Natural Convection Flow in Parallel-Plate Vertical Channels

BY

SOHAIL ANWAR

A Thesis presented to the

DEANSHIP OF GRADUATE STUDIES

In Partial Fulfillment of the
Requirementsfor the degree

MASTER OF SCIENCE

IN

MECHANICAL ENGINEERING

KING FAHD UNIVERSITY
OF PETROLEUM AND MINERALS

KING FAHD UNIVERSITY OF PETROLEUM AND MINERALS
DHAHRAN 31261, SAUDI ARABIA

DEANSHIP OF GRADUATE STUDIES

This thesis, written by **SOHAIL ANWAR** under the direction of his Thesis Advisor and approved by his Thesis Committee, has been presented to and accepted by the Dean of Graduate Studies, in partial fulfillment of the requirements for the degree of **MASTER OF SCIENCE IN MECHANICAL ENGINEERING.**

Thesis Committee

_____
Dr. Badr, Hassan M. (Thesis Advisor)

_____
Dr. Habib, M.A. (Thesis Co Advisor)

_____
Dr. Said, Syed A. M. (Member)

_____
Dr. Zubair, Syed M. (Member)

_____
Dr. Ben-Mansour, Rached (Member)

_____
Dr. Al-Sulaiman, Faleh A.
(Department Chairman)

_____
Prof. Osama A. Jannadi
(Dean of Graduate Studies)

Date

In the Name of Allah, Most Gracious, Most Merciful.

Dedicated to My Beloved Parents and Brothers
whose constant prayers, sacrifice and inspiration led to this
wonderful accomplishment

ACKNOWLEDGEMENTS

All praise and thanks are due to Allah (subhana wa taala) for bestowing me with health, knowledge and patience to complete this work. Thereafter, acknowledgement is due to KFUPM for the support given to this research through its tremendous facilities and for granting me the opportunity to purse graduate studies with financial support.

I acknowledge, with deep gratitude and appreciation, the inspiration encouragement, valuable time and guidance given to me by my thesis Committee Chairman, Dr. Hassan M. Badr.

I am grateful to my thesis Committee Co Chairman Dr. M. A. Habib for his constant help, guidance and the countless hours of attention he devoted through out the course of the work. His priceless suggestion made this work interesting and learning for me. Working with him was indeed a wonderful and learning experience with I thoroughly enjoyed. I also acknowledge the personal attention given in my thesis by my thesis Committee member Dr. S. A. M. Said. He was always friendly, understanding and concern about me. I am also grateful to my Committee members, Dr. Rached Ben-Mansour and Dr. S. M. Zubair for their constructive guidance and technical support. Thanks are also to director of PC labs Dr. M. A. Antar and Mr. Ahmed for there help in providing me adequate computing facilities thorough out this work and the department secretaries, Mr. Lateef and Mr. Jameel for their help and assistance.

I am also thank full to department Chairman Dr. Faleh A. Al-Sulaiman for providing me favorable environment where I able to utilize my skills.

Special thanks are due to my senior colleagues at the University, Mujtaba Hussain, Salman A Gaffer, Arifusalam, Baseer, Ahsan, Ovas, Iftakhar Naqvi, Arshed, Mazharuddin and Irfan S Hussaini who were always there to help me in my work. I would also like to thank my friends Arifullah Vantala, Syed Imran, Majid, Abdullah, Ali, Sameer, Amwar Basha, Fasi, Mannan, Faheem, Guruji, Shafi, Junaid, Tayyab, Zahed, Mujahed, Bilal, Hassan, Ismail, Abbas, Jalal Shah, Ameen, Ameer, Ayub, Farooq and all others who provided wonderful company and good memories that will last a life time.

Finally, thanks are due to my dearest Father, Mother, Brothers and other relatives for their emotional and moral support throughout my academic career and also for their love, patience, encouragement and prayers.

Contents

List of Tables

List of Figures

Abstract

Name: **SOHAIL ANWAR**

Title: **NATURAL CONVECTION FLOW IN PARALLEL-PLATE VERTICAL CHANNELS**

Major Field: **MECHANICAL ENGINEERING**

Date of Degree: **2 December, 2003**

The aim of this research is to investigate numerically the problem of buoyancy driven turbulent natural convection flow in a vertical channel. The importance of this problem is mainly due to many related engineering applications such as cooling of electric and electronic equipment, nuclear reactor fuel elements, home ventilation, and many others. The investigation is limited to vertical channels of uniform cross-section (parallel-plate channels) but with different modes of heating. The details of the flow and thermal fields are obtained from the solution of the conservation equation of mass, momentum and energy in addition to equation of the low Reynolds number turbulence models. The study covers Rayleigh number ranging from 10^5 to 10^9 and focuses on the effect of channel geometry on the characteristic of the flow and thermal fields as well as the local and average Nusselt number variation. The numerically predicted velocity and thermal field as well as the Nusselt number variation are validated using experimental data available in the literature.

The present results indicate that the Low Re $k-\varepsilon$ M3 Model has the capability to predict the complex buoyancy driven turbulent natural convection flow in the vertical channel in the considered Rayleigh number range. Different models were used to simulate the flow process at the channel inlet and exit sections. A uniform pressure inlet boundary condition can simulate actual flow processes for parallel-plate vertical channels. A Nusselt number correlation has been developed in terms of Modified Rayleigh number and channel aspect ratio for symmetrically heated isothermal and isoflux vertical surfaces.

MASTER OF SCIENCE DEGREE
KING FAHD UNIVERSITY OF PETROLEUM AND MINERALS
Dhahran, Saudi Arabia

Abstract (Arabic)

الملخص

الاسم: **سهيل أنور**

عنوان الرسالة: ا نتقال الحرارة بالحمل في القنوات الصفائحية العمودية المتوازية

التخصص: **الهندسة الميكانيكية**

تاريخ منح الدرجة:8 /شوال/1424

الغرض من هذه الدراسة هو البحث عن حل عددي لمسألة إنتقال الحرارة بالحمل الطبيعي المضطرب في قناة رأسية و تكمن أهمية هذا البحث في انها تتعلق بكثير من التطبيقات الهندسية كتبريد بعض المعدات الكهربائية و الالكترونية ,بعض عناصر المفاعل النووي, التهوية المنزلية, والكثير من التطبيقات الاخرى . ويعالج هذا البحث التدفق في القنوات العمودية ذات المقطع الثابت(القنوات الصفائحية المتوازية) لكن بطرق مختلفة للتسخين. فقد تم الحصول على تفاصيل التدفق والحقل الحراري من حل قانون بقاء الكتلة ,كمية الحركة والطاقة بالاضافة الى نموذج للانسياب المضطرب. و تغطي الدراسة رقم رالي من(10^5-10^9) , وتركز على تأثير شكل القناة على خصائص التدفق والحقل الحراري بالاضافة الى تغير رقم نوسلت المحلي والمتوسط.وقد تم تحقيق صحة التنبأ العددي للسرعة والحقل الحراري بالإضافة الى تغير رقم نوساتبالمقارنة مع البيانات التجريبية المتوفرة في المجلات العلمية

وقد دلت النتائج على ان نموذج low Re k-ε-M3 لديه القدرة التنبأ على التدفق طبيعي لإنتقال الحرارة بالحمل المضطرب في القنوات الصفائحية العمودية المتوازية في المجال المذكور المحدد لرقم رالي . وقد تم استخدام نماذج مختلفة لنمذجة عملية التدفق في مدخل ومخرج القناة.وقد دلت النتائج على ان افتراض الضغطالمتساوي عند المدخل يمكن ان يمثل التدفق الحقيقي للقنوات الصفائحية العمودية المتوازية.وقد تم اشتقاق علاقة توافقية لرقم نوسلتتم بدلالة رقم رالية المعدل ونسبة الطول الى العرض للقناة ذات للسطوح المسخنة بشكل متساوي للتدفق الحراري وبشكل متساوي لدرجة الحرارة .

هذه الدراسة أعدت لنيل درجة الماجستير في العلوم

جامعة الملك فهد للبترول والمعادن
الظهران ,المملكة العربية السعودية

Nomenclature

b	channel Width
C_P	specific heat at constant pressure
$C_{1\varepsilon}$, $C_{2\varepsilon}$, C_μ	empirical constants in the $k-\varepsilon$ turbulence model
$C_1, C_2, C_1^{'}, C_2^{'}, C_l$	empirical constant in RSM turbulence model
C_{ij}	convection term in equation 3.18
d	normal distance to the wall
D_{ij}^{L}	molecular diffusion term in equation 3.18
D_{ij}^{T}	turbulent diffusion term in equation 3.18
E	roughness parameter
f_1, f_2, f_μ	wall damping function
g	gravitational constant
g_i	component *i* of the gravitation vector
G_b	production of turbulent kinetic energy due to buoyancy
G_k	production of turbulent kinetic energy due to mean velocity gradient
G_{ij}	buoyancy production term in equation 3.18
Gr	Grashof number = $\left(\frac{g\beta b^3(T_W - T_O)}{\nu^2}\right)$
h	average heat transfer co-efficient
h_y	local heat transfer coefficient

k	thermal conductivity
k	kinetic energy of turbulence
$l_{ref.}$	characteristic length
L	channel Length
Nu_y	local Nusselt Number
$\overline{Nu}$	average Nusselt Number
n_i, n_j, n_k	unit vectors normal to i, j, k directions, respectively
p	pressure
P	nodal point
P_{ij}	stress production term in equation 3.18
Pr	Prandtl Number
Pr_t	turbulent Prandtl Number
q_w"	wall heat flux
Ra	Rayleigh number = (Gr. Pr)
Ra_m	modified Rayleigh number = $Ra_b(b/L)$
R_t	turbulent Reynolds number
S	surface vector
S	modulus of the mean rate of stress tenson
T	temperature
T_P	temperature at nodal point 'P'
T_w	wall temperature
T_i	ambient temperature
U_i	i th component of velocity

V	vertical velocity
$V_{avg.}$	average vertical velocity
$\bar{u}$, $\bar{v}$	time average velocity
u' , v'	fluctuating components of velocity
u, v	velocity in the x, y directions, respectively
u^+	dimensionless velocity
u_τ	characteristic velocity
x	x co-ordinate
y^+	dimensionless wall distance
y_p	Y-co-ordinate at grid node P
y	y co-ordinate

Greek Symbols

α	thermal diffusivity
β	co-efficient of thermal expansion
δ_{ij}	Kronecker delta $(=1, i=j; =0, i\neq j)$
ΔT	temperature difference between wall and ambient
∇	gradient
ε	rate of dissipation of the kinetic energy
Φ, ϕ	general field variable represented in the transport equations
ϕ_{ij}	pressure strain term in equation 3.18
Θ	non-dimensional temperature $\Theta = \frac{T - T_{amb.}}{T_W - T_{amb.}}$

Ψ	Streamline $\int \rho(u\,dy - v\,dx) + const.$ (m^2/s)
Γ	diffusion coefficient
κ	von karman constant
μ	laminar viscosity
μ_t	turbulent viscosity
ν	molecular kinematic viscosity
ρ	density
σ_k	Prandtl number for k
σ_ε	Prandtl number for ε
τ_w	wall shear stress

Subscripts

i, j	spatial coordinate indices
i	inlet condition
P	nodal point
w	wall condition
o	outlet condition
avg.	average
amb.	ambient condition
ref.	reference

Chapter 1

Introduction

1.1 Background

Heat transfer is the area that deals with the mechanisms responsible for transferring energy from one place to another when a temperature difference exists. In thermodynamics, heat is defined as energy in transient; however most of the thermodynamic processes are concerned with equilibrium or quasi equilibrium situations.

In the study of heat transfer, both equilibrium and non-equilibrium processes are encountered. The science of heat transfer allows us to determine the time rate of energy transfer caused by the more practical non-equilibrium processes. With the growing sophistication in technology and with the increasing concern with energy and the environment, the study of heat transfer has, over the past several years, been related to a very wide variety of problems, each with its own demands of precision and elaboration in the understanding of the particular processes of interest. Areas of study range from atmospheric, geophysical and environmental problems to those in heat rejection, space research and manufacturing systems.

Of the two basic processes of thermal energy transport, conduction and radiation, the formal occurs if a temperature difference exists in a material and is due to the motion of the microscopic particles that comprise the material. The motion of the particles is dependent on the local temperature in the material and diffusion of energy occurs due to

differences in the local motion. The energy transfer in the later mode, radiation, is in the form of electromagnetic waves. Energy is emitted from a material due to its temperature level, being larger for a large temperature, and is then transmitted to another surface through the intervening space, which may be vacuum or a medium that may absorb, reflect or transmit the radiation depending on the mature and extent of the medium. There is also a third mode of heat transfer, convection, in which the conductive heat transfer processes are coupled with the motion of a fluid. As a consequence of this fluid motion, the heat transfer rate, as given by conduction, is often considerably altered.

In the diversity of studies related to heat transfer, considerable effort has been directed to the convective mode, in which the relative motion of the fluid provides an additional mechanism for the transfer of energy. Convection is inevitably coupled with the conductive mechanism in most convection hear transfer processes. Also, at the solid surface, the process is predominantly conduction due to the relative fluid motion being brought to zero. A study of the convective heat transfer, therefore, involves the mechanism of conduction and, sometimes, those of radiative processes as well, coupled with those of fluid flow. This makes the study of this mode of heat transfer a very complex one, though its importance in technology and in nature can hardly be exaggerated.

The convective mode of heat transfer is further divided into two basic processes. If the motion of the fluid arises due to an external agent, such as the externally-imposed flow of a fluid stream over a heated object, the process is termed forced convection. If on the other hand, no such externally-induced flow is provided and the flow arises naturally simply due to the effect of a density difference, resulting from a temperature difference,

in a body force field, such as the gravitational field, the process is termed as natural convection.

1.2 Natural Convection

Natural convection is one of the most economical and practical methods of cooling and heating. Natural convection is caused by temperature or concentration induced density gradient within the fluid. Natural convection flow occurs as a result of the influence of gravity forces on fluids in which density gradients have been thermally established. When a vertical cold plate is placed in warm stationary fluid, the temperature of the fluid near the wall will decrease resulting in an increase in the fluid density. This density increase results in downward flow of the heavier cold fluid near the plate and upward flow of the lighter warm fluid. When a hot plate is placed in cool still fluid it results in an upward flow of the light warm fluid near the plate. Other type of natural convection flow occurs in the presence of centrifugal forces that produce variation in the fluid density.

1.3 Natural Convection adjacent to a Vertical Flat Plate

In a wide class of natural convection processes, heat transfer occurs from a heated vertical surface placed in a quiescent medium at a uniform temperature. If the plate surface temperature is greater than the ambient temperature, the fluid adjacent to the vertical surface gets heated, becomes light and rises. Heavier fluid from the neighboring areas rushes in to take the place of the rising fluid; similarly, the flow for a cooled surface is downwards. The fluid layer in contact with the surface is stationary due to the no-slip

condition and the fluid far from the vertical surface is stagnant because of the infinite quiescent medium. A boundary layer flow exists and the region outside the boundary layer is unaffected by the flow (Bejan, 1995). Laminar flow exists within the boundary layer up to a certain height of the plate, beyond which turbulence gradually develops because of the associated thermal instability.

1.4 Natural Convection through Vertical Parallel Plate Channels

In a smooth vertical parallel plate channel that are open to the ambient at top and bottom ends, natural convection occurs when at least one of the two plates forming the channel is heated or cooled. The resulting buoyancy-drive flow can be laminar or turbulent depending on the channel geometry, fluid properties and temperature difference between the plate and ambient. The Rayleigh number at which flow becomes turbulent in vertical channels is different from that of flow over a vertical flat plate. Surface thermal conditions may be idealized as being isothermal or isoflux and symmetrical or asymmetrical. For small aspect ratio (length to inter-plate spacing), independent boundary layer develops at each surface and a condition similar to that of a vertical plate in an infinite quiescent medium takes place. For large aspect ratio, however, boundary layers developed on opposing surfaces eventually merge to yield a fully developed condition. Due to modern application of cooling of electronic equipments such as printed circuit boards, there has been resurgence of interest in studying natural convection in vertical channels. Understanding the flow pattern in these equipment may significantly improve their design and consequently their operational performance Incropera and DeWitt (1996).

Chapter 2

Literature Survey

2.1 Experimental Investigation

2.1.1 Laminar Flow Regimes

Elenbaas (1942) conducted the first comprehensive experimental work, which has served as a benchmark for most subsequent studies. Laminar natural convection heat transfer in smooth parallel-plate vertical channels was investigated and a detailed study of the thermal characteristics of cooling by natural convection was reported. This work was followed by many experimental, theoretical and numerical investigations for both laminar and turbulent flow regimes.

During the last two decades, a number of studies involving experimental measurements of heat transfer in laminar free convection flows between two vertical plates were reported. Sparrow and Azevedo (1985) conducted experimental and numerical studies on the effect of inter-plate spacing on natural convection heat transfer characteristics of a one-sided heated vertical channel. The 50-fold variation of the inter-plate spacing enabled the investigation of all operation conditions between the two limits of the fully developed channel flow and the single vertical plate. The experiments were performed in water at Prandtl number Pr =5. The numerical solutions were carried out for

the same operating conditions taking into account both natural convection in the channel and conduction at the wall. It was reported that the heat transfer process is particularly sensitive to changes in inter-plate spacing for narrow channels.

The problem of natural convection heat transfer in a vertical channel with a single obstruction was investigated both experimentally and analytically by Said and Krane (1990). In the experimental part, optical techniques were used to obtain measurement of both quantitative data (heat flux and temperature) and qualitative data (flow visualization). Only uniform wall temperature boundary conditions were considered experimentally. In the numerical study, a general purpose, finite element computer code NACHOS was used with the two thermal boundary conditions of uniform wall temperature and uniform heat flux. They concluded that the location of the obstruction along the wall affects the rate of heat transfer. Moving the obstruction away from the entrance towards the exit was found to reduce the net heat transfer rate from the channel.

Kihm *et al.* (1993) investigated natural convection heat transfer characteristics in converging vertical channel flows by measuring the wall temperature gradients using a laser specklegram technique in which the wall temperature gradient was measured non-intrusively using laser. The local and average heat transfer coefficients were obtained for forty different configurations, including five different inclination angles from the vertical ($\theta = 0^{O}$, 15^{O}, 30^{O}, 45^{O} and 60^{O}) with eight different channel exit openings for each inclination angle. Correlations were obtained for the local and average heat transfer coefficients in the range of Grashof numbers up to 7.16×10^{6}, however, the flow regimes for all considered cases were laminar. They reported that as the top opening of channel decreased, both local and average Nusselt number values started decreasing below that of

a single plate. In the low Rayleigh number range, neither the single-plate limit not the fully-developed limit could properly describe the heat transfer characteristics in the converging channel. In another study, Kihm *et al.* (1995) investigated both experimentally and theoretically the phenomenon of flow reversal in natural convection flow between two isothermal vertical walls. They reported the existence of a recirculating flow region accompanied by vena-contracta-like streamlines at the entrance when Rayleigh number exceeded a certain critical value. This phenomenon resulted in insufficient volume flow rate through the channel, which in turn, limited the increase of heat transfer as Rayleigh number increases.

Naylor and Tarasuk (Part II, 1993) conducted an interferometric study on two-dimensional laminar natural convection in an isothermal vertical divided channel for two different positions of the dividing plate. The average Nusselt number obtained experimentally was found to be 10% less than the one obtained numerically (Naylor and Tarasuk, Part I, 1993); however, the general trends were in a good agreement. Tanda (1995) investigated experimentally the problem of heat transfer between two staggered vertical plates in the presence of a natural convection regime with emphasis on the effect of interplate spacing and the magnitude of vertical stagger on the heat flux from each plate. The parameters investigated included the interplate spacing, the magnitude of the vertical stagger, and the Rayleigh number based on the overall convective heat flux from each plate. The experiments were performed in air and the characteristics of the thermal field around the plates were obtained using a schlieren optical technique. They reported that staggering affects the heat transfer characteristics of the facing sides of the plates when the interplate distance was relatively small. The Nusselt number averaged on the

inner face of the lower plate was enhanced up to over 40% compared with that for the case of the unstaggered plate channel. On the other hand, the mean Nusselt number on the facing side of the upper plate was reduced by 15%.

Manca *et al.* (1995) conducted an experimental study of laminar natural convection in an asymmetrically heated vertical channel with uniform flush mounted discrete heat sources. The effect of wall emissivity was taken into account. The wall temperature profiles as a function of emissivity, strip heat flux, channel spacing, the number strips and their arrangement were presented. A correlation for Nusselt number in terms of Rayleigh number was proposed for Rayleigh numbers ranging from 10 to 106. Tanda (1997) performed experiments for studying heat transfer in natural convection flow of air in a vertical channel with one surface roughened by transverse square ribs while the opposite surface kept smooth. Isothermal condition was imposed on the ribbed side, while the other side remained unheated. A schlieren optical technique was used for measuring the thermal field characteristics and for obtaining the distribution of the local heat transfer coefficient. It was found that the presence of the square ribs results in lower heat transfer in comparison with the smooth channel. The same problem was investigated by Daloglu and Ayhan (1999) who conducted measurements of natural convection in a rectangular channel with fins connected periodically to both plates. The channel had an aspect ratio of 66 and the walls were maintained at uniform heat flux. Results were obtained for the modified Rayleigh numbers ranging from 20 to 90 and it was found that the Nusselt number for finned channels is less than that for smooth channels for all values of Rayliegh number.

A study on natural convection from an array of vertical plates with discrete and protruding heat sources was reported by Fujii *et al.* (1996). The problem was investigated both theoretically and experimentally. The governing equations of motion and energy were solved numerically using an upwind finite difference scheme for Grashof numbers up to 8.8×10^5. The velocity profiles between the central plates were measured using a laser-Doppler anemometer while the plate surface temperature was measured using thermocouples. A correlation for the local Nusselt number was proposed that is capable of predicting the protrusion surface temperature within an error band of ±20%. Hall *et al.* (1999) conducted experimental and numerical studies to determine the temperature distribution on the surfaces of vertical channels formed by parallel plates heated symmetrically and cooled by conduction, radiation and natural convection in air. Effects of wall separation, wall thickness, thermal conductivity, and emissivity on the wall temperature distribution were determined. Optimum channel width and correlation for the maximum wall temperature rise were obtained for both controlled and uncontrolled edge temperature conditions.

2.1.2 Turbulent Flow Regimes

Miyamoto *et al.* (1986) conducted the first experimental study on turbulent free convection heat transfer in an asymmetrically heated vertical channel. The channel was formed from two vertical parallel plates. One plate was heated by imposing a uniform heat flux along the plate and the opposite plate was adiabatic. The channel (4.98 m high and spanned 0.95 m) was open at the bottom and top. Experiments were performed with channel widths of 50, 100 and 200 mm. The temperature variation on the heated and adiabatic vertical plates as well as the turbulence characteristics of the free convection

flow between the plates (mean values, intensities and correlation of fluctuating velocity and temperature) were measured. These results were compared with those of a single plate. The temperature and velocity fields were presented at three vertical locations and the variation of the local heat transfer coefficient was determined along the heated wall.

La Pica *et al.* (1993) conducted an experimental study of free convection heat transfer in a vertical channel in a laboratory model of rectangular cross-section, with a wall of breadth 1.2 m and variable channel width, and a fixed height of 2.6 m. One of the channel walls was heated with uniform heat flux. Tests were conducted with different values of channel gap and heating power. On the basis of the obtained results, two correlations were reported for the average Nusselt number in terms of Rayleigh number and a geometrical parameter (channel gap/channel height).

Habib *et al.* (2001) presented experimental measurements in a vertical parallel-plate channel. Vertical velocity profiles and contours were presented for symmetric and asymmetric channels. Flow visualization in parallel- and converging-plate channels were also presented. The results indicate the significant influence of the boundary conditions on the flow field. In another study, Habib *et al.* (2002) conducted velocity field measurements for natural convection flow in symmetrically and asymmetrically heated vertical channels. In the symmetrically heated channel, both plates are heated above the ambient temperature where in the asymmetrically heated channel, one plate was kept above ambient temperature and the other one below it. Velocity measurements were performed by Laser Doppler Anemometer for two Rayleigh numbers (Ra= 2×10^6 and 4×10^6) both in the turbulent region. The results of velocity measurements indicated high velocity gradient at the shear layer close to the hot wall and a region of reverse flow at

the center of the channel close to the channel exit in the symmetrical case. In the asymmetrical case, a large vortex was formed with upward flow near the hot wall and downward flow near the cold wall. The measurements showed a thicker boundary layer close to the hot wall in comparison with that near the cold wall. It was also reported that cooling one of the two plates below ambient temperature influences the flow pattern significantly and results in a small vortex at the center of the channel at its middle section. The skewness factor for the asymmetrical flow was found to be higher than that for the symmetrical case.

2.2 Numerical Investigations

2.2.1 Laminar Flow Regimes

The first numerical solution for developing natural convection flow in an isothermal channel was carried out by Bodia and Osterle (1962) using the boundary-layer approximation. The authors assumed uniform velocity and temperature profiles and ambient pressure at the channel inlet while assuming fully-developed flow at the channel exit. The solution methodology developed by Bodia and Osterle (1962) was widely used to solve free convective channel flow problems for various boundary conditions as in the works by Aung *et al.* (1972), Miyatake and Fujii (1972), Dalbert *et al.* (1981), and Oosthuzien (1981). Very few numerical solutions to free convection in the vertical channel were carried out without using the boundary-layer approximation. Among these were the works by Kettleborough (1972) and Nakamura *et al.* (1982) who presented data from the finite-difference solutions of the full conservation equations. However, the

results were limited to two values of Grashof number and are in poor agreement with other published results in many aspects.

Naylor *et al.* (1991) conducted a numerical study on developing free convection flow between isothermal vertical plates with aspect ratios between 10 and 24. The Navier-Stokes and energy equations were solved numerically assuming a special inlet-flow boundary conditions in the range of Grashof number $50 < Gr < 5\times10^4$. The results showed a new recirculating flow zone in the entrance region when $Gr = 104$ for a channel of length to width ratio of 24. They assumed a radial flow caused by a sink positioned at the middle of the inlet section and a fully developed flow at the exit section. This was not applicable to low Rayleigh number cases since conduction far upstream from the channel inlet heats the approaching flow. At low Rayleigh number, the flow entered the channel without separation; however, in the high Rayleigh number range separation occurred followed by the formation of small eddies close to the channel wall near the leading edge. As aspect ratio increases, flow separation was found to occur for lower values of Rayleigh numbers. Both parabolic and elliptic solutions resulted in fair agreement between the pressure variations along the channel centerline at low Rayleigh numbers. However, a large difference was found especially near the channel entrance at high Rayleigh numbers. This was mainly due to flow separation in the entrance region causing a 'venturi' effect on the mainstream leading to a local pressure drop. Comparisons with the boundary-layer results show that the full elliptic solution is necessary to get accurate results in the channel entrance region. The obtained velocity and temperature profiles were not in good agreement with those reported by Kettleborough (1972) and Nakamura *et al.* (1982) at Grashof numbers of 125 and 1250. Kettleborough (1972) predicted an

interesting phenomenon of reverse flow in the channel with fluid being drawn into the channel from the channel exit section, however, the temperature profiles obtained did not agree with those predicted by Nakamura *et al.* (1982). Although the general trend of the local heat transfer distributions is the same, both parabolic and elliptic predictions obtained by Kettleborough (1972) and Nakamura *et al.* (1982) were much lower than the experimental results reported by Wirtz and Haag (1985).

Naylor and Tarasuk (Part I, 1993) obtained a numerical solution for the problem of two-dimensional laminar natural convection in a divided vertical channel. The channel was divided by an isothermal vertical plate located midway between the two isothermal channel walls. The study examined the effect of Rayleigh number, plate-to-channel length ratio, vertical plate position, and the plate thickness on the heat transfer process. Solutions for both full elliptic and parabolic forms of the Navier-Stokes and energy equations were obtained for Prandtl number Pr = 0.7. Positioning the plate at the bottom of the channel was found to give the highest average Nusselt numbers for the plate and for the channel. The average Nusselt number on the dividing plate was about two times higher than that of a single flat plate placed in a fluid of infinite extent. The computational domain was described by the same authors in their earlier work (Naylor *et al.*, 1991) and utilizing the same boundary conditions. At low Rayleigh numbers, the flow entered the channel smoothly whereas separation occurred at the channel inlet at high Rayleigh numbers. The thermal boundary layers look similar to those of two semi-infinite vertical flat plates and the two boundary layers merge before the channel exit. The authors studied the variation of the plate average Nusselt number with Rayleigh number for several length ratios. Further investigations on the separation bubble formed near the

channel entrance region were carried out by Roberts and Floryan (1998). This separation bubble was found to have a considerable effect on the local Nusselt number especially at high Grashof numbers. When this sharp-edged inlet corners were rounded, the inlet separation region disappeared for all Grashof numbers. It was found that the local Nusselt number decreases in the entrance region of the channel with square corners but with no such decrease in the case of rounded corners.

Darie *et al.* (1998) numerically studied the effect of through forced upward flow on natural convection from an asymmetrically heated vertical channel. The study focused on the effect of forced flow on heat transfer from the cold wall and the conditions required for achieving an effective thermal insulation. The study revealed that there is a critical Reynolds number that will significantly reduce the Nusselt number on the cold wall. Flow transition from buoyancy driven flow regime to forced convection flow regime was found to depend on the aspect ratio. Two critical Reynolds number were reported; the first for the heat transfer process and the second for the flow structure. The first critical Reynolds number was found to be proportional to the square of aspect ratio (independent of Ra) while the second critical Reynolds number was determined based on a fully-developed flow assumption for different aspect ratios. It was found that the analytical prediction for the second critical Reynolds number is only valid for aspect ratios less than 8.

The effect of other parameters including different forms of heating, transient regimes, chimney effect and channel geometry were investigated by a number of researchers. Shahin and Floryan (1999) studied the heat transfer enhancement generated by the chimney effect in a system of vertical channels. The increase in heat transfer with

adiabatic chimneys was studied numerically and a heat transfer correlation was presented. Chang *et al.*, (1997) performed numerical analysis of transient natural convection in vertical plates of finite length with transient symmetric isoflux heating. The parameters studied were the Grashof number ranging from 10 to 108 for aspect ratio 5. The transient thermal and flow fields, including isotherms, pressure contours, streamlines and velocity profiles for various Grashof number were obtained. A correlation of a transient-induced Reynolds number for a vertical finite-length channel with various transient Rayleigh numbers was proposed. The effect of variation of fluid properties within the thermal field was studied by Zamora and Hernandez (1997) who focused on the influence of variable property on laminar airflow induced by natural convection in a vertical, asymmetrically-heated channel. A full-elliptic model accounting for the variation of viscosity and thermal conductivity was used. They concluded that the variable property effects have a strong influence on the velocity and temperature fields. Other forms of heating was reported in the work by Lee (1999) who conducted a numerical/theoretical investigation on laminar natural convection heat and mass transfer between two vertical parallel plates with unheated entry and exit regions. Both with uniform wall temperature/concentration and uniform wall heat flux/mass flux as boundary condition. Results of dimensionless induced flow rate, average Nusselt number, Sherwood number were reported and correlations for these parameters were presented.

Theoretical studies of laminar natural convection in vertical and inclined channels with different geometries were recently reported by a number of researchers. Straatman *et al.* (1994) investigated the effect of the angle of inclination on natural convection heat transfer in a channel with isothermal walls. The overall heat transfer was found to

decrease as the inclination angle increased. The amount of decrease in heat transfer was proportional to the cosine of the inclination angle. The heat flux distribution along each wall was presented. No significant asymmetric thermal field was observed in the considered range of the parametric studies. Said (1996) conducted a numerical investigation of natural convection heat transfer in a uniform convergent vertical channel with air as the working medium. Half-angle of convergence in the range of 0^O to 10^O was employed and solutions were obtained for modified Rayleigh number ranging from 1 to $2x10^4$. To obtain a correlation for Nusselt number suitable for merging the convergent channel results with those of the parallel-walls channel, three characteristic dimensions based on the minimum, average and maximum channel interval spacing were considered. It was found that the maximum interval spacing is the most appropriate as a characteristic dimension. The effect of wall protrusions on natural convection in a vertical two-parallel-plate channel was investigated by Sarma *et al.* (1995) with the assumption that one of the plates is flat while the other has periodic protrusions. The governing equations were solved using a regular perturbation method assuming steady laminar 2-D flow. The study showed that both flow rate and heat transfer coefficient decrease in the presence of wall protrusions.

2.2.2 Turbulent Flow Regimes

Contrary to the large volume of research published on the problem of laminar natural convection flow in vertical channels, only few investigations were reported on the turbulent flow case. Nobuhide and Mitsugu (1997) investigated the fully developed, turbulent combined (forced and natural) convection between two vertical parallel plates kept at different temperatures through a series of direct numerical simulations. The

pressure gradient drives the mean flow upward, while the buoyant force acts either upward (aiding flow) near the high temperature wall or downward (opposing flow) near the low temperature wall. The Reynolds number based on the channel half-width and the friction velocity is assumed to be 150; whereas the Grashof number based on the channel width and the wall temperature difference varies from 0 to 1.6×10^6. The effect of buoyancy on the turbulence statistics including the mean velocity and temperature, the Reynolds stress tensor and the turbulent heat flux vector were examined.

Fedorov and Viskanta (1997) studied the induced flow and heat transfer in an asymmetrically heated, vertical parallel-plate channel. A low Reynolds number $k-\varepsilon$ turbulence model was used in conjunction with heat transfer analysis in the channel. The model predictions were first validated through comparisons with the experimental data reported by Miyamoto *et al.* (1986). The local Nusselt number distributions were presented and the induced flow rate and average heat transfer coefficient were obtained in terms of the relevant dimensionless parameters. The study focused on symmetrically heated vertical, parallel-plate channel with one wall heated (either uniform wall temperature or constant heat flux) and the other wall adiabatic. Air enters the channel from below at ambient temperature and moves upward by buoyancy forces. The flow was considered steady and incompressible and the heat transfer by radiation was neglected. The velocity at the inlet section was computed from the mass balance and the velocity gradient was set to zero at the channel exit section. Comparison of the available experimental data and the model predictions suggested that the low Reynolds number $k-\varepsilon$ turbulence model was capable of predicting the flow and thermal fields with reasonable accuracy. It was found that the turbulence intensity assumed at the channel

inlet affects the location of transition from laminar to turbulent flow as well as the average heat transfer coefficient. In another paper, Fedorov *et al.* (1997) predicted the heat and mass transfer from an evaporating water film falling under gravity along a heated vertical plate with countercurrent airflow in a parallel-plate channel. A low Reynolds number $k-\varepsilon$ turbulence model similar to that used by the same author (Fedorov and Viskanta, 1997) was used in conjunction with heat and mass transfer analysis in the asymmetrically heated channel. The heated wall was wetted with a film of water that flows downward by gravity, and a counter flow air stream cooling the water film. The model predictions were compared with experimental data (Miyamoto *et al.*, 1986) for validation. The variation of the local heat flux and Nusselt and Sherwood numbers were reported.

Versteegh and Nieuwstadt (1998, 1999) conducted a numerical simulation of turbulent natural convection in a differentially heated vertical channel in the Rayleigh number range Ra = 5.4 x 10^5 to 5.0 x 10^6. The emphasis in their work was on the analysis of turbulent Reynolds stresses, fluxes, variances and the related budgets based on the turbulence structure found from linear stability analysis of the laminar solution of the problem. The scaled mean profiles like velocity, temperature, and turbulence quantities (temperature flux, temperature variance, velocity variance) were presented. A numerical simulation of conjugate, turbulent natural convection air-cooling of three identical heated ceramic components mounted on a vertical adiabatic channel was carried out by Bessaih and Kadja (2000). A two-dimensional heat transfer model together with the standard $k-\varepsilon$ turbulence model was used to study the flow and thermal fields. The finite-volume method was used to solve the model equations throughout the entire physical domain. In

another paper Bessaih and Kadja (2000) presented a numerical simulation of conjugate, turbulent natural convection air cooling of three heated ceramic components having as aspect ratio of one, mounted on a vertical adiabatic channel wall. A three-dimensional, conjugate heat transfer model, and a high Reynolds number $k-\varepsilon$ turbulence model were used together with finite-volume discretization. The effects of spacing between the heated electronic components and the removal of heat input in one of the components were reported.

2.3 Turbulence Modeling for Buoyancy-driven flows

The buoyancy driven fluid motion in vertical open channels arises from heat transfer through vertical or nearly vertical walls, the greatest effects of buoyancy occur very close to the wall where the temperature is highest. This renders inapplicable the use of local-equilibrium logarithmic velocity and temperature-versus-distance variations to simplify the calculation of near-wall flows. The standard $k-\varepsilon$ model (Launder and Spalding, 1974; Rodi, 1980) was devised for high Reynolds number turbulent flows and is traditionally used in conjunction with a wall function when it is applied to wall-bounded turbulent flows. However, universal wall functions do not exist in complex flows, and it is thus necessary to develop a form of $k-\varepsilon$ model equations that can be integrated down to the wall. Jones and Launder (1973) first proposed a low Reynolds number $k-\varepsilon$ model for near-wall turbulence, which was then followed by a number of similar $k-\varepsilon$ models. The simplest example of a near-wall modified turbulence model is the van Driest (1956) damping function for the mixing length. More advanced models incorporate either a wall damping effect or a direct effect of molecular viscosity or both, on the empirical constants and functions in the turbulence transport equation devised

originally for high Reynolds number, fully turbulent flows remote from the wall. In the absence of reliable turbulence data in the immediate vicinity of a wall or at low Reynolds numbers, these modifications have been based largely upon comparisons between calculations and experiments in terms of global parameters.

In the models proposed by Chien (1982), Dutoya and Michard (1981), Hassid and Poreh (1978), Hoffmann (1975), Lam and Bremhorst (1981), Launder and Sharma (1974) and Reynolds (1976), the Reynolds stress is related to the local velocity gradient by an eddy viscosity, which is computed from model transport equations for k and ε. The models differ from their basic version by the inclusion of viscous diffusion terms as well as additional terms such as the wall roughness and a near-wall term for better representation of the near-wall behavior. The systematic evaluation of the above two-equation "low Reynolds number" turbulence models was performed by Patel *et al.* (1984) using a local variable accounting for low Reynolds number and wall proximity effects. He suggested that the performance of these models can be improved by selecting a damping function for the shear stress that is in agreement with experimental data and has an influence restricted to the sublayer and buffer zones; choosing the low Reynolds number functions in the dissipation rate equation with a mathematically consistent near–wall behavior and in accordance with empirical information.

Yang and Shih (1993) proposed a turbulence model for low Reynolds number near wall turbulent flow. This model was free from three major deficiencies. First, a near-wall pseudo-dissipation rate was introduced to remove the singularity in the dissipation equation at the wall. The definition of the near-wall pseudo-dissipation rate was quite arbitrary. Second, the model constants were different from those of the standard $k-\varepsilon$

model, making the near-wall models less capable of handling flows containing both high Reynolds number turbulence and near wall turbulence, which is often the case for a real flow situation. Patel *et al.* (1984) put the first criterion that enables the near-wall models to predict turbulent free shear flows. Third, the variable y^+ is used in the damping function of the eddy viscosity formulae. Since the definition of y^+ involves the friction velocity, any model containing y^+ cannot be used in flows with separation. The above deficiencies were overcome by choosing $k^{1/2}$ as turbulent velocity scale. The model constants are exactly the same as those in the standard $k-\varepsilon$ model that ensures the performance of the model far from the wall. A damping function is proposed in terms of R_y $\left(k^{1/2}y/\upsilon\right)$ instead of y^+, as in Lam and Bremhorst (1981) model. This allows the model to be used in more complicated flow situation as flows with separation.

2.4 Objectives of the Present Work

As evident from the above literature review, natural convection heat transfer in vertical parallel-plate channels was not studied numerically for Rayleigh number ranging from 10^5 to 10^9. Moreover, the turbulent natural convection solutions for this problem were not validated with experimental data in this Rayleigh number range. So far, there is no appropriate boundary conditions that can be used for simulating the conditions at the inlet and exit section. Accordingly, the main objectives of this study are

1. Analyzing different turbulence models that can predict flow and heat transfer characteristics in this range of Rayleigh number and validate it with existing experimental data available in literature.
2. Evaluate the boundary conditions that can simulate the actual flow process at the inlet and exit sections of the channel.
3. Study both cases of uniform wall temperature and uniform wall heat flux.
4. Develop correlations for Nusselt number in terms of Rayleigh number.

Hence, the result of the study is expected to contribute to the literature in this field and enhance the understanding of turbulent natural convection in vertical channels.

Chapter 3

Mathematical Formulation

In Natural convection, as in other convective processes, a consideration of fluid flow is necessary in the study of the energy and mass transfer mechanisms. A study of convection further necessitates a consideration of the coupling between the fluid flow and the mechanism underlying convection and conduction. This is due to the fact that the heat transported due to the moving fluid element would eventually be transferred to adjacent surfaces through conduction. In natural convection processes, unlike forced convection, the flow itself arises due to the temperature difference in the body force field. Therefore, the heat transfer and the fluid flow processes are inseparably linked together and one may not be determined independent of the other.

The physical situation involving fluid flow and heat transfer are governed by the conservation principles of mass, momentum, and energy. These principles can be expressed in terms of partial differential equations. A close examination of these equations reveals that they posses a common form Lapidus and Pinder (1982)

$$\oint \rho\phi v \cdot dA = \oint \Gamma_\phi \nabla\phi \cdot dA + \int_V S_\phi dV \tag{3.1}$$

Here ϕ is any field variable and v is the velocity vector. This equation describes the transport of scaler or vector quantity which takes place because of convection and diffusion processes.

The first term in the general transport equation is called convection term. This represents the transport of property ϕ due to mass flow though the control surfaces. The second term represents diffusion of property ϕ due to its gradient in the flow field. The third term is the source term representing the rate of generation of the transport variable ϕ within the control volume.

3.1 General Governing Equation in Physical Space

3.1.1 Mean flow equation

In many industrial applications, Natural convection flows are turbulent. "Turbulence is an irregular motion which in general makes its appearance in fluids, gaseous or liquid, when they flow past solid surfaces or even when neighboring streams of the same fluid flow past or over one another." von Karman (1937).

The crucial difference between visualization of laminar and turbulent flows is the appearance of eddying motion of a wide range of length scales in turbulent flows. A typical flow domain of 0.1m to 0.1m with a high Reynolds number turbulent flow might contain eddies down to 10 to 100μm size. This requires a computing mesh of 10^9 to 10^{12} points to be able to describe processes at all length scales. The fastest events take place with a frequency of the order of 10kHz, so it is required to discretise time into steps of about 100μs.

The present day computing powers are far behind those required to simulate turbulent flows using direct numerical simulation (i.e. using full Navier Stokes Equations without any modeling assumptions about structure of turbulence).

Engineers need computational procedures which supplies adequate information about the turbulent processes, avoiding the need of predicting the effects of each and every eddy in the flow. Because turbulence consists of random fluctuation of the various flow properties statistical approach is used. Reynolds (1895) introduced a procedure in which all quantities are expressed as the sum of mean and fluctuating parts. The time-averaged property of the flow provides equations governing mean-flow quantities ϕ to a greater extend.

The time-averaged Navier-Stokes equations of motion for steady, two-dimensional, flow in a vertical channel can be written as Fedorov and Viskanta (1997)

3.1.2 Conservation of mass (Continuity):

$$\frac{\partial\left(\rho\bar{u}\right)}{\partial x}+\frac{\partial\left(\rho\bar{v}\right)}{\partial y}=0 \tag{3.2}$$

3.1.3 Conservation of x-momentum:

$$\frac{\partial}{\partial x}\left(\rho\overline{\bar{u}\bar{u}}\right)+\frac{\partial}{\partial y}\left(\rho\overline{\bar{u}\bar{v}}\right)=-\frac{\partial p}{\partial x}+\frac{\partial}{\partial x}\left[\left(\mu+\mu_t\right)\frac{\partial\bar{u}}{\partial x}\right]+\frac{\partial}{\partial y}\left[\left(\mu+\mu_t\right)\frac{\partial\bar{u}}{\partial y}\right]-\frac{2}{3}\rho\frac{\partial k}{\partial x} \tag{3.3}$$

3.1.4 Conservation of y-momentum:

$$\begin{aligned}\frac{\partial}{\partial x}\left(\rho\overline{\bar{u}\bar{v}}\right)+\frac{\partial}{\partial y}\left(\rho\overline{\bar{v}\bar{v}}\right)=&-\frac{\partial p}{\partial y}+\frac{\partial}{\partial x}\left[\left(\mu+\mu_t\right)\frac{\partial\bar{v}}{\partial x}\right]+\frac{\partial}{\partial y}\left[\left(\mu+\mu_t\right)\frac{\partial\bar{v}}{\partial y}\right]\\&-\frac{2}{3}\rho\frac{\partial k}{\partial y}+\left(\rho-\rho_o\right)g\end{aligned} \tag{3.4}$$

3.1.5 Conservation of energy equation:

$$\frac{\partial}{\partial x}\left(\rho\bar{u}\bar{T}\right)+\frac{\partial}{\partial y}\left(\rho\bar{v}\bar{T}\right)=\frac{\partial}{\partial x}\left[\left(\frac{\kappa}{C_P}+\frac{\mu_t}{\mathrm{Pr}_t}\right)\frac{\partial T}{\partial x}\right]+\frac{\partial}{\partial y}\left[\left(\frac{\kappa}{C_P}+\frac{\mu_t}{\mathrm{Pr}_t}\right)\frac{\partial T}{\partial y}\right] \tag{3.5}$$

In equation (3.3)-(3.5), μ_t is the turbulent dynamic viscosity that is to be predicted from the knowledge of the kinetic energy of turbulence, k, and turbulent kinetic energy dissipation rate, ε. Note that in the above formulation, the governing equations are solved for incompressible flow with Boussinesq approximation.

The above governing equations are time averaged, however, they no longer form a closed set due to the additional terms representing the transport of momentum and heat of the fluctuating motion. Equations governing these fluctuating motions introduce additional unknown quantities and can only be solved when the turbulence correlations are used.

3.2 Turbulence Modeling

Different turbulence models are used to predict the natural convection heat transfer through vertical parallel plate channels. One of the widely used models of turbulence is the $k-\varepsilon$ model. The following represents the main equations in that model Rodi (1984)

Turbulent viscosity equation

$$\mu_t = \rho C_\mu f_\mu \left(\frac{k^2}{\varepsilon}\right) \tag{3.6}$$

Turbulence kinetic energy (k-equation)

$$\frac{\partial}{\partial x}\left(\rho\bar{u}k\right)+\frac{\partial}{\partial y}\left(\rho\bar{v}k\right)=\frac{\partial}{\partial x}\left[\left(\mu+\frac{\mu_t}{\sigma_k}\right)\frac{\partial k}{\partial x}\right]+\frac{\partial}{\partial y}\left[\left(\mu+\frac{\mu_t}{\sigma_k}\right)\frac{\partial k}{\partial y}\right]+G_k+G_b-\rho\varepsilon-D \quad (3.7)$$

Turbulence dissipation (ε-equation)

$$\begin{aligned}&\frac{\partial}{\partial x}\left(\rho\bar{u}\varepsilon\right)+\frac{\partial}{\partial y}\left(\rho\bar{v}\varepsilon\right)=\frac{\partial}{\partial x}\left[\left(\mu+\frac{\mu_t}{\sigma_\varepsilon}\right)\frac{\partial \varepsilon}{\partial x}\right]+\frac{\partial}{\partial y}\left[\left(\mu+\frac{\mu_t}{\sigma_\varepsilon}\right)\frac{\partial \varepsilon}{\partial y}\right]\\&+C_{\varepsilon 1}f_1\frac{\varepsilon}{k}\left(G_k+C_{\varepsilon 3}G_b\right)-C_{\varepsilon 2}f_2\rho\frac{\varepsilon^2}{k}+E\end{aligned} \quad (3.8)$$

In the k and ε equation (3.7 and 3.8), first two terms in this equation represent transport of kinetic energy of fluctuation or dissipation rate of kinetic energy by convection. Third and fourth terms represent transport of these quantities by diffusion Ince and Launder (1989). G_k represents the rate of generation of turbulent kinetic energy due to mean velocity gradients,

$$G_k=\mu_t\left(\frac{\partial\overline{u_i}}{\partial x_j}+\frac{\partial\overline{u_j}}{\partial x_i}\right)\frac{\partial\overline{u_i}}{\partial x_j}-\frac{2}{3}\rho k\delta_{ij}\frac{\partial\overline{u_i}}{\partial x_j} \quad (3.9)$$

$\rho\varepsilon$ its destruction rate and G_b is generation of turbulent kinetic due to buoyancy given by

$$G_b=\beta g_i\frac{\mu_t}{\mathrm{Pr}_t}\frac{\partial T}{\partial x_i} \quad (3.10)$$

In addition there are some extra terms, denoted by D in k-equation and E in ε-equation to account for near wall behavior. f_1 and f_2 are wall damping functions Launder and Spalding (1972) in ε-equation.

3.3 Wall Function and Near Wall Model

The natural convection flow through vertical parallel plate channels is characterized by large velocity and temperature gradients near the wall. In that region, a special numerical code must be used in order to obtain reasonable accuracy. There are two approaches to model the near-wall region. In one approach, the viscosity-affected, inner region (viscous sublayer and buffer layer) is not resolved. Instead, semi-empirical formulas called "wall function' are used to bridge the viscosity-affected region between the wall and the fully-turbulent region. The use of the wall function obviates the need to modify the turbulence models to account for the presence of the wall. In the second approach, the turbulence models are modified to enable the viscosity- affected region to be resolved with a mesh that extends all the way to the wall, including the viscous sublayer. This is termed as 'near wall modeling".

3.4 Model-1: The Standard $k-\varepsilon$ Turbulence Model

The turbulent viscosity (μ_t) in equations (3.3-3.5) has been defined using the two-equation $k-\varepsilon$ model of turbulence. The model constant and wall function (damping function) are listed in table (3.1). It can be seen that the wall damping function f_μ, f_1 and f_2 in equation (3.8) are unity and the wall roughness parameter $E = 9.8$ for a smooth wall Schlichting (1979). The near-wall value of the term D in *k*-equation (3.7) is zero. Since, the standard $k-\varepsilon$ turbulence model is not applicable in the viscosity-affected inner region (viscous sublayer and buffer layer), a semi-empirical formula (wall functions) is used to bridge the viscous region between the wall and the fully-turbulent layer. The law of the wall can be expressed as Rodi (1984)

$$u^+ = \frac{u}{u_\tau} = \frac{1}{\kappa}\ln\left(\mathrm{E}y^+\right) \tag{3.11}$$

where u_τ is the friction velocity, y^+ represents the dimensionless distance from the wall. The defining equation of u_τ and y^+ can be written as

$$u_\tau = \sqrt{\frac{\tau_w}{\rho}} \tag{3.12}$$

$$y^+ = \frac{\rho y\, u_\tau}{\mu} \tag{3.13}$$

where

κ is the von Karman constant and its value is 0.4 (Launder and Spalding, 1974).

τ_w is the shear stress at the wall.

E is roughness parameter

y is the actual distance from the wall.

3.5 Model-2: Low Re $k-\varepsilon$ Turbulence Model 2.

This turbulence model has same equation for Turbulence kinetic energy and its dissipation energy equation (3.7 and 3.8) as the standard $k-\varepsilon$ turbulence model but modifications are applied to enable it to cope with low Reynolds number flows. The wall damping function is applied to ensure that viscous stresses take over from turbulent Reynolds stresses at low Reynolds numbers and in the viscous sub-layer adjacent to solid walls Launder and Sharma (1974). These functions are themselves functions of the

turbulence Reynolds number (R_t) with extra term D and E in equation 3.7 and 3.8 as shown in table 3.1. The turbulence Reynolds number is defined as

$$R_t = \frac{k^2}{v\varepsilon} \tag{3.14}$$

3.6 Model-3: Low Re $k-\varepsilon$ Turbulence Model 3.

This turbulence model has an equation for turbulence viscosity and transport equations for k and ε (3.6-3.8) same as in the standard $k-\varepsilon$ turbulence model. But it eliminates singularity that would appear if the standard $k-\varepsilon$ model is applied down to the wall because of vanishing *k* at the wall. As the wall is approached, both the turbulence length scale and turbulent velocity approach zero Yang and Shih (1993). However, the ratio of these quantities approaches a nonzero value which is order of *y*. The wall damping function f_μ is expressed in the form Yang and Shih (1993).

$$R_y = \frac{k^{1/2} y}{v} \tag{3.15}$$

$$f_\mu = \left[1 - \exp\left(-a_1 R_y - a_3 R_y^3 - a_5 R_y^5\right)\right] \tag{3.16}$$

where $a_1 = 1.5\text{x}10^{-4}$, $a_3 = 5.0\text{x}10^{-7}$ and

$a_5 = 1.0\text{x}10^{-10}$

3.7 Model-4: The Renormalization Group (RNG) $k-\varepsilon$ Turbulence Model.

The RNG $k-\varepsilon$ turbulence model is derived from the instantaneous Navier-Stokes equations, using a mathematical technique called "renormalization group method" (RNG). The resulting model has constants different from those in the standard $k-\varepsilon$ model and additional terms and function in the transport equations for k and ε (Yakoth and Steven, 1986). These equations are the same as equations (3.7) and (3.8) with the only difference in the diffusion term where this model uses $\alpha_\phi \mu_{eff}$ in place of $\left(\mu + \frac{\mu_t}{\sigma_\phi}\right)$.

As well an additional term R in the ε-equation is incorporated and is defined as

$$R = \frac{C_\mu \rho \eta^3 \left(1 - \eta/\eta_o\right)}{1 + \beta \eta^3} \frac{\varepsilon^3}{k} \tag{3.17}$$

where α_ϕ is the diffusivity of transport property, $\eta \equiv S\,k/\varepsilon$, S is the modulus of the mean rate of strain tensor, $\eta_o = 4.38$, $\beta = 0.012$ Choudhury (1993).

A comparison between the four $k-\varepsilon$ turbulence models is detailed in Table 3.1. All the four $k-\varepsilon$ turbulence models differ from their basic version by the inclusion of the viscous diffusion terms and damping functions f to modify the constant C. Also, extra terms denoted by D and E, are added in some cases to better represent the near-wall behavior.

Table 3.1: Comparison of different Turbulence Model constants, damping functions and extra terms

Model	D	$\varepsilon_w - B.C$	C_μ	$C_{\varepsilon 1}$	$C_{\varepsilon 2}$	$C_{\varepsilon 3}$	σ_k	σ_ε
Standard $k-\varepsilon$	0	Wall function	0.09	1.44	1.92	1.0	1.0	1.3
Low-Re-$k-\varepsilon$-M2 (Launder-Sharma)	$2\nu\left(\frac{\partial k^{(1/2)}}{\partial y}\right)$	0	0.09	1.44	1.92	1.0	1.0	1.3
Low-Re-$k-\varepsilon$-M3 (Yang-Shih)	$2\nu\left(\frac{\partial k^{(1/2)}}{\partial y}\right)$	0	0.09	1.44	1.92	1.0	1.0	1.3
RNG	0	Wall function	0.0845	1.42	1.68	1.0	1.0	1.2

Model	f_μ	f_1	f_2	E
Standard $k-\varepsilon$	1.0	1.0	1.0	9.8
Low-Re-$k-\varepsilon$-M2 (Launder-Sharma)	$\exp\left[\frac{-3.4}{(1+R_T/50)^2}\right]$	1.0	$1-0.3\exp\left(-R_T^2\right)$	$2\mu\mu_t\left(\frac{\partial^2 u}{\partial y^2}\right)^2$
Low-Re-$k-\varepsilon$-M3 (Yang-Shih)	$\left[1-\exp\begin{bmatrix}-a_1R_y\\-a_3R_y^3\\-a_5R_y^5\end{bmatrix}\right]$	1.0	1.0	$2\mu\mu_t\left(\frac{\partial^2 u}{\partial y^2}\right)^2$
RNG	1.0	1.0	1.0	R

3.8 Model-5-The Reynolds Stress Model (RSM).

The Reynolds stress model involves calculation of the individual Reynolds stresses, $\overline{u_i' u_j'}$ through solving their differential transport equations. The individual Reynolds stresses are then used to obtain closure of the Reynolds-averaged momentum equation (Launder et al. 1975). The model equations for the transport of the Reynolds stresses $\rho\overline{u_i' u_j'}$ may be written as follows.

$$C_{ij} = D_{ij}^{T} + D_{ij}^{L} + P_{ij} + G_{ij} + \varphi_{ij} + \varepsilon_{ij} \tag{3.18}$$

where

$$C_{ij} = \frac{\partial}{\partial x_k}\left(\rho \bar{u}_i \overline{u_i u_j}\right)$$ is the convection term, (3.18a)

$$D_{ij}^{T} = -\frac{\partial}{\partial x_k}\left[\frac{\mu_t}{\sigma_k}\frac{\partial \overline{u_i u_j}}{\partial x_k}\right]$$ is the turbulent diffusion term, (3.18b)

$$D_{ij}^{L} = \frac{\partial}{\partial x_k}\left[\mu \frac{\partial}{\partial x_k}\left(\overline{u_i u_j}\right)\right]$$ is molecular diffusion term, (3.18c)

$$P_{ij} = \left(\overline{u_i u_j}\frac{\partial U_j}{\partial x_k}\right) + \left(\overline{u_j u_k}\frac{\partial U_i}{\partial x_k}\right)$$ is stress production term, (3.18d)

$$G_{ij} = \beta \frac{\mu_t}{\mathrm{Pr}_t}\left(g_i \frac{\partial T}{\partial x_j} + g_j \frac{\partial T}{\partial x_i}\right)$$ is the buoyancy production term, (3.18e)

$$\phi_{ij} = \phi_{ij,1} + \phi_{ij,2} + \phi_{ij}^{w}$$ is the pressure Strain term, (3.18f)

$$\phi_{ij,1} = -C_1 \rho \frac{\varepsilon}{k}\left[\overline{u_i u_j} - \frac{2}{3}\delta_{ij} k\right]$$ is the slow pressure strain term, (3.18g)

$$\phi_{ij,2} = -C_2\left[\left(P_{ij} + F_{ij} + G_{ij} - C_{ij}\right) - \frac{1}{3}\delta_{ij}\left[P_{kk} + G_{kk} - C_{kk}\right]\right]_{k=1,2,3}$$ is the rapid pressure strain term, (3.18h)

$$\phi_{ij}^{w} = C_1^{'}\frac{\varepsilon}{k}\left(\overline{u_k u_m} n_k n_m \delta_{ij} - \frac{3}{2}\overline{u_i u_k} n_j n_k - \frac{3}{2}\overline{u_j u_k} n_i n_k\right)\frac{k^{3/2}}{C_l \varepsilon d}$$
$$+ C_2^{'}\left(\phi_{km,2} n_k n_m \delta_{ij} - \frac{3}{2}\phi_{ik,2} n_j n_k - \frac{3}{2}\phi_{jk,2} n_i n_k\right)\frac{k^{3/2}}{C_l \varepsilon d}$$ is the wall reflection term, (3.18i)

n_k is the x_k component of the unit normal to the wall, $C_l = \frac{C_\mu^{3/4}}{k}$, d is the normal distance to the wall.

$$\varepsilon_{ij} = -2\mu\overline{\frac{\partial u_i}{\partial x_k}\frac{\partial u_j}{\partial x_k}}$$ is the dissipation term. (3.18j)

Model-6-Modified Reynolds Stress Model (Modified RSM)

The model constant $C_1, C_2, C_1^{'}, C_2^{'}, C_l, C_\mu$ and κ are given in the table 3.2 for both Reynolds stress model and modified Reynolds stress model. Modification of linear pressure strain (ϕ_{ij}) term will account for the low Reynolds number turbulence Launder and Shima (1989) which occurs in natural convection heat transfer in vertical parallel plate channels.

Table 3.2: RSM Turbulence Model constants for both general RSM and Low Reynolds number Modified RSM.

Model	C_1	C_2	$C_1^{'}$	$C_2^{'}$	C_l	C_μ	κ
RSM	1.8	0.6	0.5	0.3	$\frac{C_\mu^{3/4}}{k}$	0.09	0.41
RSM (Low-Re Modification)	$1+2.58A\sqrt{A}$ $\left\{1-\exp\left[-\left(0.0067\,\mathrm{Re}_t\right)^2\right]\right\}$	$0.75\sqrt{A}$	$-\frac{2}{3}C_1+1.67$	$\max\left[\frac{\frac{2}{3}C_2-\frac{1}{6}}{C_2},0\right]$	$\frac{C_\mu^{3/4}}{k}$	0.09	0.41

where $\mathrm{Re}_t=\frac{\rho k^2}{\mu\varepsilon}$, $A\equiv\left[1-\frac{9}{7}\left(A_2-A_3\right)\right]$, $A_2\equiv a_{ik}a_{ki}$, $A_3\equiv a_{ik}a_{kj}a_{ji}$ and a_{ij} is the anisotropic part of the Reynolds stress tensor, define as

$$a_{ij}=-\left(\frac{-\rho\overline{u_i u}+\frac{2}{3}\rho k\delta_{ij}}{\rho k}\right) \tag{3.19}$$

3.9 Problem Statement and Boundary Conditions

3.9.1 Problem Statement

The problem considered is depicted schematically in Figure 3.1 and refers to the two-dimensional flow in a vertical parallel-plate channel with length 'L', and distance between the plates 'b'. The plates are either kept at constant temperature or subjected to constant heat flux condition. The inlet and exit section of the channel are open to the ambient. The Cartesian coordinate system is chosen and the origin is shown in Figure.

The present study considers steady-state, turbulent, incompressible, two-dimensional natural convection flow of air in the vertical parallel-plate channel. All the thermophysical properties are assumed to be constants, except for the density in the buoyancy force term which can be adequately modeled by Boussinesq approximation (Jaluria, 1980). The compression work, viscous dissipation and radiative transport are all neglected. The particular form of the general transport equations which govern the process of natural convection are presented in equation (3.2-3.5).

3.9.2 Boundary Conditions

On each of the computational domain boundaries, conditions are required to solve the differential equations. Generally there are four types of boundaries in this problem, namely, the inlet section, the outlet section, the solid walls and the axis of symmetry.

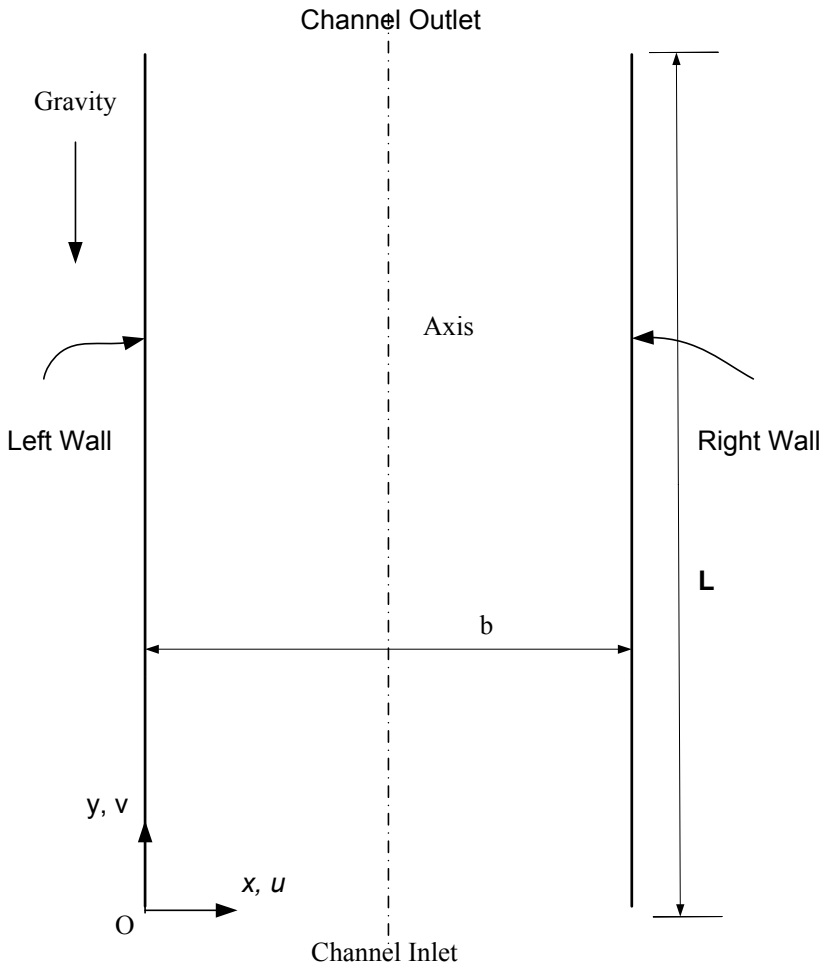

Figure 3.1: Vertical parallel-plate channel

Boundary Condition at the walls

A no slip boundary condition is imposed on the velocity components at the walls.

$$\bar{u}_i = 0 \text{, for } 0 \le y \le L \text{, } x = 0 \text{ and } x = b$$

Turbulence kinetic energy vanishes at the wall,

$$k = 0 \text{, for } 0 \le y \le L \text{, } x = 0 \text{ and } x = b$$

In this work, either uniform heat flux or uniform temperature boundary condition is imposed at the heated walls and accordingly,

$$T = specified\ temperature$$
$$or$$
$$Temperature\ gradient\ specified$$

Inlet Condition

At the inlet section of the channel, the pressure is set equal to ambient pressure and the temperature is set equal to the ambient temperature,

$$\begin{matrix} P_i = Ambient\ \ pressure \\ T_i = Ambient\ temperature \end{matrix}, \qquad \text{at } y = 0$$

Outlet Condition

At the outlet section of the channel, the pressure is set equal to ambient pressure.

$$P_o = Ambient\ \ pressure, \qquad \text{at } y = L$$

Axis of Symmetry

Here the derivative of the variables (velocity, temperature, kinetic energy and its dissipation) is set equal to zero.

$$\frac{\partial \bar{u}_i}{\partial x} = 0, \frac{\partial T}{\partial x} = 0, \frac{\partial k}{\partial x} = 0 \ and \ \frac{\partial \varepsilon}{\partial x} = 0 \qquad (3.20)$$

3.10 Heat Transfer Parameters

3.10.1 Surface Heat Transfer Coefficient

The local heat transfer from the heated wall to the air stream depends on the temperature gradient at the wall. The convective heat flux from the wall to the air stream can be expressed in terms of the local heat transfer coefficient $\left(h_y\right)$ as:

$$h_y = \frac{q_w''}{\left(T_w - T_{ref}\right)}, \text{ at } x = 0 \text{ and } x = b \tag{3.23}$$

where $q_w^{"}$ represents the wall heat flux.

3.10.2 Heat flux at the wall

In natural convection through the channel flow becomes turbulent at low Reynolds numbers. The equation to be used for calculating the wall heat flux depends on the thickness of the viscous sublayer. In case if the viscous layer thickness y^+ is less than y_T^+ ($y_T^+ = 11.63$), equation (3.21) is used. However, if $y^+ > y_T^+$, equation (3.22) is used (Versteeg and Malalasekera, 1995).

$$q_w'' = \frac{\left(T_w - T_p\right)\rho C_p C_\mu^{1/4} k_p^{1/2}}{\Pr\left[U^+ + P\right]} \qquad (y^+ > y_T^+) \tag{3.21}$$

$$q_w'' = \frac{\left(T_w - T_p\right)\rho C_p C_\mu^{1/4} k_p^{1/2}}{\Pr\, y^+} \qquad (y^+ < y_T^+) \tag{3.22}$$

where U^+ is defined in equation 3.11, P is a correction function dependent on the ratio of laminar to turbulent Prandtl number (Launder and Spalding, 1974)

3.10.3 Local Nusselt Number

For the purpose of generalizing the heat transfer results, the local Nusselt number along the heated wall is defined as

$$Nu_y = \frac{h_y\, l_{ref}}{k} \tag{3.24}$$

Hear l_{ref} = b (width of the channel).

Chapter 4

Numerical Solution

4.1 Introduction

Numerical methods are useful for solving fluid dynamics, heat and mass transfer problems and other partial-differential equations of mathematical physics when these cannot be handled by exact analysis due to nonlinearities, complex geometries and complicated boundary conditions. The development of high-speed computers significantly enhanced the use of numerical methods in various branches of science and engineering. Many complicated problems can now be solved at very little cost and in a very short time with the available computing power.

A numerical solution of a differential equation consists of a set of numbers from which the distribution of the dependent variable, ϕ, can be constructed. A numerical method treats as its basic unknowns the values of the dependent variable at a finite number of locations called the grid points in the computational domain. The method includes the tasks of formulating algebraic equation for these unknowns and prescribing an algorithm for solving these equations. These numerical methods can be categorized into:

1. Finite-difference method.
2. Finite-element method.
3. Finite-volume method.

4. Boundary-element method.

There are many distinct streams of numerical solution techniques. The main difference between the streams is associated with the way in which the flow variables are approximated and with the discretization processes.

4.2 Discretization

The discretization process is essentially an exercise of engineering judgment. The number, shape, size and configuration of the discrete volumes (control volumes) must be in such a way that the original body is simulated as close as possible. The general objective of such a discretization is to divide the body into finite control volumes sufficiently small so that the simple models can adequately approximate the true solution. At the same time, one must remember that too fine a subdivision leads to extra computational effort.

For a given differential equation, the discretization equations can be derived in many ways as follows:

4.2.1 Taylor Series Formulation

The usual procedure for deriving finite-difference equations consists of approximating the derivatives in the differential equations via a truncated Taylor series. This is explained in detail by Lapidus and Pinder (1982).

4.2.2 Variational Formulation

The discritization equation in this method is based on the calculus of variations. The calculus of variations shows that solving certain differential equations is equivalent to minimizing a related quantity called the functional. This equivalence is known as a variational principle. If the function is minimized with respect to the grid point values of the dependent variable, the resulting conditions give the required discretization equations. This method is discussed by Desal and Abel (2000).

4.2.3 Method of Weighted Residuals

A powerful method for solving differential equations is the method of weighted residuals described in detail by Finalayson (1972).

4.2.4 Finite Volume Formulation

This discretization technique is used in the present numerical calculations. In this discretization technique, the solution domain is divided into a number of nonoverlapping control volumes such that there is one control volume surrounding each grid point. The differential equation is integrated over each control volume to yield the discretization equation. Thus, the discretization equation represents the same conservation principle over a finite region as the differential equation over an infinitesimal region. This direct interpretation of the discretization equation makes the method easy to understand in physical terms; the coefficients in the equation can be identified, even when they appear in a computer program, as familiar quantities such as flow rate, conductance, areas, volumes, diffusivities, etc. The control volume approach can be regarded as a special case of the method weighted residuals Patankar (1980) in which the weighted function is

chosen to be unity over a control volume and zero everywhere else. Although the main reasons for choosing the control volume formulation are its simplicity and easy physical interpretation, the formulation has also been shown, for a limited set of test problems, to be more accurate than the Galerkin method Patankar (1980) which is a more popular weighted residual technique.

4.3 Discretization of the Governing Transport Equations

Discretization of the governing equations can be illustrated most easily by considering the steady-state conservation equation for transport of a scalar quantity ϕ. This is demonstrated by the following equation written in integral form for an arbitrary control volume V as follows

$$\oint \rho \phi v \cdot dA = \oint \Gamma_\phi \nabla \phi \cdot dA + \int_V S_\phi dV \tag{4.1}$$

where ρ is the density, v is the velocity vector ($u\,\hat{i} + v\,\hat{j}$), A is the surface area vector, Γ_ϕ is the diffusion coefficient for ϕ, S_ϕ is the source of ϕ per unit volume and $\nabla\phi$ is given by

$$\nabla \phi = \left(\partial\phi / \partial x \right) \hat{i} + \left(\partial\phi / \partial y \right) \hat{j} \tag{4.2}$$

The above equation is applied to each control volume or cell in the computation domain. The two-dimensional cell shown in the Figure 4.1 is an example of such a control volume. Discretization of the above equation (4.1) for a steady state convection-diffusion equation for the transport of general property ϕ is given by

$$\nabla \cdot \left(\rho u \phi \right) = \nabla \cdot \left(\Gamma \; grad \; \phi \right) + S_\phi \tag{4.3}$$

The integration over a control volume gives

$$\int_{CA} n \cdot (\rho \phi u) dA = \int_{CA} n \cdot (\Gamma \; grad \; \phi) dA + \int_{CV} S_\phi dV \tag{4.4}$$

This equation represents the flux balance in a control volume. The principal problem in the discretisation of the convection terms is the calculation of the value of transported property ϕ at the control volume faces and its convective flux across these boundaries.

Applying the divergence theorem to the above equation, we get

$$\frac{\partial}{\partial x}(\rho u \phi) + \frac{\partial}{\partial y}(\rho v \phi) = \frac{\partial}{\partial x}\left(\Gamma \frac{\partial \phi}{\partial x}\right) + \frac{\partial}{\partial y}\left(\Gamma \frac{\partial \phi}{\partial y}\right) + S \tag{4.5}$$

A portion of the two dimensional grid used for the discretisation is shown Figure 4.1

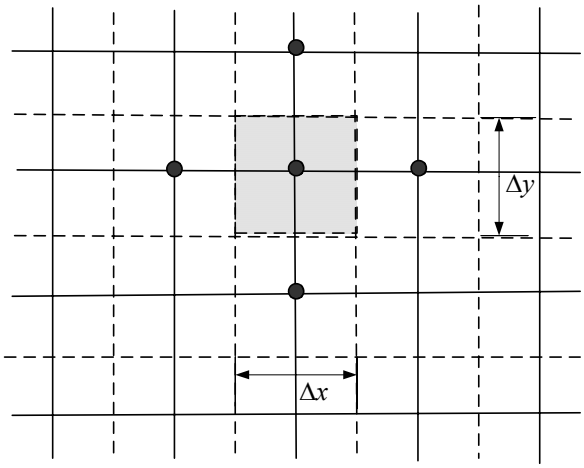

Figure 4.1: A part of the two-dimensional control volume grid.

4.3.1 Domain Discretization

The first step in the finite volume method is to divide the domain into discrete control volumes. The boundary of control volumes are positioned mid way between adjacent nodes. Thus, each node is surrounded by a control volume or cell. It is common practice to set up control volumes near the edge of the domain in such a way that the physical boundaries coincide with the control volume boundaries.

A general nodal point is identified by 'P' and its neighbors in two-dimensional geometry. The nodes of the west and east are identified by 'W' and 'E' and the nodes of the north and south by 'N' and 'S' respectively. The west side face of the control volume is referred to by 'w' and other corresponding faces on east, north and south of the control volume by 'e', 'n', 's' respectively. The distance between the nodes W and P is identified by δx_{WP} and between face w and P by δx_{wP}. Similarly, the other distances are computed. The widths of the control volume is given by $\Delta x = \delta x_{we}$ and $\Delta y = \delta y_{ns}$.

The key step of the finite volume method is the integration of the governing equation (or equations) over a control volume to yield a discretized equation at its nodal point P. For the above defined control volume this integration gives,

$$\int_{\Delta V} \frac{\partial}{\partial x}(\rho u \phi) dx.dy + \int_{\Delta V} \frac{\partial}{\partial y}(\rho v \phi) dx.dy = \int_{\Delta V} \frac{\partial}{\partial x}\left(\Gamma \frac{\partial \phi}{\partial x}\right) dx.dy + \int_{\Delta V} \frac{\partial}{\partial y}\left(\Gamma \frac{\partial \phi}{\partial y}\right) dx.dy + \int_{\Delta V} S_{\phi} dV \tag{4.6}$$

So, noting that $A_e=A_w=\Delta y$ and $A_n=A_s=\Delta x$, we obtain

$$\left[(\rho uA\phi)_e-(\rho uA\phi)_w\right]+\left[(\rho vA\phi)_n-(\rho vA\phi)_s\right]=\left[\left(\Gamma A\frac{\partial\phi}{\partial x}\right)_e-\left(\Gamma A\frac{\partial\phi}{\partial x}\right)_w\right]+\left[\left(\Gamma A\frac{\partial\phi}{\partial x}\right)_n-\left(\Gamma A\frac{\partial\phi}{\partial x}\right)_s\right]+\overline{S}\Delta V \tag{4.7}$$

The flow must also satisfy continuity and accordingly,

$$\frac{\partial(\rho u)}{\partial x}+\frac{\partial(\rho v)}{\partial y}=0 \tag{4.8}$$

and its integration over the control volume gives

$$\left[(\rho uA)_e-(\rho uA)_w\right]+\left[(\rho vA)_n-(\rho vA)_s\right]=0 \tag{4.9}$$

The nonlinearity of the source term can be removed by representing it in a linear form.

$$\overline{S}\Delta V=S_u+S_p\phi_P \tag{4.10}$$

Using linear central differencing approximation we can write expressions for the flux through the control volume faces as:

$$\text{Flux across the west face}=\Gamma_w A_w\left.\frac{\partial\phi}{\partial x}\right|_w=\Gamma_w A_w\frac{(\phi_P-\phi_W)}{\delta x_{WP}} \tag{4.11}$$

Similar expressions can be written for flux through other faces.

To obtain discretized equations for the convection / diffusion problem we must approximate the terms in above equation 4.7. It is convenient to define two variables F

and D to represent the convective mass flux per unit area and diffusion conductance at cell faces: $F = \rho u$ and $D = \frac{\Gamma}{\delta x}$.

The cell face values of the variables F, D and P_e can be written as

$$F_w = (\rho u)_w,\ D_w = \frac{\Gamma_w}{\delta\, x_{WP}} \text{.and } P_W = \frac{F_W}{D_W} \tag{4.12}$$

For the convective terms for a uniform grid, we can write the cell face values of property ϕ as $\phi_e = \phi_P - \phi_E / 2$ and similarly for other face values.

The general discretized equation form for interior nodes reduces to

$$a_P \phi_P = a_W \phi_W + a_E \phi_E + a_N \phi_N + a_S \phi_S + S_u \tag{4.13}$$

and from conservation equation we have $(F_E - F_W) + (F_N - F_S) = 0$

where $a_W = D_W A(|P_W|) + |\,|F_W, 0|\,|$

$a_E = D_E A(|P_E|) + |\,|-F_E, 0|\,|$

$a_S = D_S A(|P_S|) + |\,|F_S, 0|\,|$

$a_N = D_N A(|P_N|) + \lceil |-F_N, 0| \rceil$

and $a_P = a_W + a_E + a_S + a_N - S_P A$

The value of $A(|P|)$ for the upwind scheme is 1.0 Patankar (1980).

In the present work, the first and second order upwind schemes have been used.

4.3.2 First-Order Upwind Scheme

In the first-order upwind scheme, quantities at cell faces are determined by assuming that the cell-center values of any field variable represent a cell-average value and hold throughout the entire cell; the face quantities are identical to the cell quantities. Thus in first-order upwinding, the face value ϕ_f is set equal to the cell-center value of ϕ in the upstream cell.

4.3.3 Second-Order Upwind Scheme

In second-order upwind scheme, quantities at cell faces are computed using a multidimensional linear reconstruction approach Barth and Jespersen (1989). In this approach, higher-order accuracy is achieved at cell faces through a Taylor series expansion of the cell-centered solution about the cell centroid. Thus, when second-order upwinding is selected, the face value ϕ_f is computed using the following expression:

$$\phi_f = \phi + \nabla\phi \cdot \Delta s \tag{4.14}$$

where ϕ and $\nabla\phi$ are the cell-centered value and its gradient in the upstream cell, and Δs is the displacement vector from the upstream cell centroid to the face centroid. This formulation requires the determination of the gradient $\nabla\phi$ in each cell. This is computed using the divergence theorem, which in discrete form can be written as

$$\nabla\phi = \frac{1}{V}\sum_{f}^{N_{faces}} \tilde{\phi}_f A \tag{4.15}$$

Here the face values $\widetilde{\phi}_f$ are computed by averaging ϕ from the two cells adjacent to the face. Finally, the gradient $\nabla\phi$ is limited so that no new maxima or minima are introduced.

4.4 Solution Procedure

4.4.1 Grid Generation

A non-uniform grid arrangement is used for numerical simulation of natural convection heat transfer and fluid flow in vertical parallel plate channel and is shown in Figure 4.2. A finer grid is constructed near the wall because of the large velocity and temperature gradients in that region.

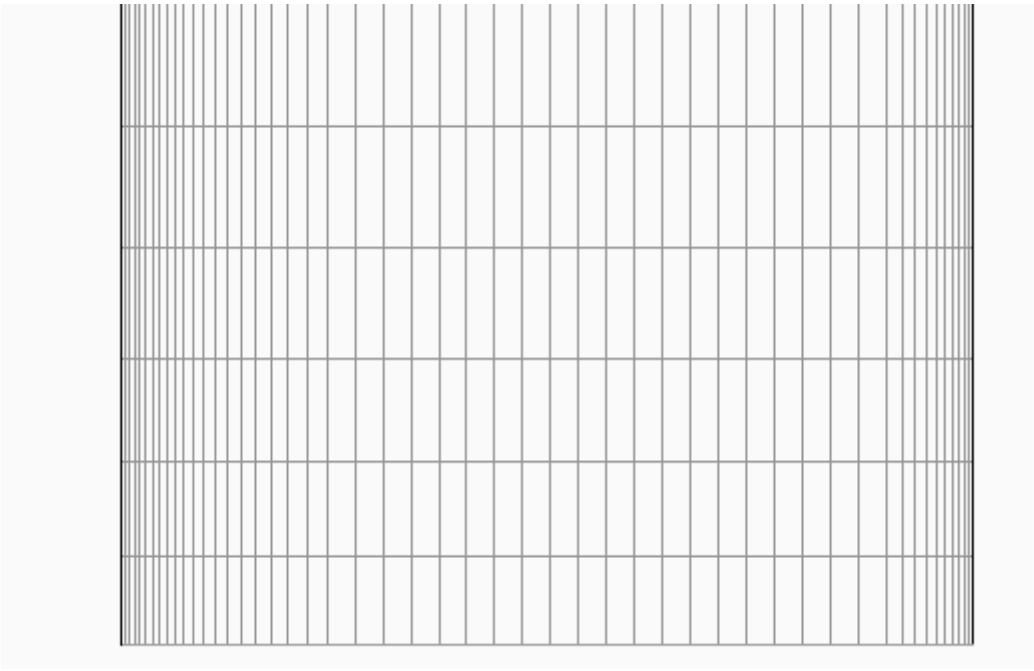

Figure 4.2: Finite Volume mesh in the channel with boundary-layer flow regions at both walls.

4.4.2 Solution Algorithms for Pressure-Velocity Coupling

If the pressure field, which appears as a major part of the source term, is unknown then equation (4.13) applied at all the nodal points yields a set of algebraic equations but the resulting velocity field may not satisfy the continuity equation. The problems of determining the pressure and satisfying continuity are overcome by adjusting the pressure field using pressure-velocity coupling. In the present study the SIMPLE algorithm Patankar and Spalding (1972) is used for the pressure-velocity coupling. The acronym SIMPLE stands for Semi-Implicit Method for Pressure-Linked Equations. In this algorithm, the pressure field p^* is first assumed. The discretized momentum equations are then solved using the assumed pressure field to yield velocity components u^* and v^*. Now the correction, p', defined as the difference between the correct pressure field p and the assumed pressure field p^*, is calculated and a better approximation of the pressure field can be obtained using $p = p^* + p'$. Similarly, the velocity components are corrected by adding the increments u' and v' to the assumed velocity components u^* and v^*. The whole process of the SIMPLE algorithm is explained in the flow diagram given in Figure 4.3.

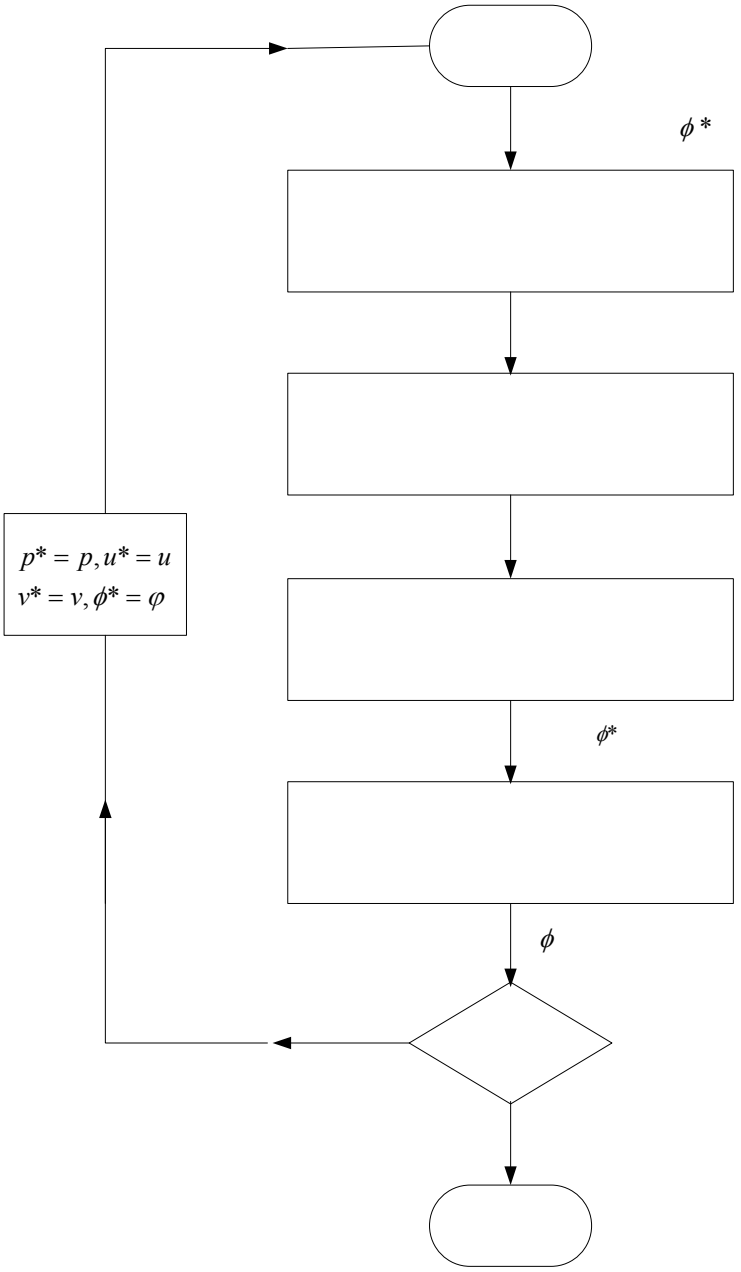

Figure 4.3: The SIMPLE Algorithm

4.4.3 The Calculation Procedure

In this procedure, the governing equations are solved sequentially (i.e., segregated from one another). Since the equations are non-linear (and coupled), several iterations of the solution loop must be performed before a converged solution is obtained. Each iteration consists of the steps illustrated in Figure 4.4 and is outlined below:

1. Fluid properties are updated, based on the current values of pressure and temperature. (If the calculation has just begun the fluid properties will be updated based on the initial values).
2. The *u* and *v* momentum equations are solved in turn using current values for pressure and face mass fluxes in order to update the velocity field.
3. Since the velocities obtained in Step 2 may not satisfy the continuity equation, a "Poisson-type" equation for the pressure correction is used. This satisfies the continuity equation (SIMPLE Algorithm) and the linearized momentum equations. The pressure correction equation is solved and resulting pressure and velocity fields are obtained.
4. Equations for scalars such as energy, turbulence kinetic energy and its dissipation rate are solved using the previously updated values of these variables.
5. A check for convergence of the equation set is made.

These steps are continued until the convergence criteria are met.

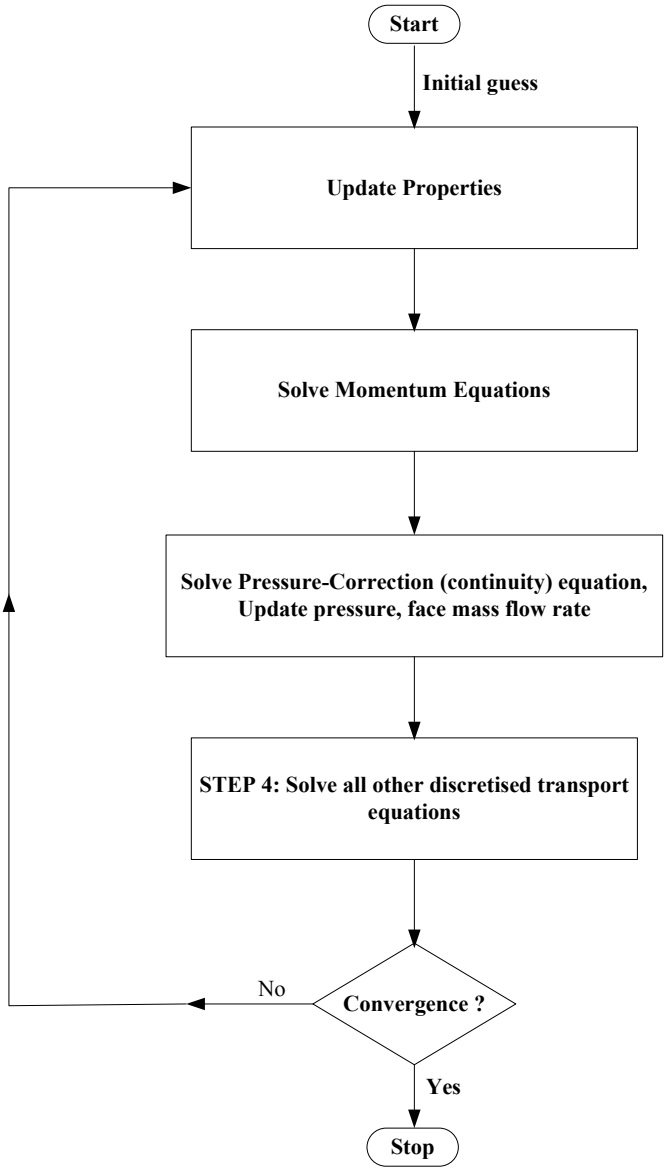

Figure 4.4: Overall view of solution Algorithm

4.4.4 Convergence Criterion

The use of an iterative solution method necessitates the definition of a convergence and stopping criteria to terminate the iteration process. The measure of convergence is a norm on the change in the solution vector between successive iterations. The iterative algorithm is terminated after a fixed number of iterations if the convergence has not been achieved. This criteria is used to prevent slowly convergent or divergent problems from wasting computation time. Convergence in this present study is defined to have been obtained after all the following criteria are achieved.

Changes in the x - and y - velocity component are less than	$1x10^{-6}$
Changes in the energy is less than	$1x10^{-6}$
Change in the turbulence kinetic energy is less than	$1x10^{-6}$
Change in the turbulence dissipation rate is less than	$1x10^{-6}$

Chapter 5

Results and Discussions

The heat transfer and fluid flow characteristics of natural convection in a Vertical Parallel-plate channel are studied for both laminar and turbulent regimes. A non-uniform grid with high refinement near the walls is used to increase the accuracy of the computational result in the proximity of walls. The details of the flow and thermal fields are obtained from the solution of the conservation equation of mass, momentum and energy in addition to equation of the low Reynolds number turbulence model. In this study different turbulence models are analyzed to simulate the complex flow structure of natural convection heat transfer through vertical parallel plates.

5.1 Validation of the Computational Scheme

For the validation of the present computational method, the computational results of some selected cases were compared with the experimental results of Wirtz and Haag (1985), La Pica *et al.* (1993) and Miyamoto *et al.* (1986) and the numerical results of Naylor *et al.* (1991), Fedorov and Viskanta (1997). The above selected cases cover both laminar and turbulent regimes and the details are as follows:

a) Laminar flow in a vertical parallel-plate channel with symmetrically heated isothermal surfaces, with Ra = 74.64, channel aspect ratio L/b = 26.25, Pr = 0.707. The experimental results were reported by Wirtz and Haag (1985).

b) Laminar flow in a vertical parallel-plate channel with symmetrically heated isothermal surfaces with Ra = 74.64, channel aspect ratio, L/b = 24, Pr = 0.707. The numerical results were reported by Naylor *et al.* (1991).

c) Laminar flow in vertical parallel-plate channel with symmetrically heated isothermal surfaces with Ra = 7000, channel aspect ratio, L/b = 24, Pr = 0.707. The numerical results were reported by Naylor *et al.* (1991).

d) Turbulent flow in vertical parallel-plate channel with asymmetrically heat isoflux surfaces with channel aspect ratio, L/b = 20.83 and heat flux range 144 to 240 W/m^2. The experimental results were reported by La Pica *et al.* (1993).

e) Turbulent flow in vertical parallel-plate channel with asymmetrically heat isoflux surfaces with channel aspect ratio, L/b = 50 and surface heat flux 104 and 208 W/m^2. The experimental results were reported by Miyamoto *et al.* (1986).

f) Turbulent flow in vertical parallel-plate channels with asymmetrically heat isothermal surfaces for a range of Rayleigh number 10^4 to 10^6. The numerical results were reported by Fedorov and Viskanta (1997).

g) Turbulent flow in vertical parallel-plate channels with asymmetrically heat isothermal surfaces with one surface heat 10^OC above ambient and other surface 10^OC below ambient for a channel aspect ratio, L/b = 3.125. The experimental results were reported by Habib *et al.* (2002).

5.1.1 Comparison of Laminar flows

Comparison of present calculation with the experimental local Nusselt number distribution measured in air by Wirtz and Haag (1985) and the numerical results by Naylor *et al.* (1991) is shown in Figure 5.1. Present calculations of the local Nusselt

number are closer to the experimental values than the numerical values obtained by Naylor *et al.* (1991). The experiments by Wirtz and Haag (1985) were performed in air as the working medium with channel aspect ratio, L/b = 26.25, and Rayleigh number of 74.64. The numerical study by Naylor *et al.* (1991) was done with the channel aspect ratio, L/b = 24, and Ra = 74.64. To verify the accuracy of the present numerical code, the present calculations are carried out for a channel with aspect ratio, L/b = 24 and Ra = 74.64. As can be seen in Figure 5.1, the results of the present study show a better agreement with the experimental results of Wirtz and Haag (1985) than the numerical results of Naylor *et al.* (1991). The difference with the experimental results might be due to the difference in the channel aspect ratio.

Figure 5.2 shows a comparison between the obtained average Nusselt number and that reported by Naylor *et al.* (1991) for Rayleigh number ranging from 1 to 1000 (laminar regime). The present results are about 20% higher that those predicted by Naylor *et al.* (1991) and that makes our results closer to the experimental measurements carried out by Wirtz and Haag (1985) as indicated in Figure 5.1.

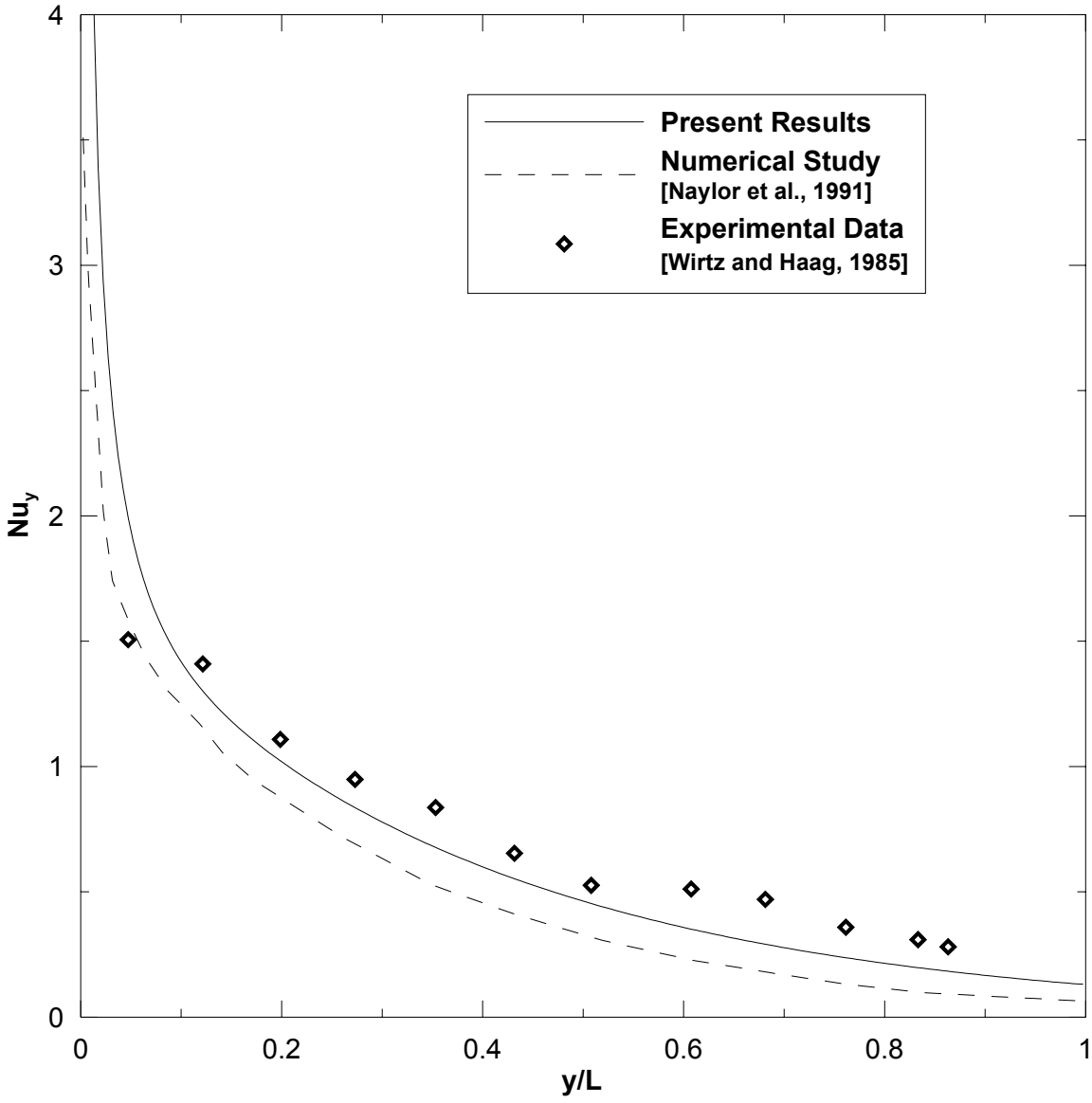

Figure 5.1: Comparison of local Nusselt number with previous laminar flow experimental and numerical data for L/b = 24, Ra = 74.64. (Nusselt number based on half channel width)

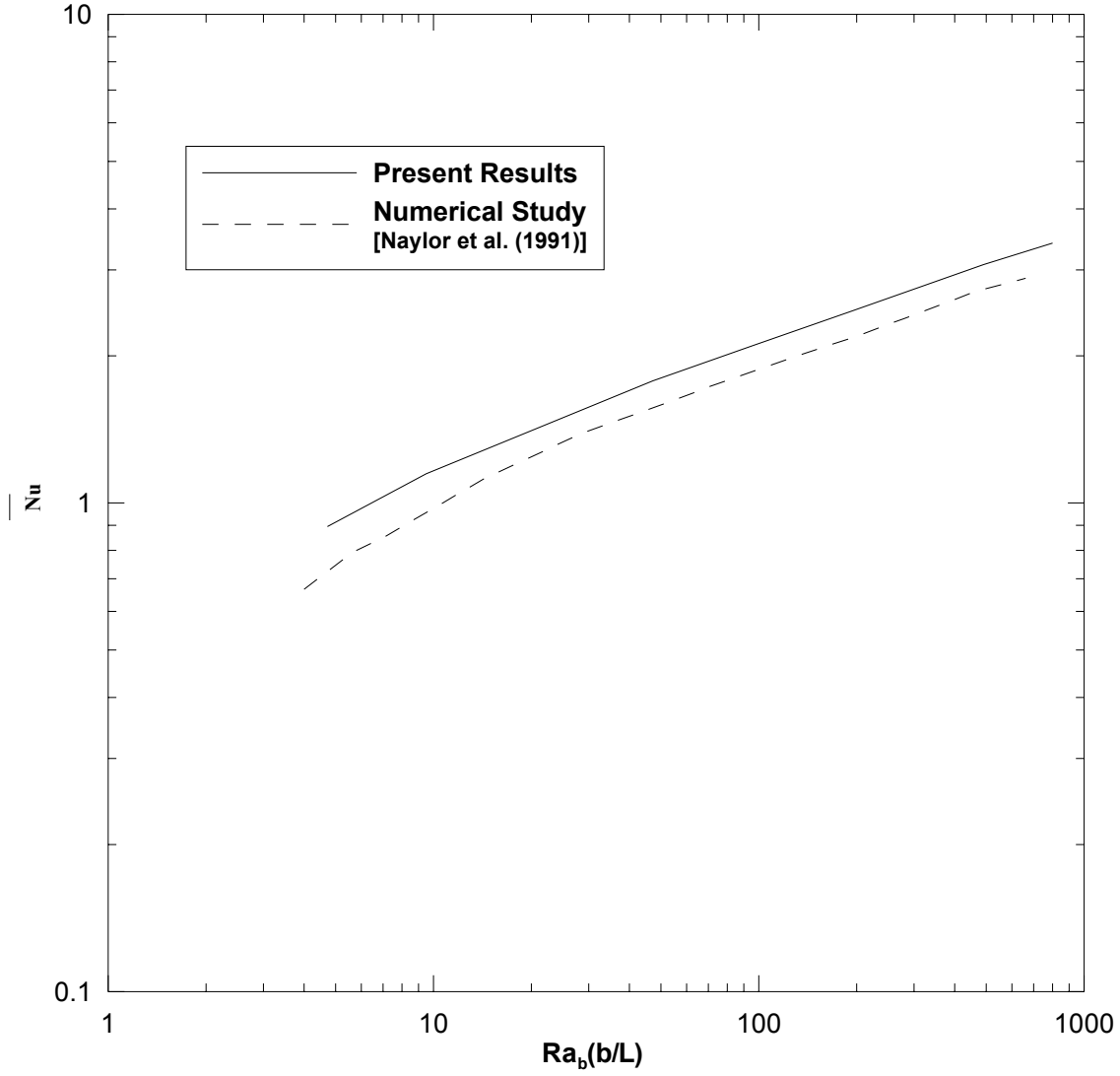

Figure 5.2: Comparison of average Nusselt number for laminar natural convection flow in vertical parallel plate channel

5.1.2 Comparison of Turbulent flows

The second comparison was carried out for the case of turbulent natural convection in a parallel-plate channel of aspect ratio, L/b = 20.8 for modified Rayleigh numbers ranging from $3x10^6$ to $7x10^6$. The obtained results are compared with the experimental findings of La Pica *et al.* (1993) and the numerical results reported by Fedorov and Viskanta (1997). The present calculations were carried out using the low Reynolds number $k-\varepsilon$ M3 model. Figure 5.3 shows the calculated average Nusselt number as function of modified Rayleigh number (Rayleigh number based on channel width multiplied by the inverse of channel aspect ratio). The figure also shows the experimental data of La Pica *et al.* (1993). It is clear from the figure that the difference between $\overline{Nu}$ obtained using the Low Re $k-\varepsilon$ M3 model and the experimental values reported by La Pica *et al.* (1993) is very small up to $Ra_b(b/L) = 5x10^6$. However, that difference increased as the modified Rayleigh number increased to $6x10^6$. The maximum difference of $\overline{Nu}$ in the entire range of the modified Rayleigh number did not exceed 7%.

Figure 5.4 shows a comparison of average Nusselt number with the numerical work by Fedorov and Viskanta (1997). The Nusselt number was based on double the channel width. The average Nusselt number predicted in present calculation is higher then the numerical results by Fedorov and Viskanta (1997). It is worth mentioning that Fedorov and Viskanta (1997) results were not validated against any experimental data. Since the present calculations are close to experimental data as shown in Figure 5.3, it can be concluded that the present prediction will be close to experimental values.

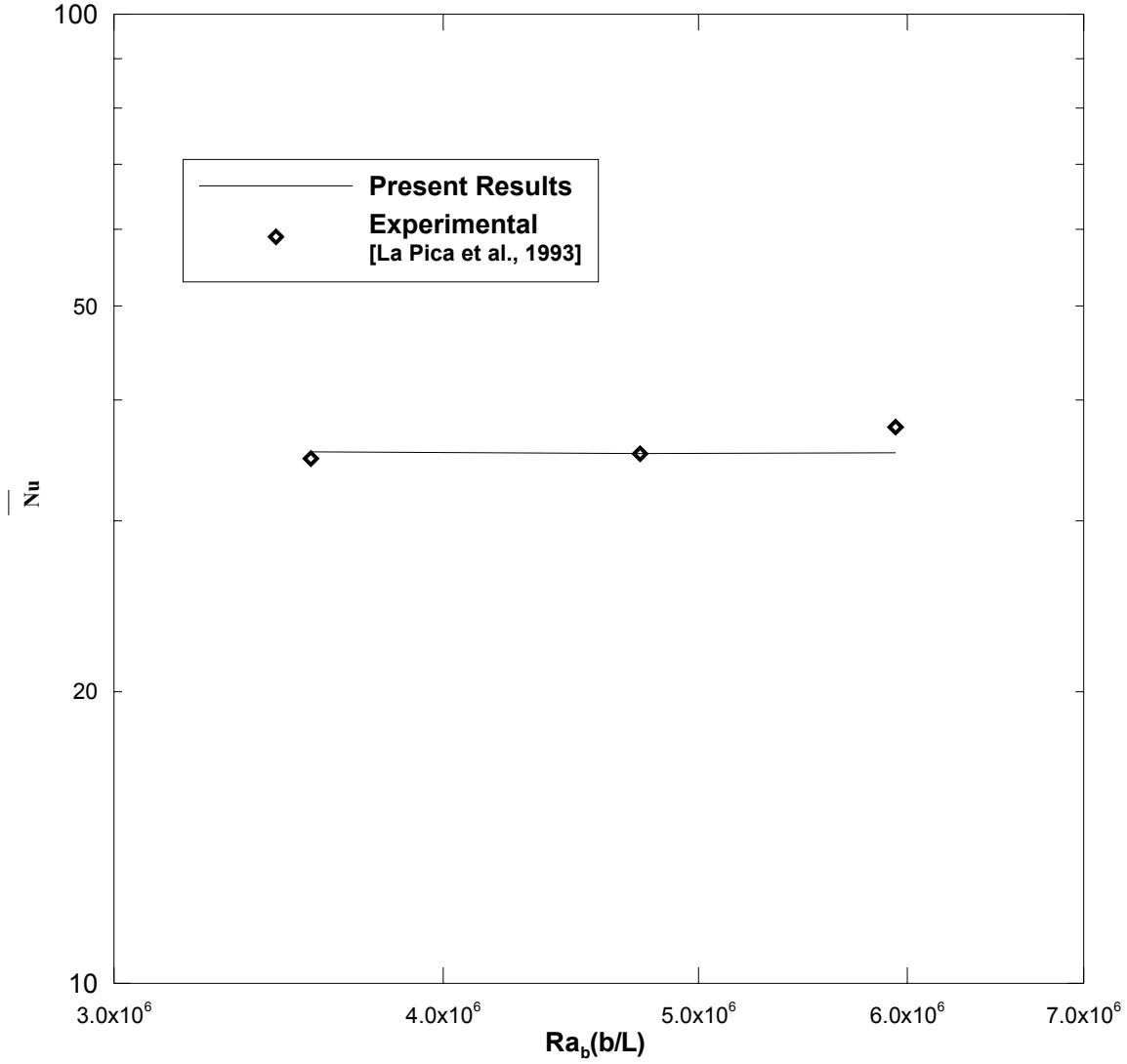

Figure 5.3: Comparison of average Nusselt number obtained by present selected turbulence model with experimental data of La pica *et al.* (1993) for a channel aspect L/b = 20.8.

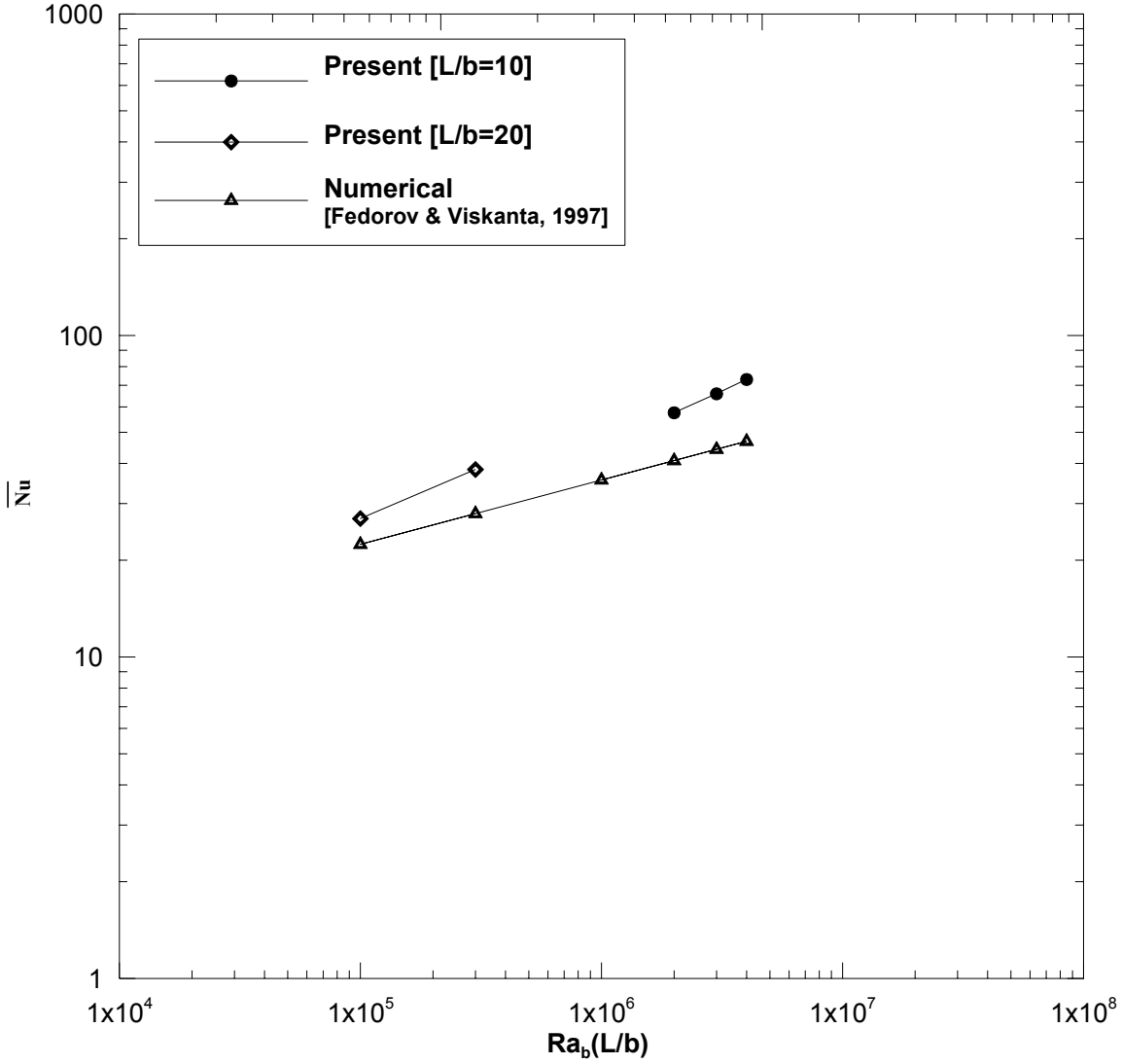

Figure 5.4: Comparison of average Nusselt number with numerical work by Fedorov and Viskanta (1997) with Nusselt number based on double the channel width.

5.1.3 Grid Independence Test

A grid independence test was carried out to make sure that the grid size does not affect the computational results. Computations were carried out using four different grid sizes: 25 x 100, 50 x 100, 50 x 200 and 100 x 300 grid points. Figure 5.5 shows the vertical velocity profile at the height y = 3865 mm from the channel inlet section in vertical parallel plate channel for all different grid sizes. As can be seen that the difference in results obtained using 50 x 100, 50 x 200 and 100 x 300 grid size is very small. Therefore in this study a grid size of 50 x 200 is used in order to utilize the computation time efficiently without compromising the accuracy of results.

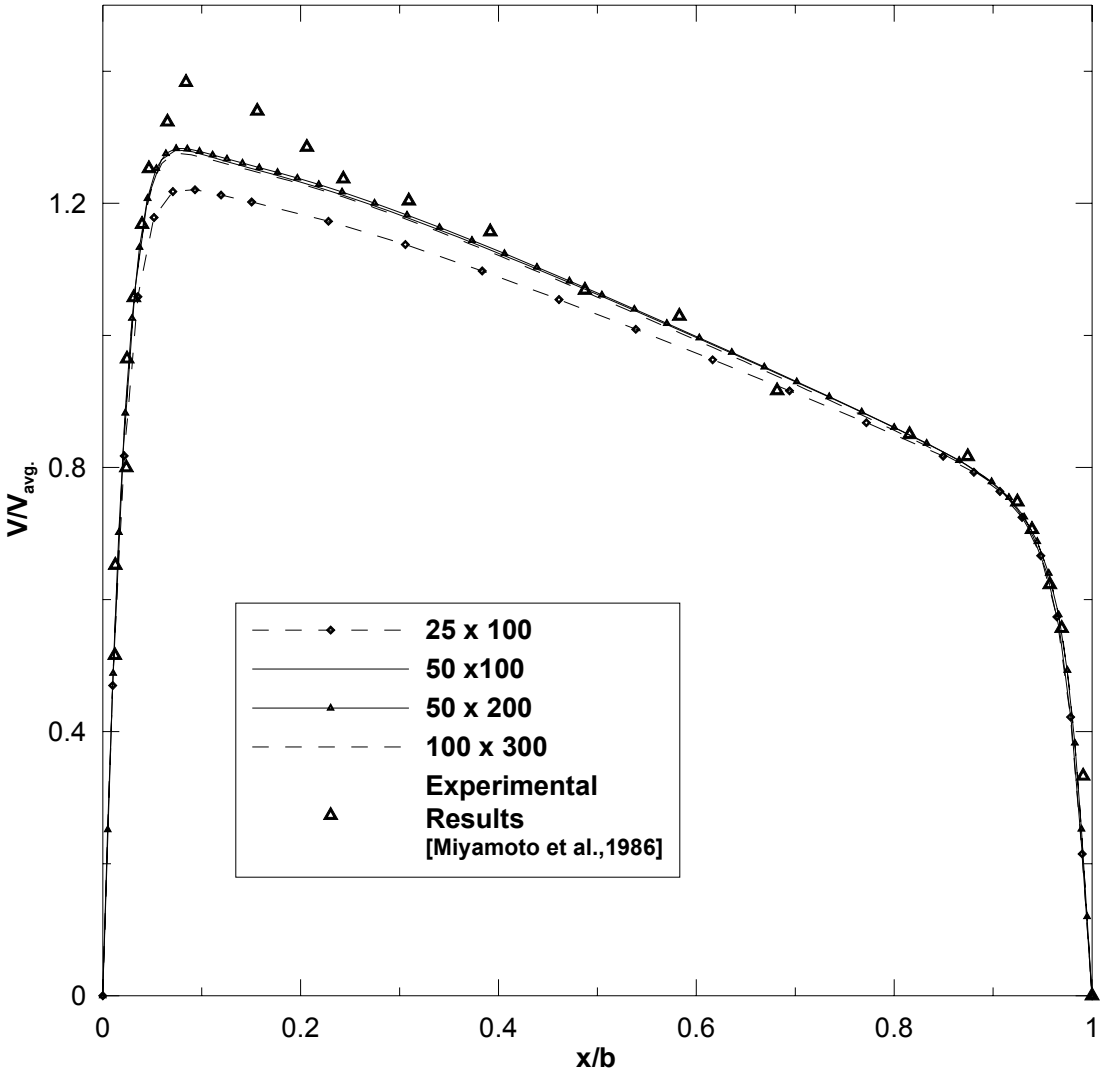

Figure 5.5: Vertical velocity distribution at the section y/L = 0.77 in the vertical parallel-plate channel for q_w" = 208 W/m^2 and b = 0.1m.

5.2 Comparison of different Turbulence Models

In this study, six different turbulence models have been studied to predict the low Reynolds number turbulence which occurs in natural convection problem. To validate the exact turbulence model, velocity and temperature profiles at three different sections of the vertical parallel-plate channel are compared with existing work reported in the literature by Miyamoto *et al.* (1986) and Habib *et al.* (2002).

5.2.1 Comparison with Miyamoto *et al.* (1986)

5.2.1.1. Description of the experiment

Experimental data has been reported by Miyamoto *et al.* (1986) on turbulent natural convection flow and heat transfer in an asymmetrically heated vertical channel. The channel was formed by two vertical parallel plates. One plate was heated by imposing a uniform heat flux along the plate and the opposite plate was adiabatic. The two plates were 4980 mm height and 950 mm width. The channel was open at both bottom and top and was installed in a laboratory room of height 6107 mm. Experiments were performed with channel widths of 50, 100 and 200 mm, and local velocity and temperature profile at three different sections of channel were reported along with the local heat transfer coefficients and temperature distribution on the heated wall. The experimental data reported is used to check the validity and appropriateness of the turbulent, two-dimensional flow and heat transfer model.

5.2.1.2. Comparison with Uniform Inlet Pressure

Natural convection flow through the vertical parallel-plate channel becomes turbulent at high Rayleigh number ($Ra > 10^5$). Turbulence starts in the thin boundary-

layer along the heated walls of the channel. The velocity and temperature gradients within this thin boundary-layer are very large and require the use of many computational grid points in the proximity of the wall. Because of buoyant fluid motion arising from heat transfer through the vertical walls, the greatest effect of buoyancy occurs very close to the wall where viscous effects are appreciable. This renders inapplicable the use of local-equilibrium logarithmic velocity and temperature profiles that are normally used to simplify the calculation of near-wall flows. Therefore, using the Standard $k-\varepsilon$ model with wall functions does not give an accurate solution in that region. This drawback was also reported in literature by To and Humphrey (1985), Ince and Launder (1989), Tsuji and Nagano (1987) and many others. Hence the Standard $k-\varepsilon$ model was modified and named as low Reynolds number $k-\varepsilon$ model by To and Humphrey (1985) and many others. In the present study, Reynolds stress model (RSM) and its modification for low Reynolds number turbulence near the wall have been also studied. In addition, Renormalization Group Analysis of Turbulence (RNG) model is used and the results are compared with the experimental results of Miyamoto *et al.* (1986) in order to choose the one that will exhibit a good agreement. Figure 5.6 shows the vertical computational domain with ambient pressure and temperature at the inlet section and ambient pressure at exit section of the channel. It has been named as Uniform Inlet Pressure.

Wall Temperature distribution

Figure 5.7 shows a comparison of theoretically predicted and measured (Miyamoto *et al.*, 1986) wall temperature variation along the heated vertical wall for a constant heat flux of 104 Wm^{-2} and a channel width of 0.1 m. As shown in the figure, the Standard $k-\varepsilon$ turbulence model, RNG model, RSM model and Low Re $k-\varepsilon$ M2

model predict lower temperature along the vertical wall. The modified RSM and Low Re $k-\varepsilon$ M3 turbulence model predictions are close up to a channel height of 2 m above which their predictions are slightly higher.

Vertical velocity distribution at different sections

A comparison between the predicted and measured mean (i.e. time-averaged) vertical velocity distribution at three different heights along the channel is given in Figure 5.8, 5.9 and 5.10. The chosen sections are the ones for which the velocity distributions were reported by Miyamoto *et al.* (1986).

Figure 5.8 compares the velocity profile at the channel section close to the exit (y/L = 0.77). At that section, the Low Reynolds number $k-\varepsilon$ model M3 predictions are close to the experimental values near the adiabatic wall. Near the heated wall, their predictions are exact in viscous sublayer but in the buffer layer between viscous sublayer and turbulent core region, the model is slightly below the experimental values. But these underpredictions are less than any other turbulence model except RSM turbulence model.

The RSM turbulence model does not incorporate the wall turbulence; however, the modified RSM model is used to incorporate the wall turbulence. The resulting velocity profiles are in good agreement with the experimental profiles but near the heated wall (left wall) its predictions is below that obtained by the low Re $k-\varepsilon$ M3. All other turbulence models studied seem to be underpredicting near the wall and overpredicting in the turbulent core region. Similarly, Figure 5.9 (y/L = 0.53) shows that the low Re $k-\varepsilon$ M3 and modified RSM predictions are close to experimental data.

Figure 5.10 shows the velocity profiles at section y/L = 0.16. At this section none of the turbulence models considered can predict exactly the mean vertical velocity profile as obtained by Miyamoto *et al.* (1986). This can be attributed to the laminar/turbulent transition occurring in that region But if previously discussed section (y/L = 0.77 and 0.53) are examine it can be concluded that at this section (y/L = 0.16) also low Re $k-\varepsilon$ M3 model prediction are in good agreement.

In case when the channel width is considerable, the free convection flow near each plate is expected to be similar to that of free convection from a single flat plate. In a single flat vertical heated surface, fluid at a far distance is stagnant. The fluid at the surface is also stationary due to the no-slip condition. The temperature decreases continuously from surface temperature to ambient temperature. Therefore, the maximum velocity occurs at some distance away from the vertical surface. Similarly, in a vertical channel there is a no-slip condition at both the walls and maximum velocity (or velocity hump) occurs close to the heated wall. The exact location and magnitude of $V_{\max.}$ to be determined through analysis. However, as the flow proceeds vertically, the flow gets more and more disordered and disturbed, eventually becoming turbulent. The flow region between the laminar and the turbulent flow regions is called transition region. The location and spread of which is a function of several variables such as surface temperature, the nature and magnitude of external disturbances.

Temperature distribution at different section

A comparison between the predicted and measured normalized temperature distributions in air at the same three vertical locations (y/L = 0.77, 0.53, 0.16) along the channel is shown in Figure 5.11, 5.12 and 5.13. At sections (y/L = 0.77 and y/L = 0.53)

both modified RSM model and Low Re $k-\varepsilon$ M3 model underpredict whereas all the other models overpredict. At the section near the inlet (y/L = 0.16), the low Re $k-\varepsilon$ M3 model is in close agreement with experimental values. On the other hand, the low Re $k-\varepsilon$ M2 model overpredicts at a section y/L = 0.77 near the heated wall and underpredicts near the adiabatic wall. From the velocity profiles predicted by the M2 model at all section, it is clear that all model predictions are consistently lower than the experimental values. This raises doubts about the suitability of that model. The numerical results are based on the assumption of an adiabatic right wall with no radiation, but radiation from the hotter left wall apparently heated the right wall and made it non-adiabatic. This is clearly indicated by a small rise in the experimental air temperature date in the vicinity of the right wall. However, despite these differences the measured and predicted temperature profile in air at the hot wall are in very good agreement with each other.

Local Nusselt Number along the heated wall

Distribution of local Nusselt number along the heat wall is shown in Figure 5.14 for different turbulence model. The M3 and Modified RSM predictions are lower than all other turbulence models. The standard $k-\varepsilon$ Model and RNG $k-\varepsilon$ Turbulence Model prediction are the highest. This is due to the fact that a wall function is used to calculate velocity and temperature in near wall cells in the standard $k-\varepsilon$ Model, RNG $k-\varepsilon$ Model and RSM. The first cell where calculations are performed by the model is in the turbulent core region and the values in near the wall cells are interpolated using the wall function. This approximation is valid for high Reynolds number turbulence but not for turbulent natural convection near walls. Therefore, for natural convection near vertical

surfaces a modification for this turbulence model is required to incorporate near wall turbulence. The low Re $k-\varepsilon$ M3 model has this modification because it applies a wall damping function which is of the order of the cell location (distance) from the wall as shown in equation 3.15 and 3.16. This clearly gives confidence in the M3 model for predicting flow of natural circulation in vertical parallel-plate channels.

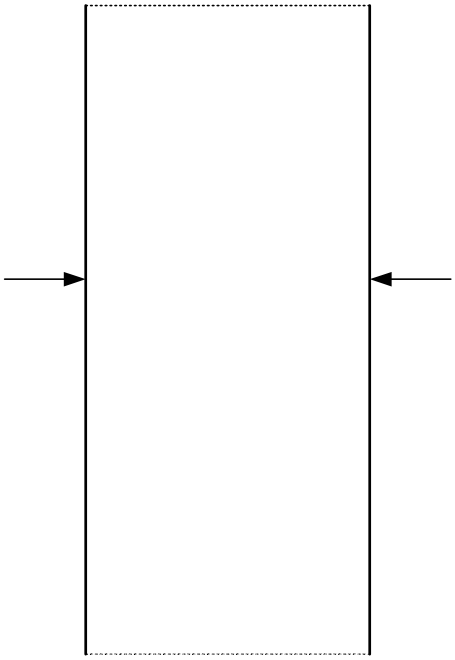

Figure 5.6: Uniform Pressure Inlet

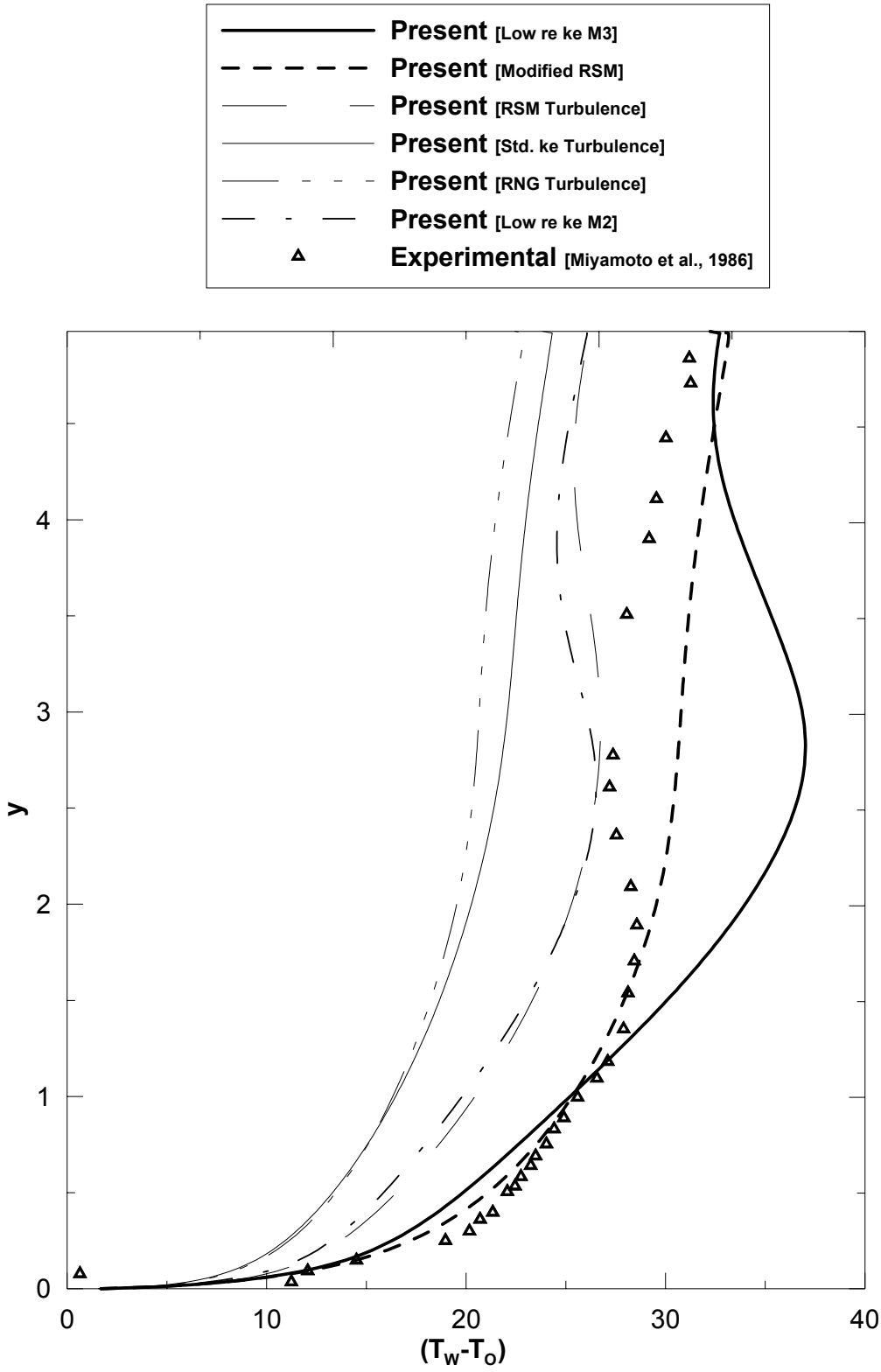

Figure 5.7: Comparison of predicted and measured wall temperature variations along a heated vertical wall for q_w" = 104Wm^{-2} and b = 0.1m.

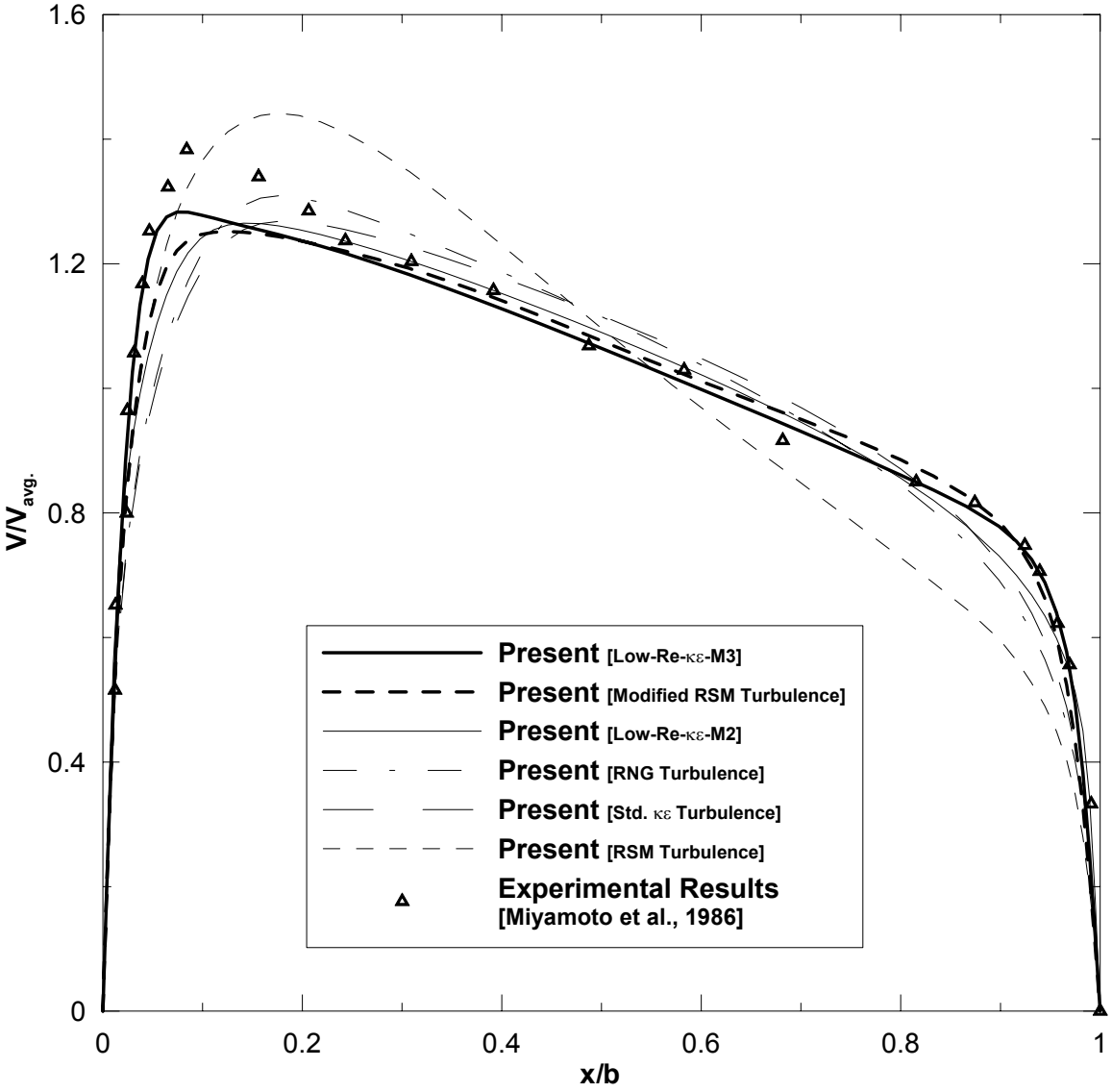

Figure 5.8: Normalized vertical velocity at section y/L = 0.77 from the channel inlet for Uniform pressure inlet condition with q_w" = 208 Wm^{-2}, b=0.1m and L/b=50.

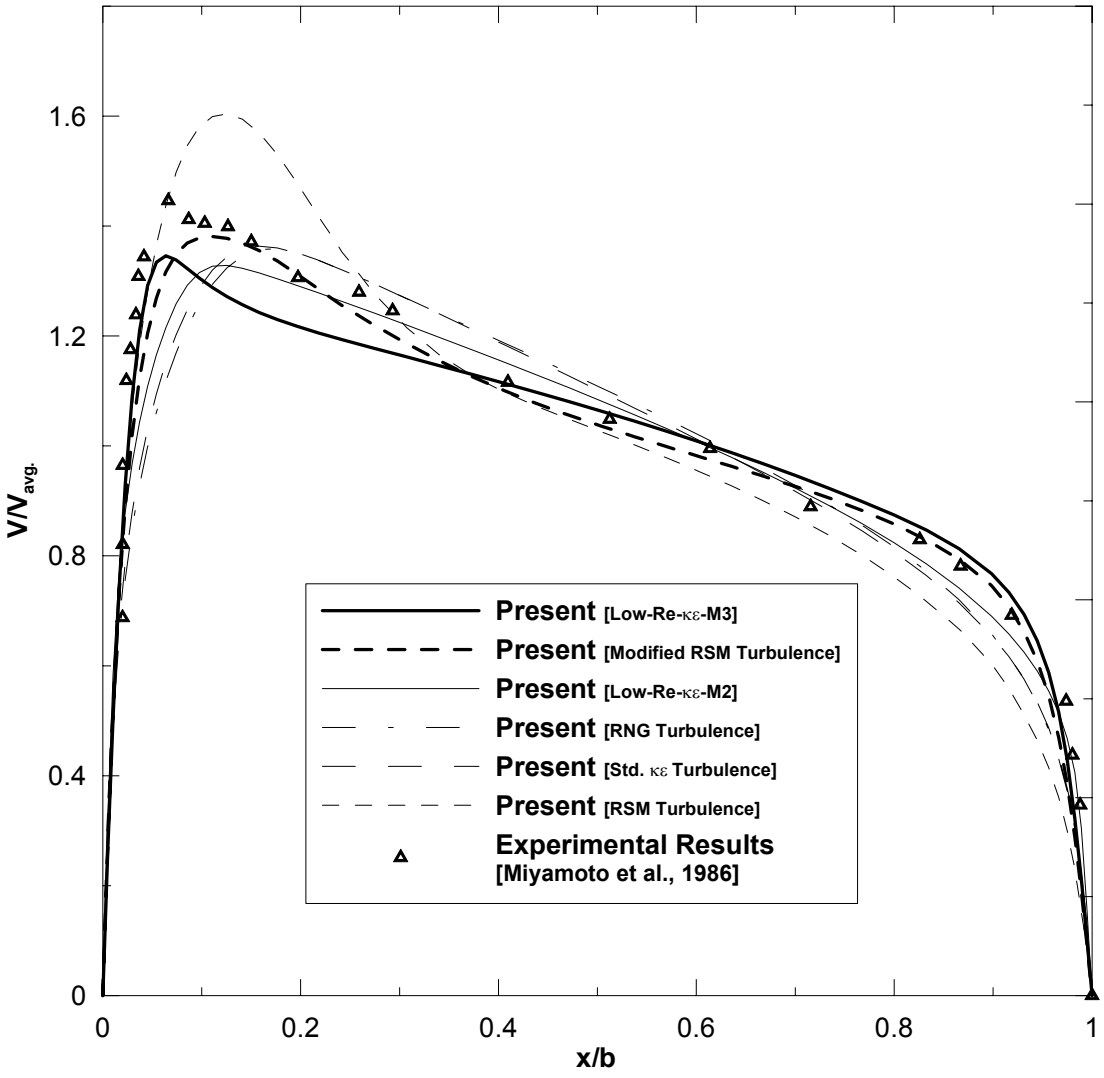

Figure 5.9: Normalized vertical velocity at section y/L = 0.53 from the channel inlet for uniform pressure inlet with q_w"= 208 Wm^{-2}, b= 0.1m and L/b=50.

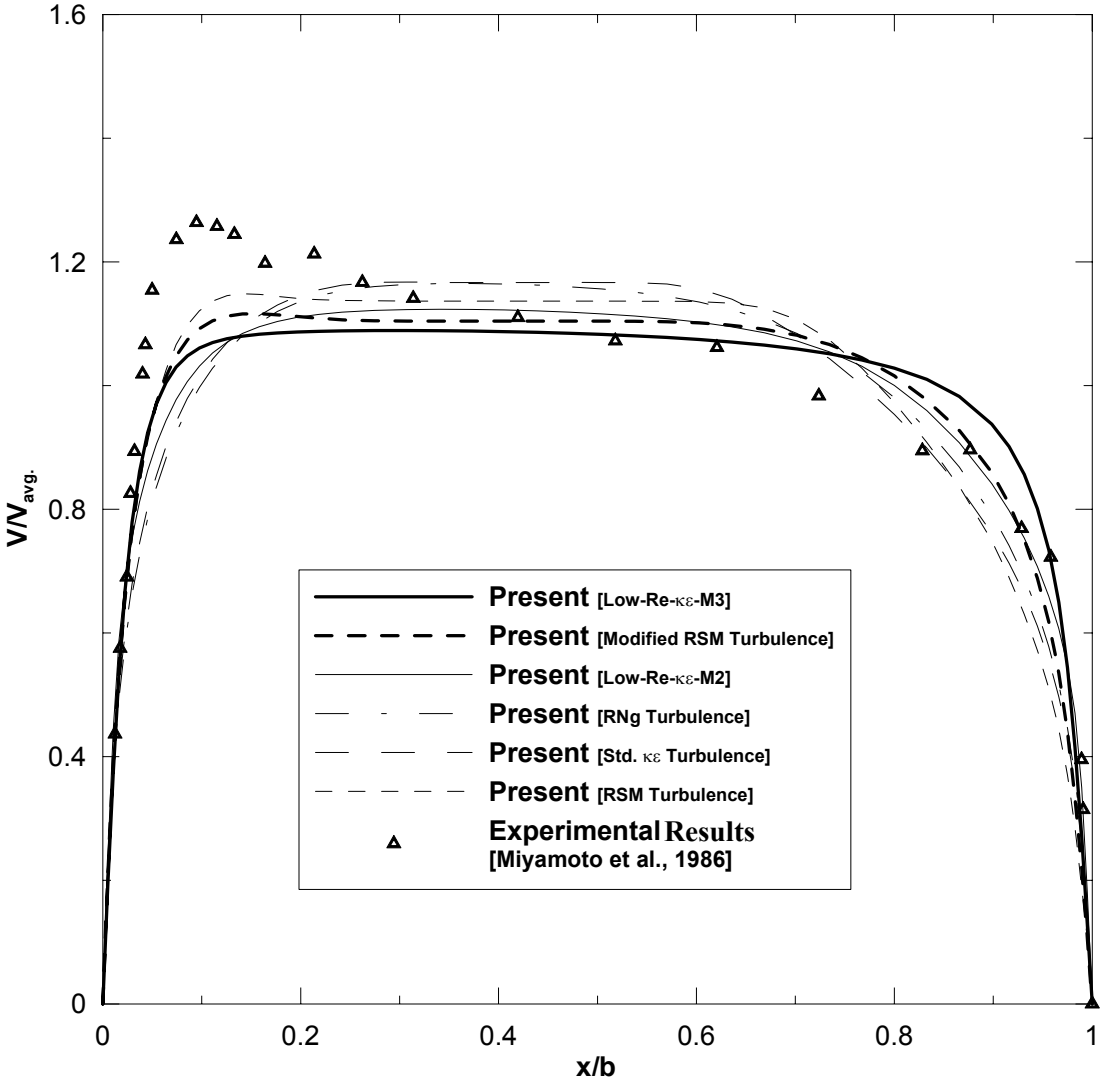

Figure 5.10: Normalized vertical velocity at section y/L = 0.16 from the channel inlet for Uniform pressure inlet with q_w"= 208 Wm^{-2}, b= 0.1m and L/b=50.

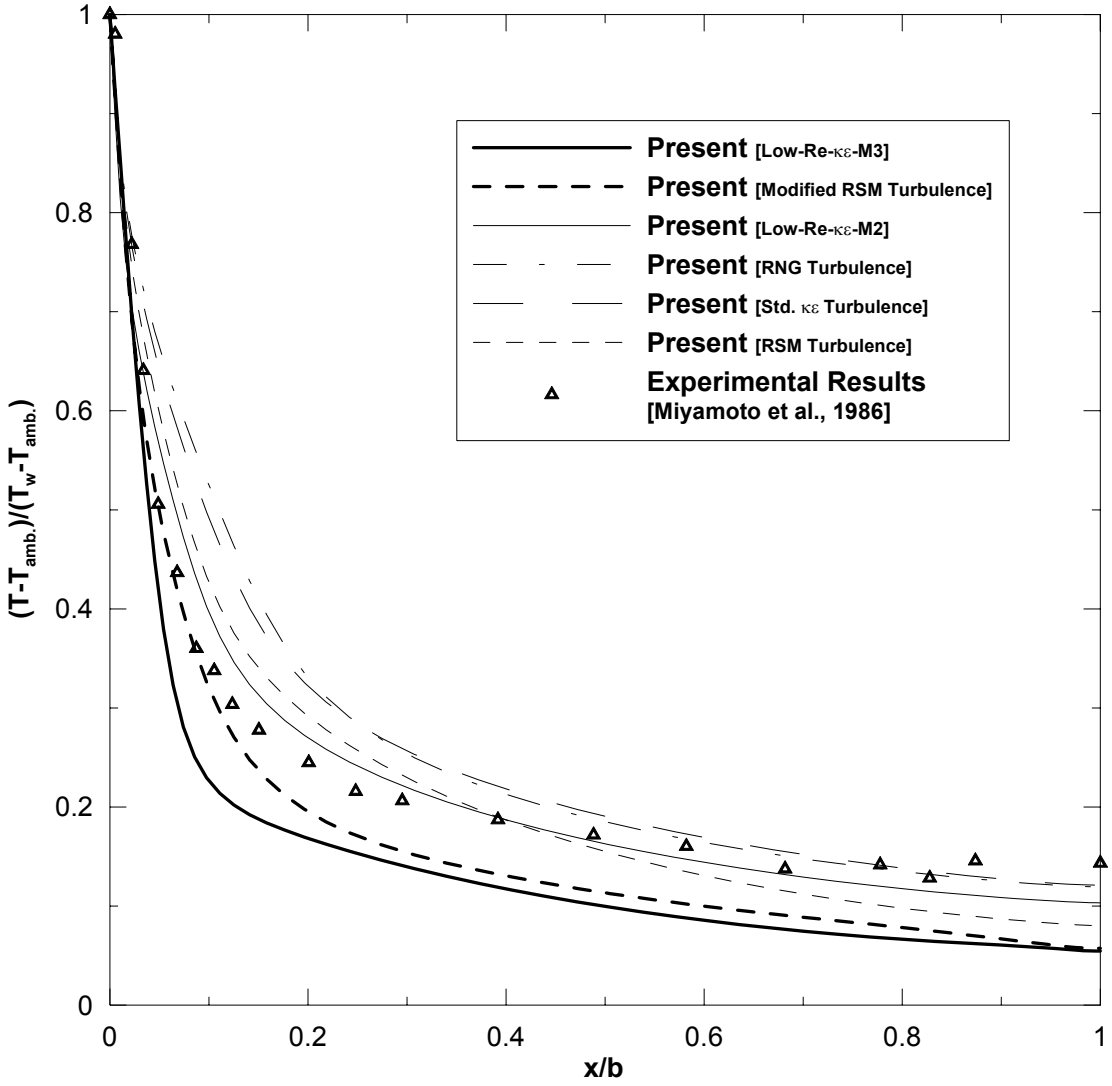

Figure 5.11: Normalized temperature at section y/L = 0.77 from the channel inlet for Uniform pressure inlet with q_w" = 208 Wm^{-2}, b= 0.1m and L/b=50.

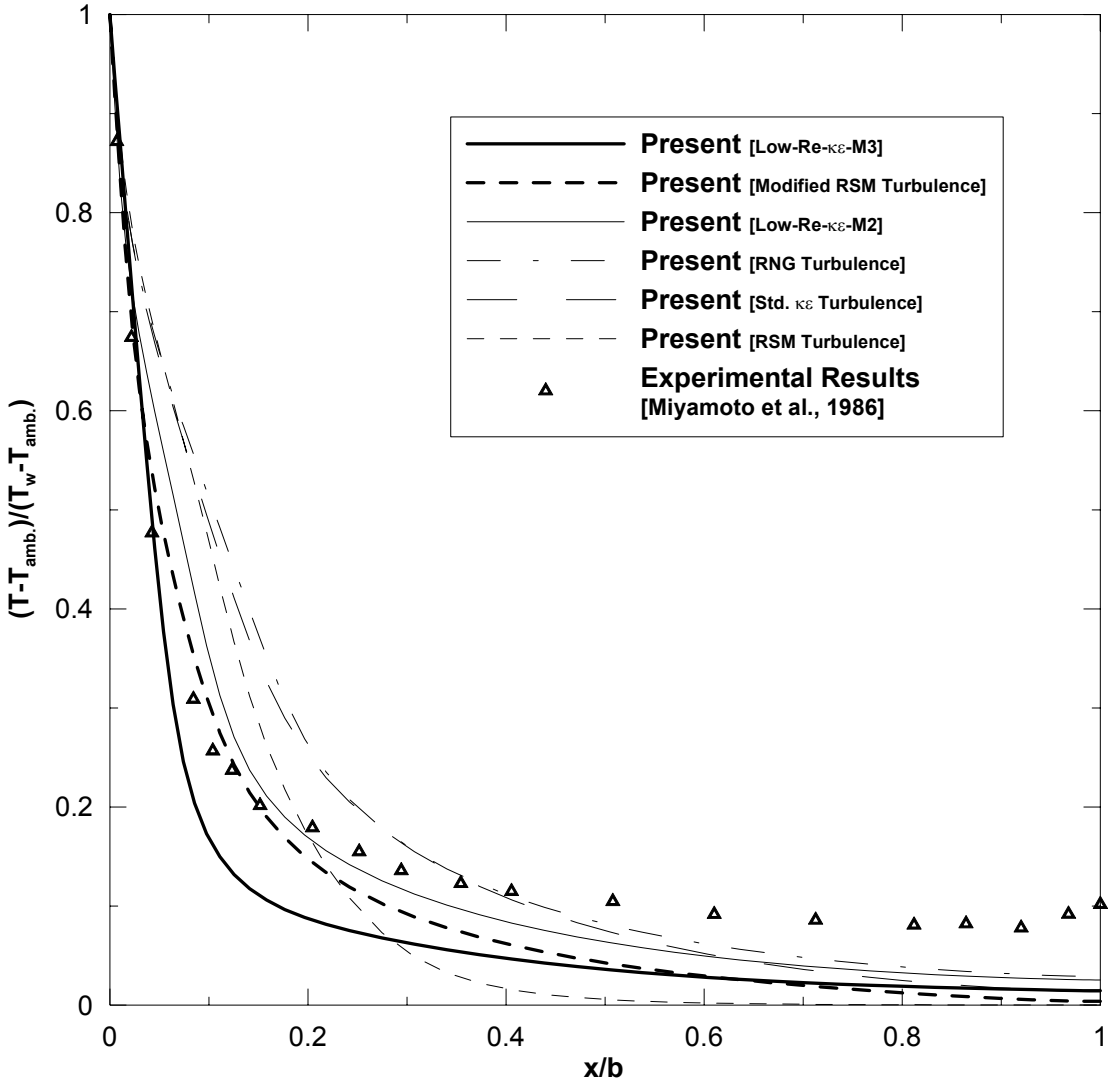

Figure 5.12: Normalized temperature at section y/L = 0.53 from the channel inlet for Uniform pressure inlet with q_w"= 208 Wm^{-2}, b= 0.1m and L/b=50.

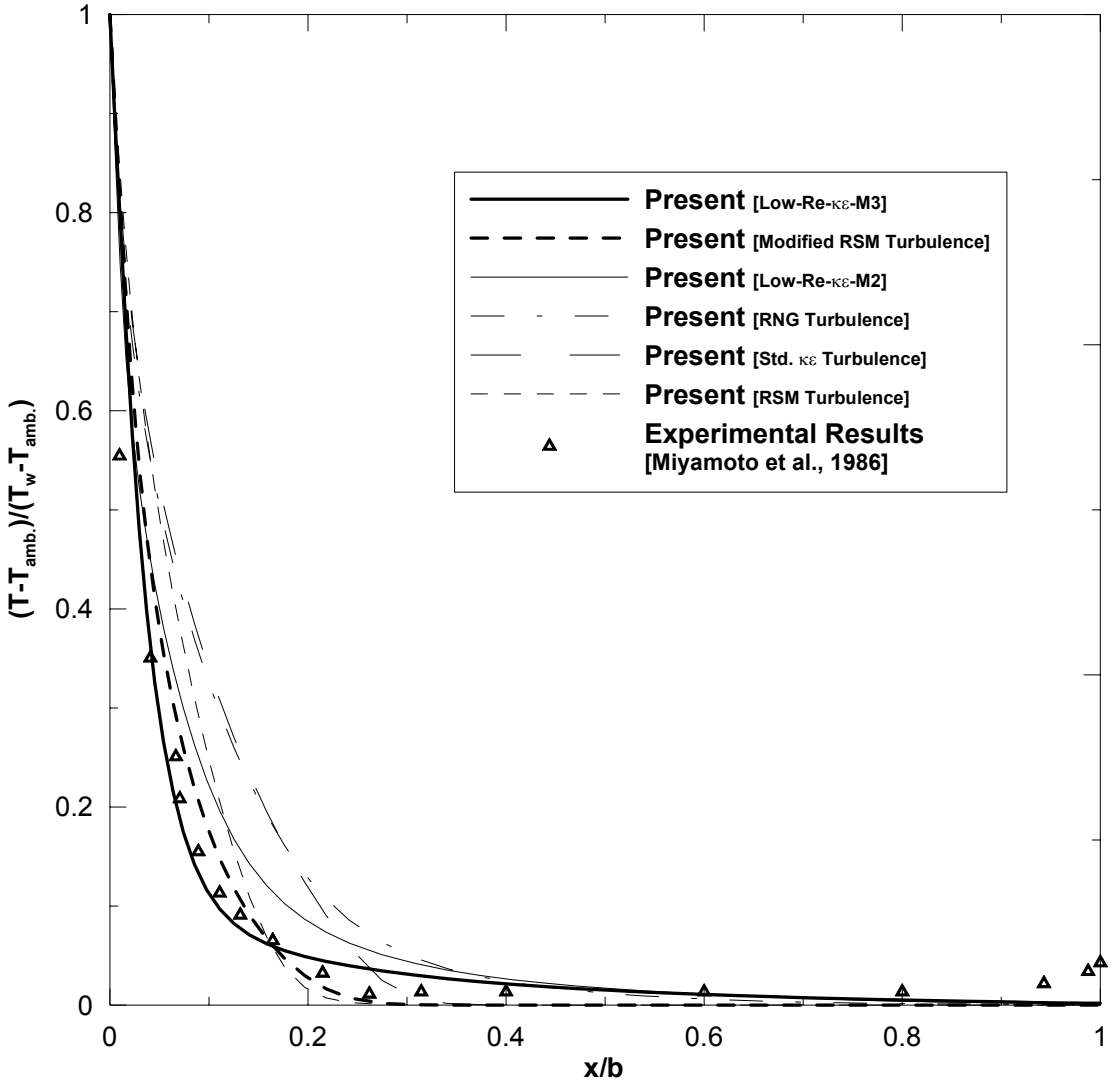

Figure 5.13: Normalized temperature at section y/L = 0.16 from the channel inlet for Uniform pressure inlet with q_w" = 208 Wm^{-2}, b= 0.1m and L/b=50.

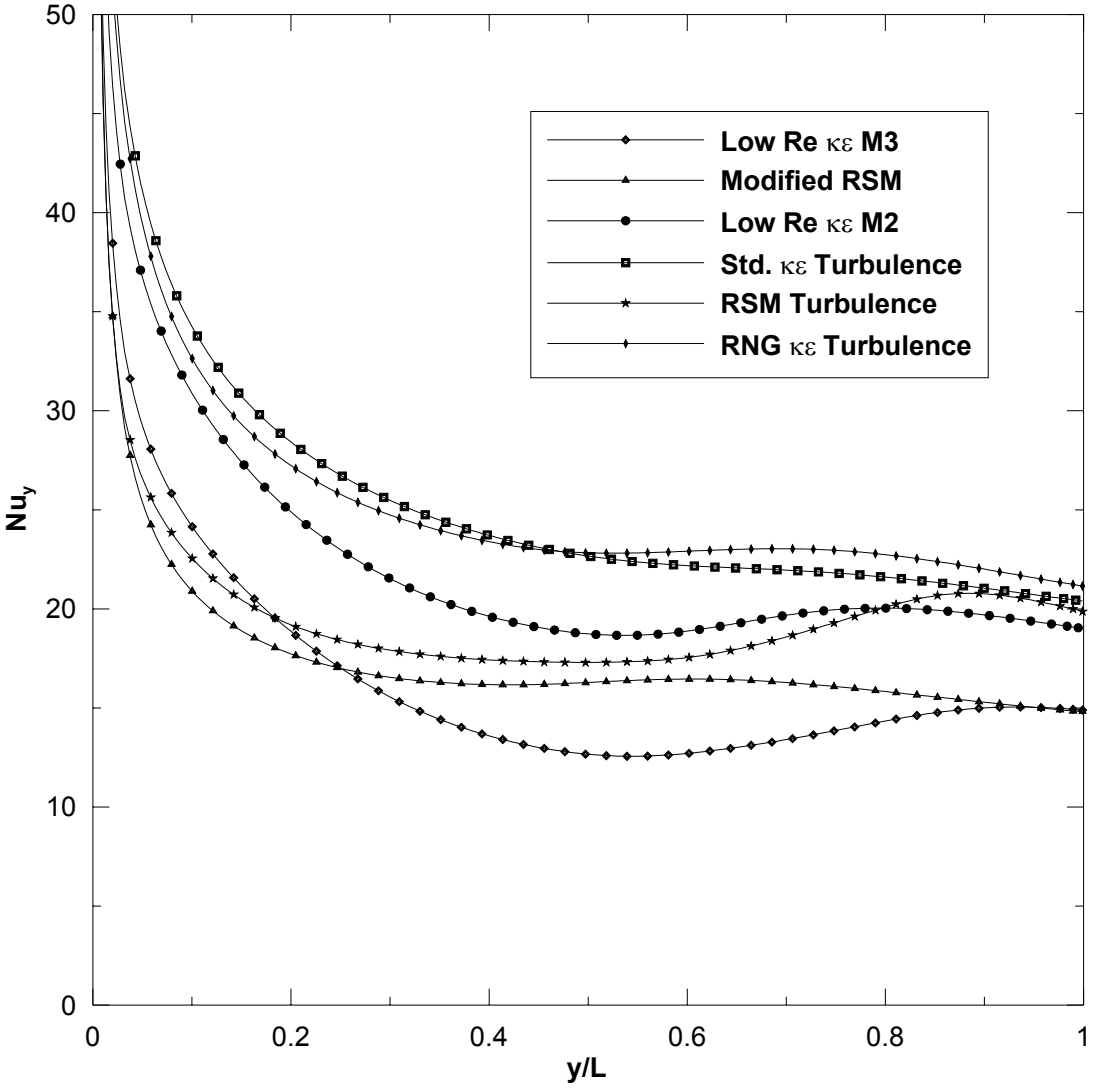

Figure 5.14: Comparison of local Nusselt number along the heated wall for different turbulence model for Uniform pressure inlet with q_w" = 208 Wm^{-2}, b= 0.1m and L/b=50.

5.2.1.3. Comparison for Extended Inlet condition

Comparison of Velocity distribution at different sections

A comparison between the predicted and measured (Miyamoto *et al.*, 1986) mean vertical velocity profiles and temperature profiles at three different heights along the channel is given for the second computational domain i.e., for the extended inlet condition shown in Figure 5.15.

Mean vertical velocity profile at section y/L = 0.77 and y/L = 0.53 shown in Figure 5.16 and Figure 5.17 clearly indicate that the M3 model predictions agree with the experimental data at both heated and adiabatic walls and is close even in the turbulent core region. All the other turbulence models results in lower velocities compared to the experimental values and totally disagree near the heated wall and also in the turbulent core region. Figure 5.18 Shows a comparison of the velocity profiles at y/L = 0.16. It is clear from the figure that all models predictions are far from the experimental values except for the Low Re $k-\varepsilon$ M3 which gave reasonable agreement with experimental values.

Figures 5.19 and 5.20 show the mean vertical temperature profile at sections y/L = 0.77 and 0.53. At these sections, the RSM model seems to be closest to the experimental data whereas the modified RSM model predicts higher mean temperatures. The predictions of the low Re $k-\varepsilon$ M3 is lower than experimental data. This might be due to the difference in flow rate as shown in Table 5.3 for all turbulence models.

Temperature distribution at different section

The temperature distributions at a sections y/L = 0.77, 0.53 and 0.16 shown in Figures 5.19, 5.20 and5.21 clearly indicate that the Low Re $k-\varepsilon$ M3 gives closer

prediction than any other model. At all three sections where experimental values where reported, there was a small rise in the air temperature in the vicinity of the right adiabatic wall. This clearly indicates radiation from the heated left wall heats the right adiabatic wall and makes it non-adiabatic. However, despite these differences the measured and predicted temperature gradients in air at the hot wall are in very good agreement with each other. This finding is encouraging and suggests that the Low Re $k-\varepsilon$ M3 turbulence model has the capability to predict local convective heat flux in a vertical channel under natural circulation condition.

The difference in flow rate between the experimental data and the different turbulence models using uniform pressure inlet condition (i.e. first computation domain shown in Figure 5.6) is given in Table 5.1 It is assumed that 100% of the heat flux is convected by the flow.

Table 5.2 shows the flow rate for the same uniform pressure inlet condition with 85% of the heat flux is convected by the fluid. This assumption is based on the experimental work by Miyamoto *et al.* (1986) who reported that only 85% of the total heat flux was contributing to heat convection.

Similarly, for the Extended Inlet condition (i.e. second computational domain shown in Figure 5.15) the differences in flow rates predicted by different turbulence models are shown in Table 5.3 with 100% heat flux contributing to heat convection. Table 5.4 shows the same but with 75% total heat flux contributing to heat convection.

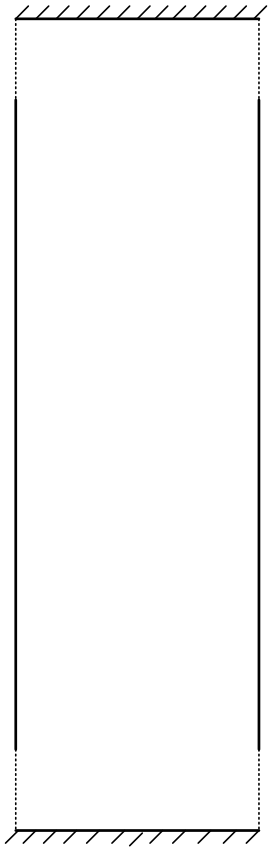

Figure 5.15: Extended inlet condition

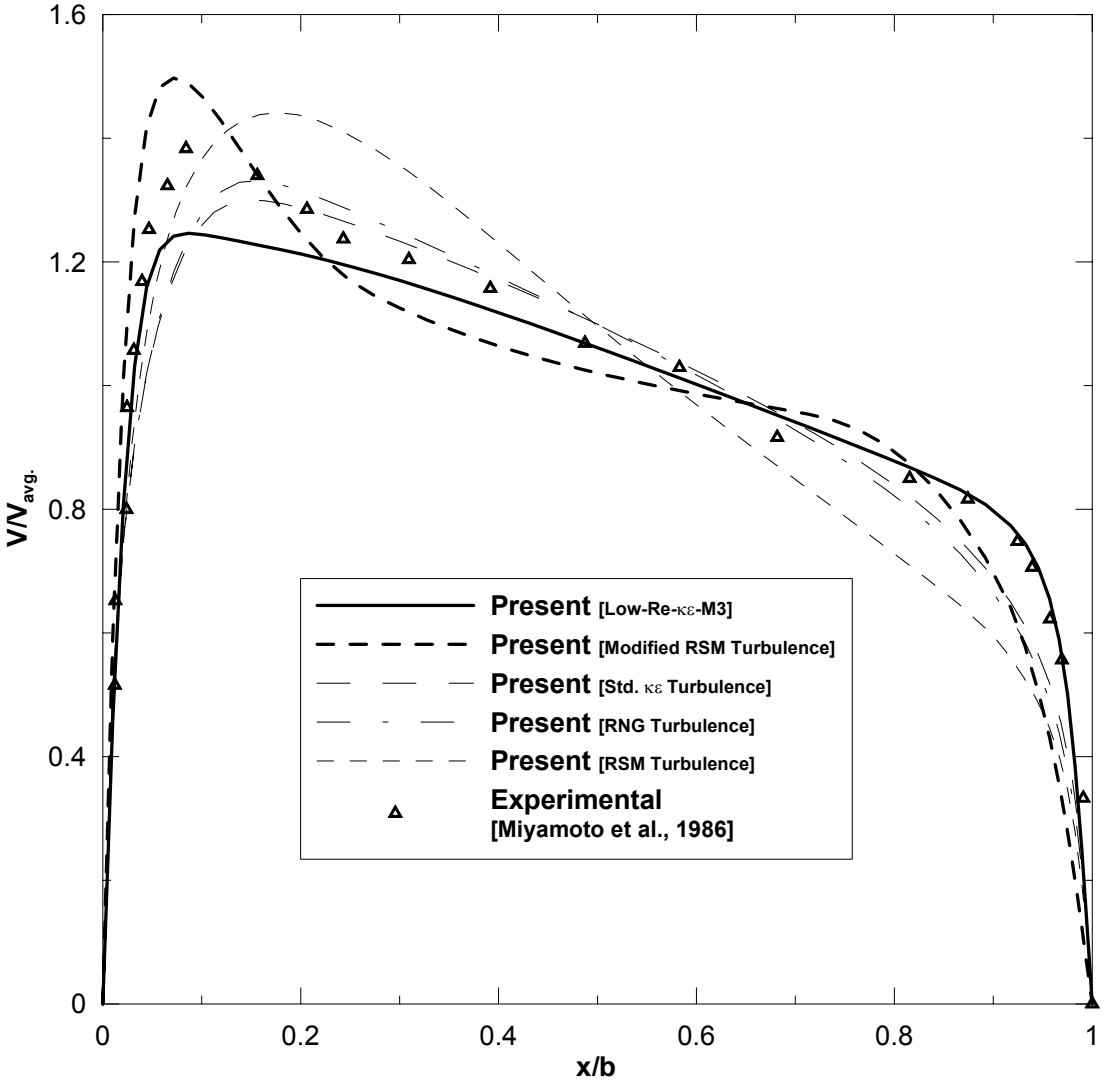

Figure 5.16: Normalized vertical velocity at section y/L = 0.73 from the channel inlet for Extended inlet condition.

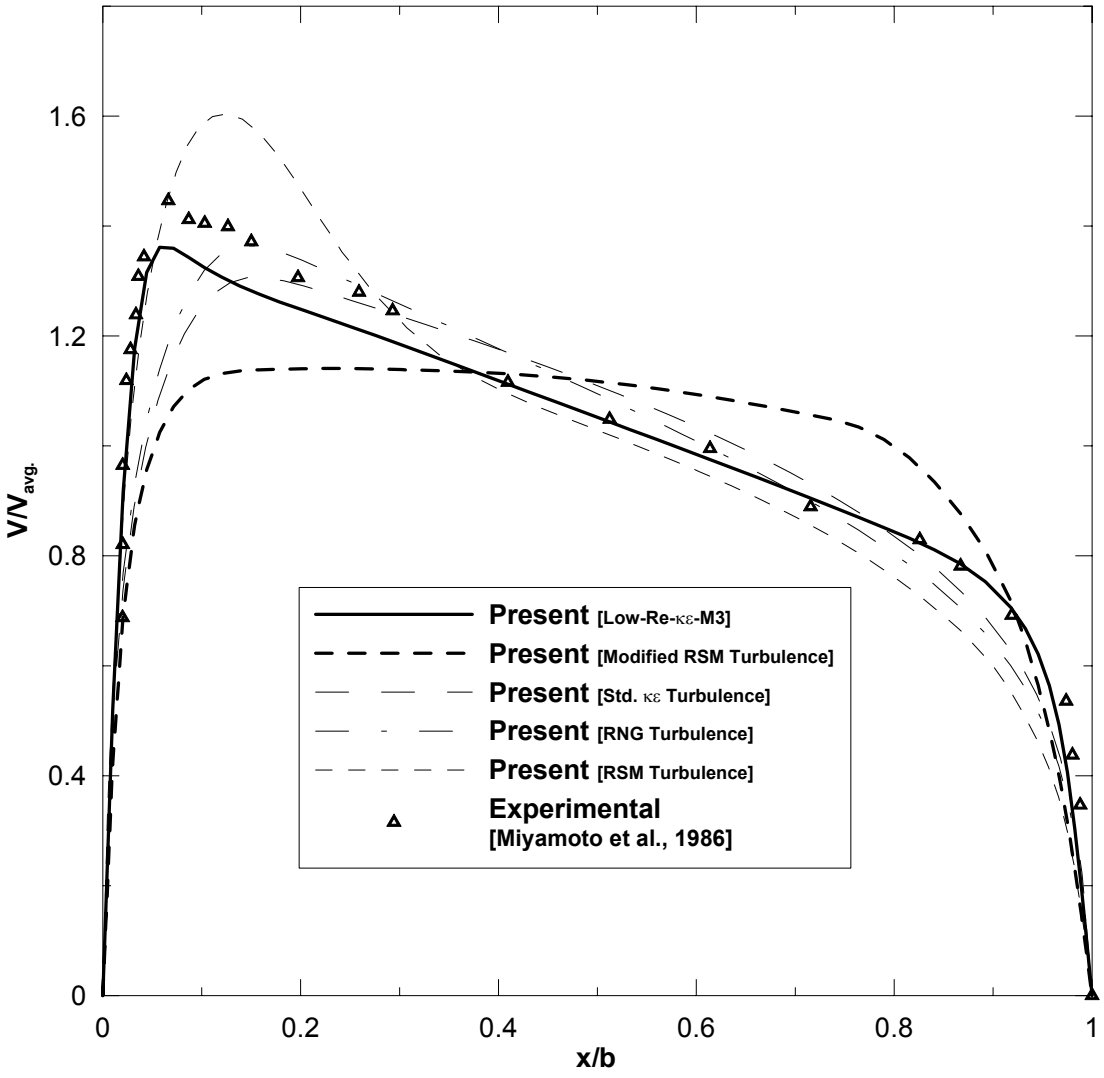

Figure 5.17: Normalized vertical velocity at section y/L = 0.53 from the channel inlet for Extended inlet condition.

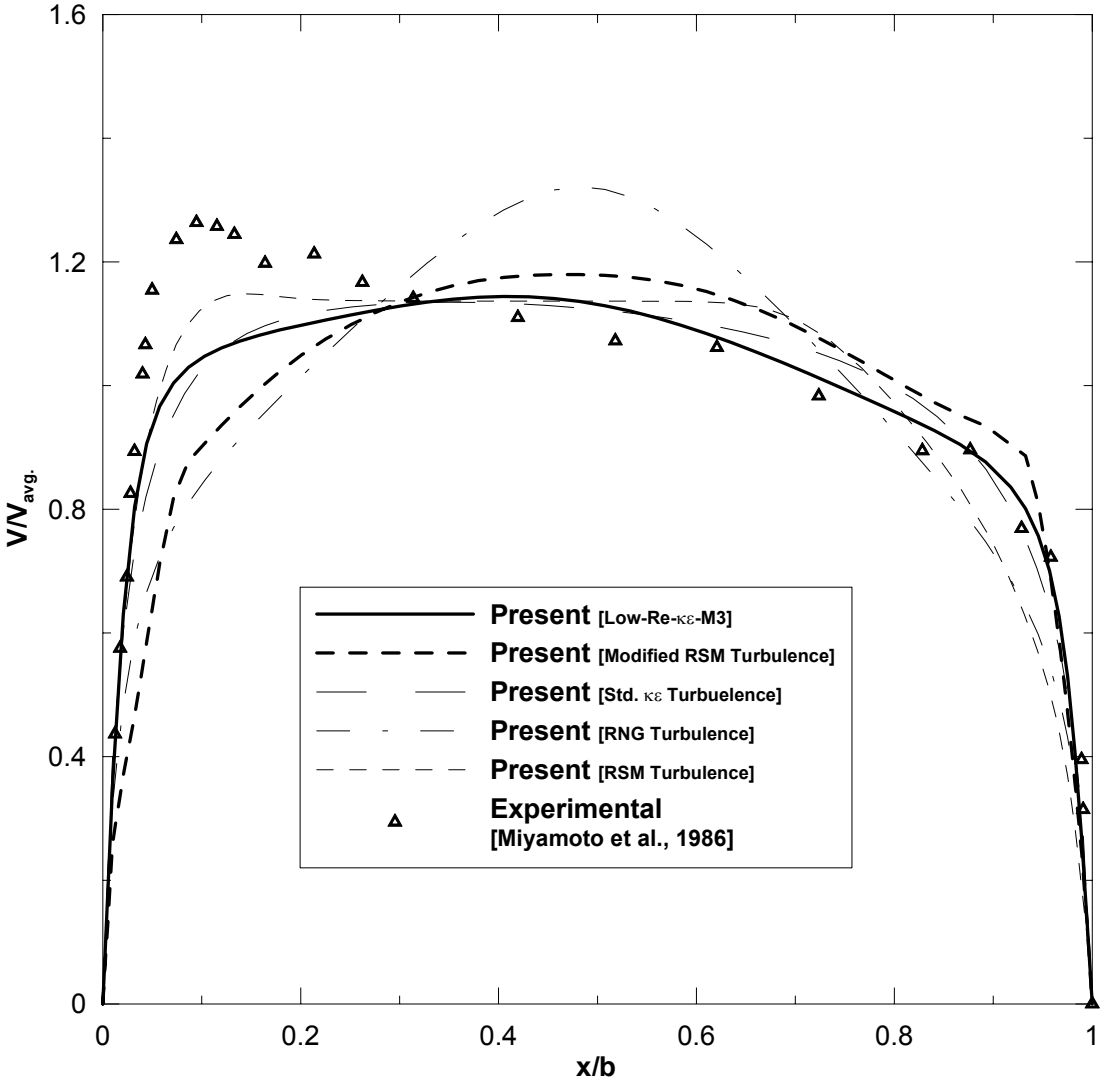

Figure 5.18: Normalized vertical velocity at section y/L = 0.16 from the channel inlet for Extended inlet condition.

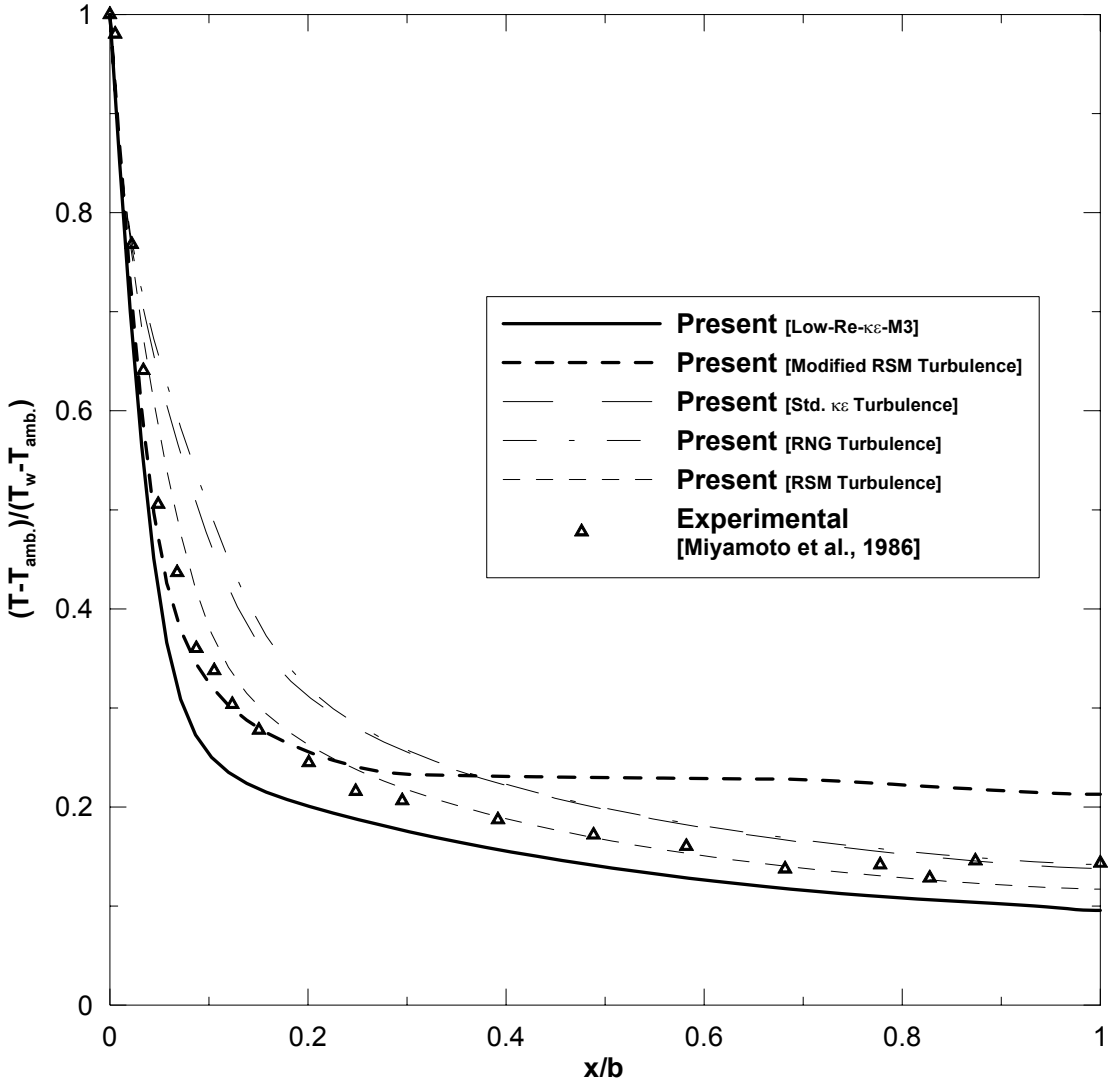

Figure 5.19: Normalized temperature at section y/L = 0.73 from the channel inlet for Extended inlet condition.

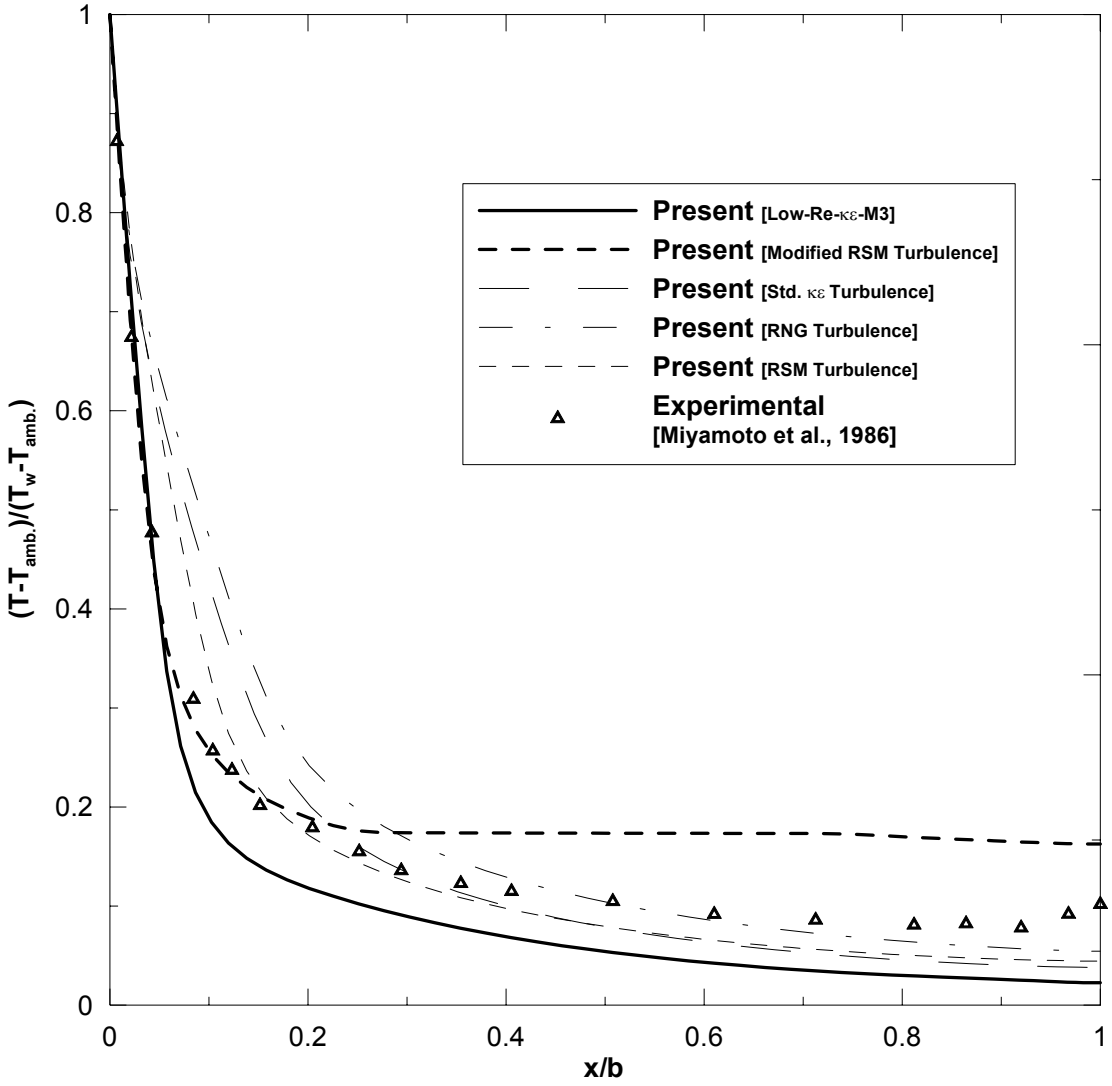

Figure 5.20: Normalized temperature at section y/L = 0.53 from the channel inlet for Extended inlet condition.

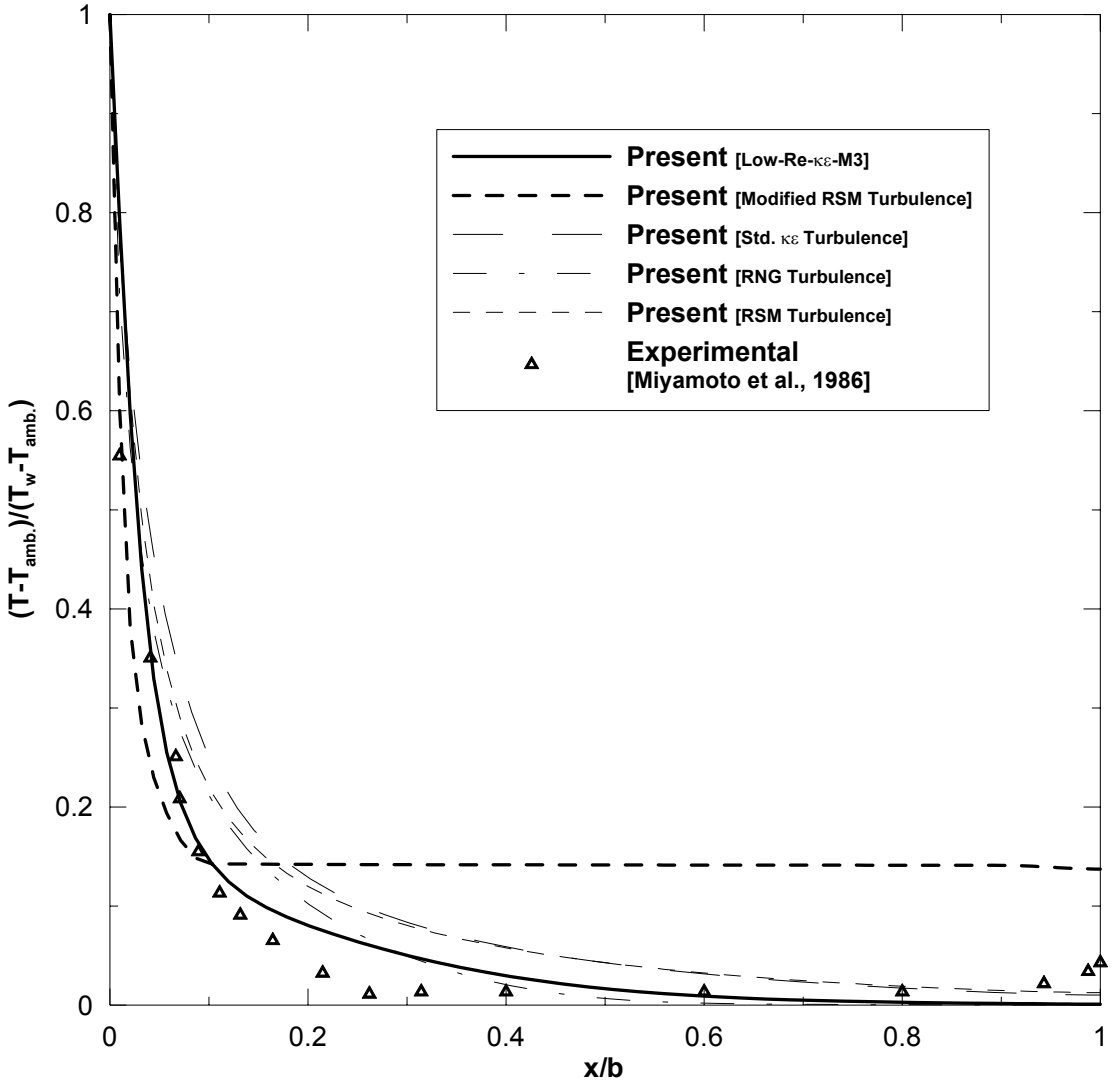

Figure 5.21: Normalized temperature at section y/L = 0.16 from the channel inlet for Extended inlet condition.

Comparison of flow rate for vertical parallel plate channels

Table 5.1: Flow rate for Uniform pressure inlet condition with Heat flux 208 W/m^2. (i.e.100% convective heat flux)

Turbulence Model	Flow rate (m^3/s) at y=820 mm	Flow rate (m^3/s) at y=3865 mm	% Error at (y=820mm)	% Error at (y=3865mm)
Std. $k-\varepsilon$ Turbulence	0.73	0.73	28	28
Modified RSM Turbulence	0.82	0.82	43	43
RNG Turbulence	0.73	0.73	28	28
RSM Turbulence	0.72	0.72	26	26
Low Re $k-\varepsilon$ M2 Turbulence	0.77	0.77	34	34
Low Re $k-\varepsilon$ M3 Turbulence	0.84	0.84	45	45
Experimental	0.57	0.57	-	-

Table 5.2: Flow rate for Uniform pressure inlet condition with Heat flux 176 W/m^2. (i.e.85% convective heat flux)

Turbulence Model	Flow rate (m^3/s) at y=820 mm	Flow rate (m^3/s) at y=3865 mm	% Error at (y=820mm)	% Error at (y=3865mm)
Std. $k-\varepsilon$ Turbulence	0.69	0.69	21	21
Modified RSM Turbulence	0.76	0.76	33	33
RNG Turbulence	0.69	0.69	21	21
RSM Turbulence	0.68	0.68	20	20
Low Re $k-\varepsilon$ M2 Turbulence	0.72	0.72	26	26
Low Re $k-\varepsilon$ M3 Turbulence	0.79	0.79	38	38
Experimental	0.57	0.57	-	-

Table 5.3: Flow rate for Extended inlet condition with Heat flux 208 W/m^2.(i.e.100% convective heat flux)

Turbulence Model	Flow rate (m^3/s) at y=820 mm	Flow rate (m^3/s) at y=3865 mm	% Error at (y=820mm)	% Error at (y=3865mm)
Std. $k-\varepsilon$ Turbulence	0.65	0.65	14	14
Modified RSM Turbulence	0.45	0.45	-21	-21
RNG Turbulence	0.66	0.66	15	15
RSM Turbulence	0.56	0.56	-1	-1
Low Re $k-\varepsilon$ M3 Turbulence	0.73	0.73	27	27
Experimental	0.57	0.57	-	-

Table 5.4: Flow rate for Extended inlet condition with Heat flux 176 W/m^2.(i.e.85% convective heat flux)

Turbulence Model	Flow rate (m^3/s) at y=820 mm	Flow rate (m^3/s) at y=3865 mm	% Error at (y=820mm)	% Error at (y=3865mm)
Std. $k-\varepsilon$ Turbulence	0.62	0.61	7	8
Modified RSM Turbulence	0.38	0.38	-33	-33
RNG Turbulence	0.62	0.62	8	9
RSM Turbulence	0.5	0.5	-12	-12
Low Re $k-\varepsilon$ M3 Turbulence	0.69	0.69	20	20
Experimental	0.57	0.57		

5.2.2 Comparison with Habib *et al.*, (2002)

5.2.2.1. Experimental description

Velocity measurements were carried out for turbulent natural convection flow in an asymmetrically heated vertical channel. The plates taken were 12.5mm thick with length 125mm and width 200mm. The gap between the plates, b, was 40 mm; hence the aspect ratio was 3.125. One plate was kept at 10^{O}C above and the other at 10^{O}C below the ambient temperature. The profiles of mean velocity are measured by using a Laser Doppler Anemometer and are presented at three different vertical positions taken at planes near the entrance, middle and exit of the channel.

5.2.2.2. Comparison of Low Re $k-\varepsilon$ M3 and modified RSM

The comparison of the vertical velocity profile by Low Re $k-\varepsilon$ M3 and Modified RSM for three locations for which experimental mean vertical velocity profile were reported is shown in Figure 5.22 at section y/L = 0.11, in Figure 5.23 at section y/L = 0.55 and in Figure 5.24 at section y/L = 0.98. From the figures 5.22 – 5.24, it is clear that prediction by Low Re $k-\varepsilon$ M3 model are better than modified RSM. The M3 model predictions are close to experimental data of Habib *et al.* (2002) at near wall region.

5.2.2.3. Grid Independence Test

A grid independence test was carried out to make sure that the grid size does not affect the accuracy of results. Computations were carried out using five different grid sizes: 20 x 50, 30 x 50, 50 x 100, 60 x 150 and 200 x 200 grid points. Figure 5.25 to 5.27 show the mean vertical velocity profile at different locations y/L = 0.11, 0.55 0.98

respectively using these different grid sizes. As can be seen the difference in results obtained from using 60 x 150 grid and the 200 x 200 grid is very small. Therefore in this study a grid size of 60 x 150 is used in order to utilize the computation time efficiently without compromising on the accuracy of the computation.

5.2.2.4. Velocity Contours and Velocity Vectors

Figure 5.28(a) shows the vertical velocity contours for the asymmetrical flow obtained from the present numerical solution while Figure 5.28(b) shows the experimental velocity contours. Figure 5.29(a) shows the velocity vectors and Figure 5.29(b) shows the streamlines for the same asymmetrical flow. Habib *et al.* (2002) reported that flow accelerates up the hot side and decelerates down the cold plate. The starting point of each boundary layer is different and concludes that there are two fully interacting opposing boundary layers. They have also reported two large vortices inside the channel near the channel centerline a small stagnation fluid region in between. This phenomenon is clearly visible in the velocity vector contours Figure 5.29(a) and streamlines Figure 5.29(b) with larger vortices near the channel centerlines and streamlines intersection at point of stagnation.

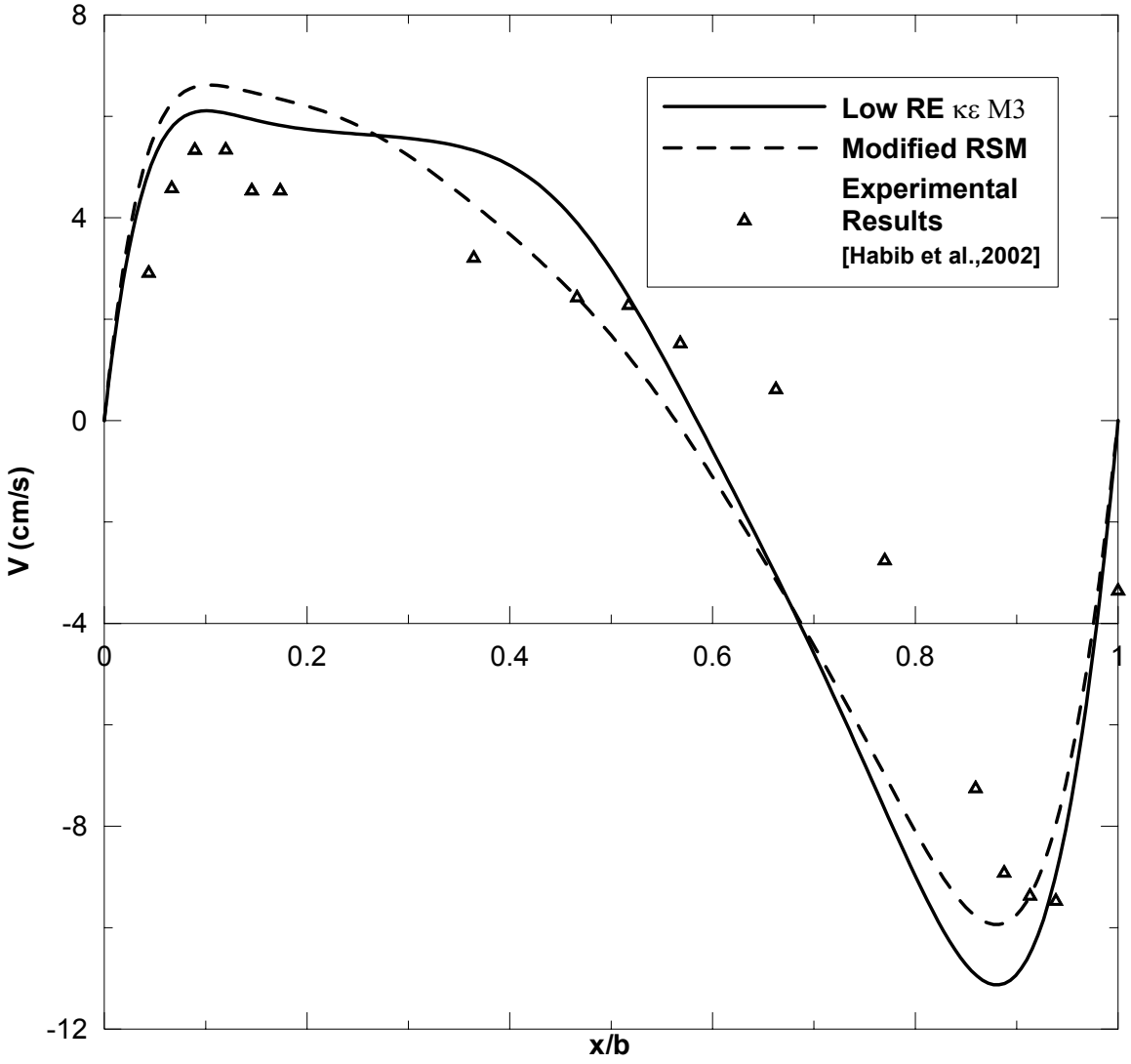

Figure 5.22: Profile of the mean vertical velocity component of the asymmetrical flow at y/L=0.11.

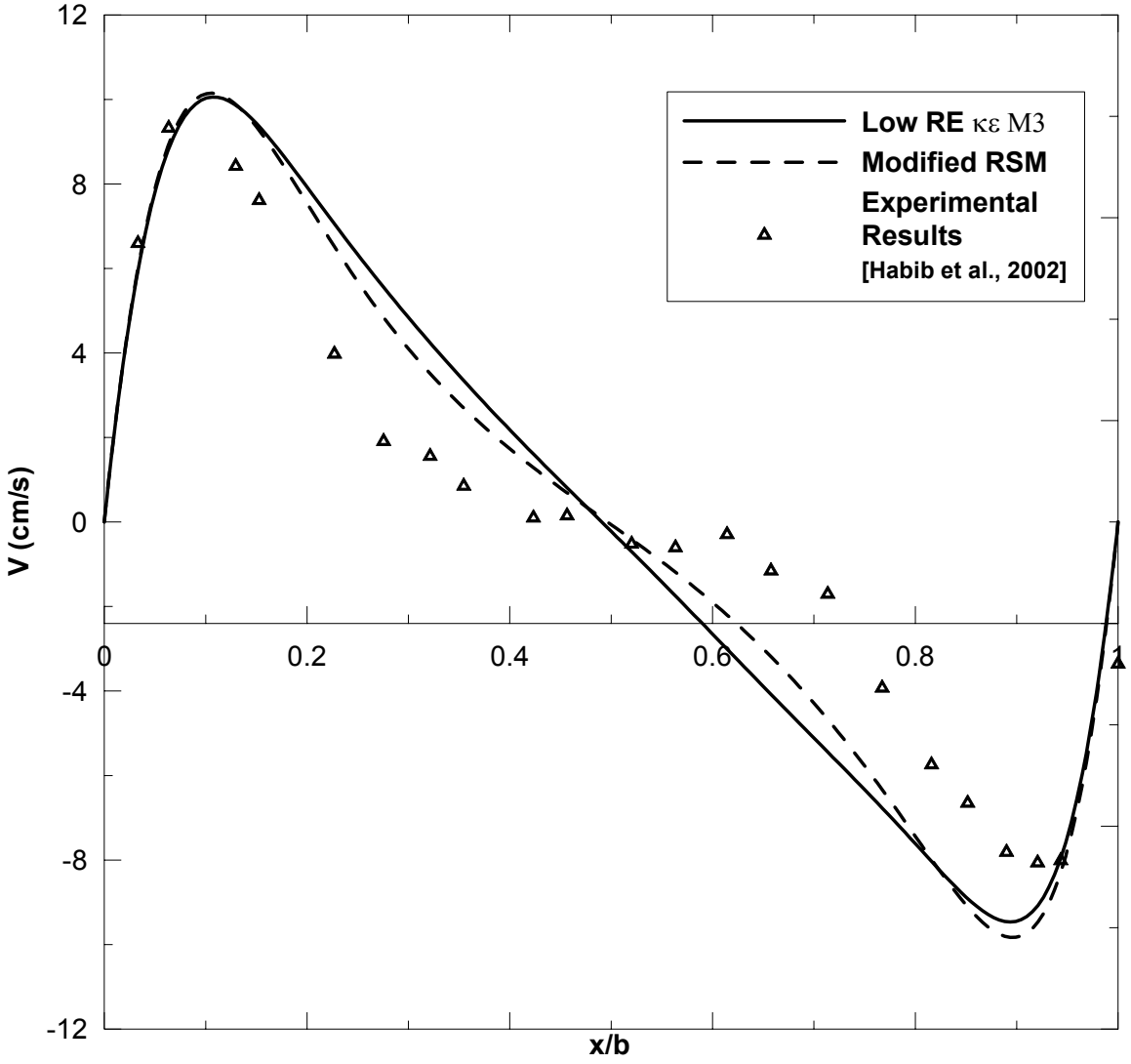

Figure 5.23: Profile of the mean vertical velocity component of the asymmetrical flow at y/L=0.55.

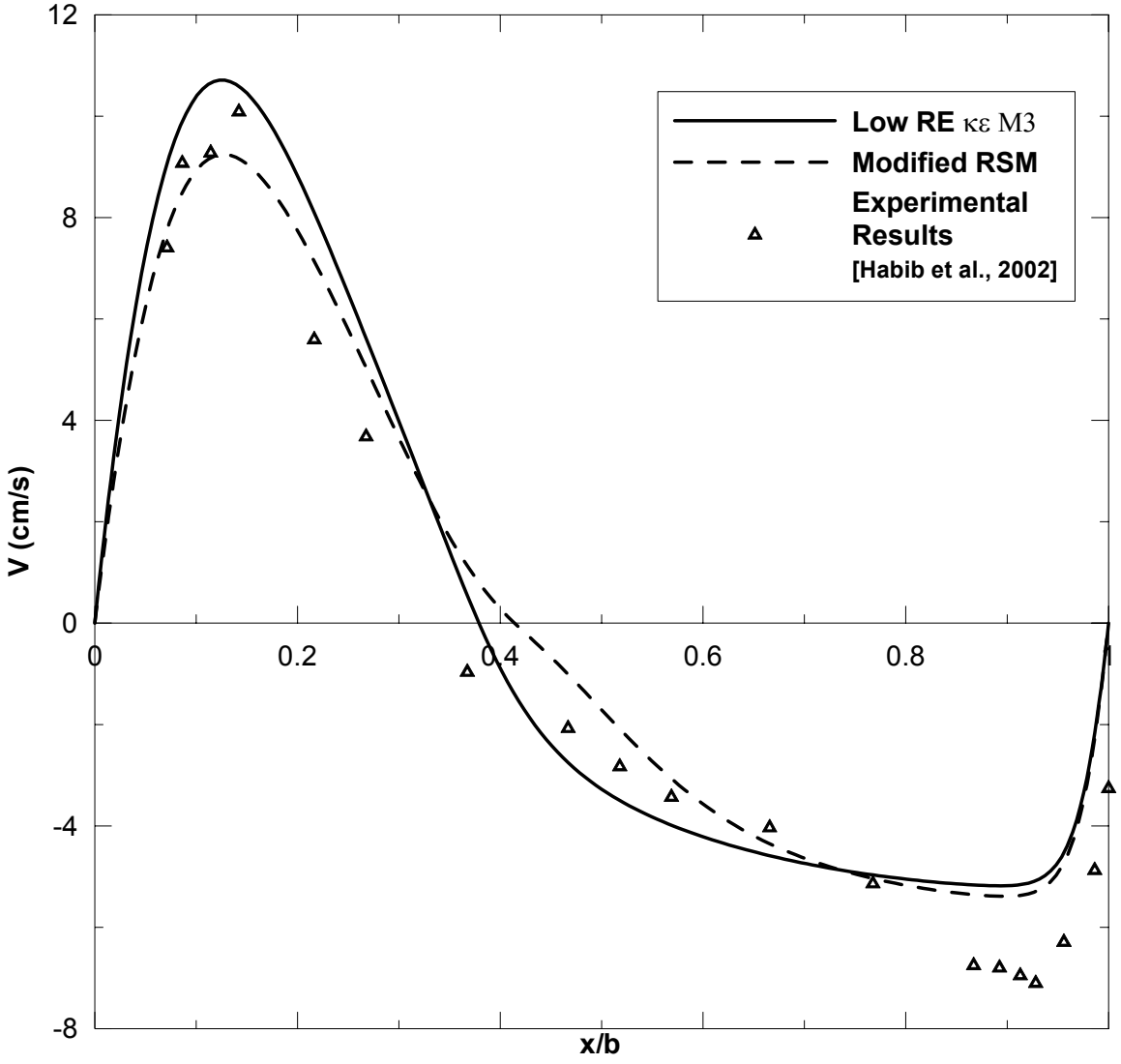

Figure 5.24: Profile of the mean vertical velocity component of the asymmetrical flow at y/L=0.98.

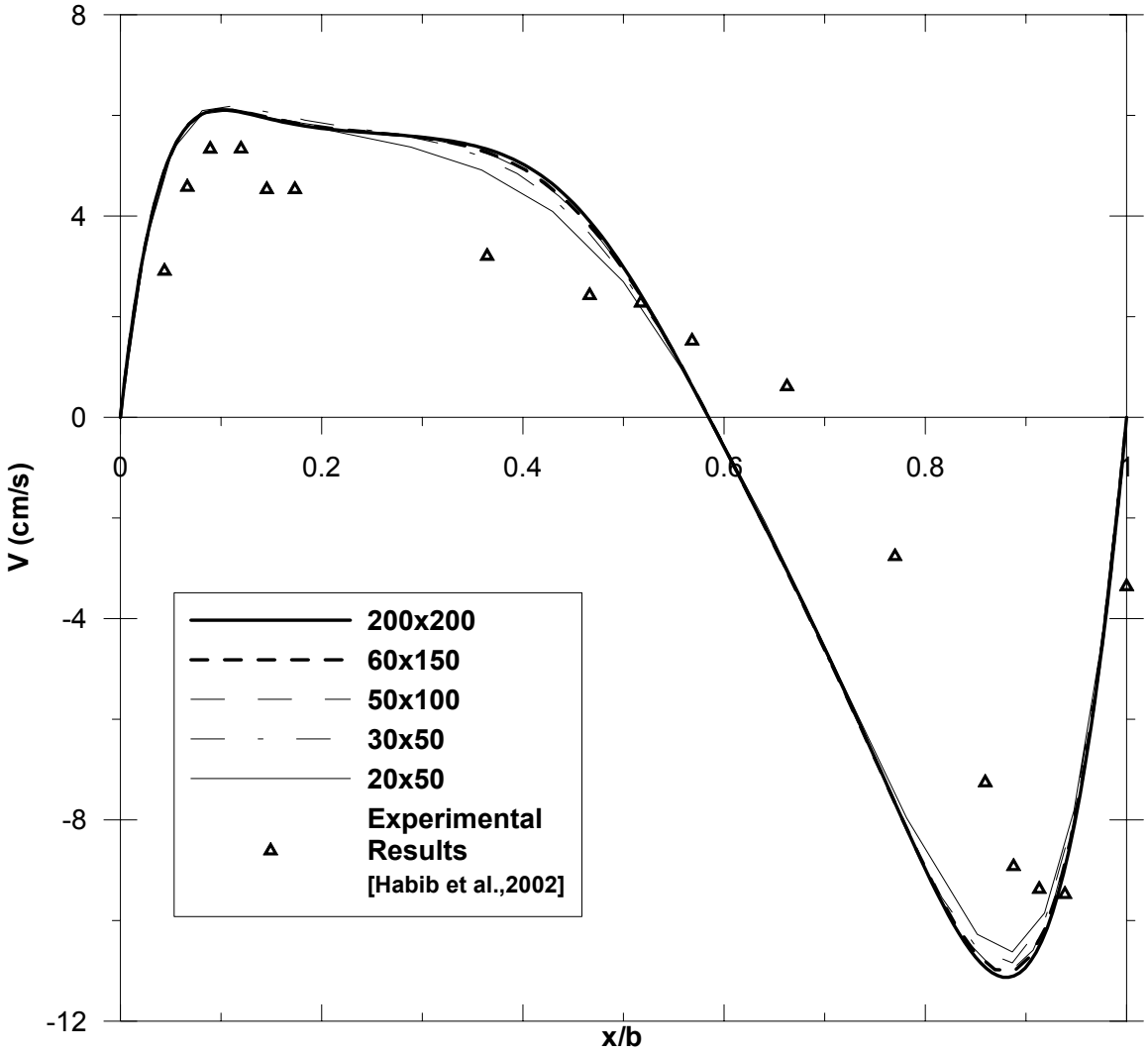

Figure 5.25: Vertical velocity at a section y/L = 0.11 with different mesh size for low Re $k-\varepsilon$ M3.

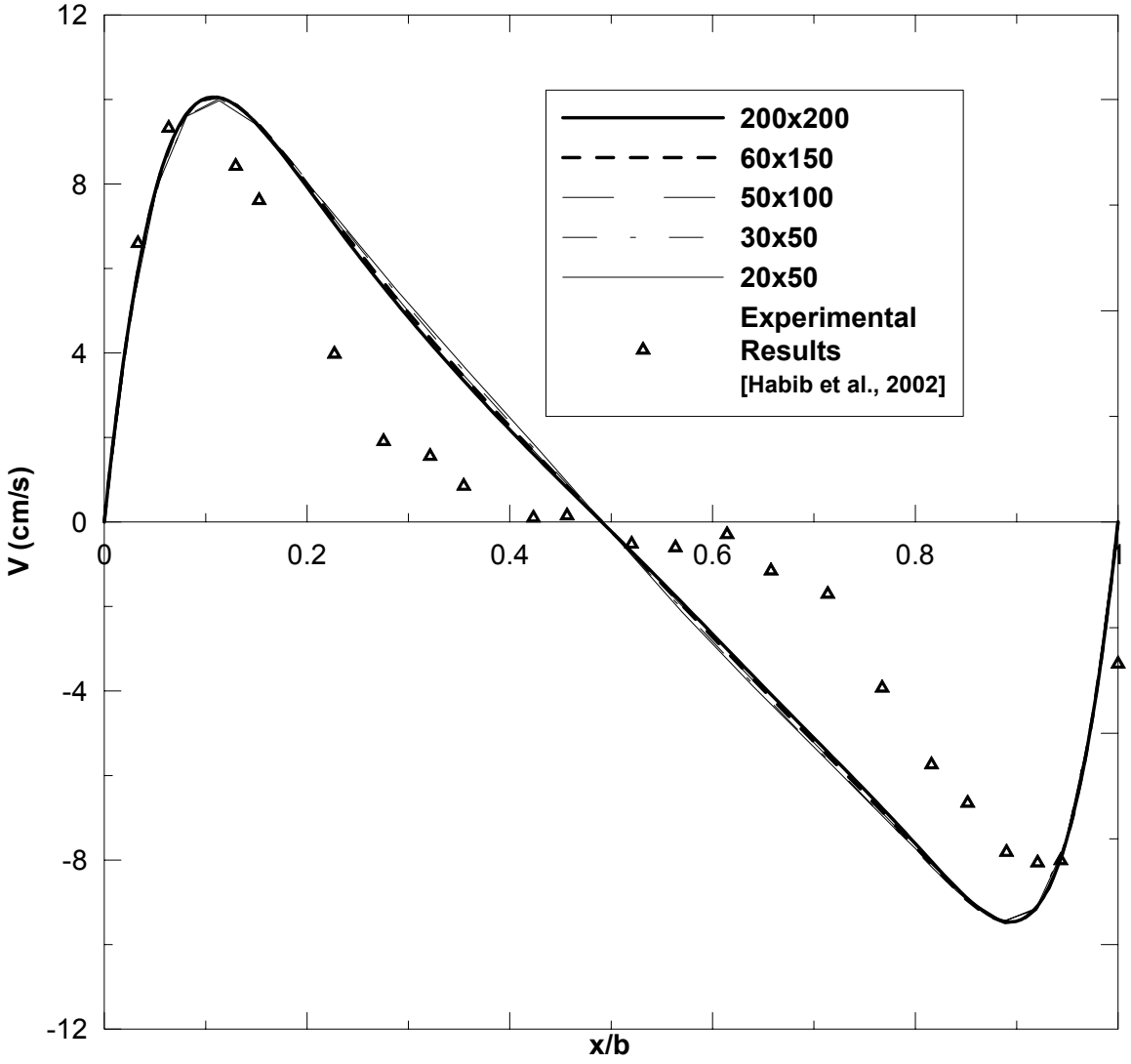

Figure 5.26: Vertical velocity at a section y/L = 0.55 with different mesh size for low Re $k-\varepsilon$ M3.

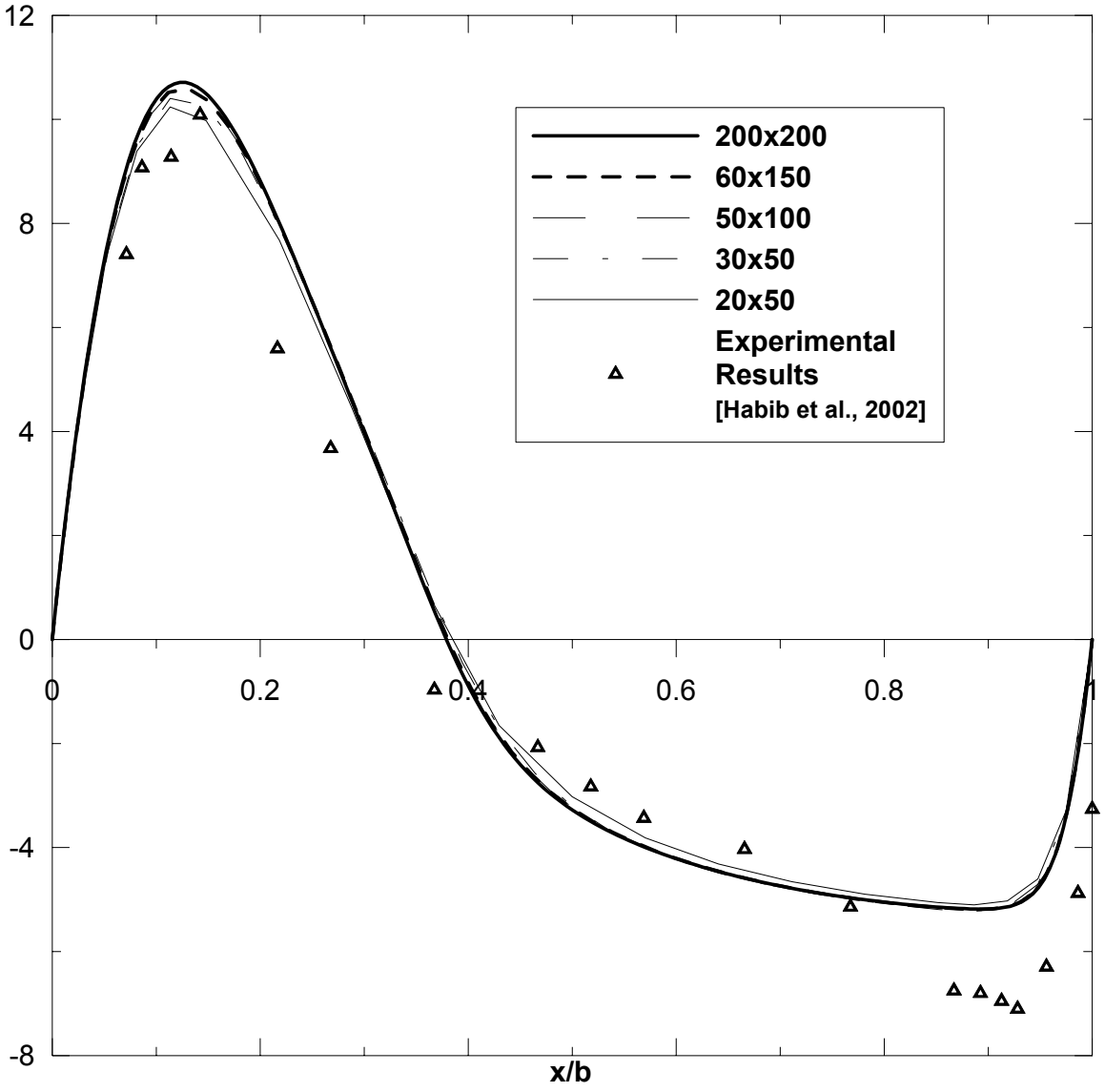

Figure 5.27: Vertical velocity at a section y/L = 0.98 with different mesh size for low Re $k-\varepsilon$ M3.

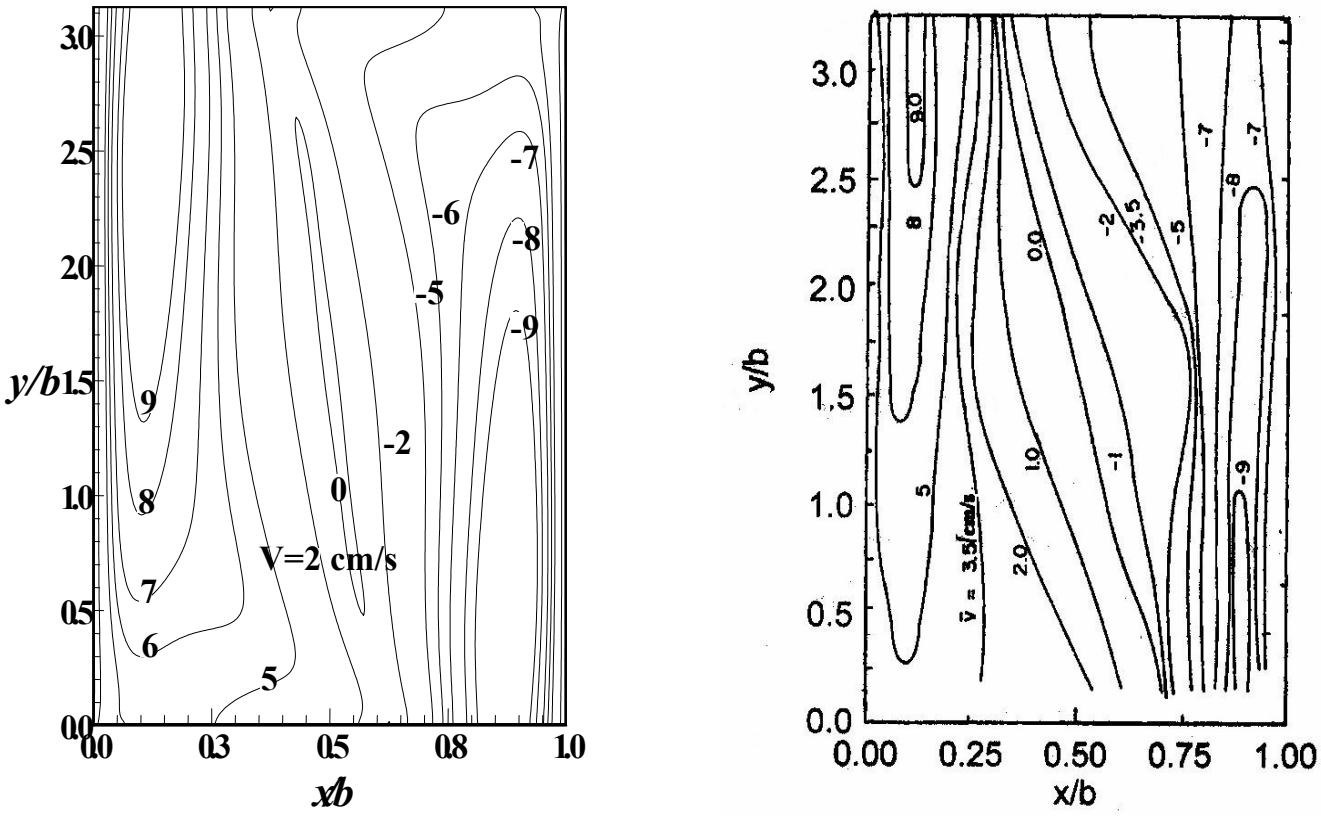

(a) Present contours (b)Experimental contours Habib *et al.* (2002)

Figure 5.28: Mean vertical velocity component for the asymmetrical flow

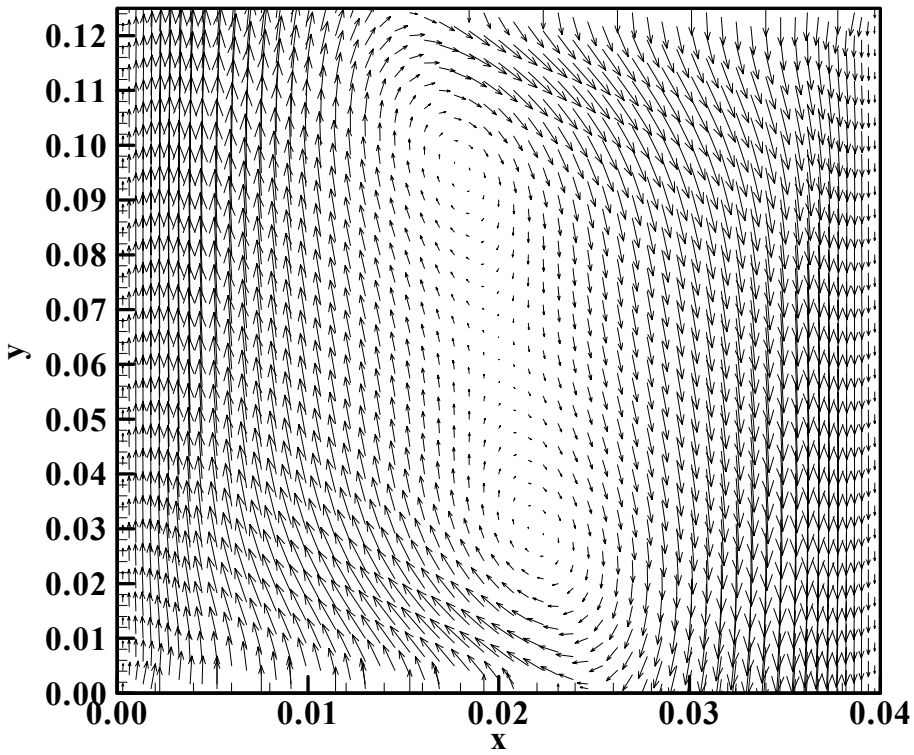

Figure 5.29 a: Velocity vector for asymmetry flow

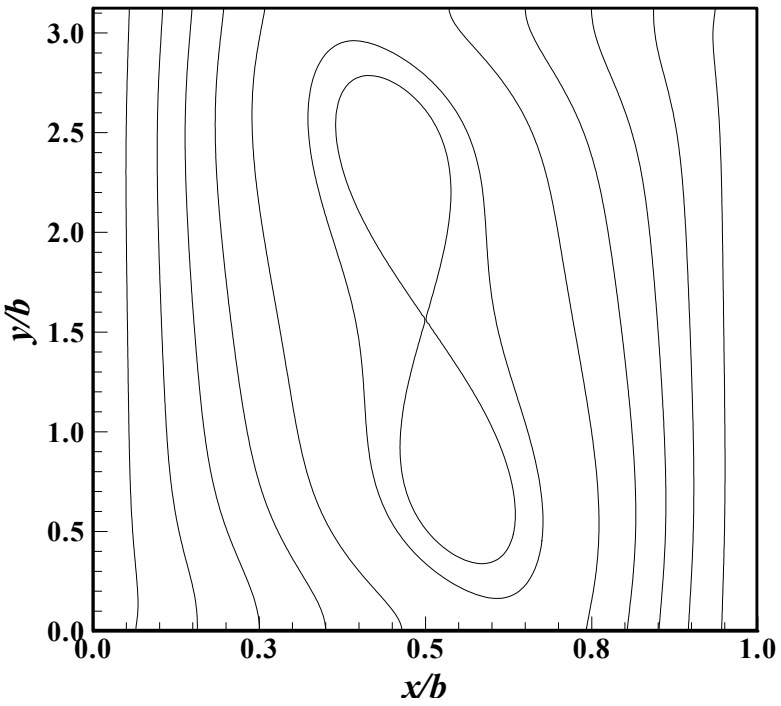

Figure 5.29 b: Streamlines for asymmetry flow

5.3 Influence of Different Inlet Conditions

In addition to the two considered inlet conditions (uniform pressure inlet (Figure 5.6) and Extended inlet (Figure 5.15)), two additional conditions have been studied, namely, the radial flow inlet (Figure 5.30) and the uniform velocity inlet.

The influence of different inlet conditions on the resulting flow and thermal fields have been studied both for laminar and turbulent natural convection flows through the vertical parallel-plate channel.

5.3.1 Influence of different inlet conditions in the laminar regime

Streamlines and Temperature Contours

Streamlines (Ψ) for the above four different inlet conditions are shown in Figures 5.31, 5.32, 5.33 and 5.34 respectively at a modified Rayleigh number of $7.3x10^3$. The streamlines resulting from uniform pressure inlet and uniform inlet velocity conditions are shown in Figures 5.31 and 5.34. Both figures show similar vertical streamlines. However, the streamlines resulting from the extended and radial flow inlet conditions (Figures 5.32 and 5.33) are bent toward the channel wall close to the exit section.

The isotherms ($T-T_O$) for the above mentioned inlet conditions are shown in Figures 5.35 to 5.38. The figures indicate that the isotherms for uniform pressure inlet and uniform velocity inlet are similar. Air within the heated-layer near the heated wall has high temperature. The rest of the domain is unaffected by the flow. The heated layer is comparatively thicker for the extended and radial flow cases than the uniform pressure inlet and uniform velocity inlet conditions.

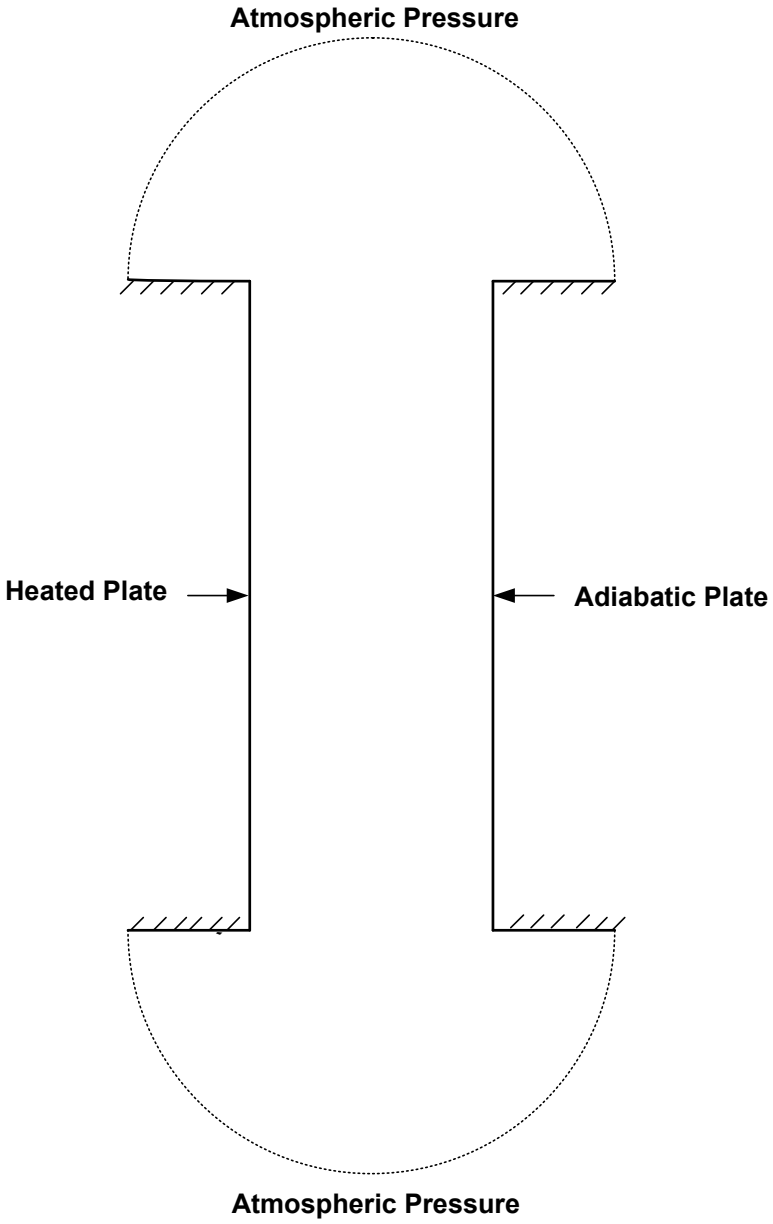

Figure 5.30: Radial inlet flow condition

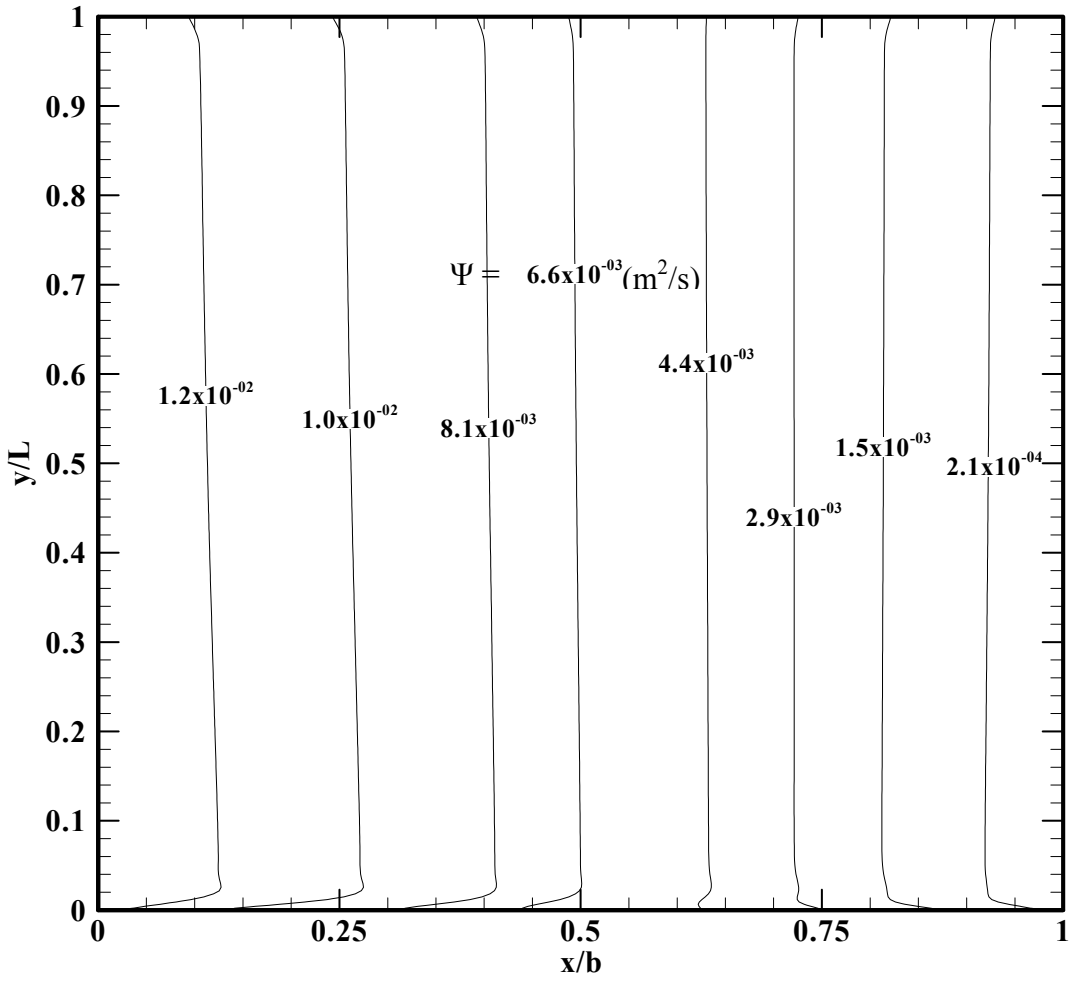

Figure 5.31: Streamlines for uniform pressure inlet condition at $Ra_b(b/L) = 7.3x10^3$.

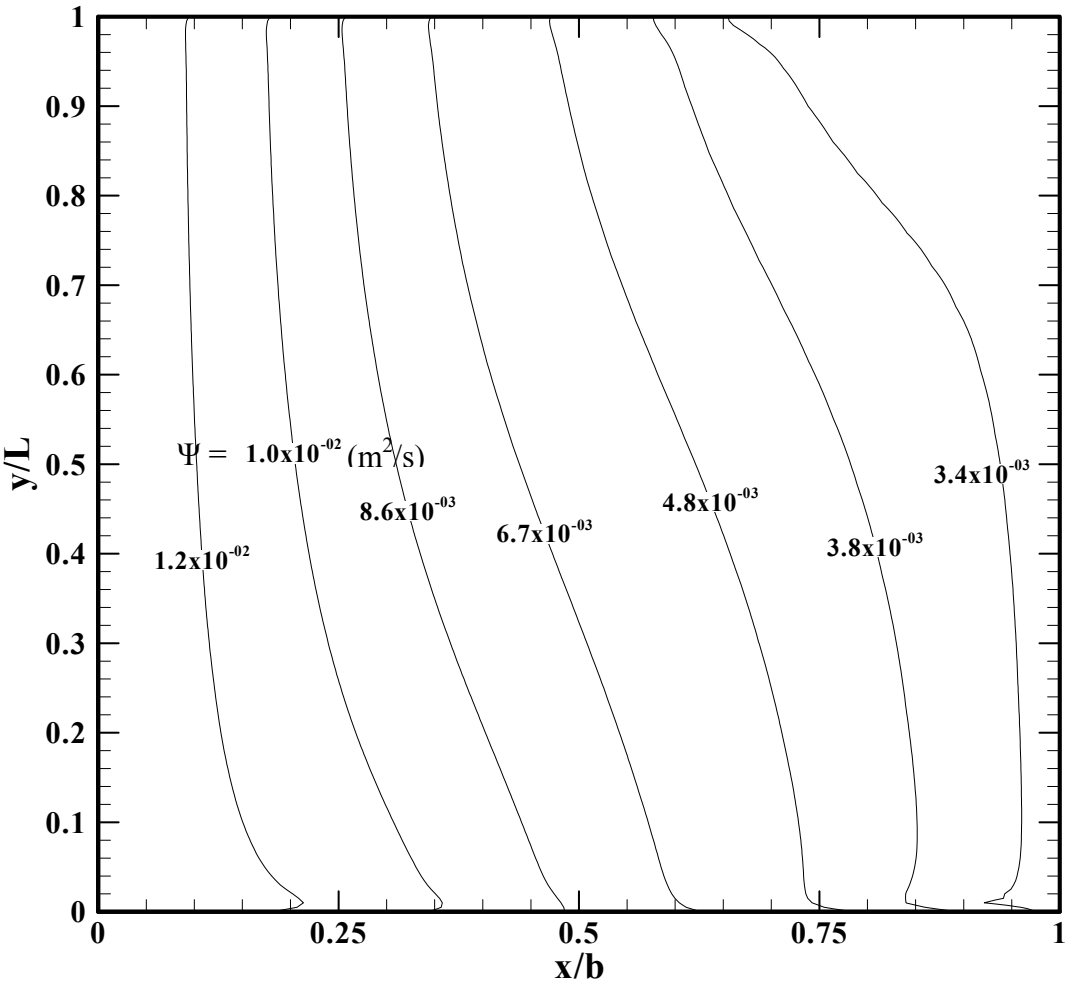

Figure 5.32: Streamlines for extended inlet condition at $Ra_b(b/L) = 7.3x10^3$.

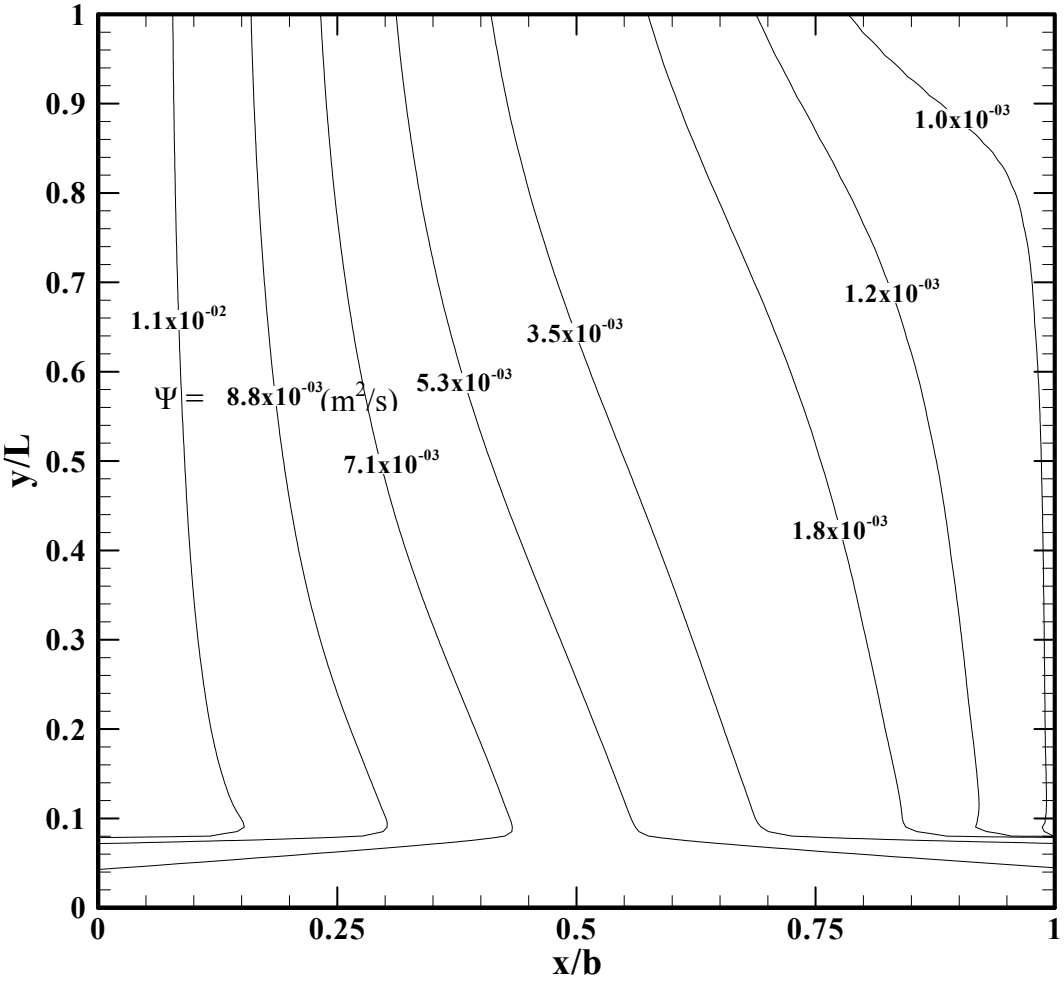

Figure 5.33: Streamlines for radial flow inlet condition at $Ra_b(b/L) = 7.3x10^3$.

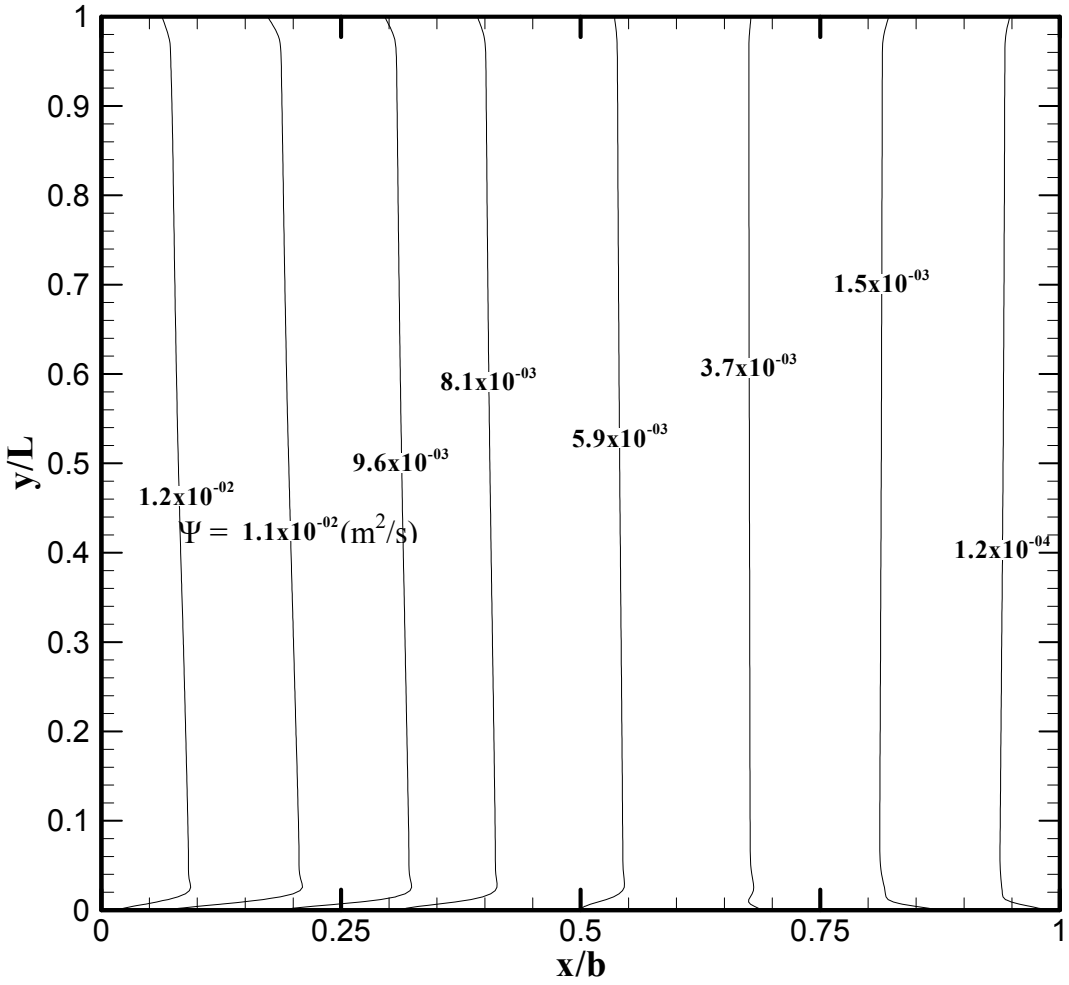

Figure 5.34: Streamlines for uniform inlet velocity condition at $Ra_b(b/L) = 7.3x10^3$.

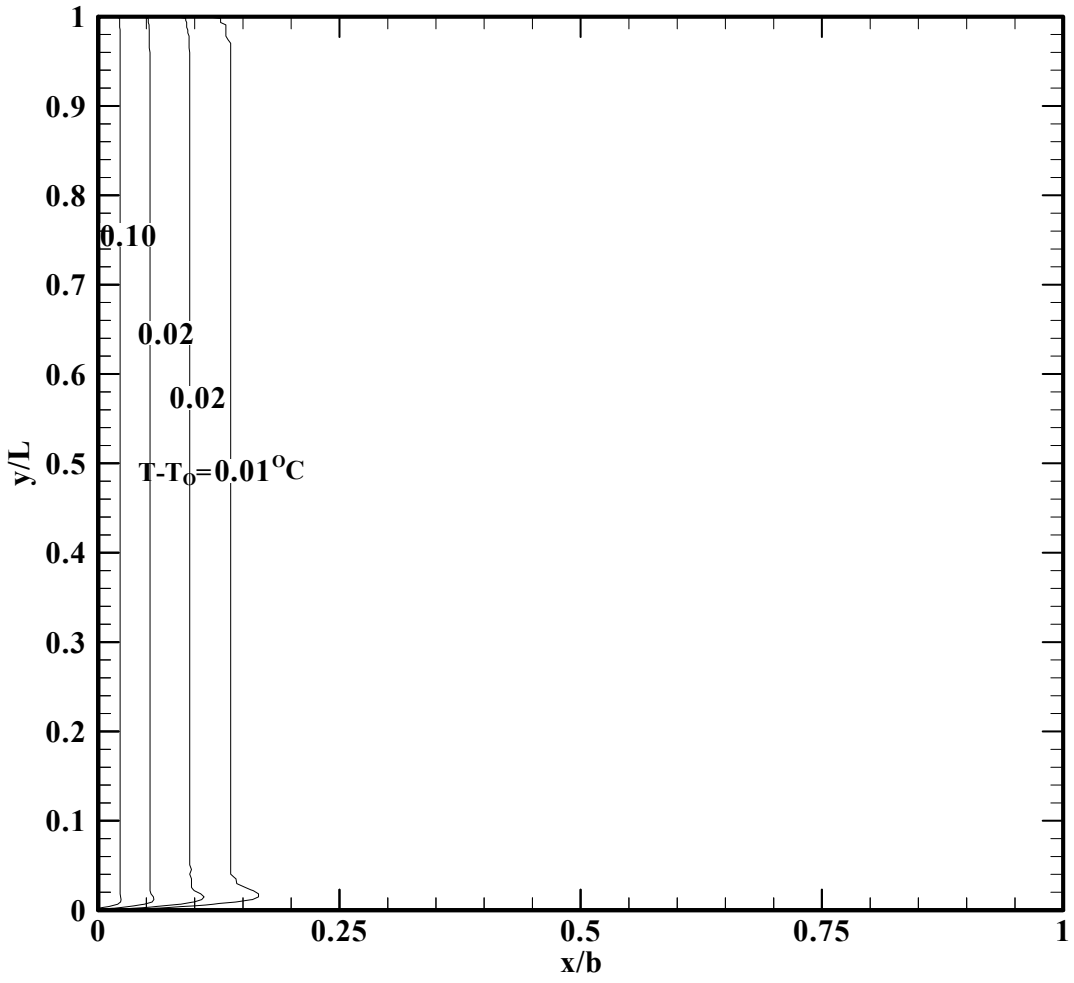

Figure 5.35: Isotherms for uniform inlet pressure condition at $Ra_b(b/L) = 7.3x10^3$.

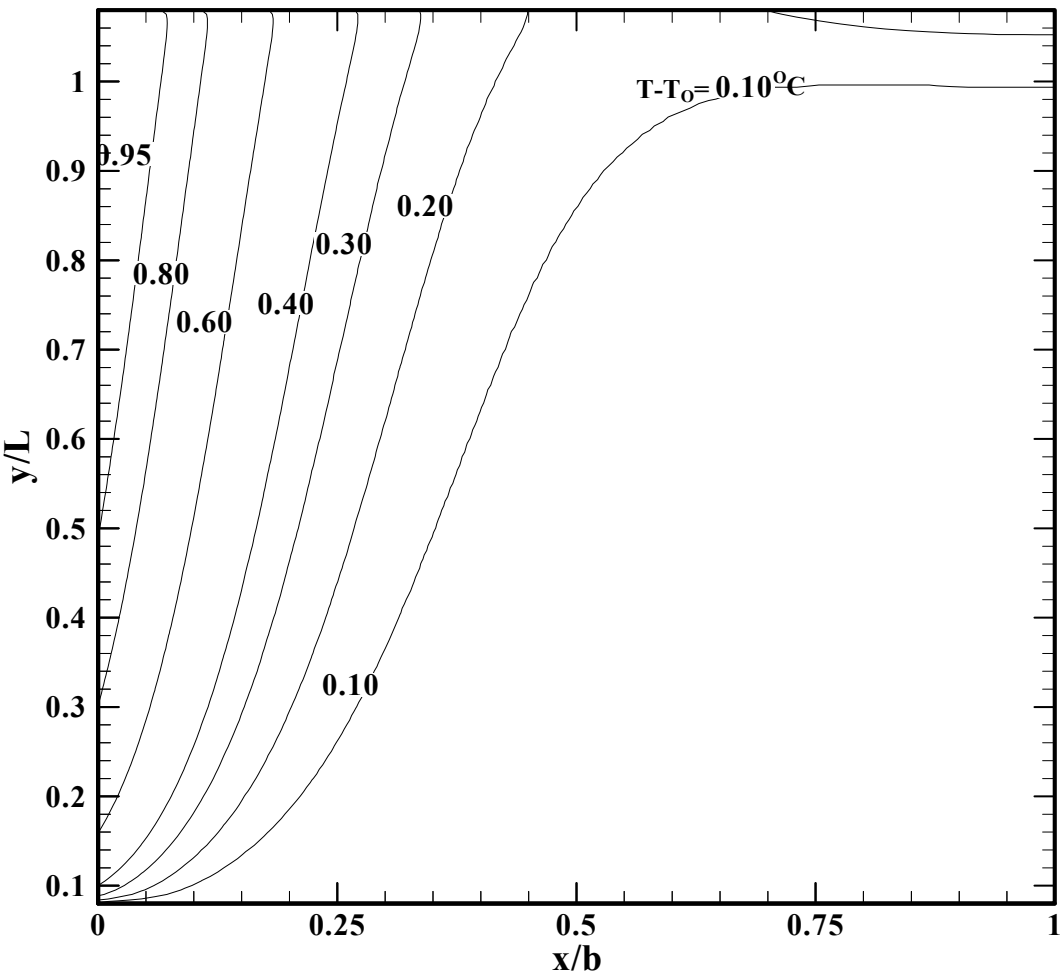

Figure 5.36: Isotherms for extended inlet condition at $Ra_b(b/L) = 7.3x10^3$.

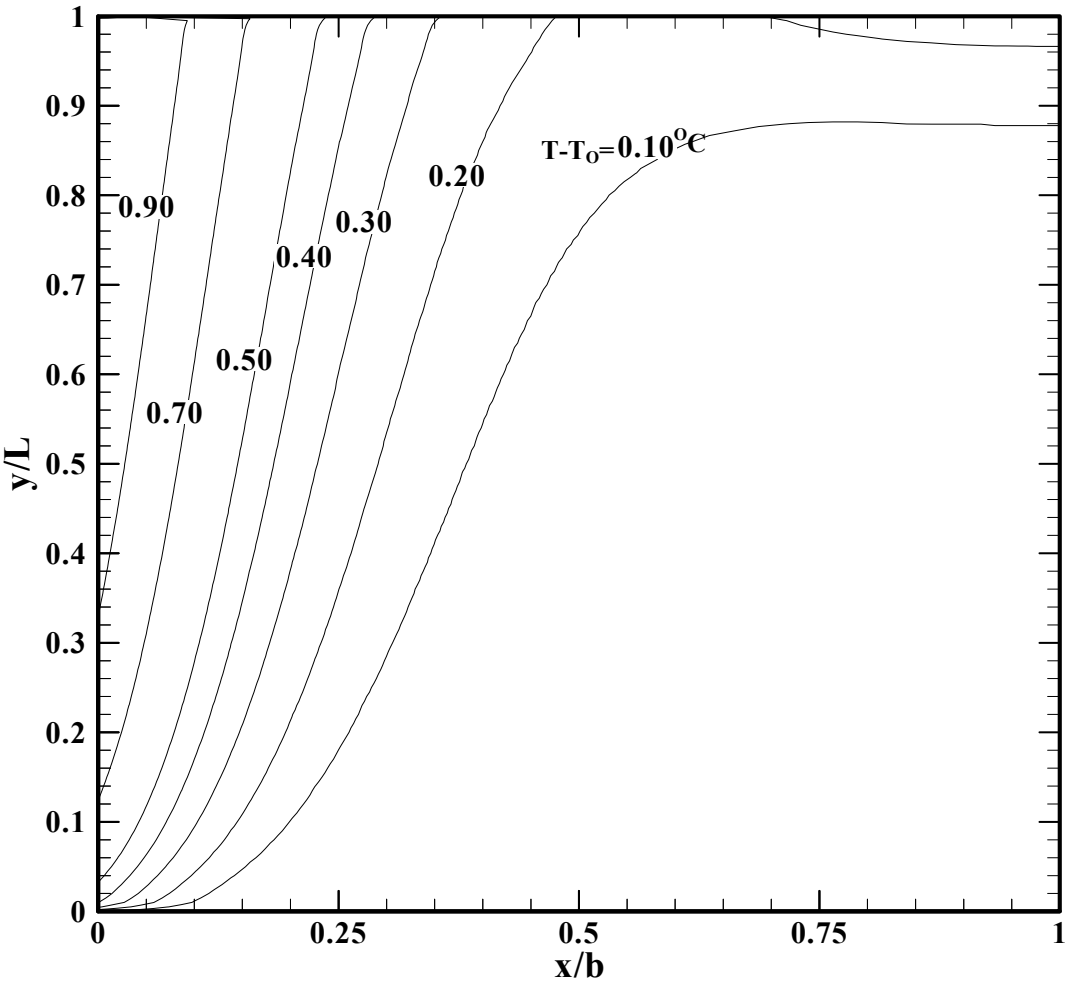

Figure 5.37: Isotherms for radial flow inlet condition at $Ra_b(b/L) = 7.3x10^3$.

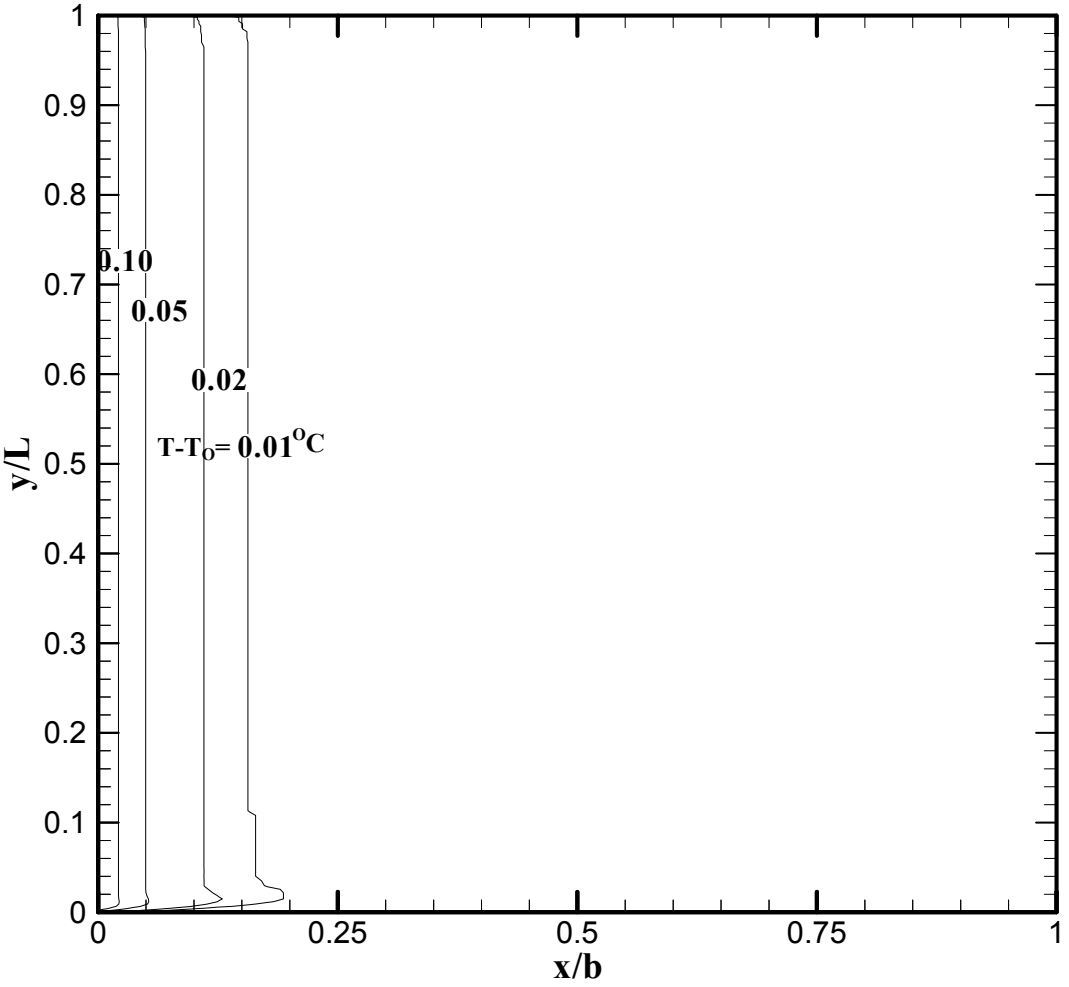

Figure 5.38: Isotherms for uniform inlet velocity condition at $Ra_b(b/L) = 7.3x10^3$.

5.3.2 Influence of different inlet conditions in the turbulent regime

Velocity and Temperature Profiles

The vertical velocity distribution at the inlet section for the four analyzed inlet conditions are shown in Figure 5.39. The uniform pressure inlet condition has high velocity gradient close to both walls. The velocity gradient is less for radial flow inlet. For the extended inlet condition a negative velocity is visible near the wall and this may be attributed to a small vortex formation in that region.

The vertical velocity profiles at sections y/L = 0.77, 0.53 and 0.16 are shown in Figures 5.40-5.42. At all these sections, the mean vertical velocity resulted from the uniform pressure inlet, the extended inlet and uniform inlet velocity are almost the same and they compare well with the experimental data by Miyamoto *et al.* (1986). However, the radial flow inlet condition resulted in a different velocity profile. The comparison between the mean vertical velocity profile at the three different sections and the experimental velocity profile indicates that all inlet conditions have similar velocity profiles but the one closest to experimental data is the uniform pressure inlet condition.

The normalized temperature profiles at the same three sections are shown in Figures 5.43 to 5.45. The temperature profiles for uniform pressure inlet condition are close to experimental data at sections y/L = 0.53 and 0.16 but underpredict by 25% at y/L = 0.77. For radial flow inlet condition, the normalized temperature distributions are underpredicted at all sections due to high flow rates.

Streamlines and Temperature Contours

The streamlines (Ψ) for the four different inlet conditions are shown in Figure 5.46, 5.47, 5.48 and 5.49 at a modified Rayleigh number of 1.5 x10^6. The streamlines

resulting from the uniform pressure inlet and uniform velocity inlet condition shown in Figure 5.46 and 5.49 are similar. However, two small vortices are formed for the extended inlet condition (Figure 5.47) close to walls at inlet.

The isotherms ($T-T_O$) for the above mentioned inlet conditions are shown in Figure 5.50-5.53. The figures indicate that the isotherms for uniform pressure inlet and uniform velocity inlet are similar. However, the isotherms for extended and radial flow inlet conditions (Figure 5.51 and 5.52) are different. Isotherm of 27^OC in radial flow inlet appears till a channel height of y/L = 0.5 whereas for all the other inlet conditions the same isotherm is visible only till a channel height y/L = 0.2. All the inlet conditions studied show a high temperature gradient near the heated wall.

Local Nusselt Number and Velocity Vectors

The local Nusselt number distributions along the heated left wall are shown in Figure 5.54. The difference between the local Nusselt numbers above a channel height of y/L = 0.2 is within a range of 10 to 20%. Velocity vectors from inlet section of channel to height y/L = 0.1 are shown in Figure 5.55 to 5.58 for all the abovementioned inlet conditions. It is clear in Figure 5.54 that the local Nusselt number distribution for radial flow inlet is lowest from inlet section to a channel height y/L = 0.2. This is due to the small velocity close to the wall as shown in Figure 5.57. The extended inlet condition has highest local Nusselt number from inlet section to y/L = 0.2 due to the small region of circulation. The circulation causes localized cooling in vicinity of the wall. This small circulation is clearly visible in the velocity vectors shown in Figure 5.56.

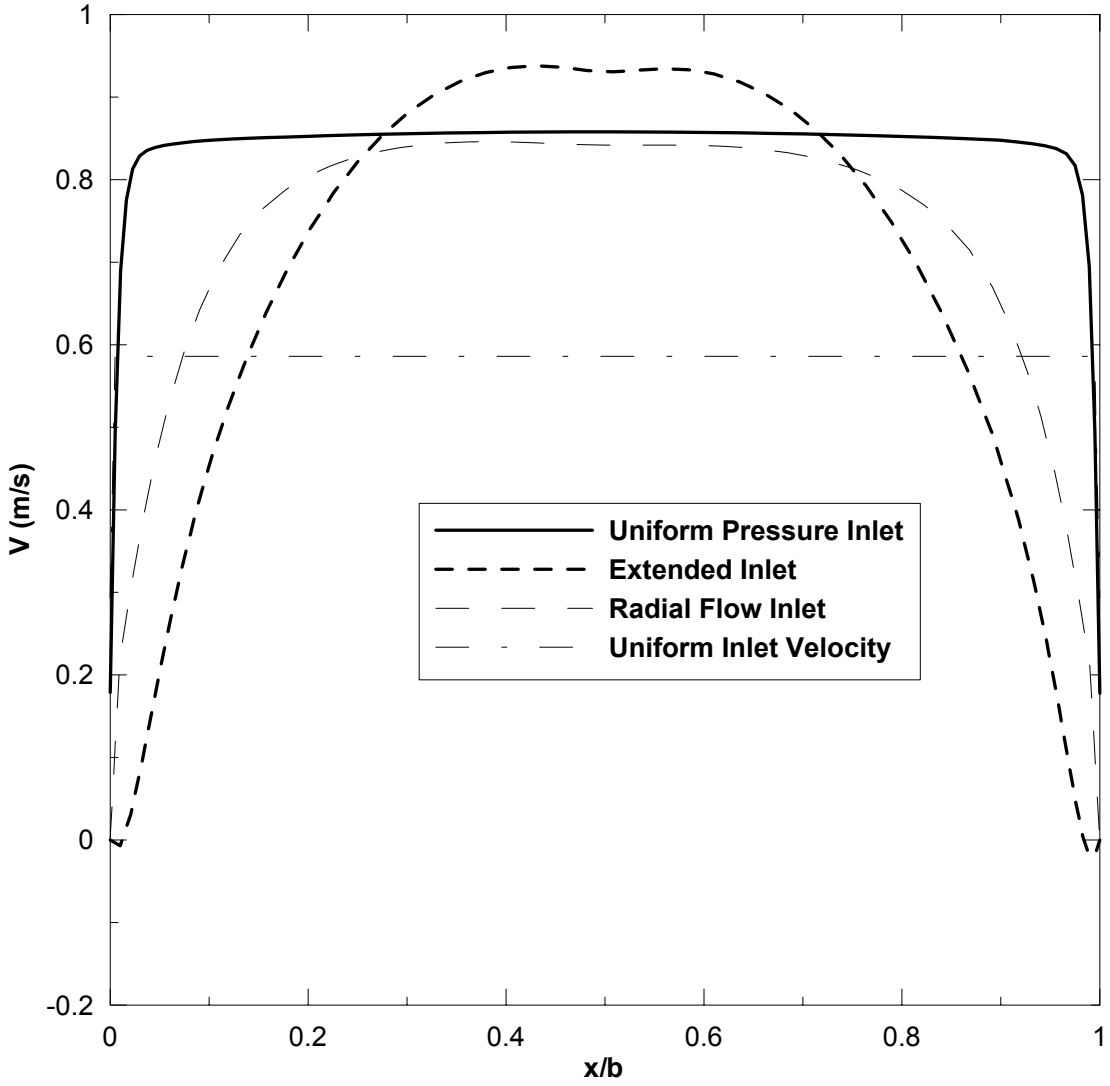

Figure 5.39: Vertical velocity component at inlet section of four different conditions

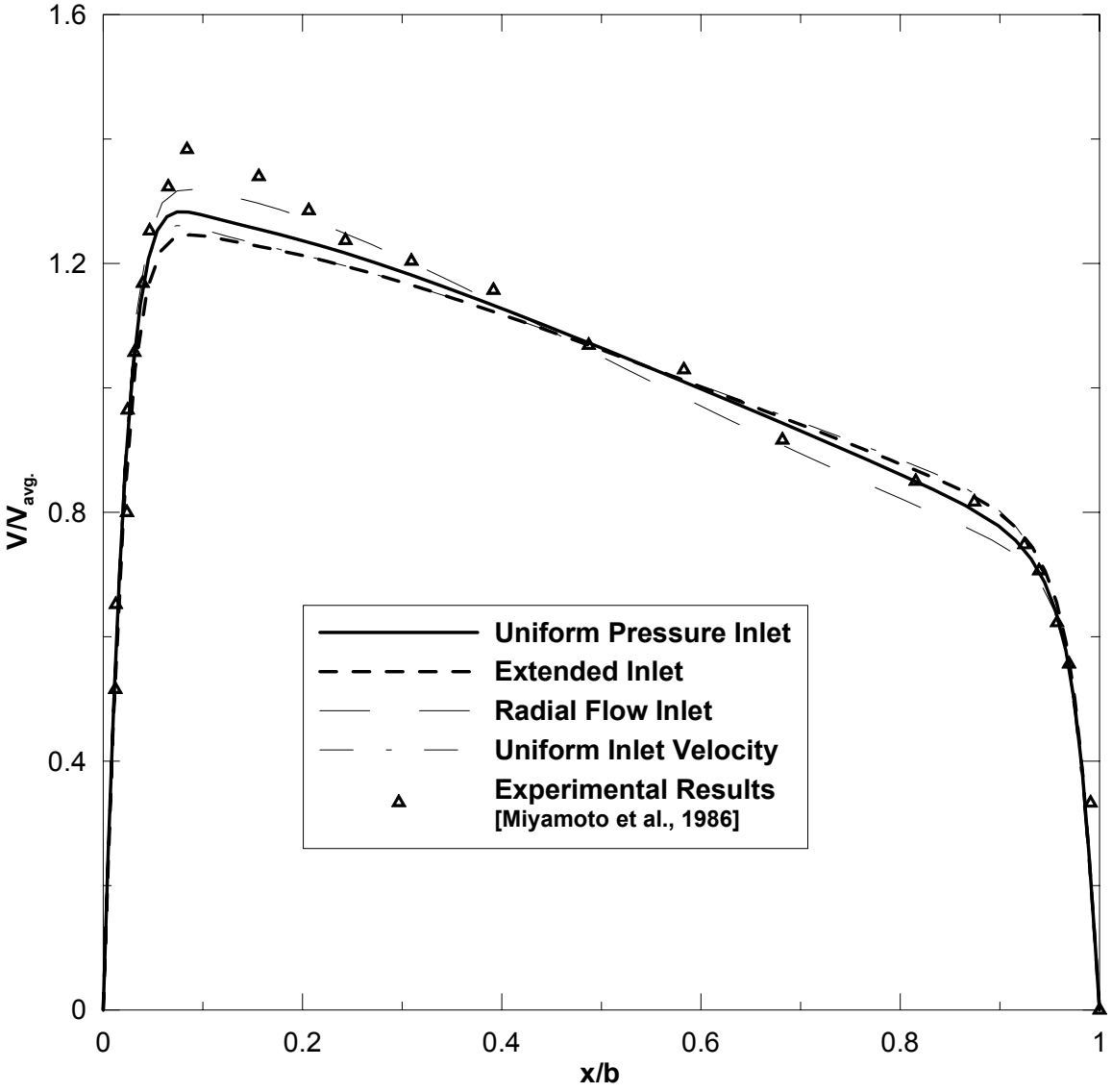

Figure 5.40: Normalized vertical velocity at section y/L = 0.77 from the channel inlet for all inlet conditions by low Re $k-\varepsilon$ M3 turbulence model.

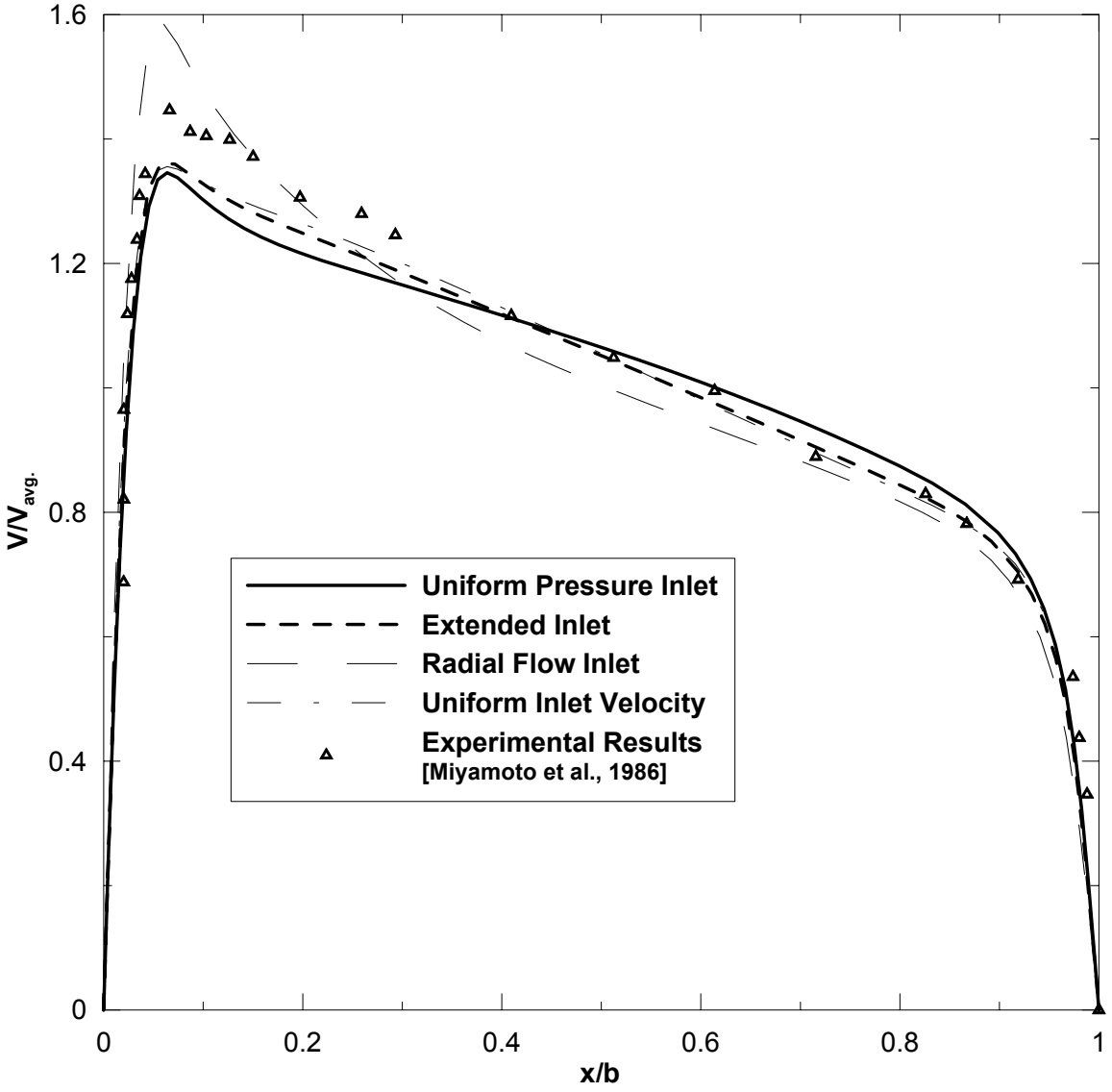

Figure 5.41: Normalized vertical velocity at section y/L = 0.53 from the channel inlet for all inlet conditions by low Re $k-\varepsilon$ M3 turbulence model.

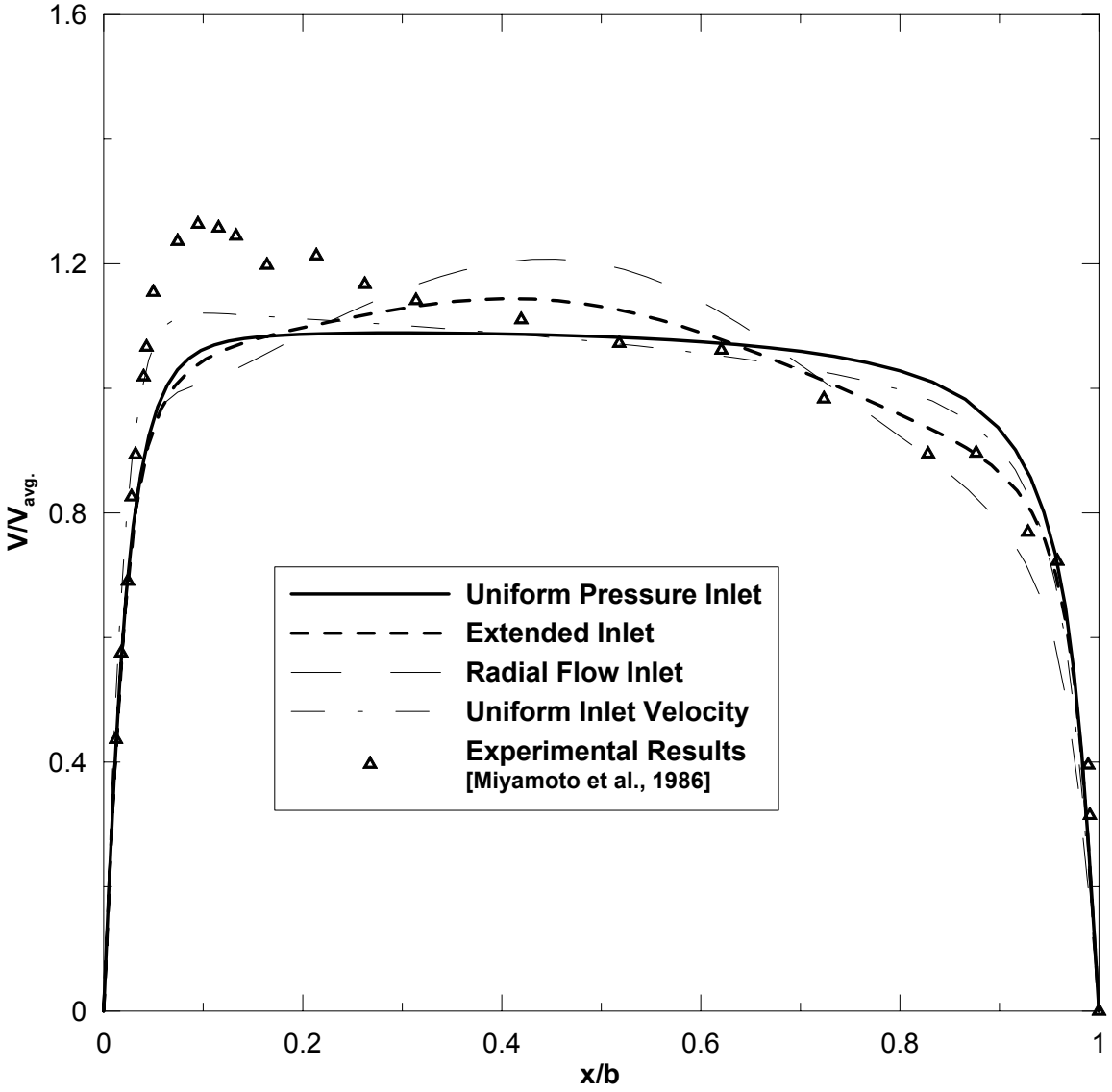

Figure 5.42: Normalized vertical velocity at section y/L = 0.16 from the channel inlet for all inlet conditions by low Re $k-\varepsilon$ M3 turbulence model.

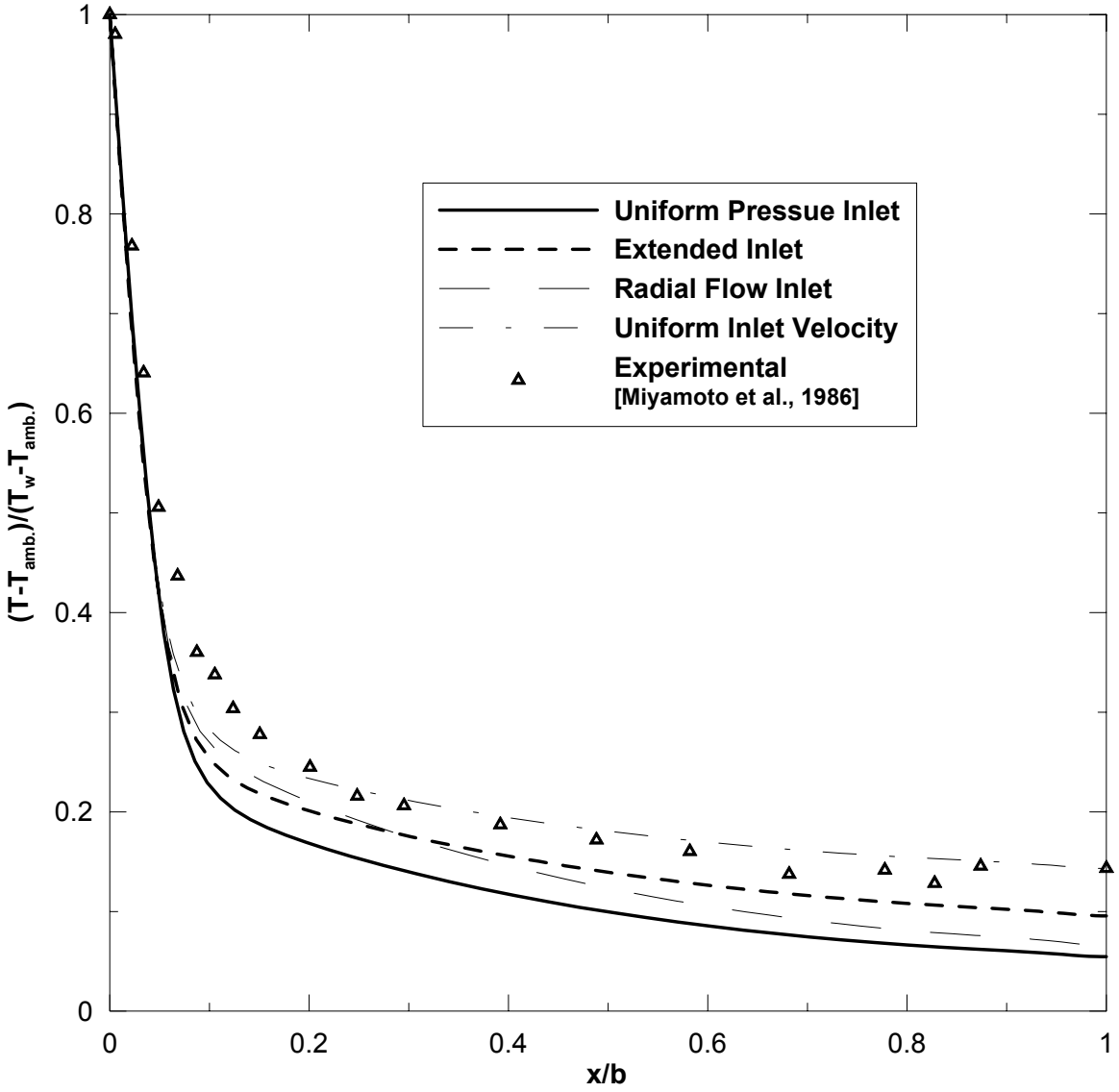

Figure 5.43: Normalized temperature at section y/L = 0.77 from the channel inlet for all inlet conditions by low Re $k-\varepsilon$ M3 turbulence model.

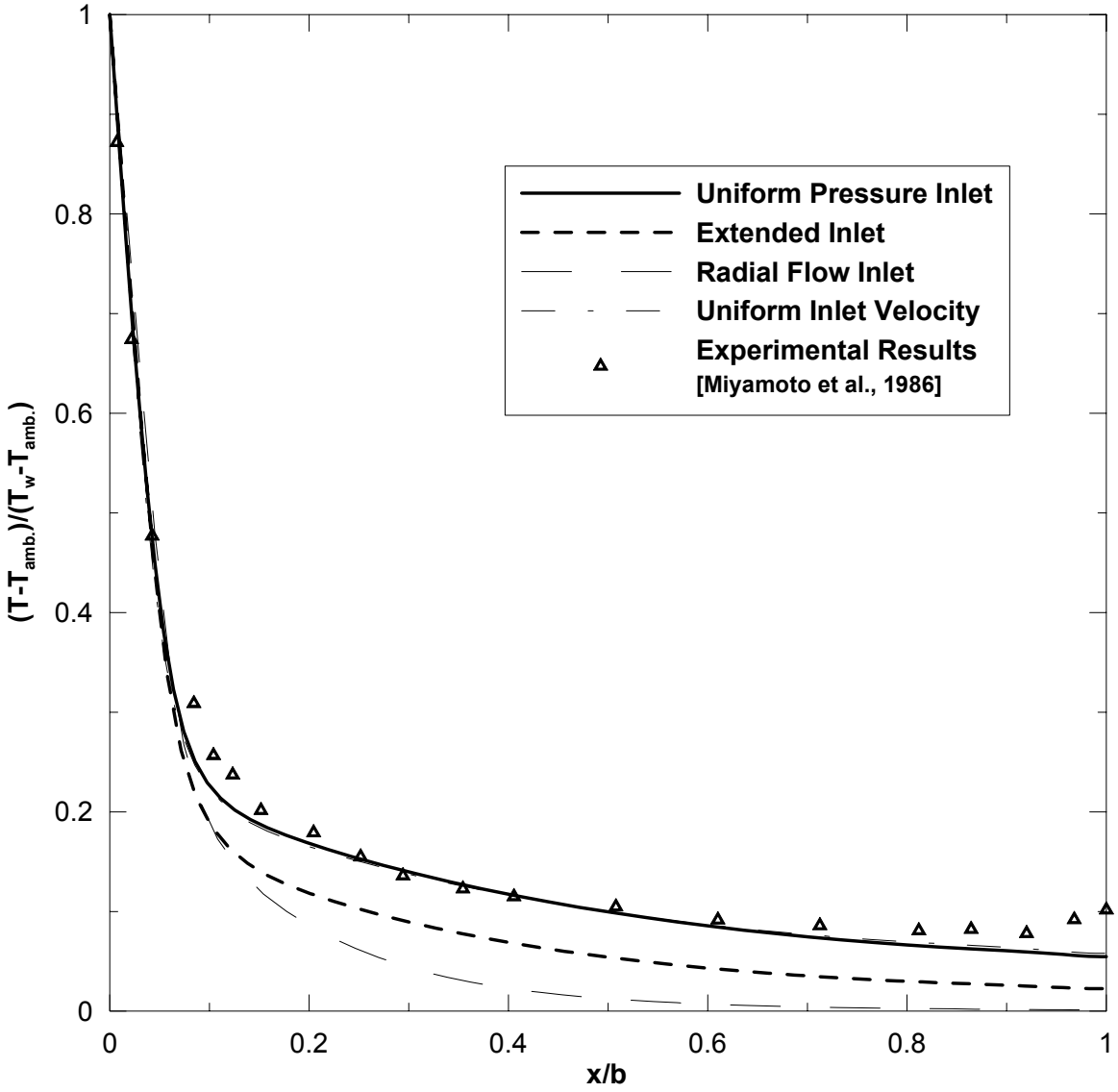

Figure 5.44: Normalized temperature at section y/L = 0.53 from the channel inlet for all inlet conditions by low Re $k-\varepsilon$ M3 turbulence model.

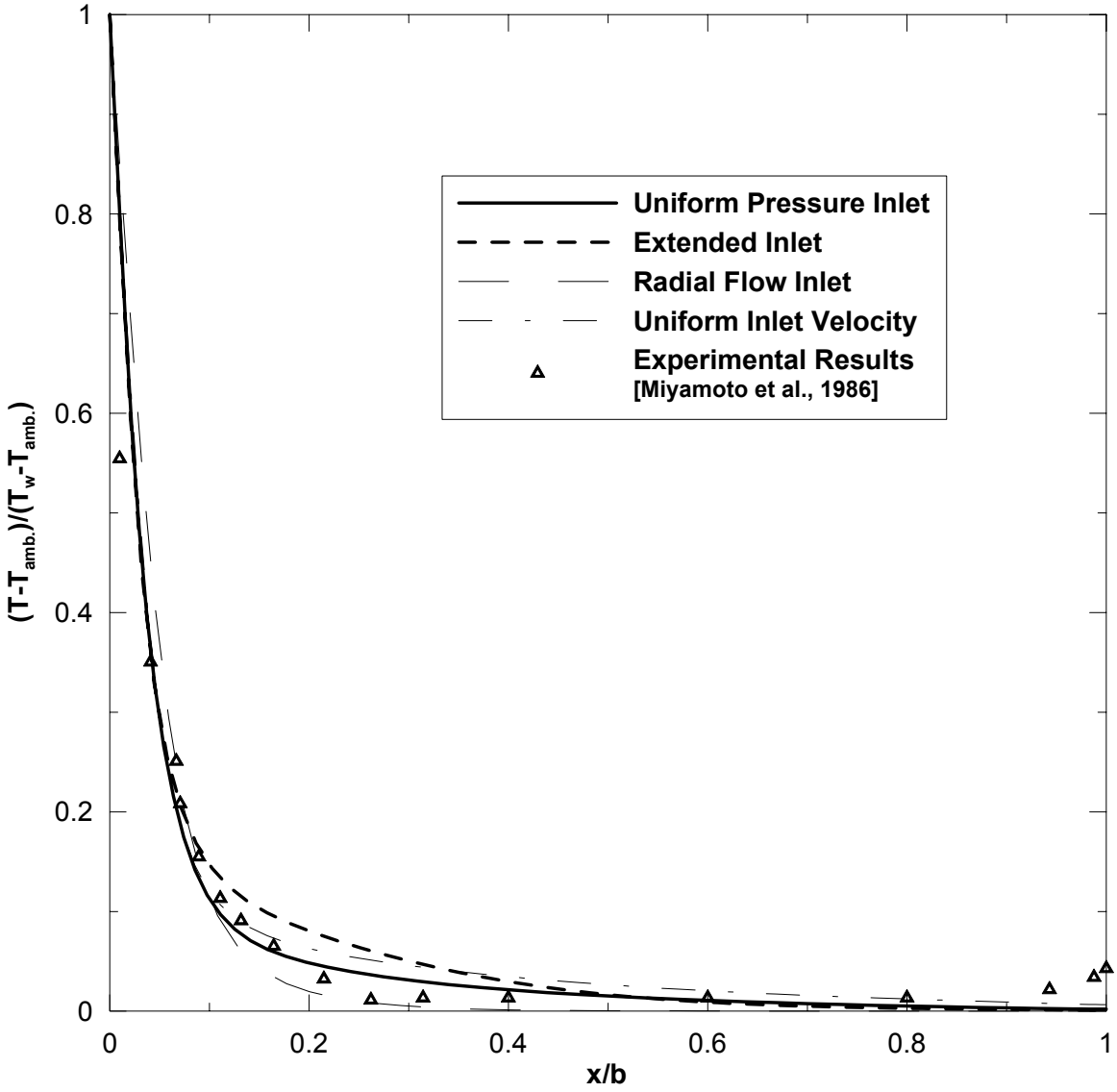

Figure 5.45: Normalized temperature at section y/L = 0.16 from the channel inlet for all inlet conditions by low Re $k-\varepsilon$ M3 turbulence model.

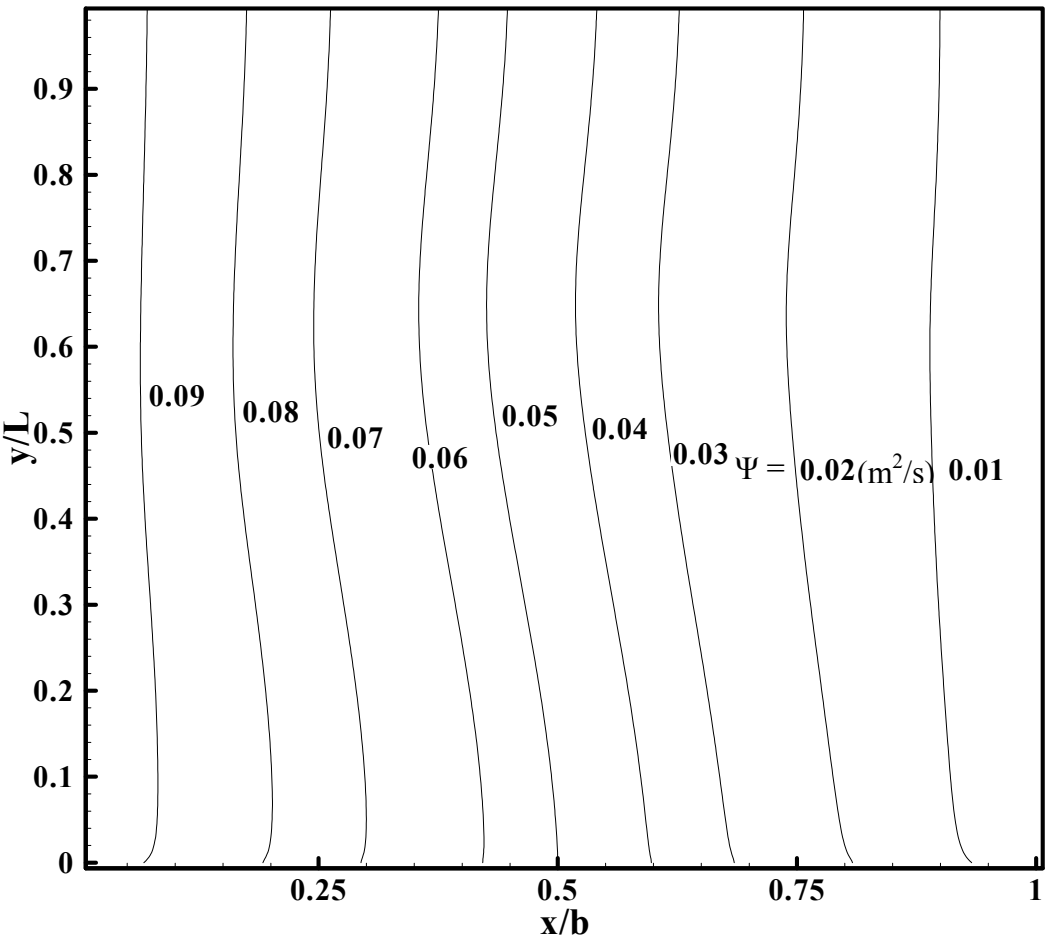

Figure 5.46: Streamlines for uniform pressure inlet condition

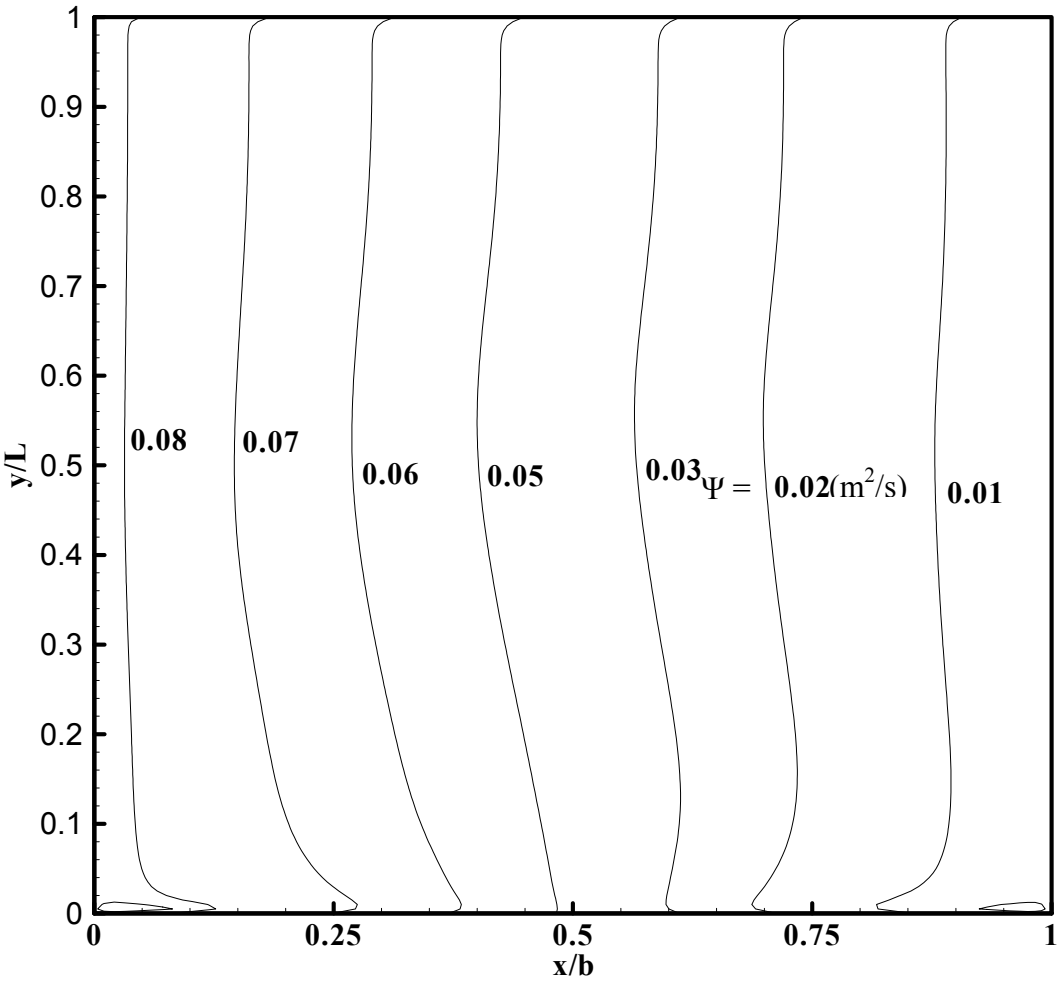

Figure 5.47: Streamlines for extended inlet condition

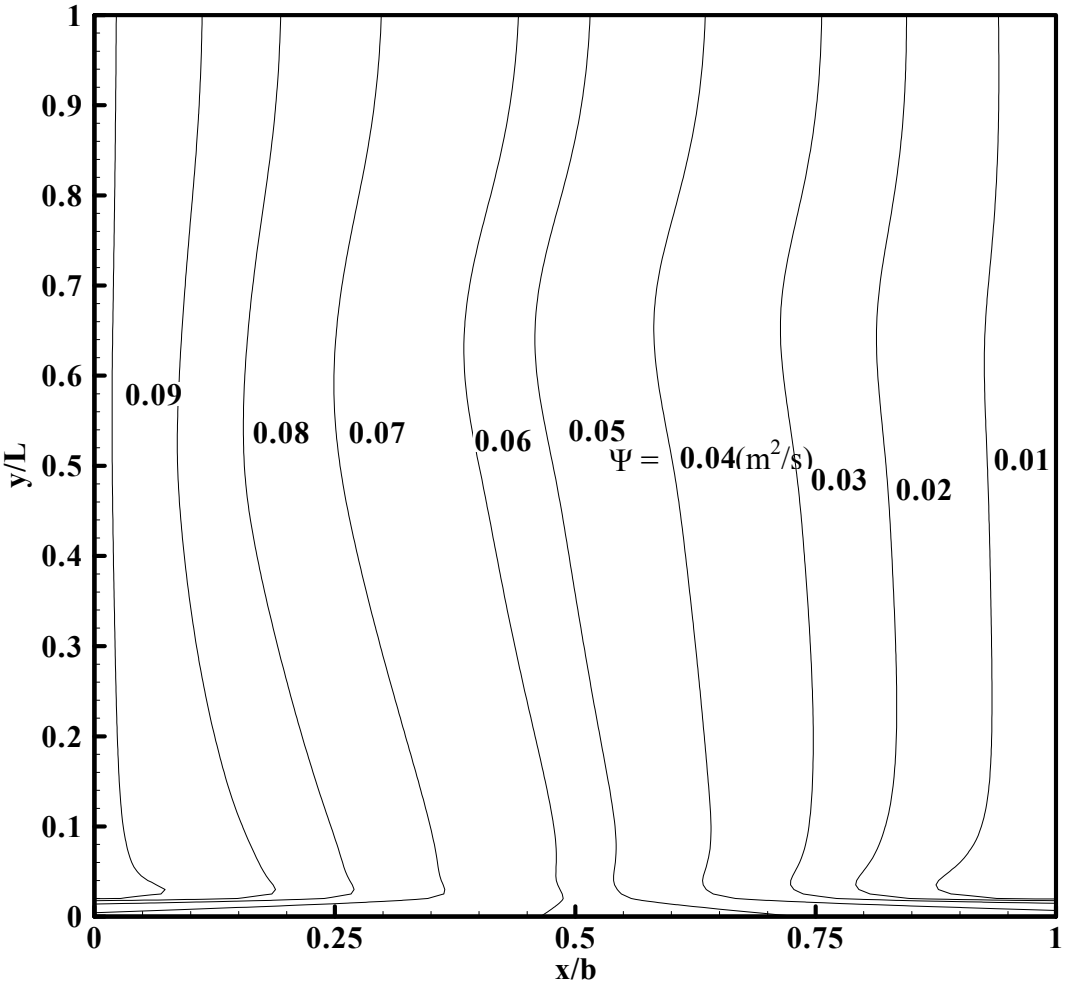

Figure 5.48: Streamlines for radial flow inlet condition

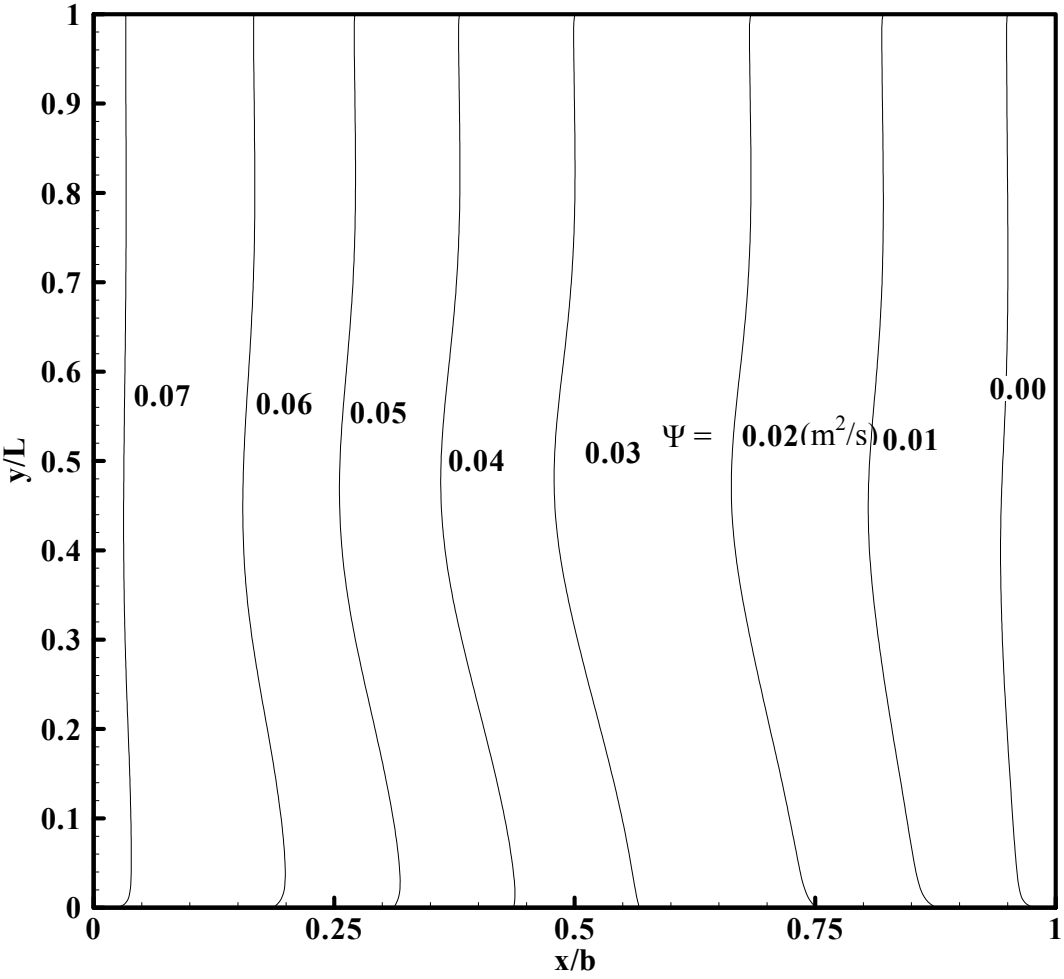

Figure 5.49: Streamlines for uniform inlet velocity condition

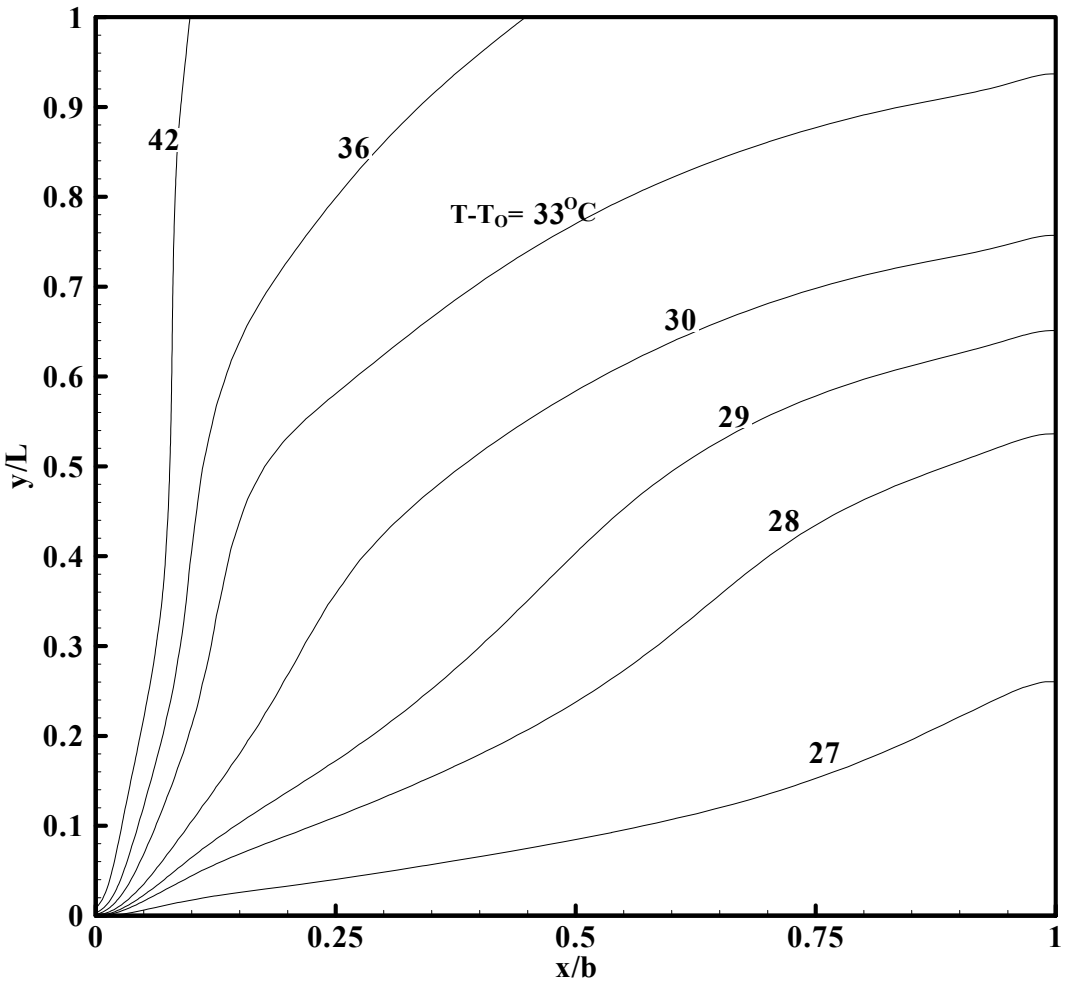

Figure 5.50: Isotherms for uniform inlet pressure condition

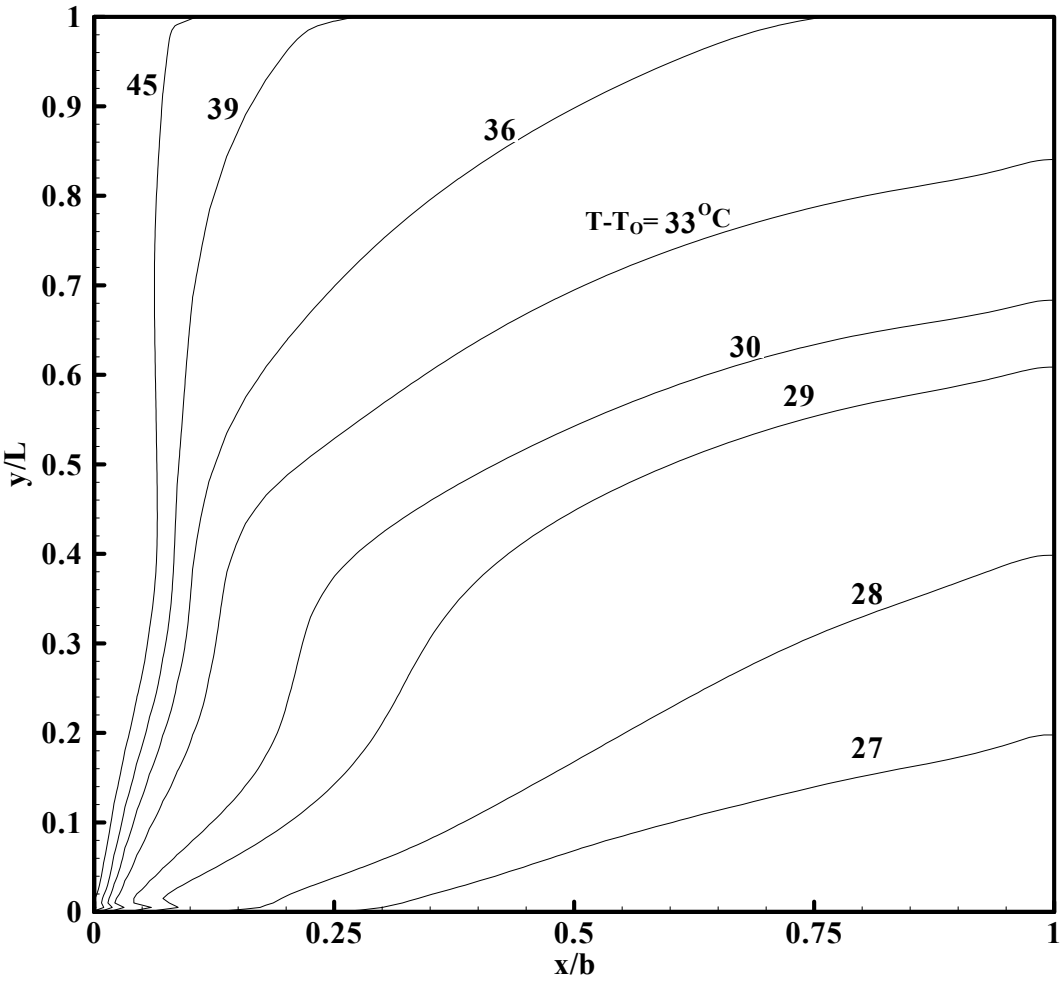

Figure 5.51: Isotherms for extended inlet condition

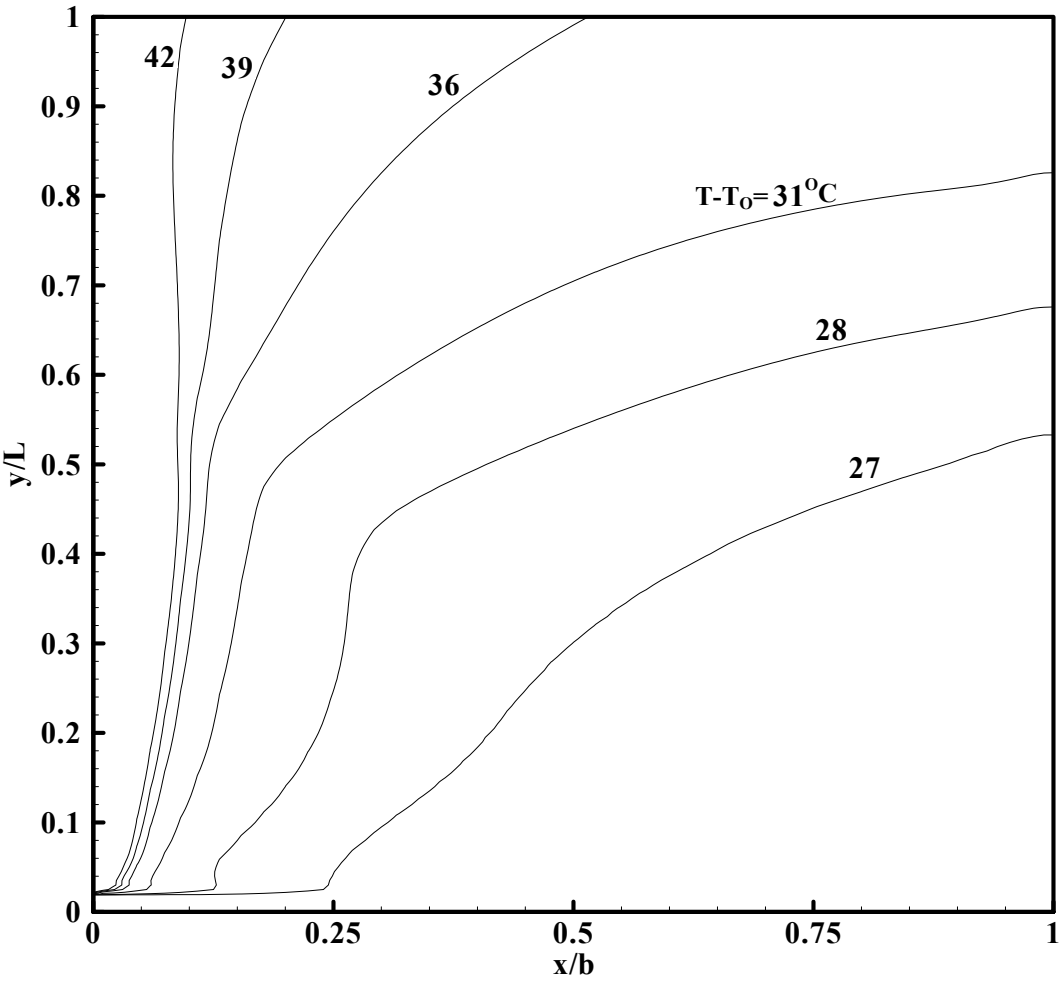

Figure 5.52: Isotherms for radial flow inlet condition

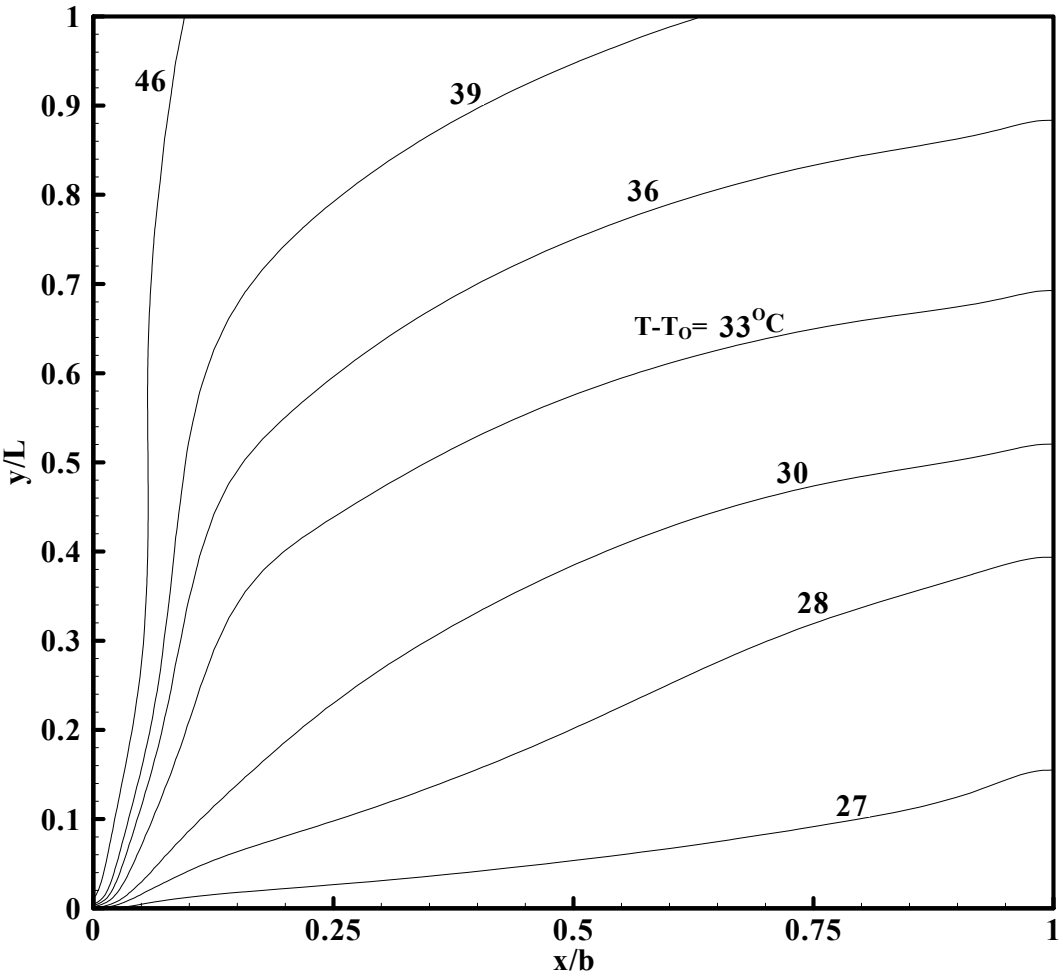

Figure 5.53: Isotherms for uniform inlet velocity condition

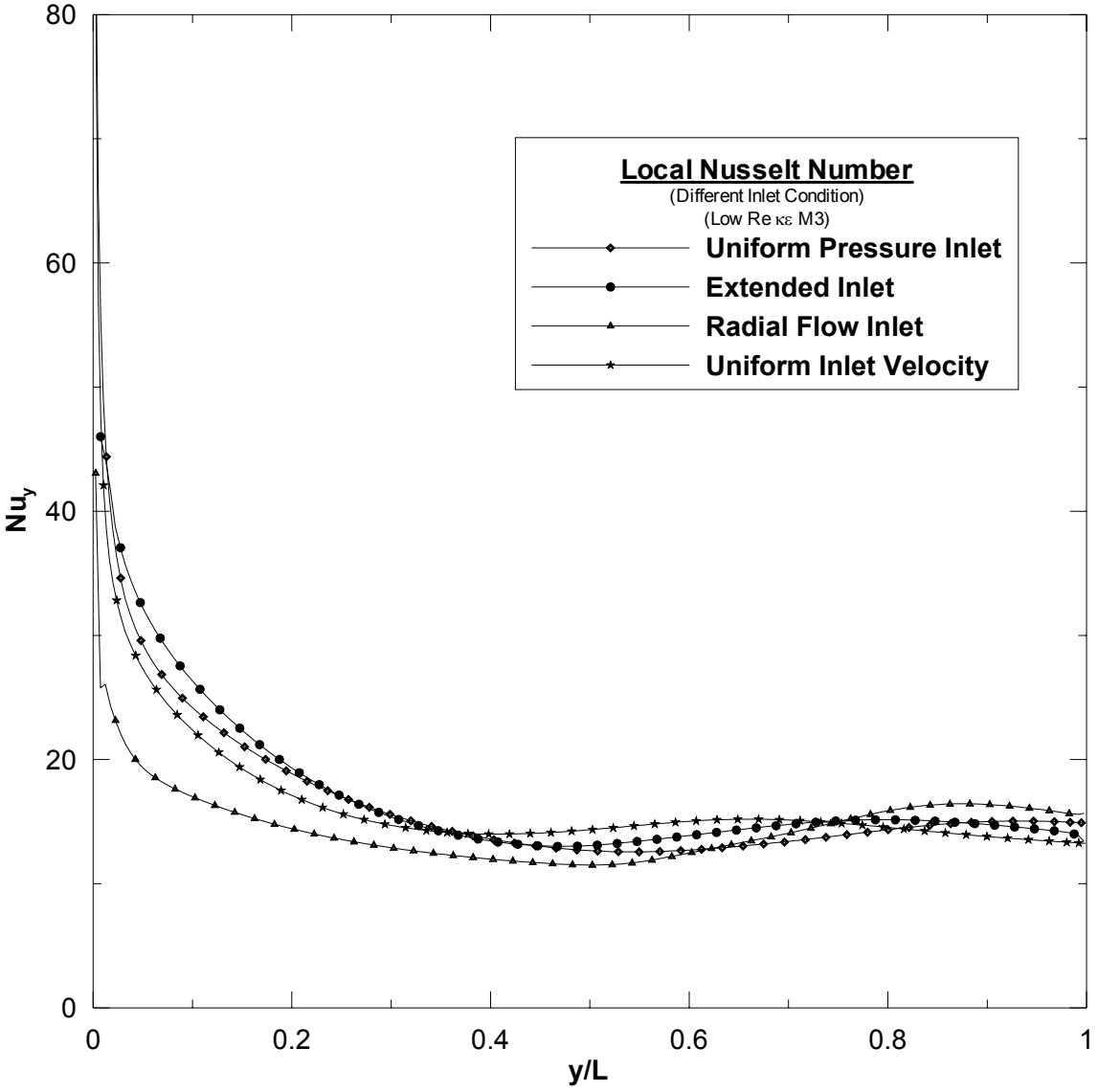

Figure 5.54: Local Nusselt number distribution along a heated wall for low Re $k-\varepsilon$ M3 turbulence model.

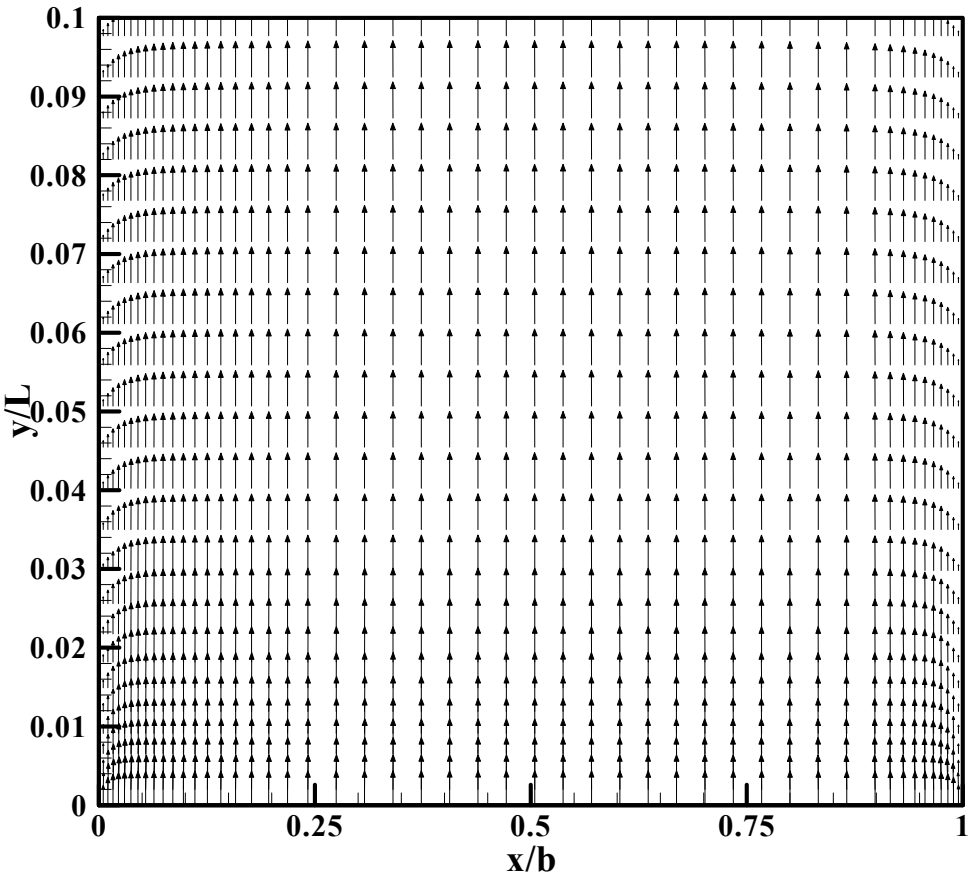

Figure 5.55: Velocity vectors at the inlet region for uniform pressure inlet

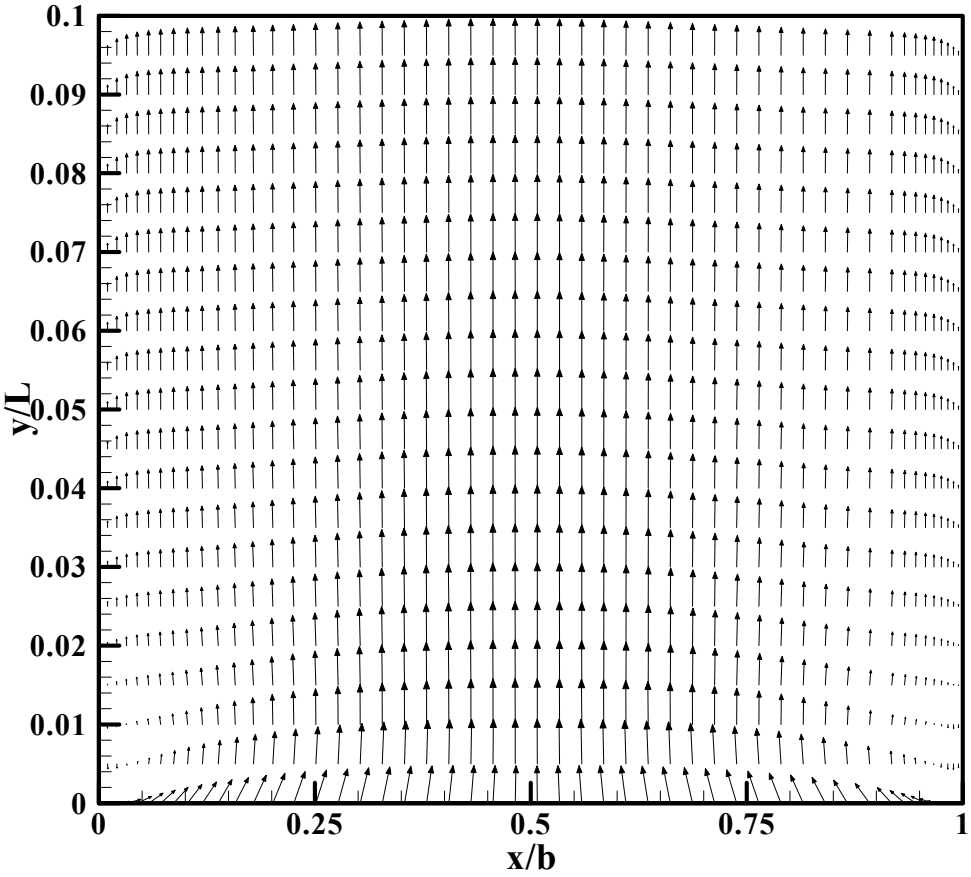

Figure 5.56: Velocity vectors at the inlet region for extended inlet condition.

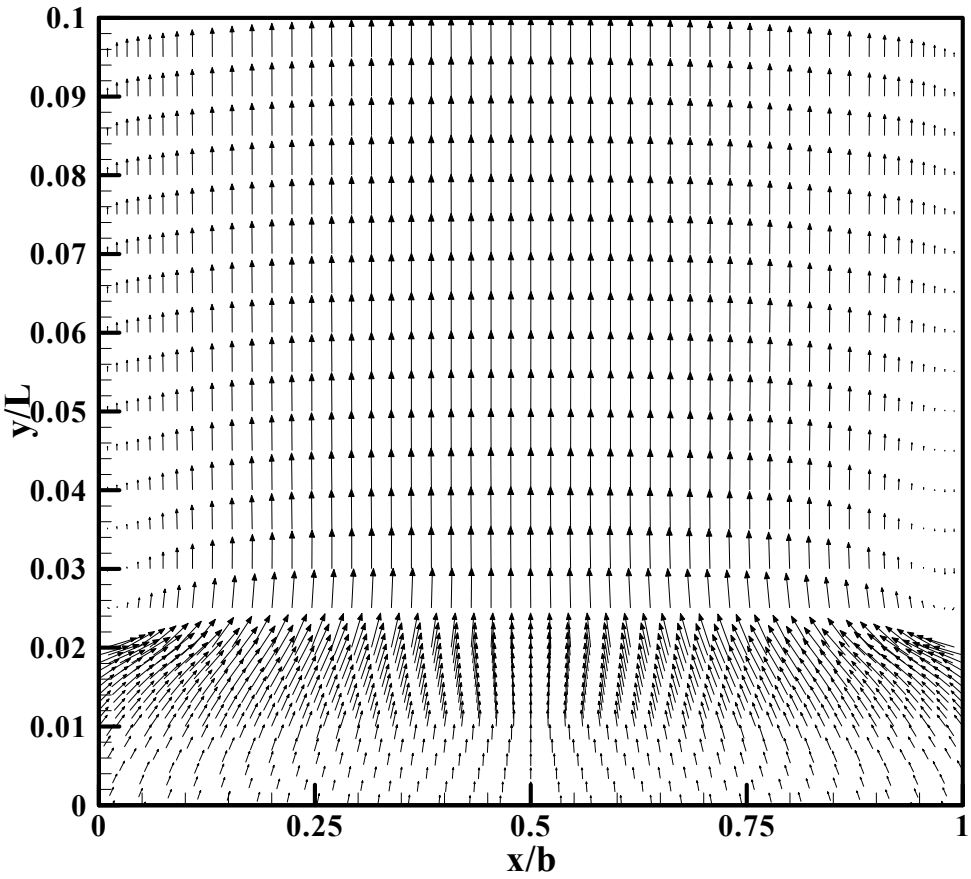

Figure 5.57: Velocity vectors at the inlet region for radial flow inlet condition.

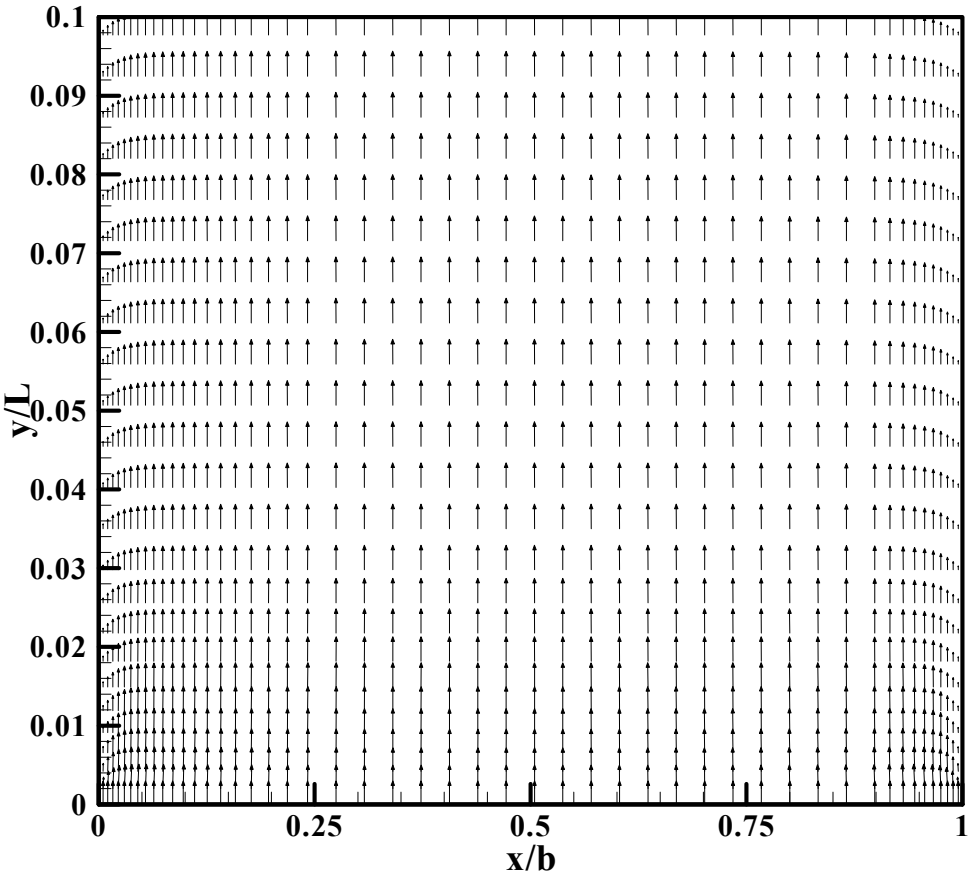

Figure 5.58: Velocity vectors at the inlet region for uniform inlet velocity condition.

5.4 Influence of Rayleigh number

5.4.1 Influence of Rayleigh number on the Laminar flow regimes

In this study, the modified Rayleigh number (Ra_m) range 50 to $3x10^4$ has been covered for symmetrically heated isothermal vertical surfaces. The aspect ratio of the channel was kept constant (L/b = 12). Figure 5.59 shows the variation of the average Nusselt number versus the modified Rayleigh for vertical parallel-plate channel. It can be noted that the average Nusselt number increases with the increase of Rayleigh number.

To study the influence of Rayleigh number on the flow field and heat transfer characteristics, the vertical velocity and temperature profiles as well as the isotherms are presented for four different Rayleigh numbers.

The variation of the mean vertical velocity across the channel at different channel cross-sections (y/L = 0, 0.5, 1.0) are plotted for a specific value of the modified Rayleigh number (Ra_m) and shown in Figure 5.60-5.63. The vertical velocity profile in Figure 5.60 shows fully developed flow at the channel exit section when Ra_m = 80. However, as Rayleigh number increases, two velocity peaks occur at the same section as shown in Figures 5.61-5.63. These vertical velocity peaks become sharp and move towards the channel walls with the increase of the modified Rayleigh number (Ra_m).

The vertical velocity distributions across the channel are plotted in Figure 5.64 at section y/L = 0.5 and in Figure 5.65at section y/L = 1.0 for different values of Ra_m. It can be noted that the dimensional vertical velocity increases as the Rayleigh number

increases as expected. Accordingly, one would expect the mass flow rate to increase with the increase of Ra_m.

Figures 5.66-5.69 shows the dimensionless temperature distribution across the channel for four different modified Rayleigh numbers (Ra_m = 80, 3040, 7865 and 15732). These are plotted in Figure 5.70 at channel mid-plane (y/L =0.5) and in Figure 5.71 at channel exit section (y/L = 1.0). It can be noted that the dimensionless temperature decreases in the core region as the Rayleigh number increases.

Figures 5.72-5.75 show the isotherms (θ) for modified Rayleigh numbers 80, 3040, 7865 and 15732. These plots show that at low Rayleigh number the flow in Figure 5.72 and 5.73 gets heated in the core region from inlet section of channel while at moderate Rayleigh numbers (Figure 5.74 and 5.75), the flow is heated in a layer close to the walls. It can be seen that the heated layer thickness decreases as the modified Rayleigh number increases.

Figure 5.76 shows the variation of local Nusselt number along the channel for four different Ra_m. It can be seen that as the modified Rayleigh number increases the local Nusselt number also increases over the entire length of the channel.

This is expected since the increase in Rayleigh number results in an increase of the flow velocity which tends to a reduction in the thermal layer thickness.

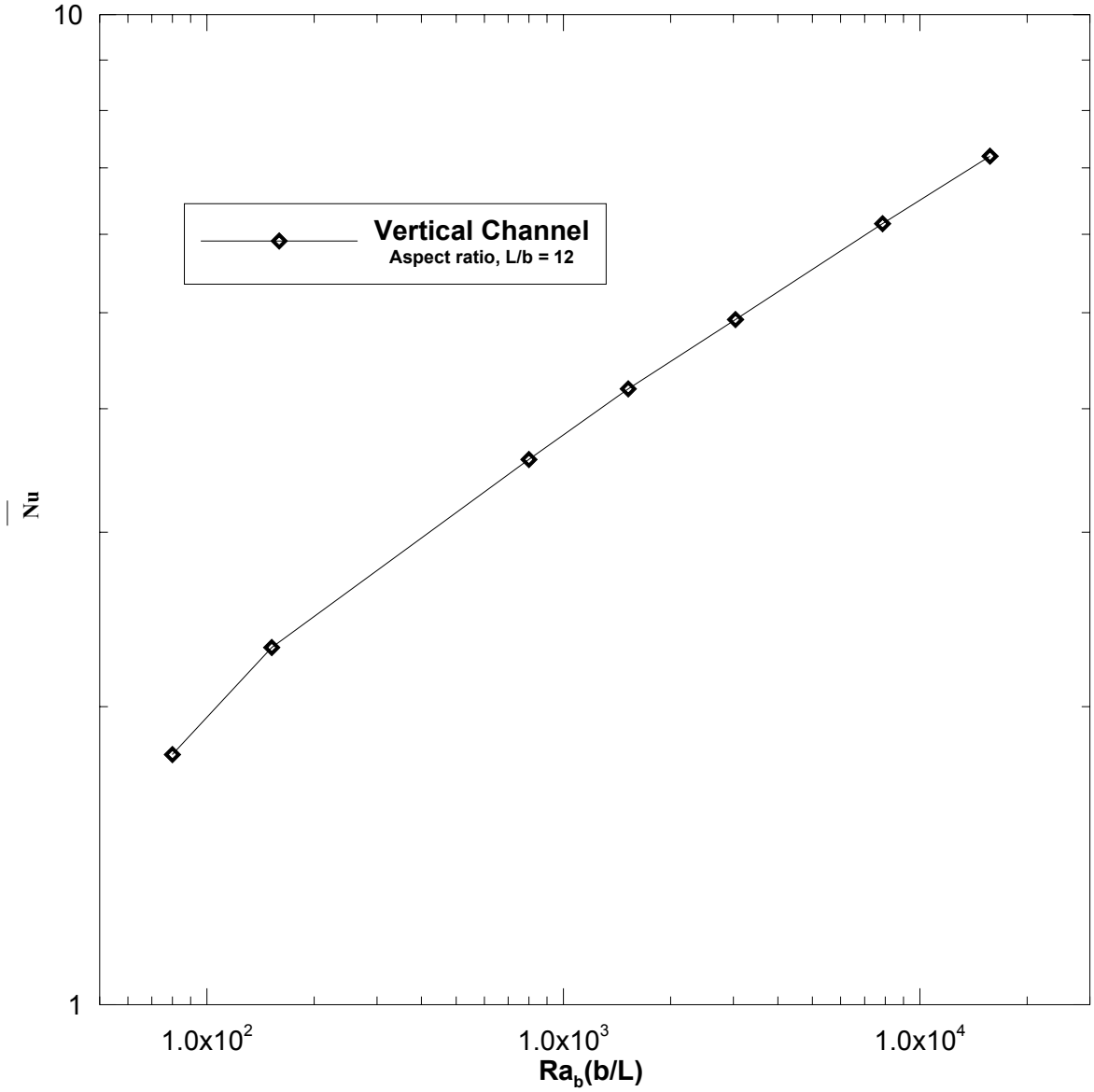

Figure 5.59: The variation of the average Nusselt number versus the modified Rayleigh number in laminar regime for vertical parallel-plate channel

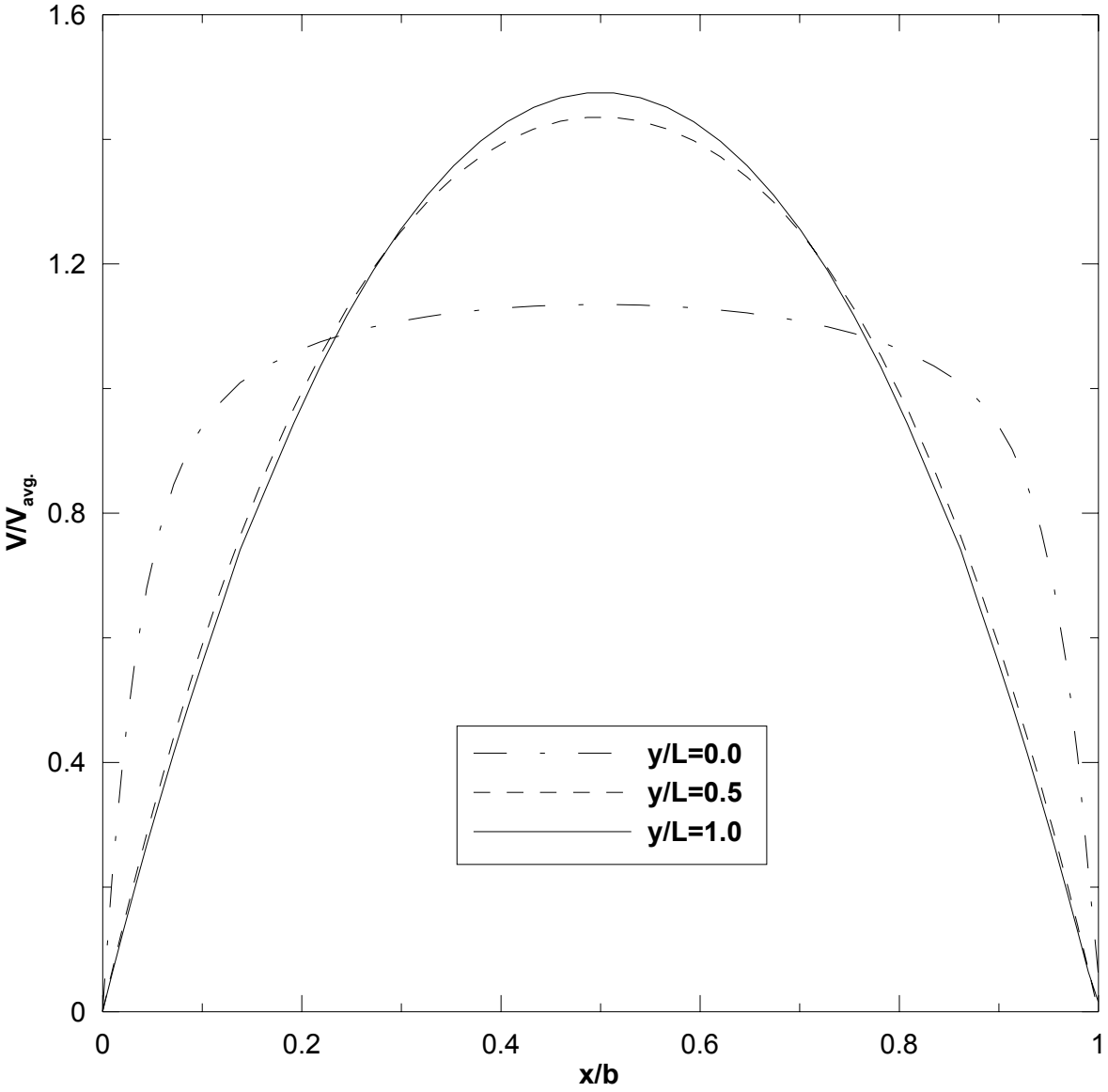

Figure 5.60: Mean vertical velocity distribution at different cross-section in the channel for $Ra_b(b/L) = 80$.

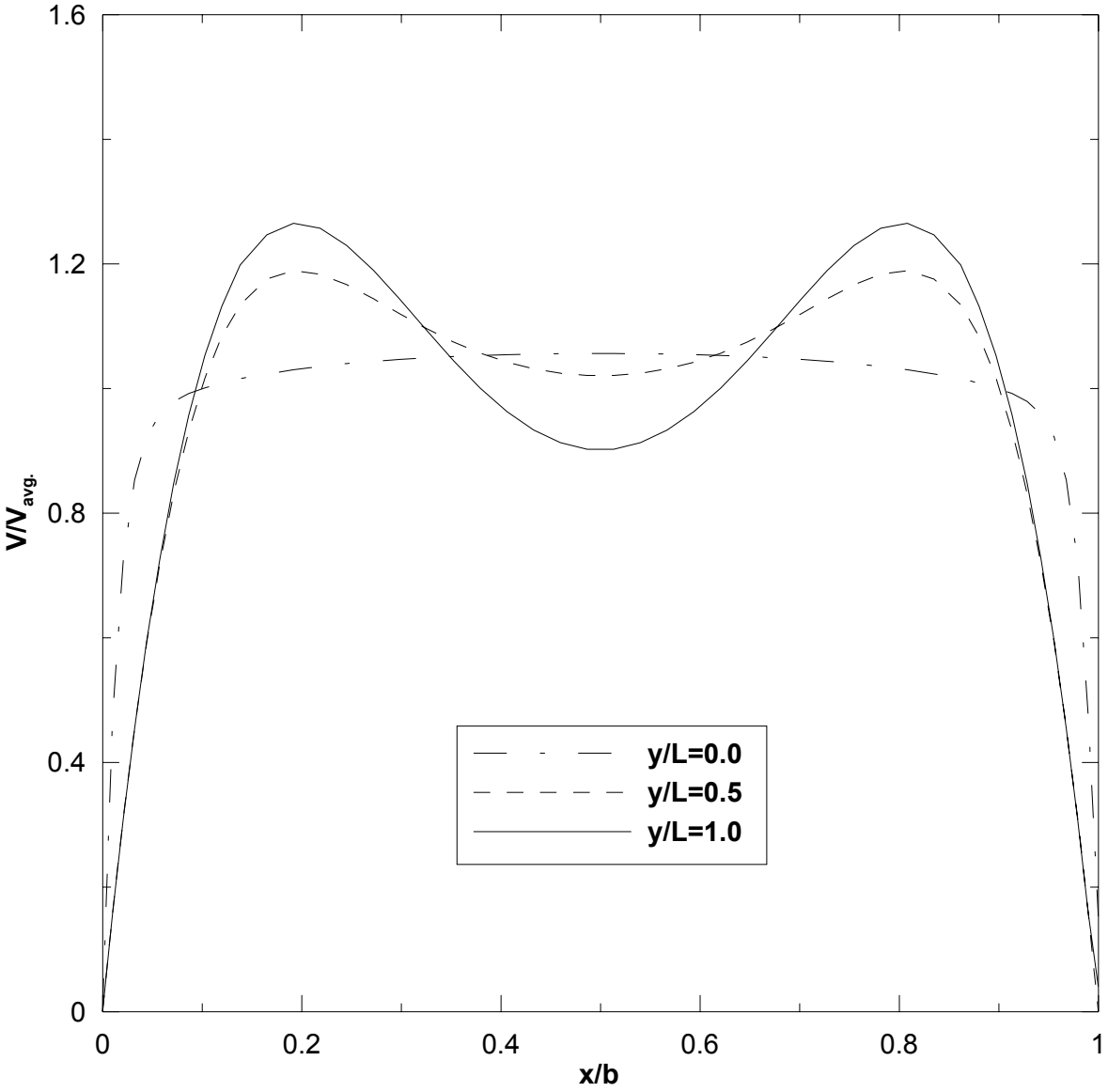

Figure5.61: Mean vertical velocity distribution at different cross-section in the channel for $Ra_b(b/L) = 3040$.

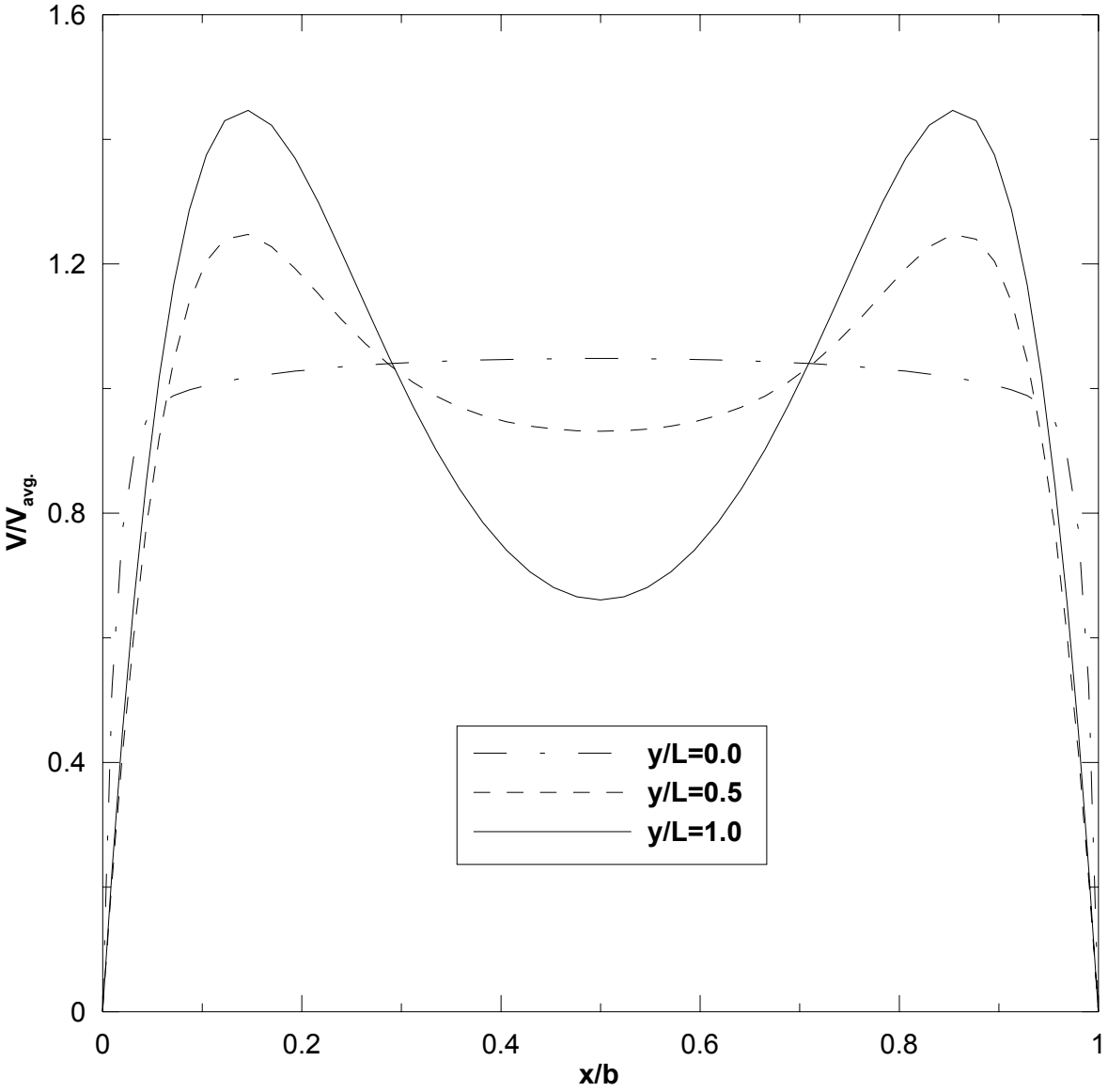

Figure5.62: Mean vertical velocity distribution at different cross-section in the channel for $Ra_b(b/L) = 7865$.

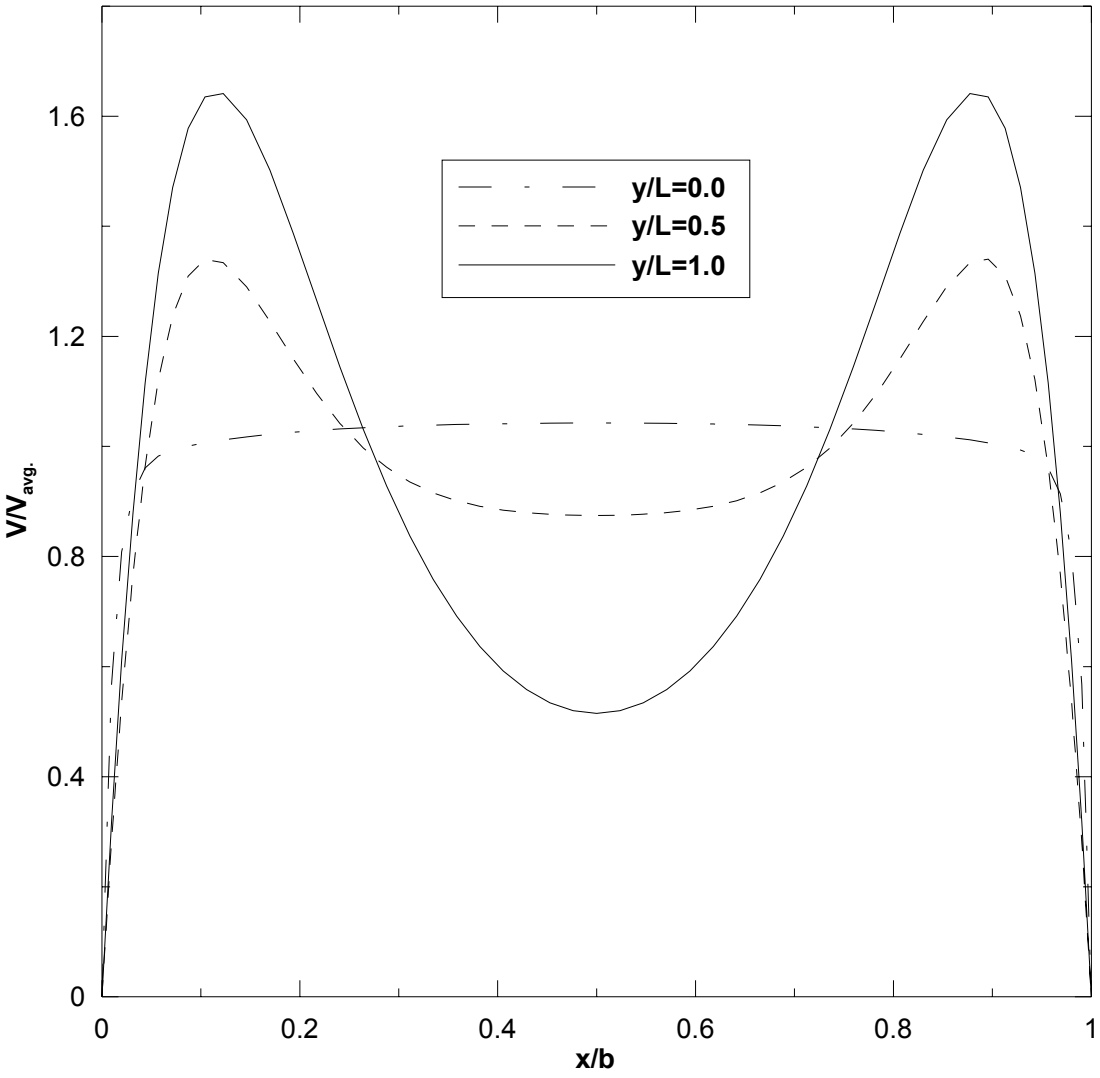

Figure5.63: Mean vertical velocity distribution at different cross-section in the channel for $Ra_b(b/L) = 15732$.

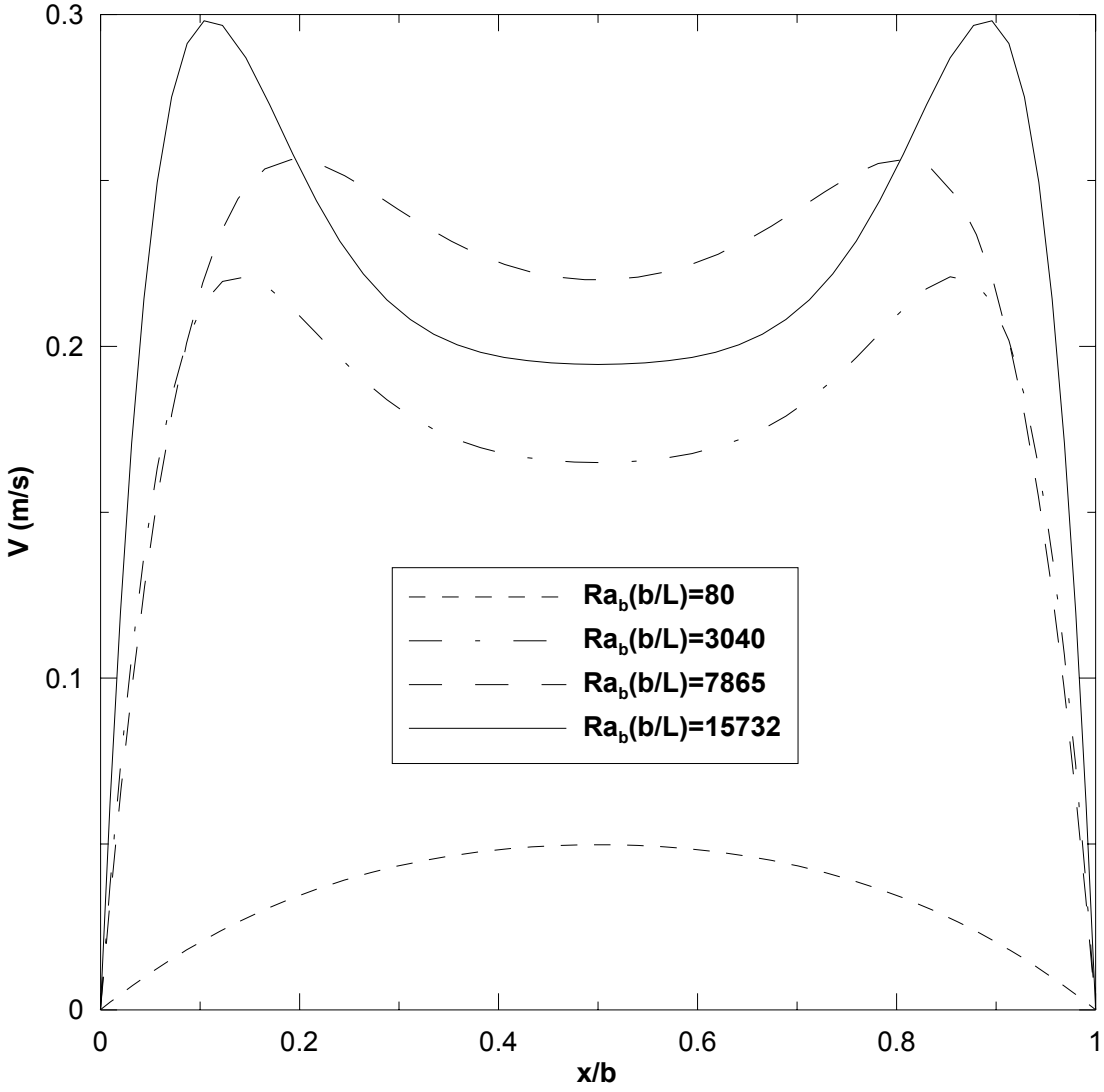

Figure5.64: Vertical velocity distribution at cross section (y/L = 0.5) for four different modified Rayleigh numbers in laminar regime.

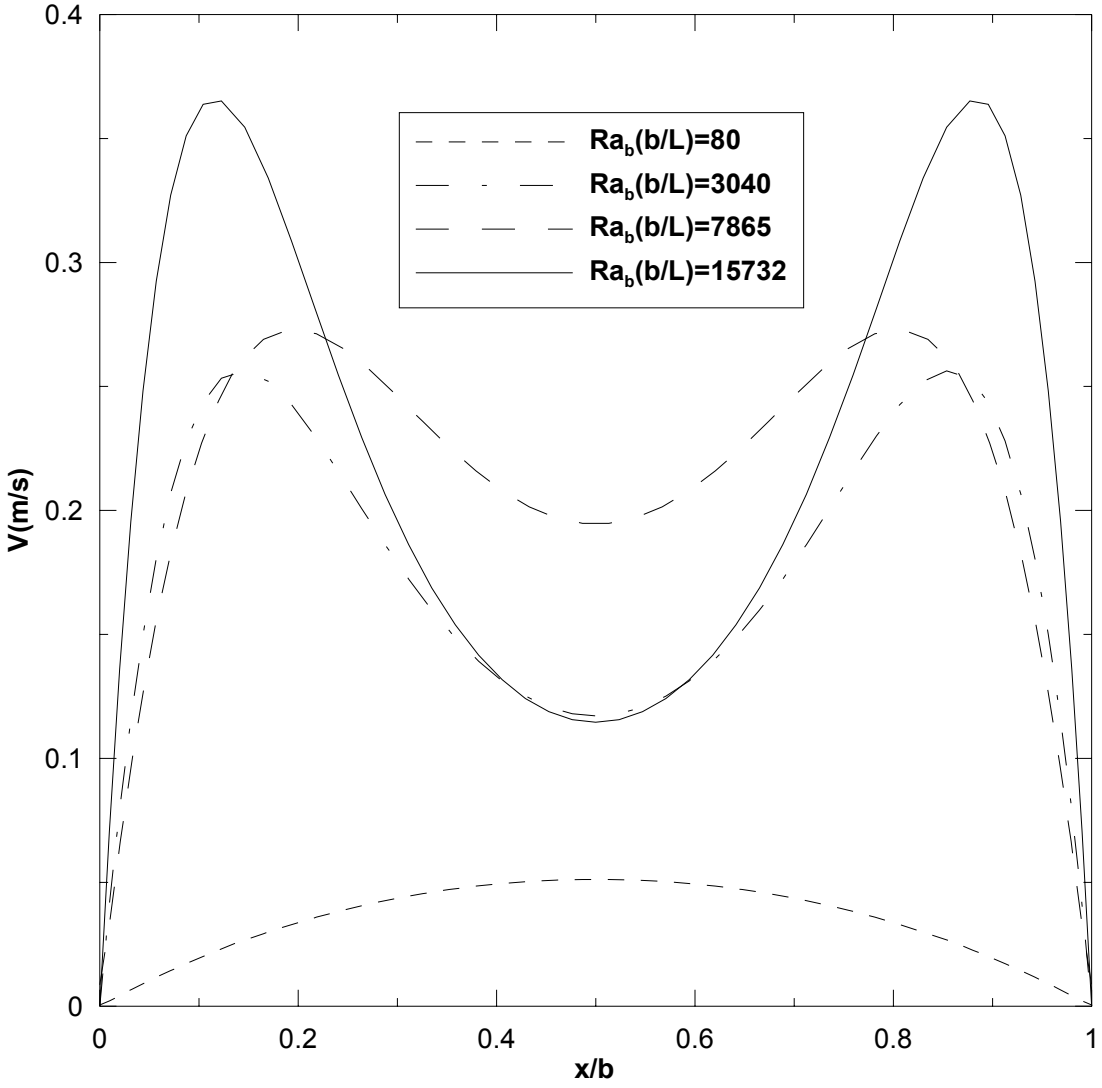

Figure 5.65: Vertical velocity distribution at cross section (y/L = 1.0) for four different modified Rayleigh numbers in laminar regime.

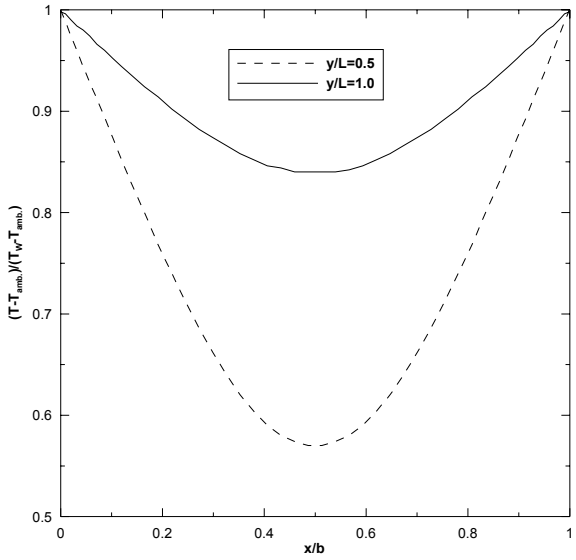

Figure 5.66: Dimensionless temperature distribution at different cross-section in the channel for $Ra_b(b/L) = 80$.

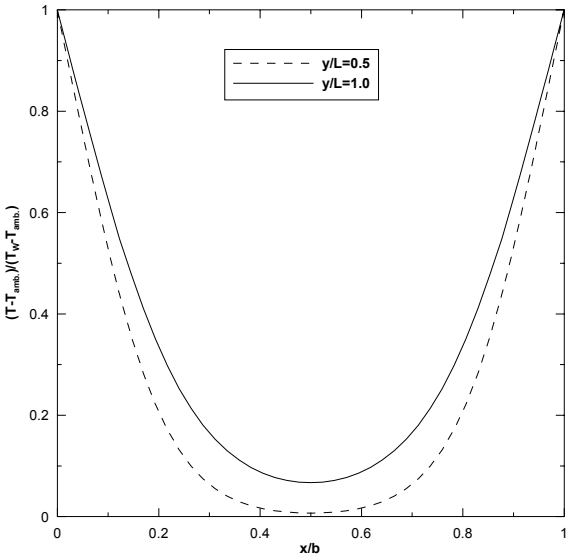

Figure 5.68: Dimensionless temperature distribution at different cross-section in the channel for $Ra_b(b/L) = 7865$.

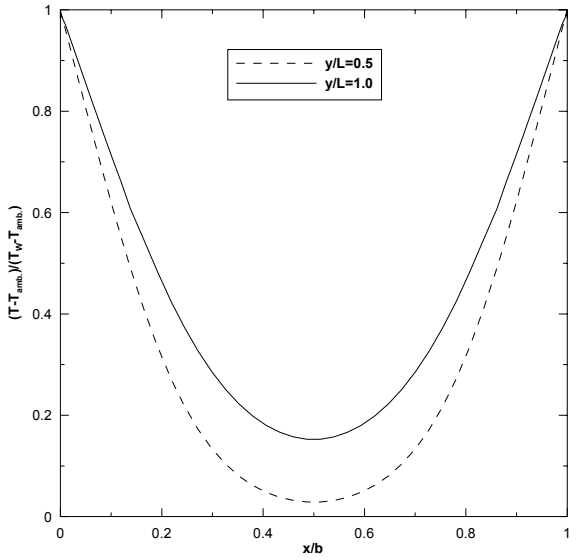

Figure 5.67: Dimensionless temperature distribution at different cross-section in the channel for $Ra_b(b/L) = 3040$.

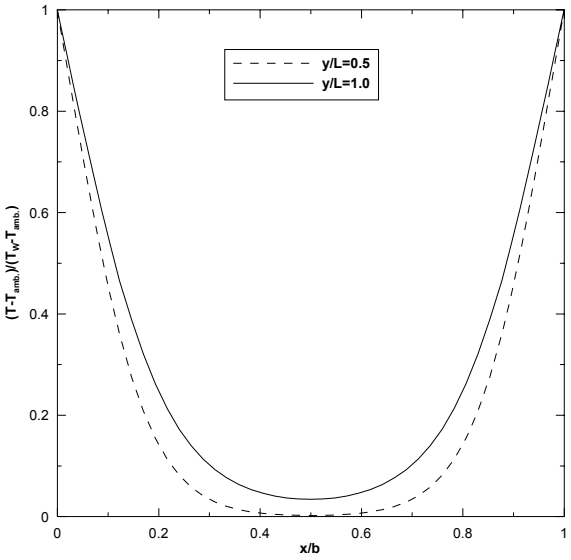

Figure 5.69: Dimensionless temperature distribution at different cross-section in the channel for $Ra_b(b/L) = 15732$.

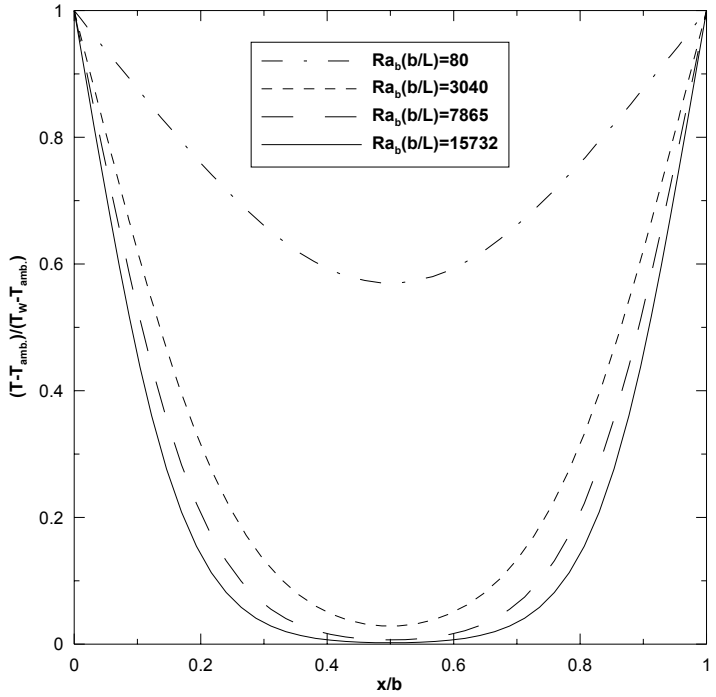

Figure 5.70: Dimensionless temperature distribution for different modified Rayleigh number in laminar regime at channel cross section y/L = 0.5.

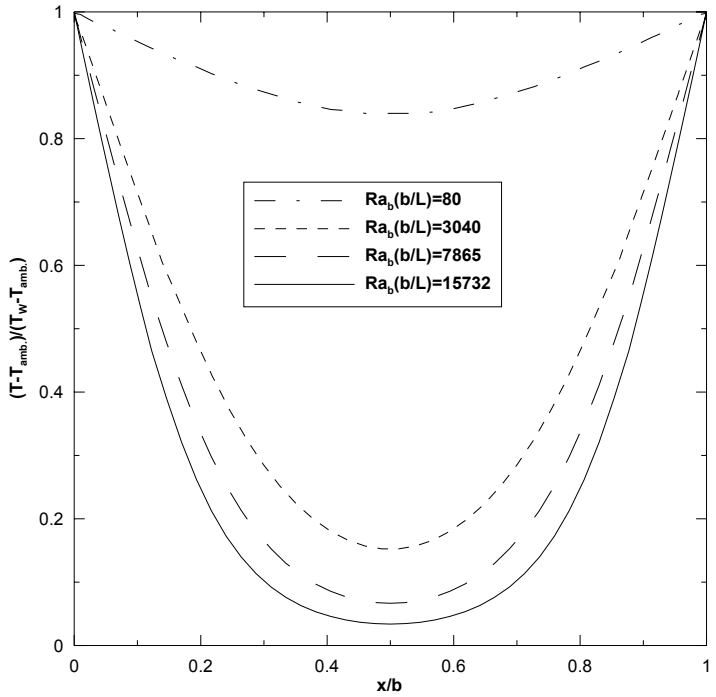

Figure 5.71: Dimensionless temperature distribution for different modified Rayleigh number in laminar regime at channel cross section y/L = 1.0.

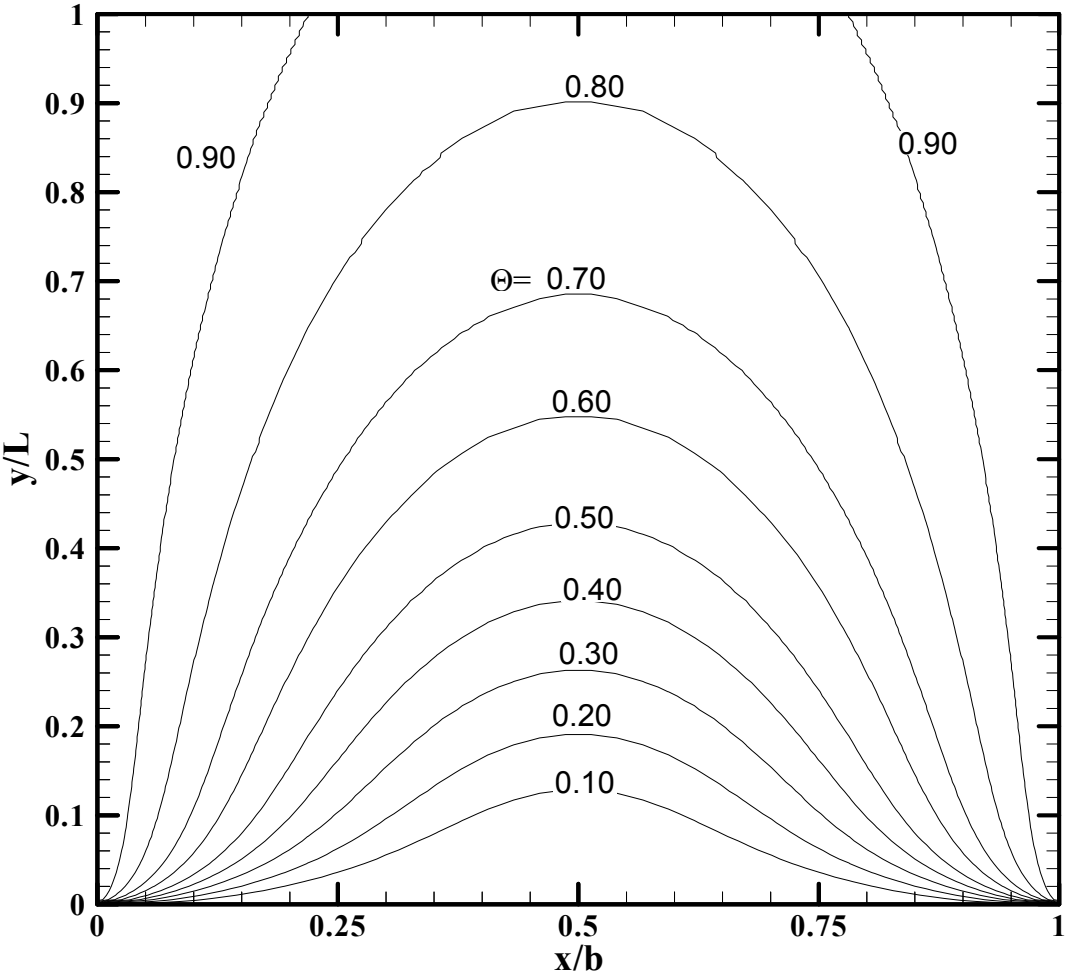

Figure 5.72: Isotherm for a modified Rayleigh number 80.

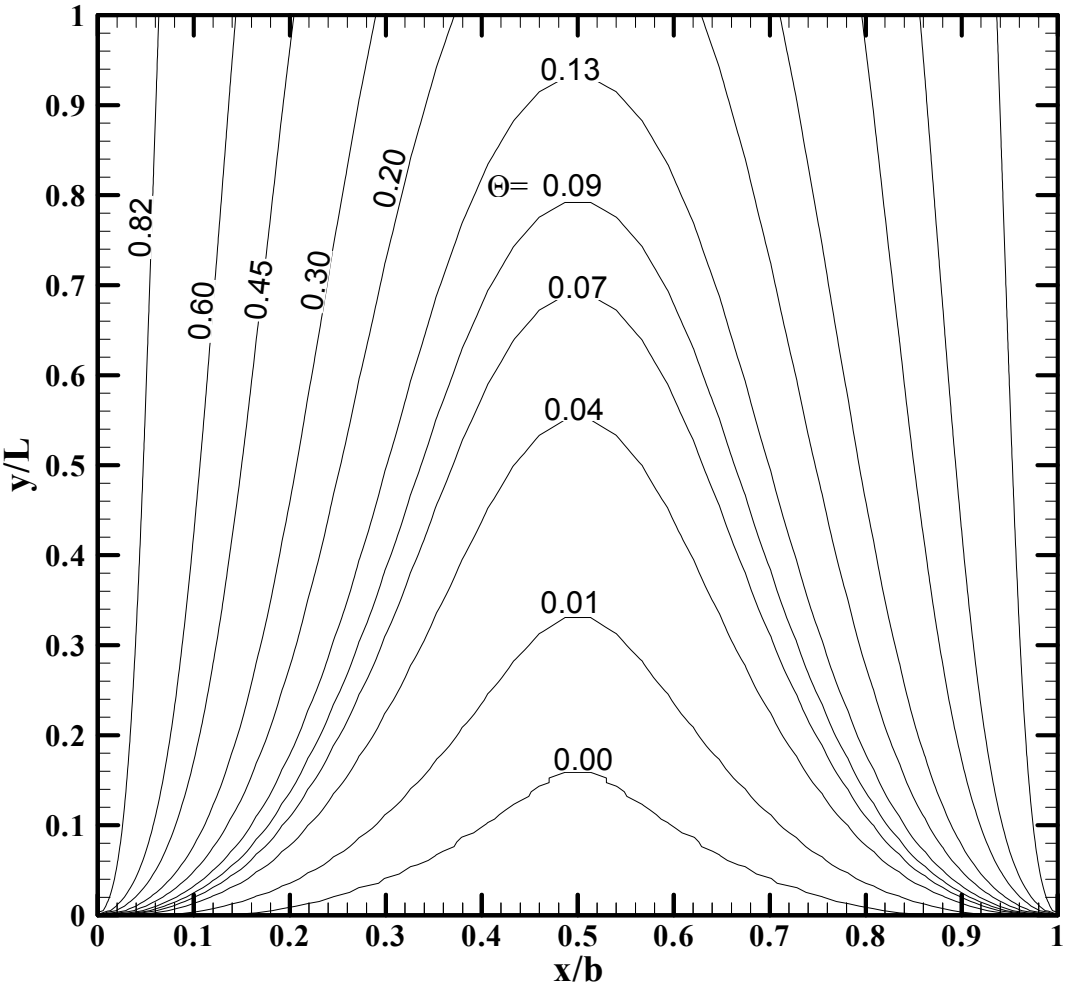

Figure 5.73: Isotherm for a modified Rayleigh number 3040.

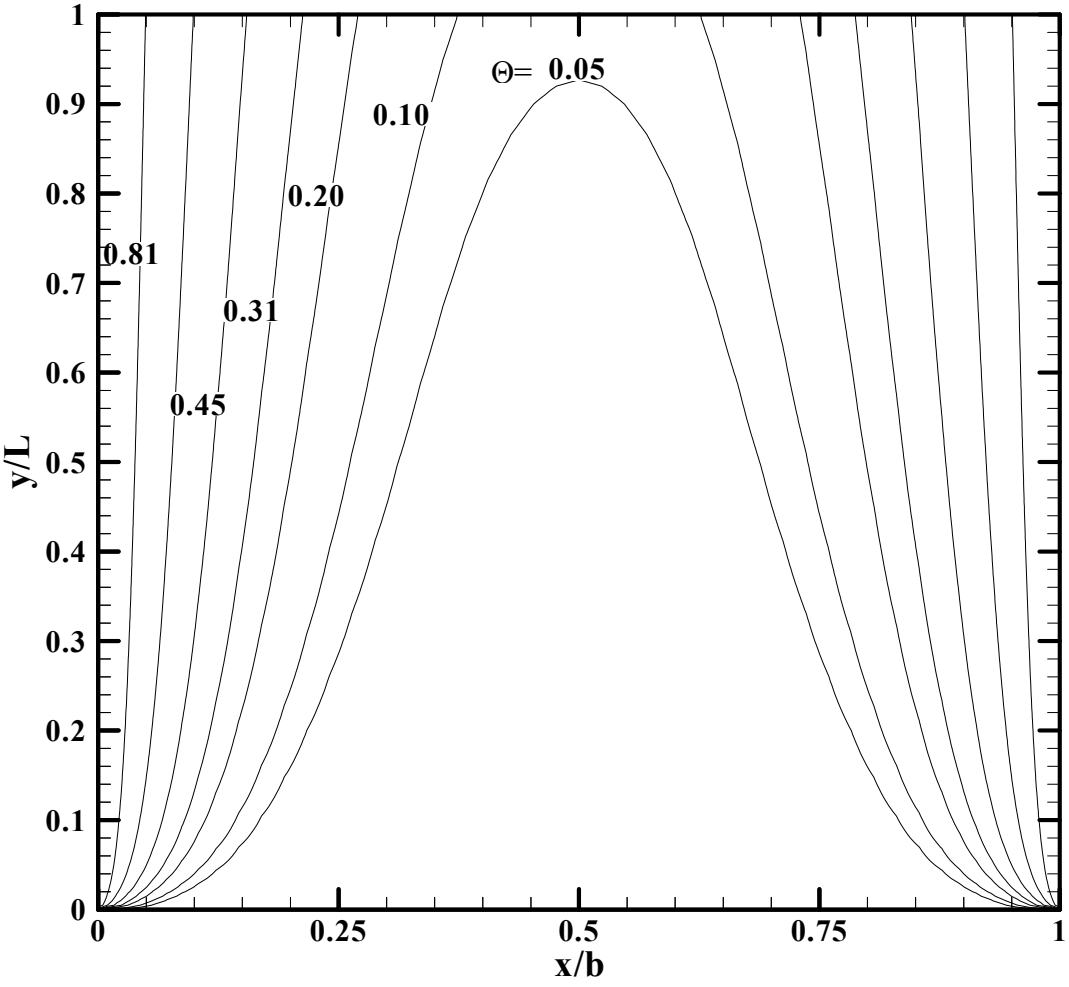

Figure 5.74: Isotherm for a modified Rayleigh number 7865.

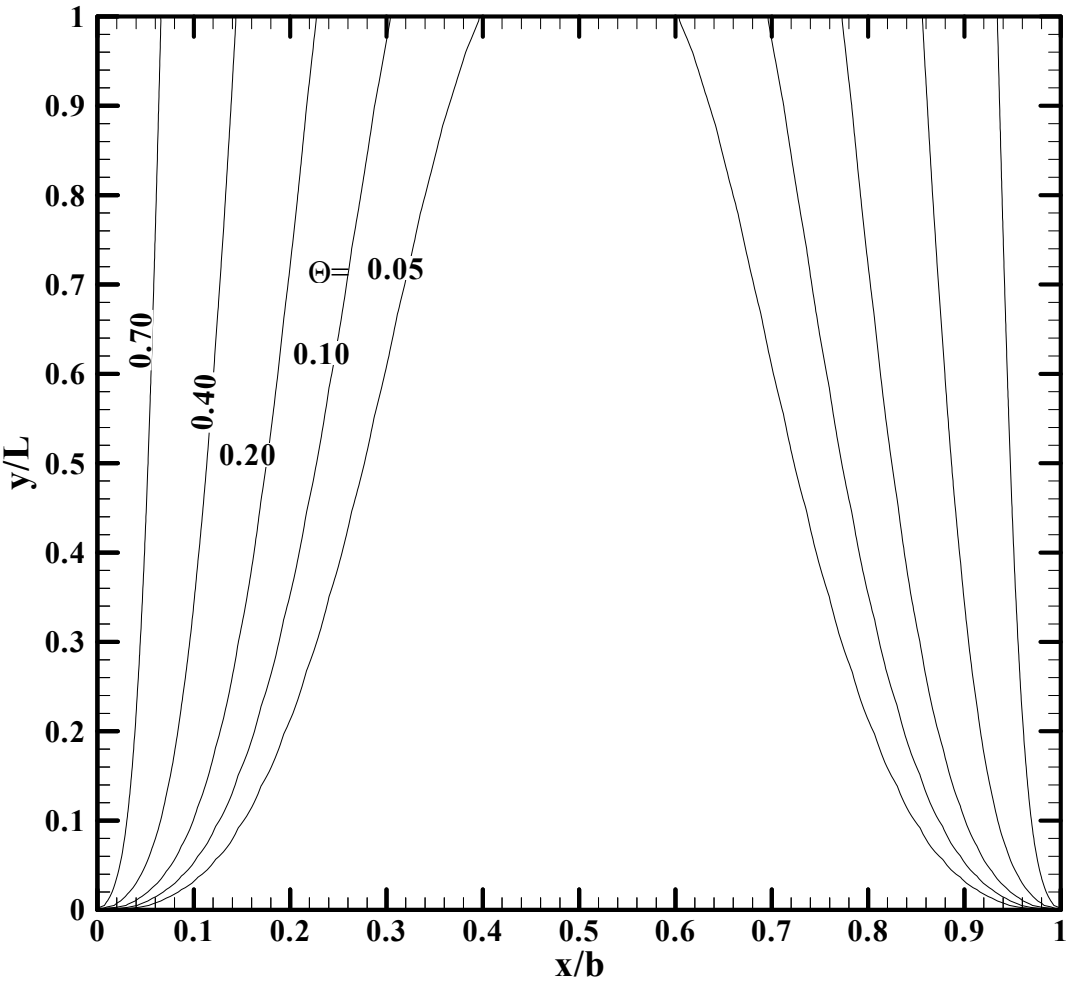

Figure 5.75: Isotherm for a modified Rayleigh number 15732.

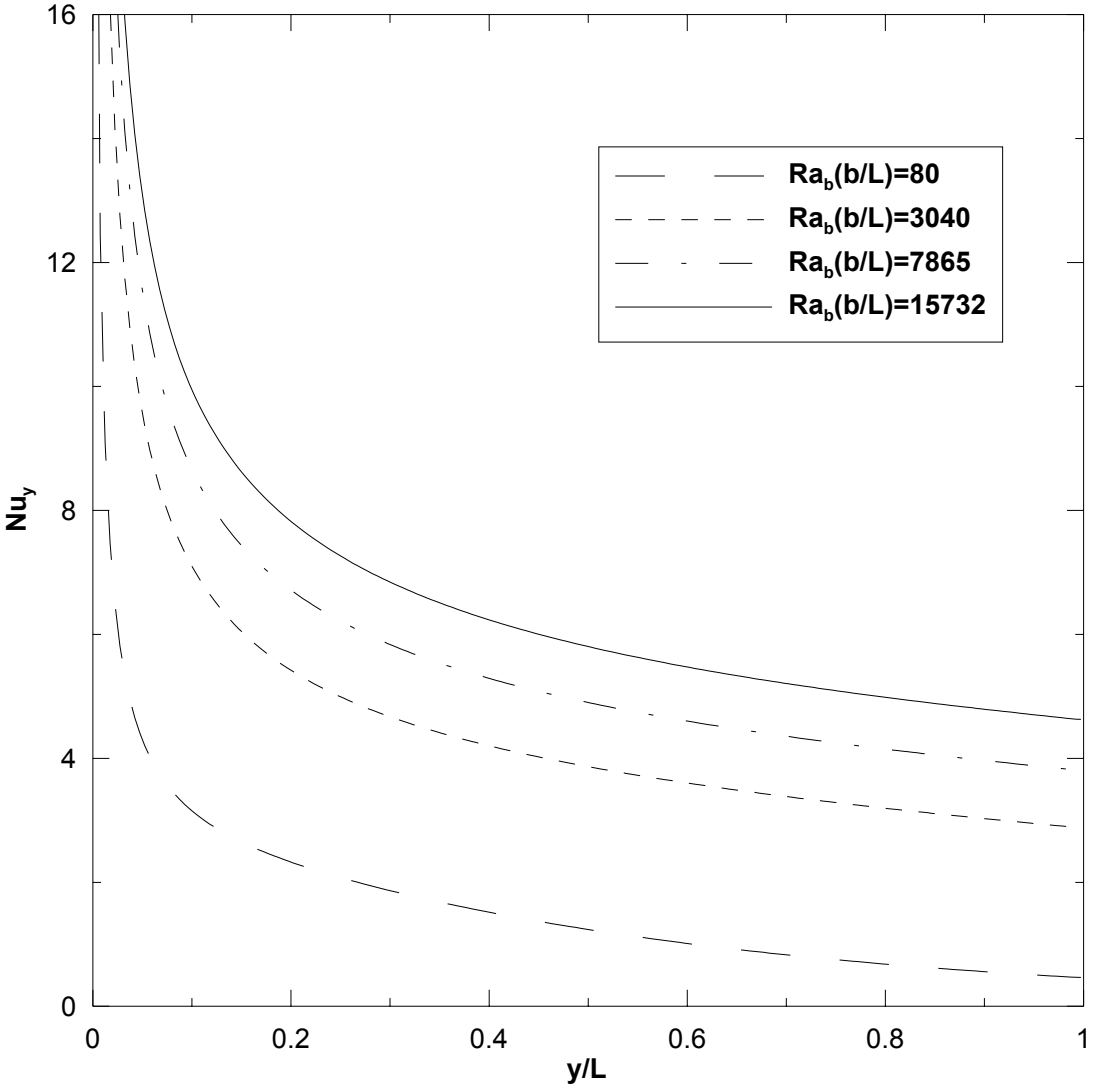

Figure 5.76: Local Nusselt number distributions along the channel for different modified Rayleigh numbers.

5.4.2 Influence of Rayleigh number on the Turbulent flow regime

This study covers the range of modified Rayleigh number from $1x10^5$ to $1x10^7$ for symmetrically heated isothermal vertical surfaces. The aspect ratio of the channel was kept constant (L/b = 12). Figure 5.77 shows the variation of the average Nusselt number versus Ra_m for vertical parallel-plate channel. It can be noted that the average Nusselt number increases continuously with the increase of Rayleigh number.

To study the influence of Rayleigh number on the flow field and heat transfer characteristics the vertical velocity and temperature profiles as well as isotherms are presented for four different Rayleigh numbers ($1.9x10^5$, $9.04x10^5$, $1.84x10^6$ and $7.06x10^6$). The plots of dimensionless mean vertical velocity versus the dimensionless distance across the channel at different channel cross-sections (y/L = 0, 0.5, 1.0) are plotted for a specific value of the Ra_m as shown in Figures 5.78-5.81. From these figures, it can be seen that the vertical velocity profiles have two velocity peaks in the entire range of Rayleigh number considered. These velocity peaks become sharp and move towards the channel walls with the increase of modified Rayleigh number. The vertical velocity profiles across the channel for four values of Ra_m are plotted at section y/L = 0.5 and y/L = 1.0 and are shown in Figures 5.82 and 5.83, respectively. It can be seen that for turbulent flows the dimensional vertical velocity increases as the Ra_m increases. Accordingly, the mass flow rate through the channel increases with increase of Ra_m as expected.

Figures 5.84-5.87 show the dimensionless temperature distribution across the channel for four different Rayleigh numbers $1.9x10^5$, $9.04x10^5$, $1.84x10^6$ and $7.06x10^6$

which are all in the turbulent flow regime. At all these Rayleigh numbers the temperature at outlet section is higher than mid-section. The fluid temperature increases along the flow direction as expected. Figures 5.88 and 5.89 show the dimensionless temperature distribution across the channel at section y/L = 0.5 and 1.0 for the abovementioned Rayleigh numbers. It can be seen that as the Rayleigh number increases the temperature at both sections decreases.

Figures 5.90-5.93 show isotherms for the above modified Rayleigh numbers. In the considered Rayleigh number range there is no thermally fully developed flow visible. In the turbulent flow regime, as Ra_m increases the thickness of heated layer decreases. Figure 5.94 shows the variation of local Nusselt number along the channel for the four different values of Ra_m. It can be seen that as Ra_m increases the local Nusselt number also increases due to decrease of the thermal layer thickness.

In the turbulent flow regime, it can be concluded that the average Nusselt number increases with the increase of the modified Rayleigh number as observed earlier in the laminar flow regime. This is due to increase in flow rate and decrease in the heated layer thickness discussed in this section.

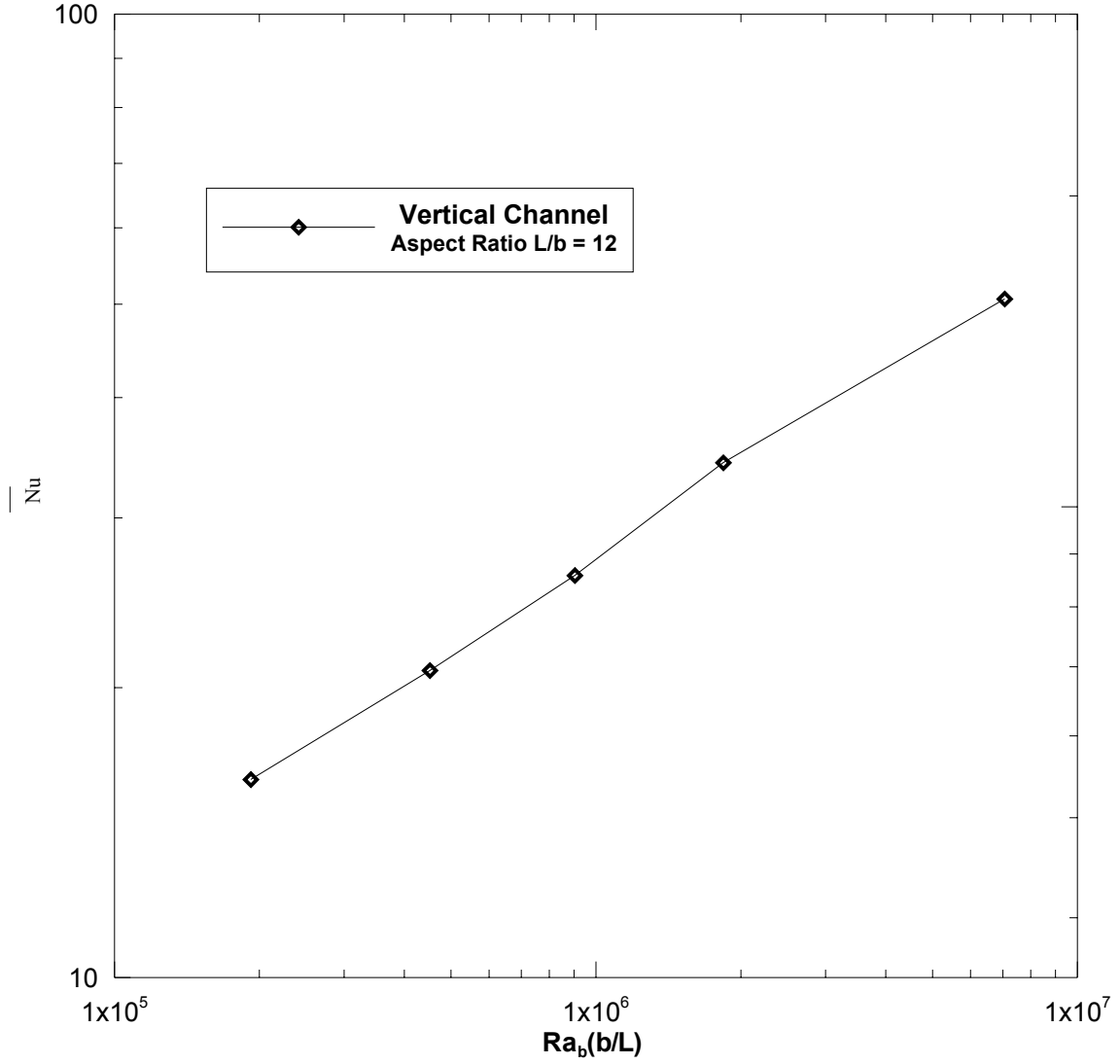

Figure 5.77: The variation of the average Nusselt number versus the modified Rayleigh number in turbulent regime for vertical parallel-plate channel.

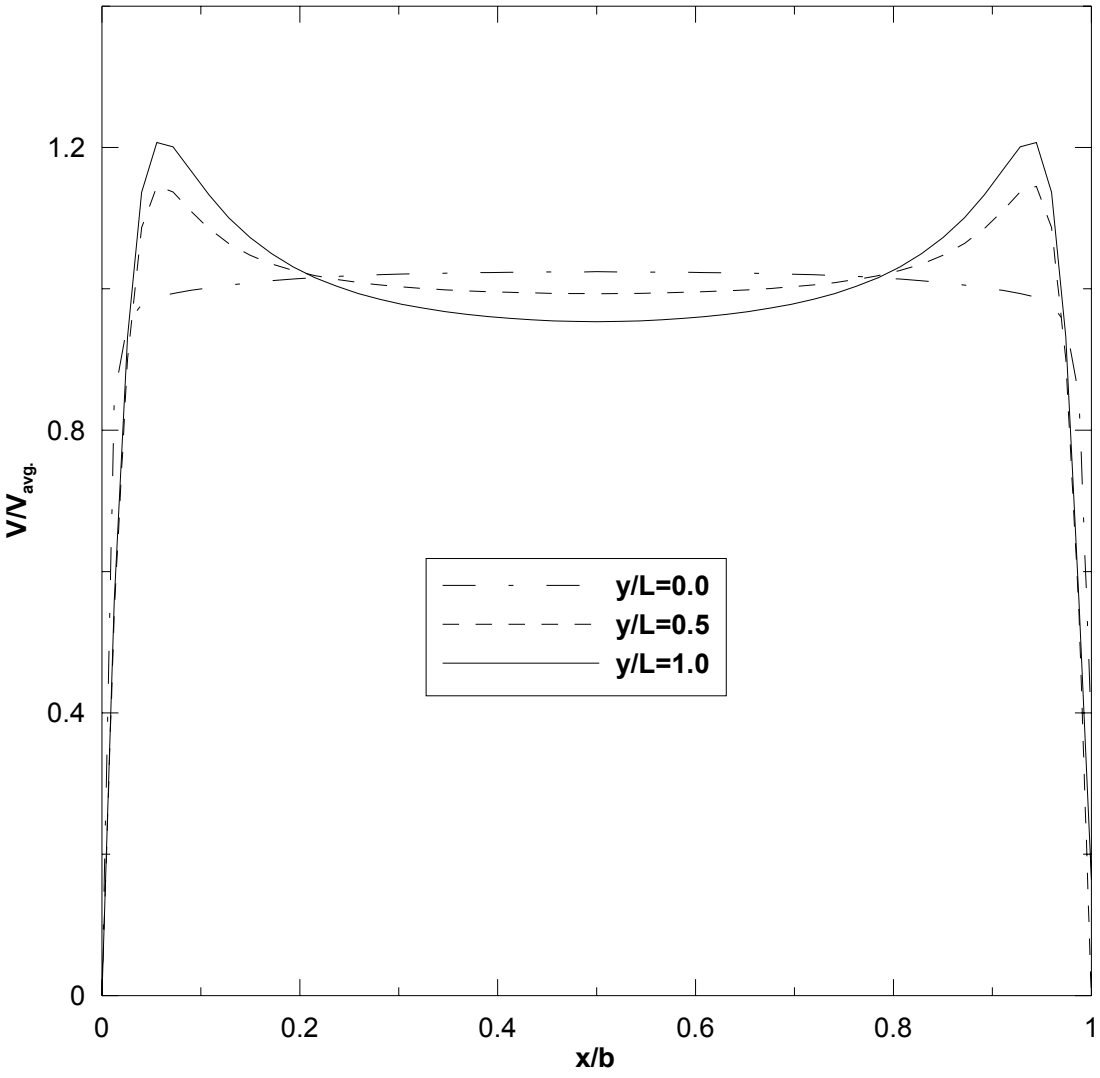

Figure 5.78: Mean vertical velocity distribution at different cross-section in the channel for $Ra_b(b/L) = 1.9x10^5$.

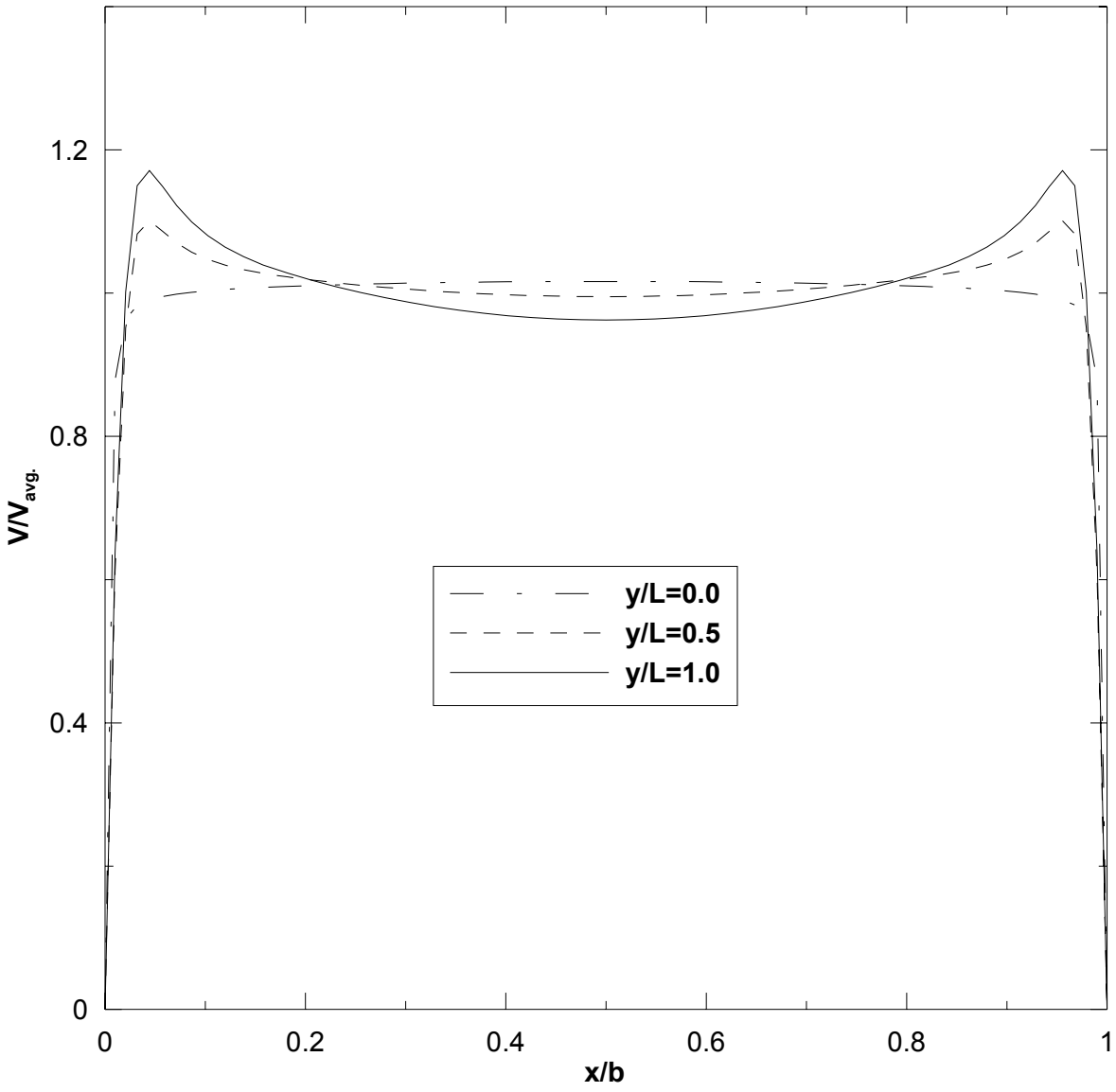

Figure 5.79: Mean vertical velocity distribution at different cross-section in the channel for $Ra_b(b/L) = 9.04x10^5$.

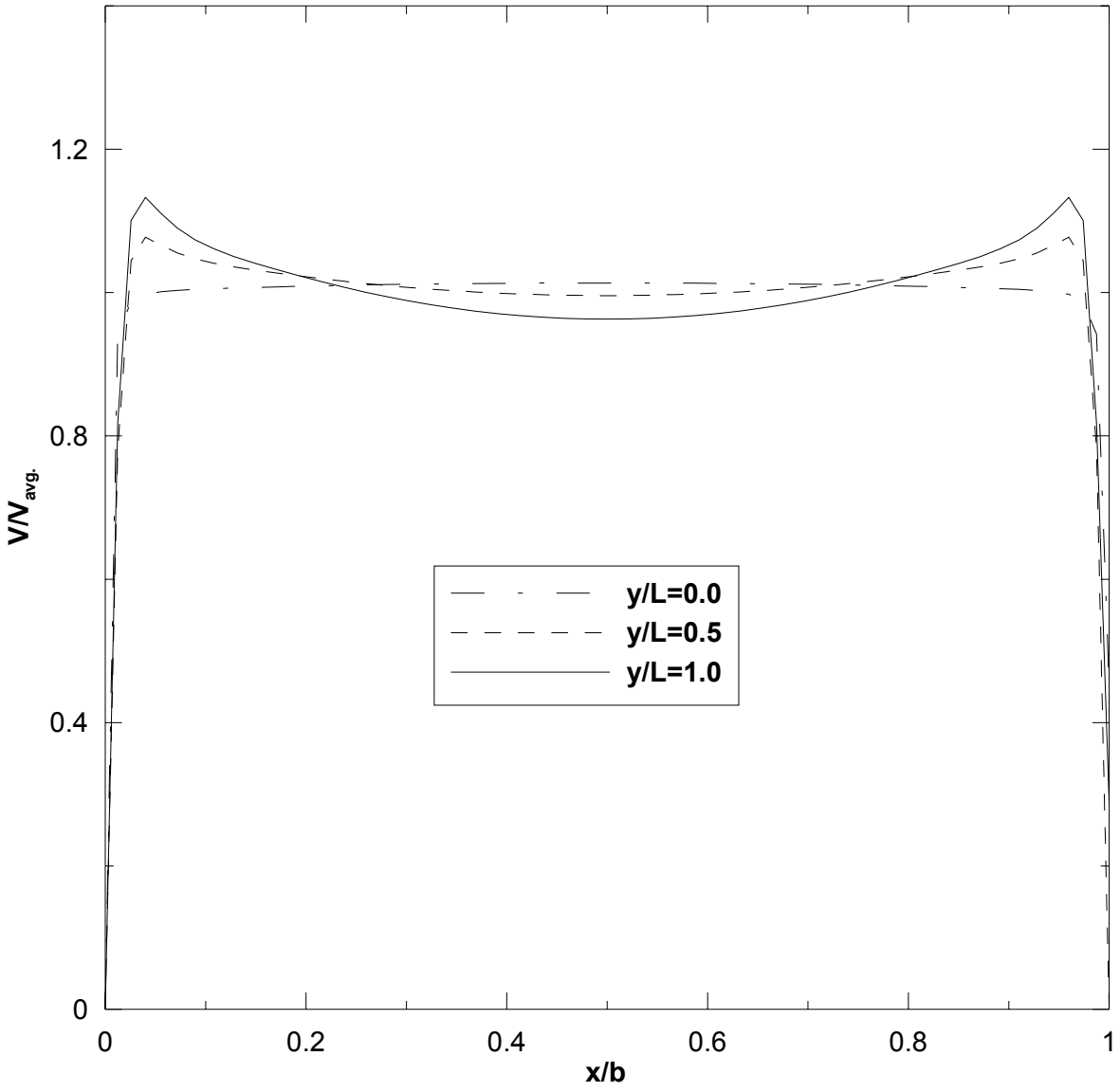

Figure 5.80: Mean vertical velocity distribution at different cross-section in the channel for $Ra_b(b/L) = 1.84x10^6$.

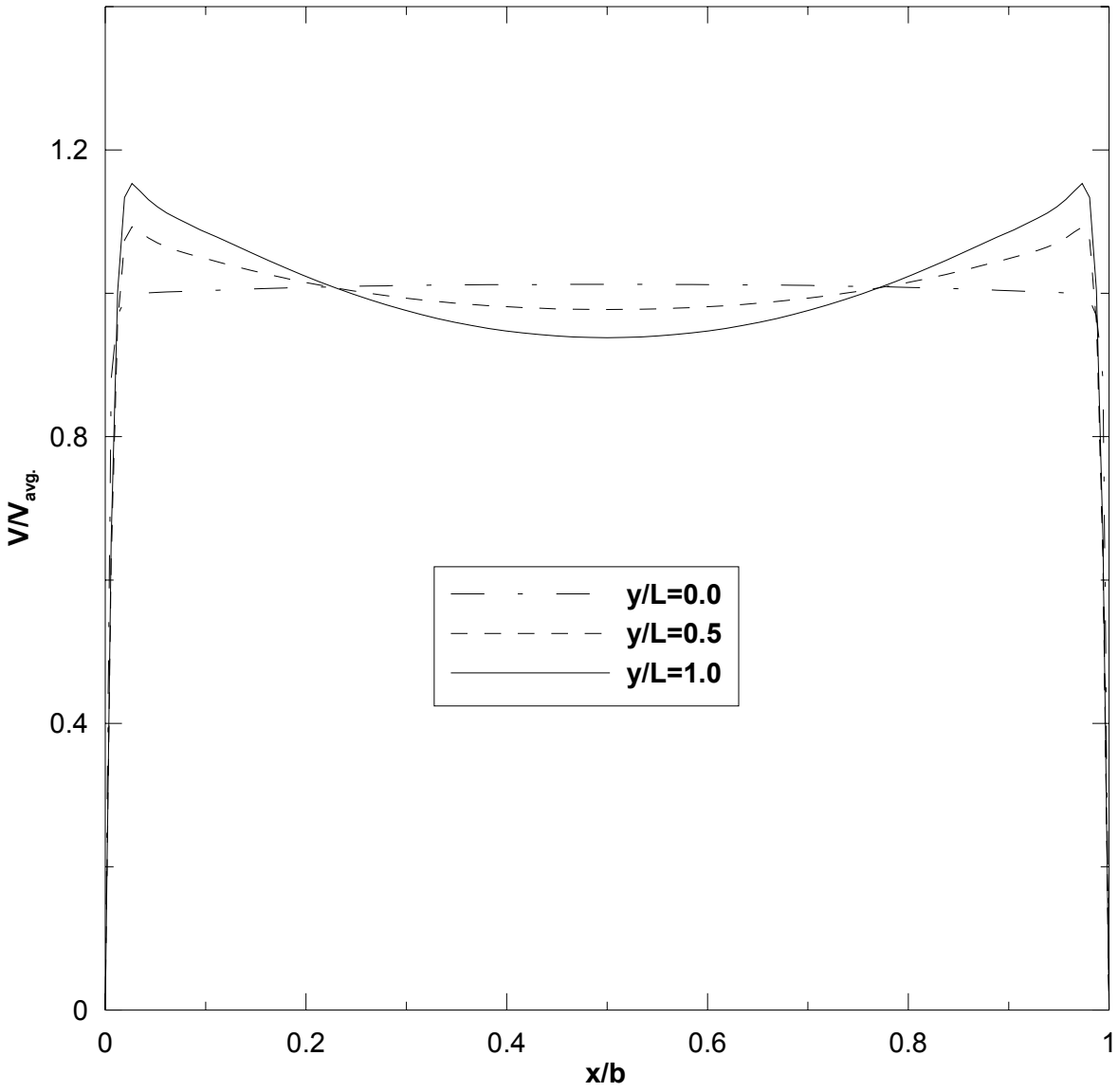

Figure 5.81: Mean vertical velocity distribution at different cross-section in the channel for $Ra_b(b/L) = 7.06x10^6$.

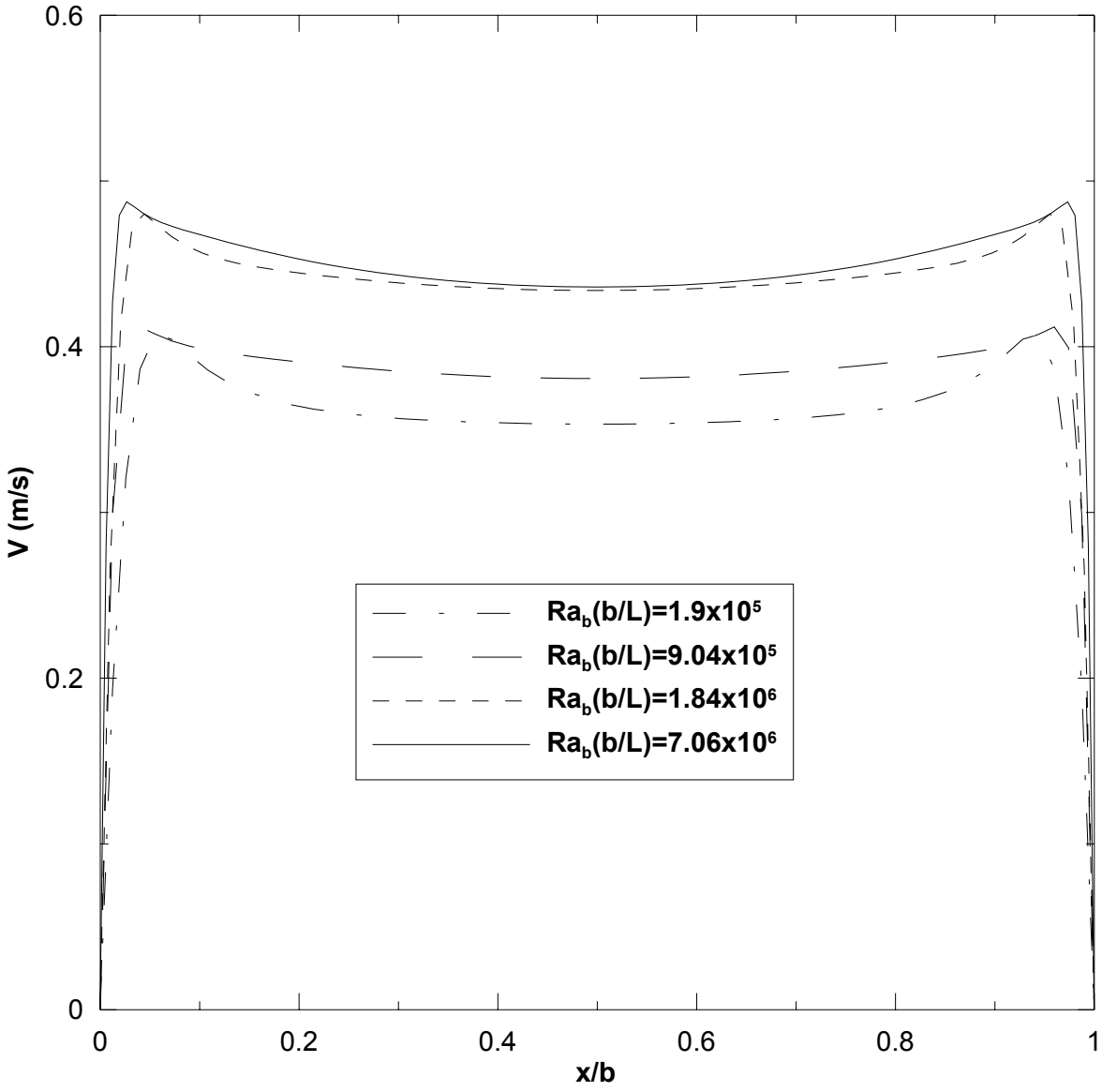

Figure 5.82: Vertical velocity distribution at cross-section (y/L = 0.5) for four different modified Rayleigh number in turbulent regime.

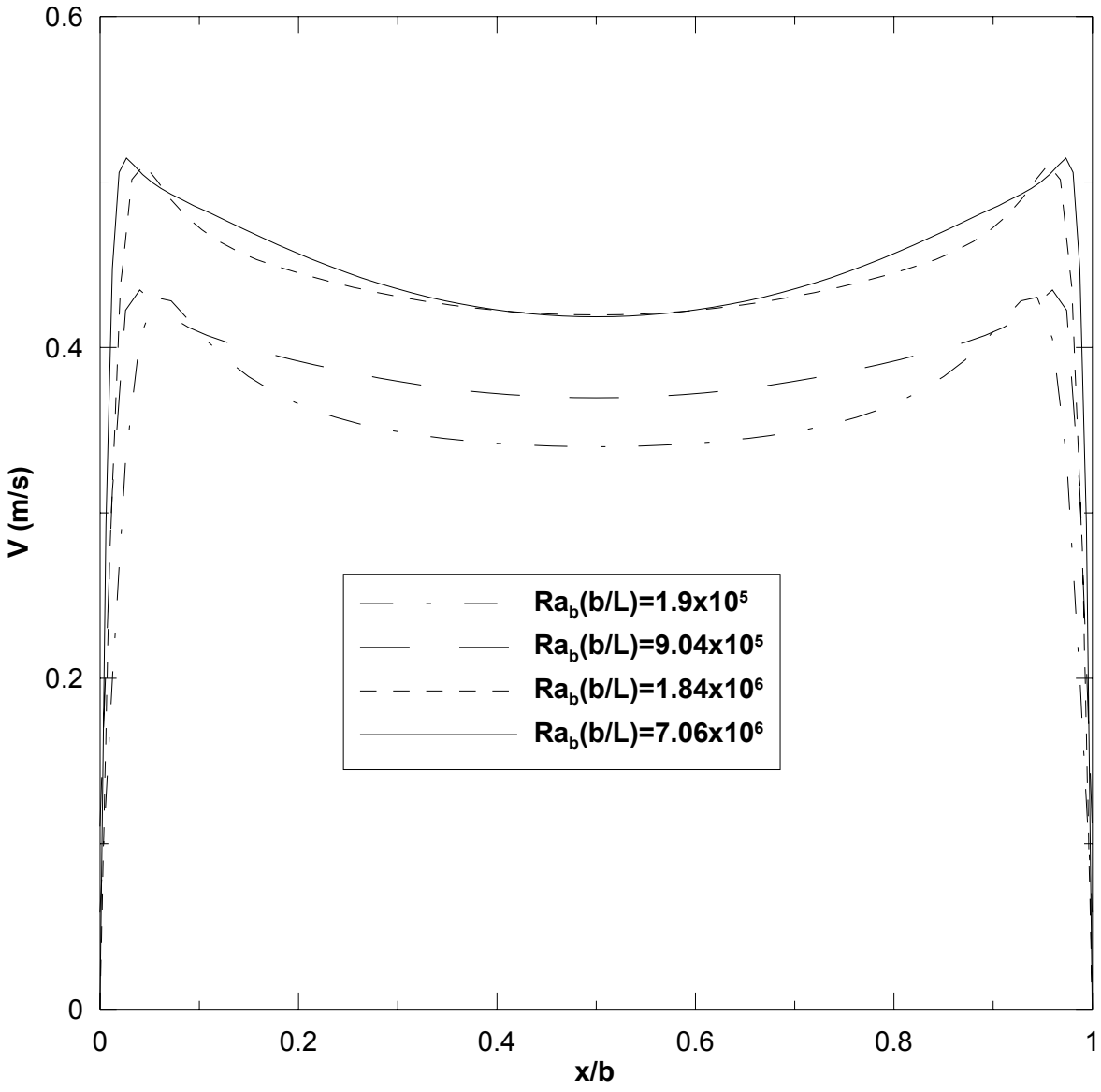

Figure 5.83: Vertical velocity distribution at cross-section (y/L = 1.0) for four different modified Rayleigh number in turbulent regime.

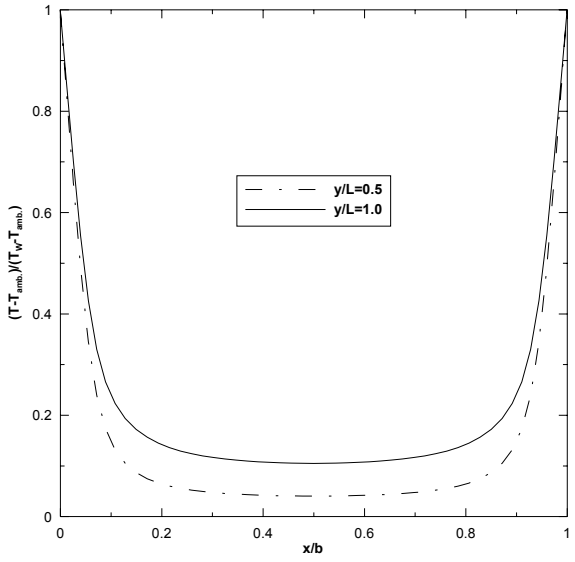

Figure 5.84: Dimensionless temperature distribution at different cross section in the channel for $Ra_b(b/L)= 1.9x10^5$.

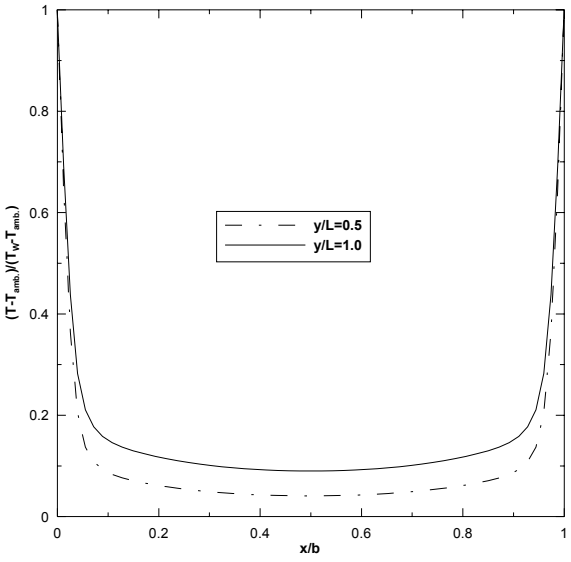

Figure 5.86: Dimensionless temperature distribution at different cross section in the channel for $Ra_b(b/L)= 1.84x10^6$.

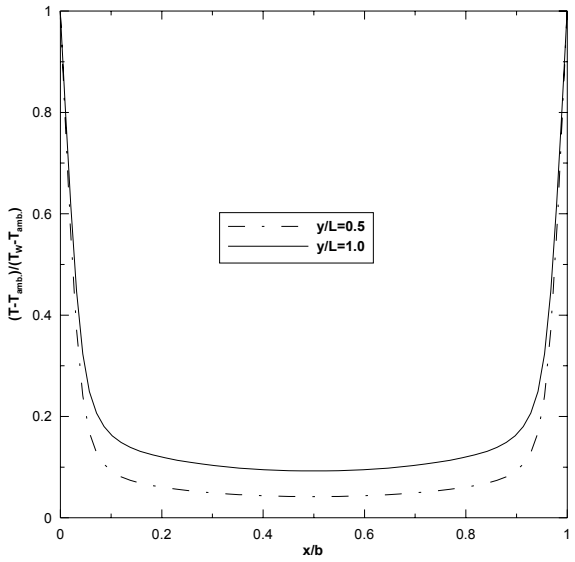

Figure 5.85: Dimensionless temperature distribution at different cross section in the channel for $Ra_b(b/L)= 9.04x10^5$.

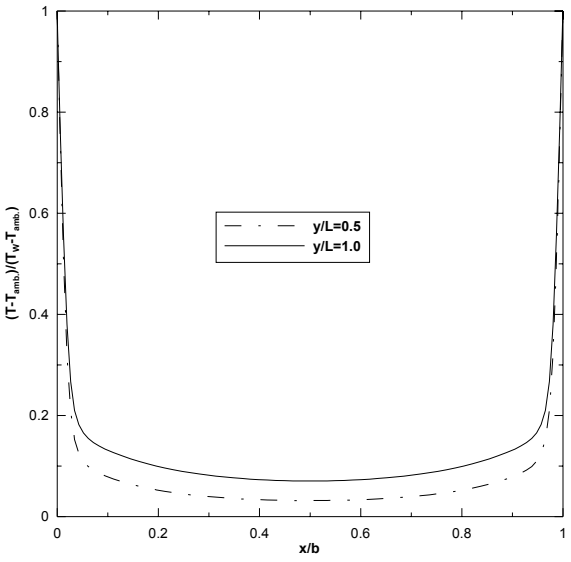

Figure 5.87: Dimensionless temperature distribution at different cross section in the channel for $Ra_b(b/L)= 7.06x10^6$.

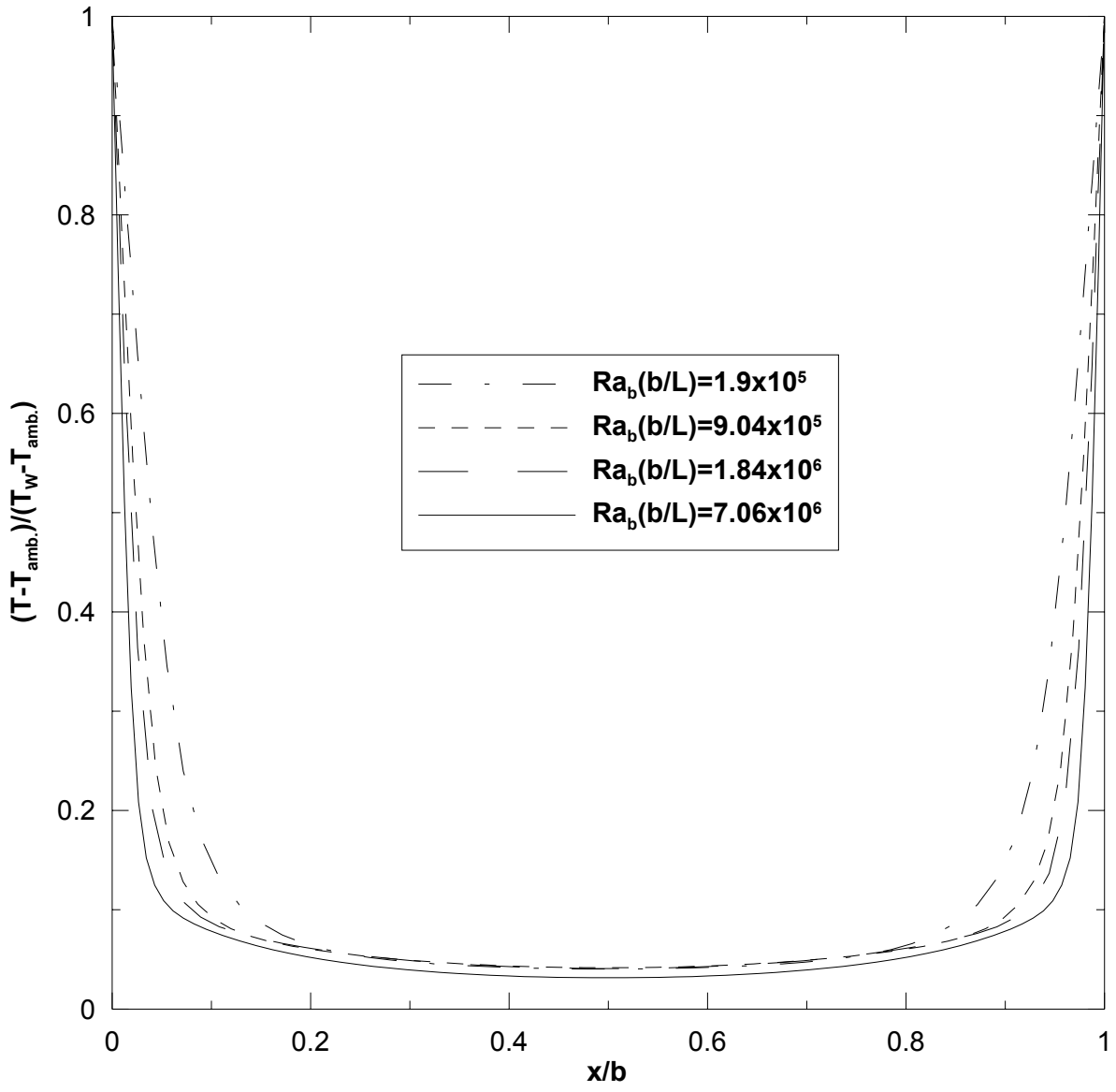

Figure 5.88: Dimensionless temperature distribution for different modified Rayleigh number in turbulent regime at channel cross-section y/L = 0.5.

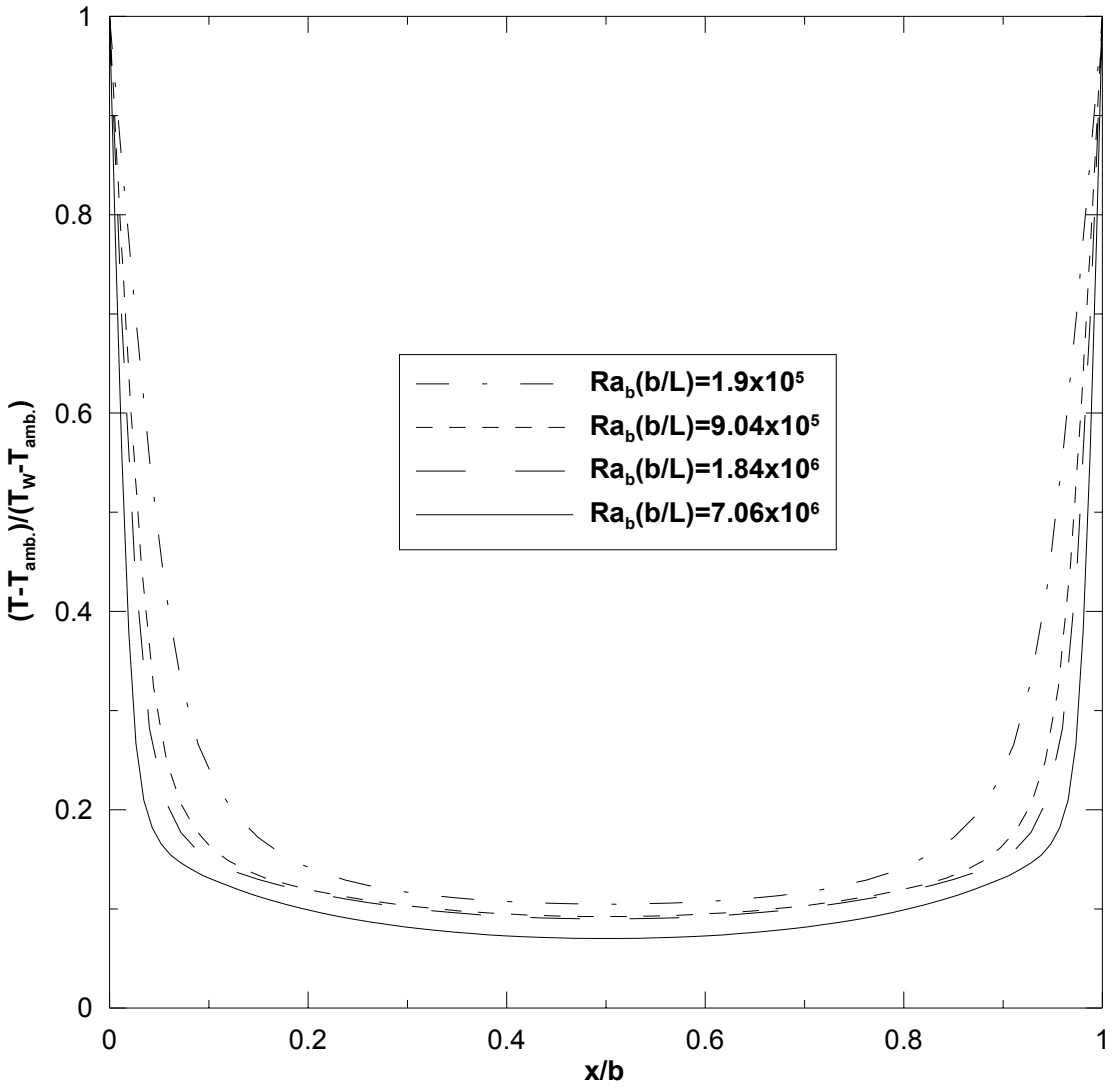

Figure 5.89: Dimensionless temperature distribution for different modified Rayleigh number in turbulent regime at channel cross-section y/L = 1.0.

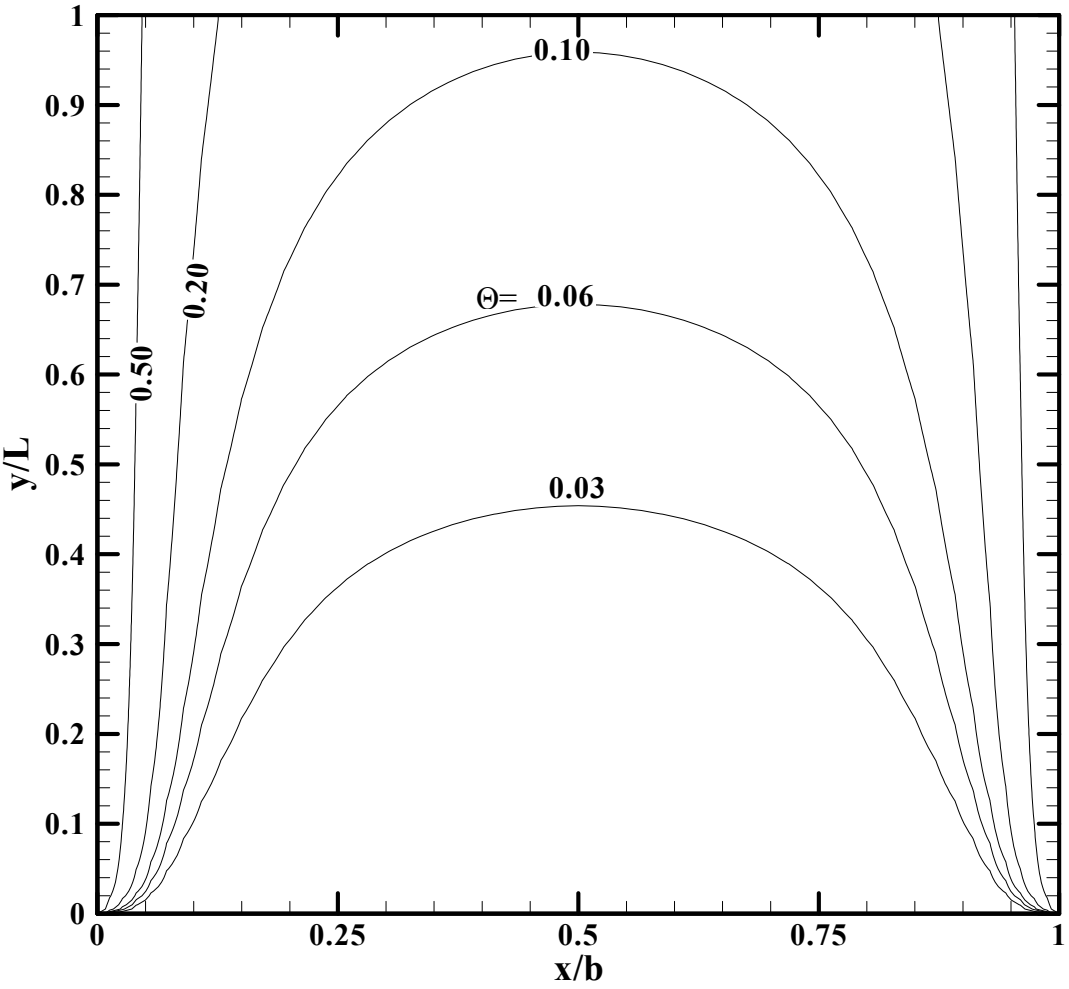

Figure 5.90: Isotherm for a modified Rayleigh number 1.9×10^5.

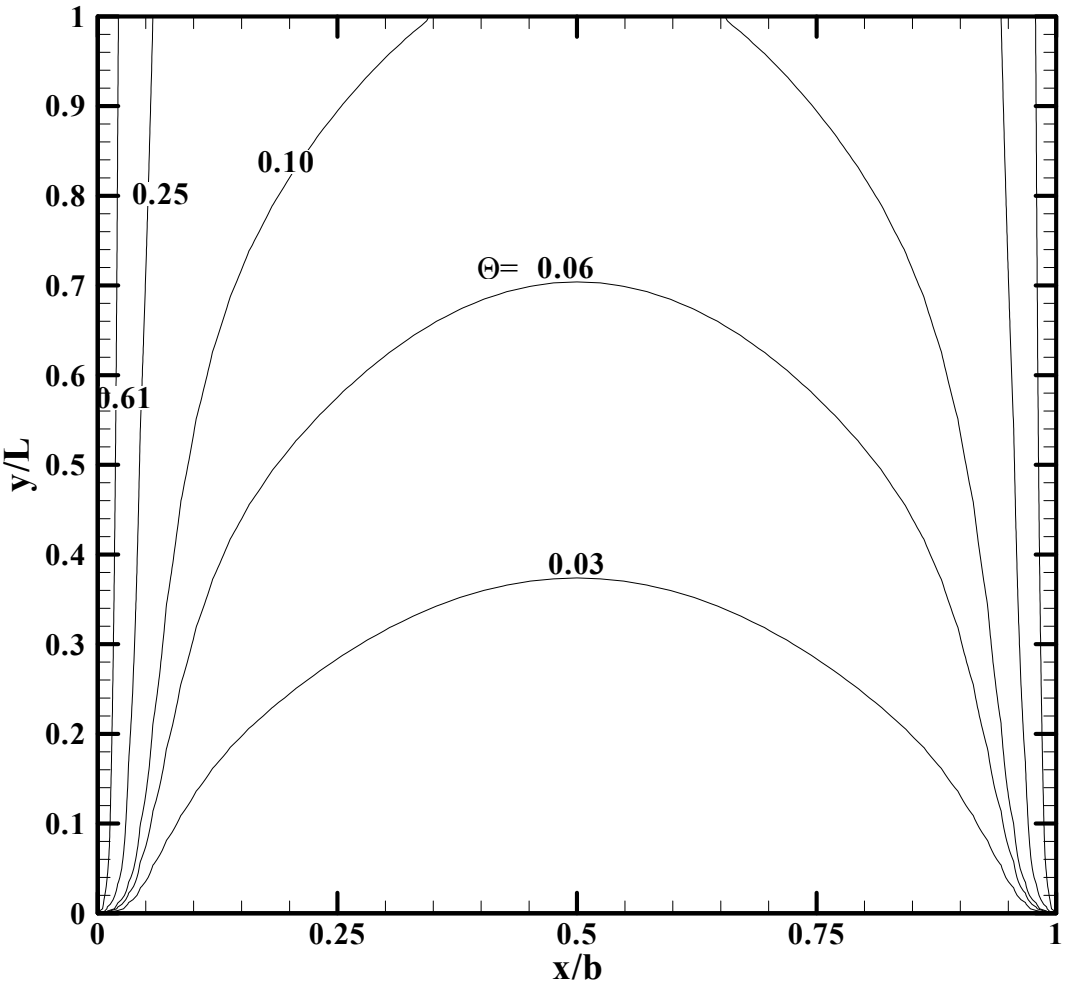

Figure 5.91: Isotherm for a modified Rayleigh number 9.05×10^5.

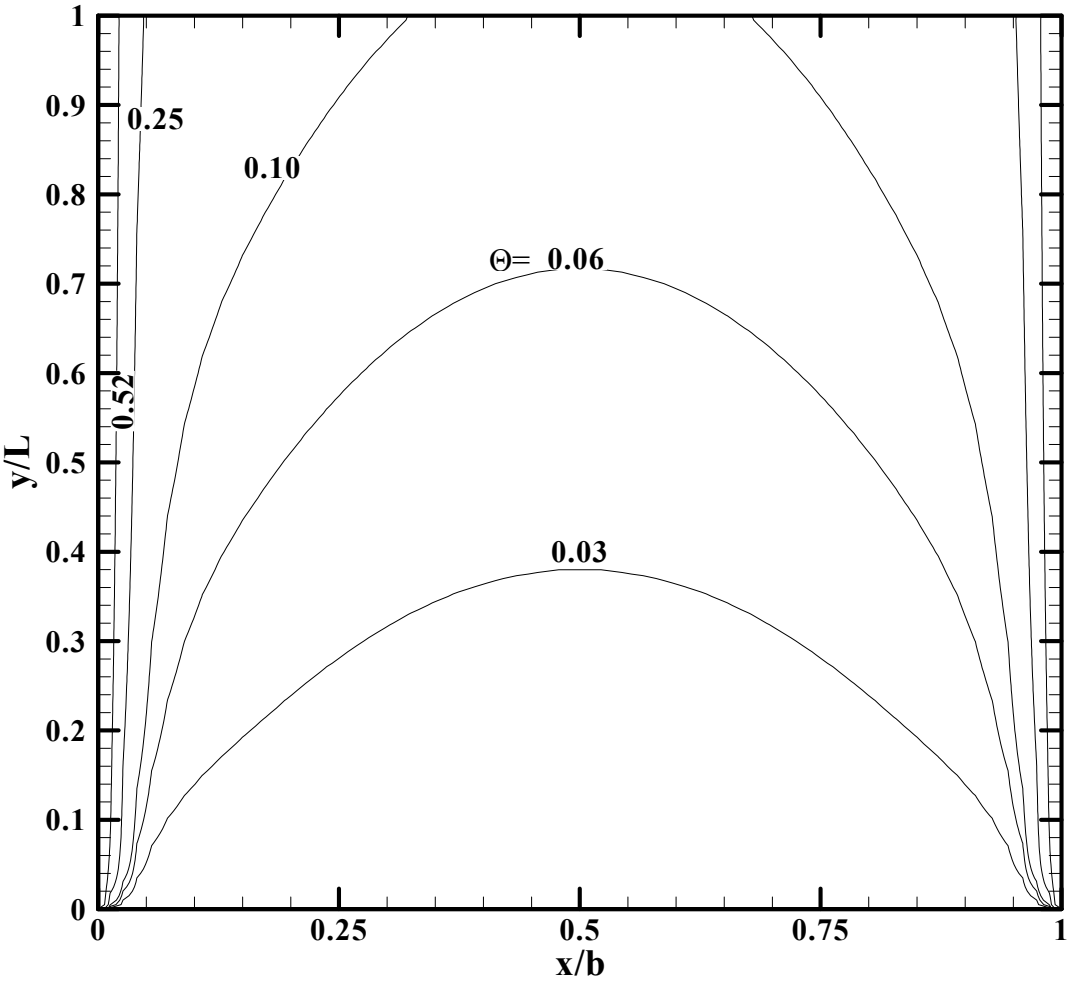

Figure 5.92: Isotherm for a modified Rayleigh number 7.06×10^6.

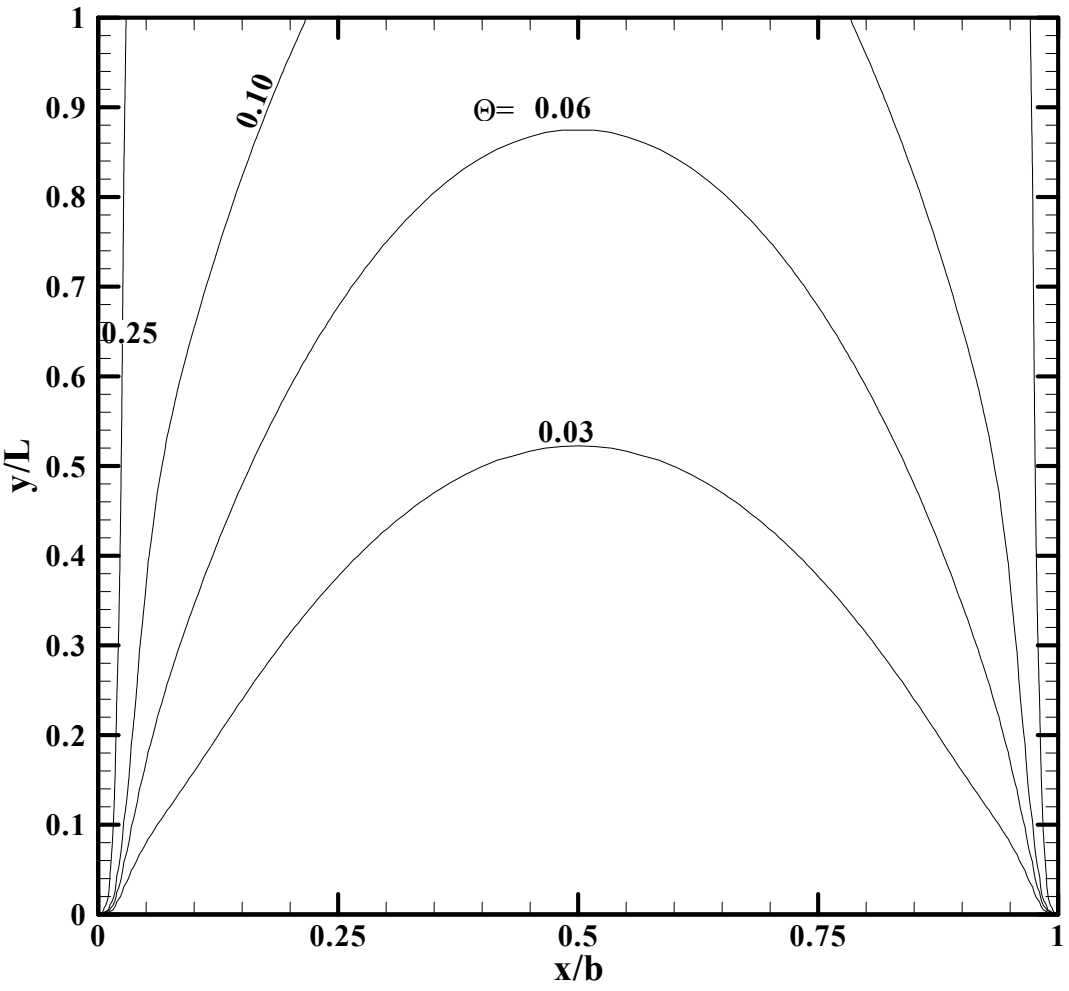

Figure 5.93: Isotherm for a modified Rayleigh number 1.84×10^6.

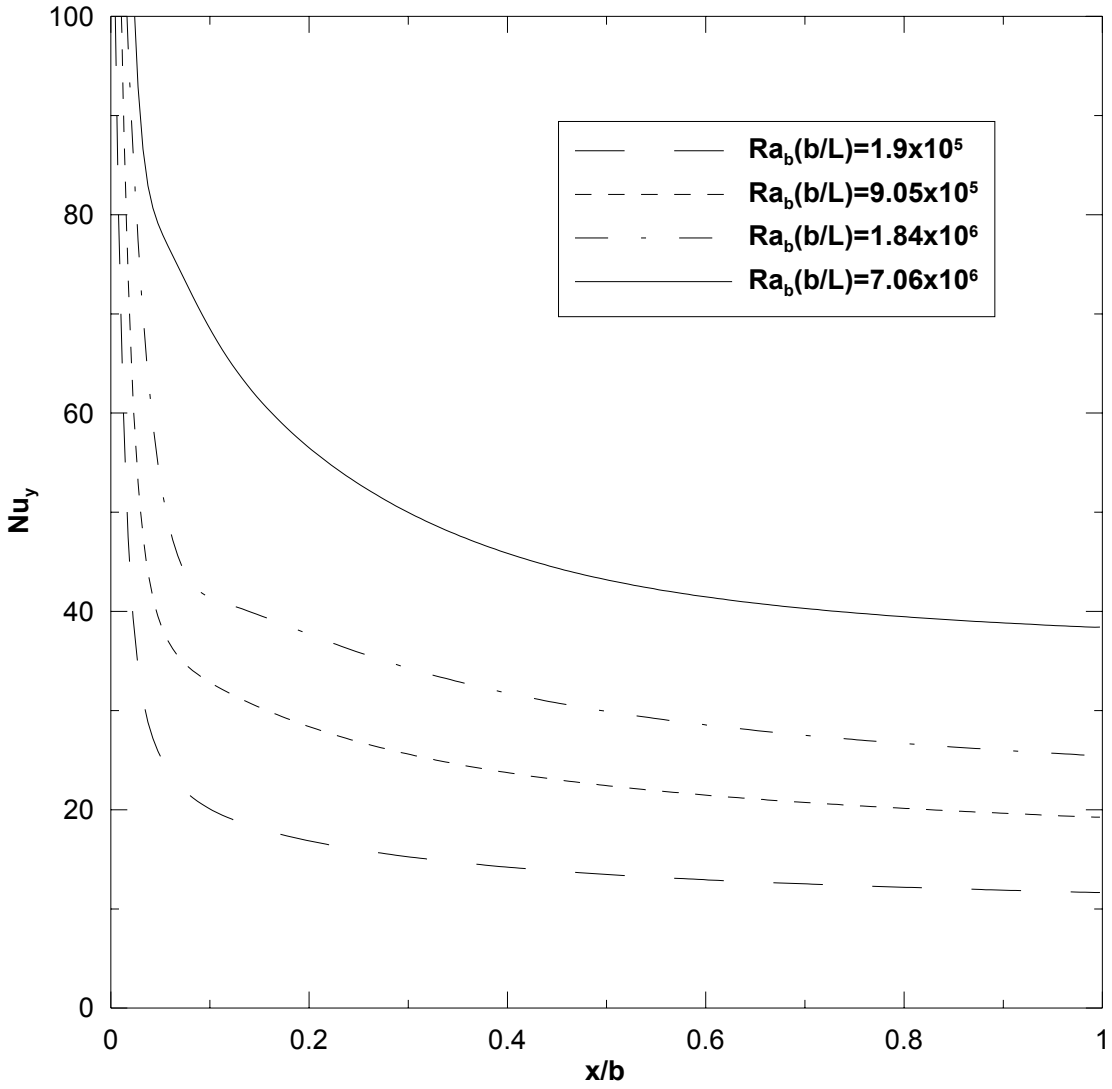

Figure 5.94: Local Nusselt number distributions along the channel for different modified Rayleigh number in turbulent regime.

5.5 Influence of Channel Spacing

The local and average heat transfer characteristics for parallel plate vertical channel were studied for the two cases of isothermal and isoflux surfaces for different channel spacing. From the literature review, it is clear that there has been no research on symmetrically heated vertical channels in the turbulent flow regimes. Therefore, this study will cover symmetrically heated vertical channel with both uniform wall temperature and uniform wall heat flux in turbulent flow regimes using Uniform pressure inlet condition.

5.5.1 Isothermal Vertical Surfaces.

Local Nusselt Number Distribution along the Channel

Figures 5.95, 5.96 and 5.97 show the variation of local Nusselt number along the channel for a range of temperature difference of 20^{O} to 70^{O} between the ambient and the channel walls considering aspect ratios of 12.5, 50 and 100. The length of the channel is kept constant while the channel width changes. As can be seen from Figure 5.95 as the temperature difference between ambient and walls increases, the local Nusselt number increases.

Figure 5.98 shows the variation of local Nusselt number along the channel for a temperature difference of 40^{O} between ambient and channel walls for different channel widths. It can be seen that as the channel width increases there is an increase in local Nusselt number. For a channel width of b = 0.4m, it can be seen that the local Nusselt number is high at the entrance region followed by a sharp decrease till a channel height of

y/L = 0.2 and then increases gradually due to the increase in the fluid velocity as observed in Figures 5.99 and 5.100. These figures show the mean vertical velocity at channel sections y/L = 0.5 and y/L = 1.0, respectively.

Bulk Temperature variation along the channel

The variation of bulk temperatures along the channel was investigated for three different channel aspect ratios of 25, 50 and 100 and the results are shown in Figures 5.101, 5.102 and 5.103, respectively. From Figure 5.101 it can be seen that the bulk temperature is lowest for $\Delta T=20^{O}$ (temperature difference between channel wall and ambient) and is highest for $\Delta T=70^{O}$. Similar trend could be observed in Figure 5.102 and 5.103. So it can be concluded that as the temperature difference between channel wall and ambient increases the bulk temperature also increases at any location in the channel.

Comparing the bulk temperature for different aspect ratios, it can be seen that as the channel aspect ratio increases the bulk temperature of the channel at any particular temperature difference increases. Comparing the bulk temperature of the channel for $\Delta T = 70^{O}$ for different channel aspect ratio it can be seen in Figure 5.104 that for an aspect ratio of 25, the maximum temperature reached close to channel exit is 311 K while for a channel aspect ratio of 50 and 100 it is 322 K and 344 K, respectively.

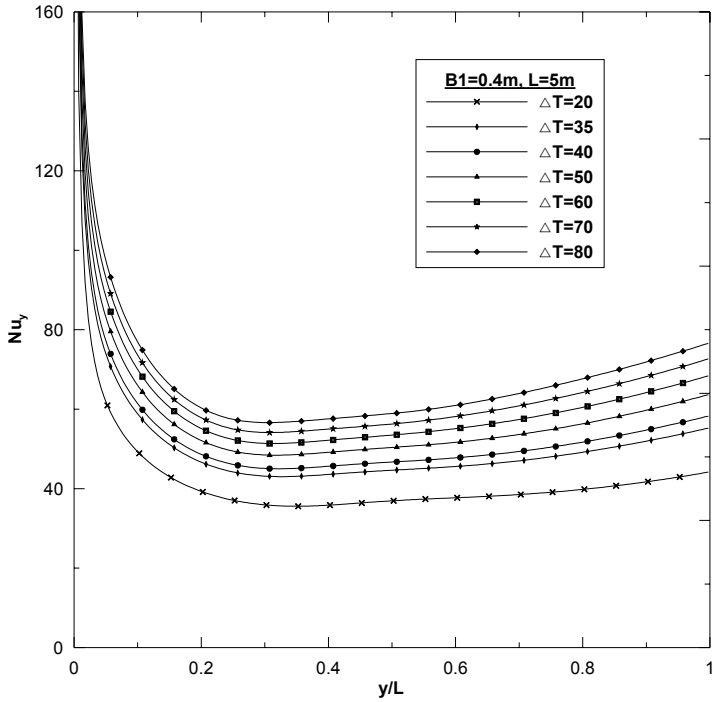

Figure 5.95: Local Nusselt number along the wall for channel width b = 0.4m and length L = 5m at different wall temperatures.

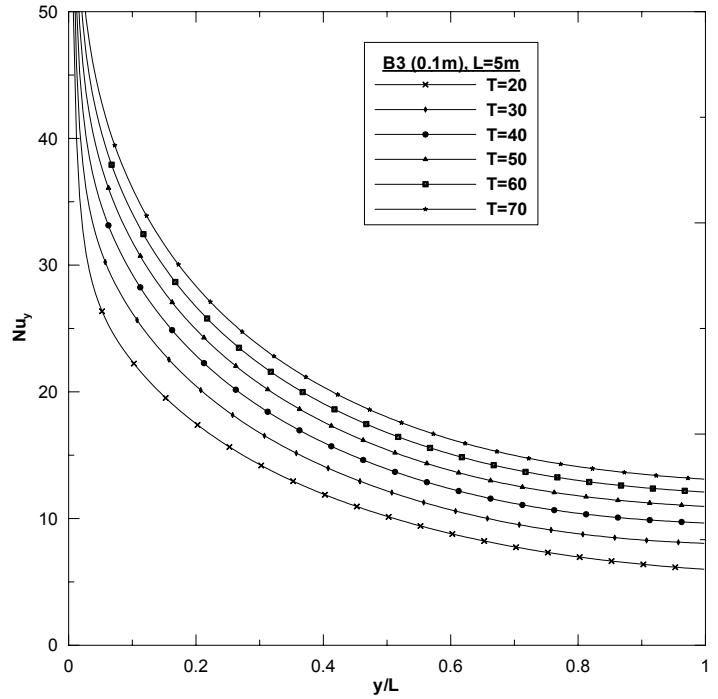

Figure 5.96: Local Nusselt number along the channel for channel width b = 0.1m and length L = 5m with different temperatures.

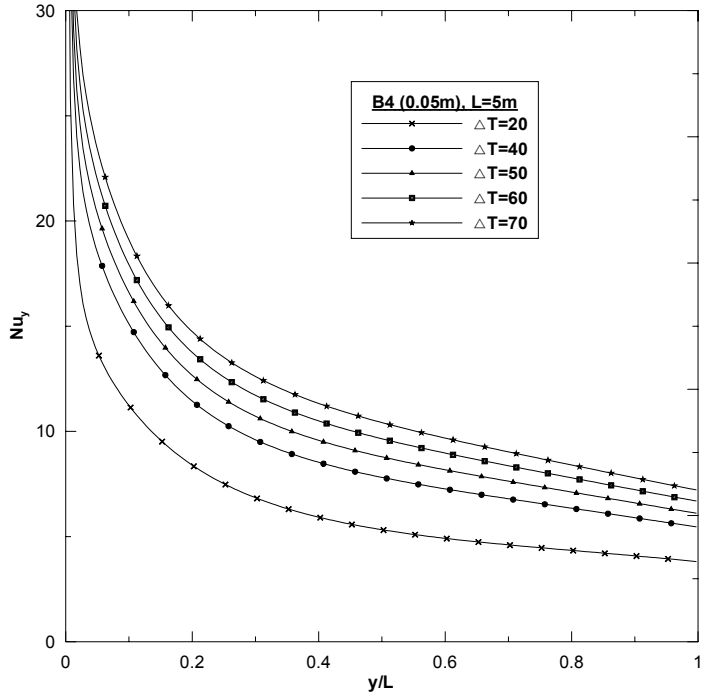

Figure 5.97: Local Nusselt number along the channel for channel width b = 0.05m and length L = =5m with different temperatures.

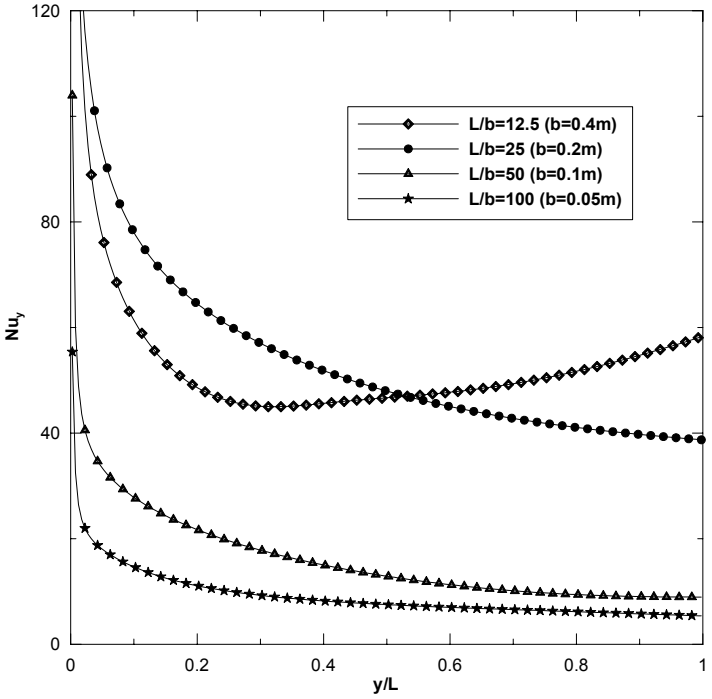

Figure 5.98: Local Nusselt number along the channel for ΔT = 40 with different channel aspect ratio.

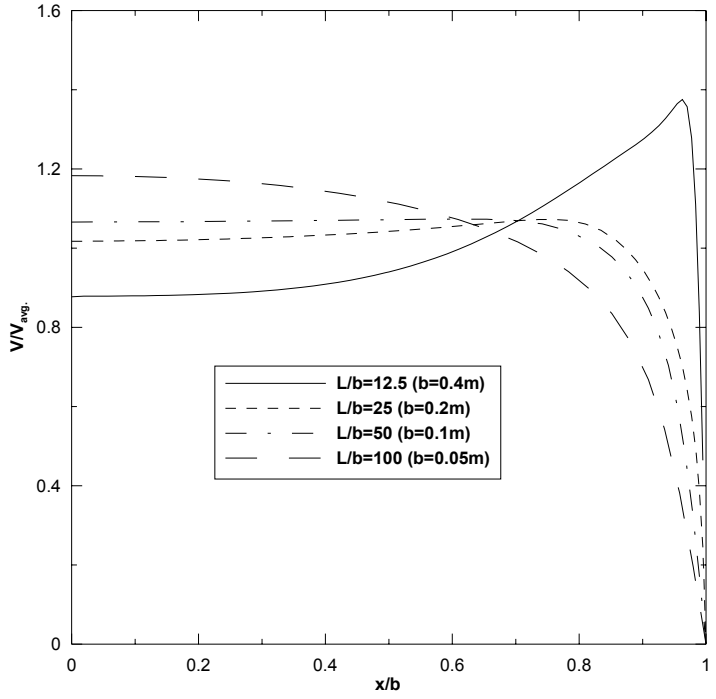

Figure 5.99: Mean vertical velocity at a section y/L =0.5 and ΔT = 40 for different channel aspect ratio

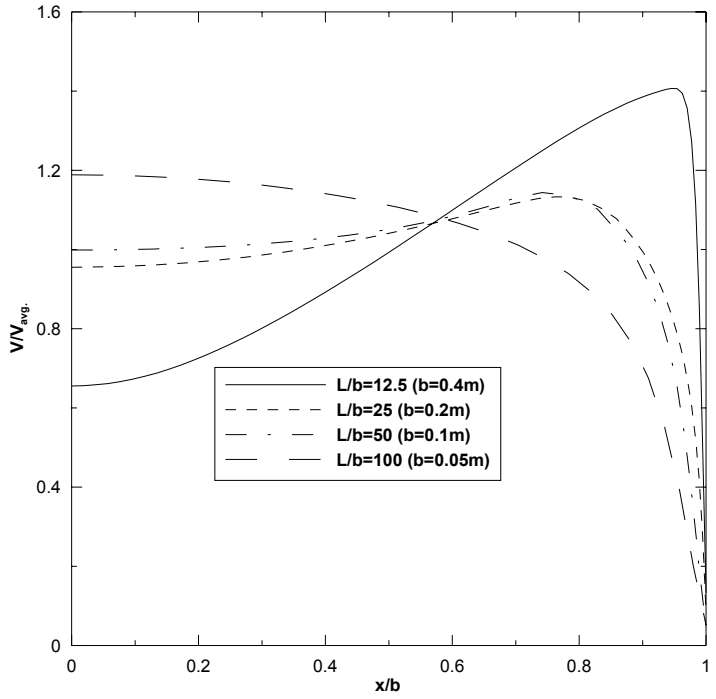

Figure 5.100: Mean vertical velocity at a section y/L =1.0 and ΔT = 40 for different channel aspect ratio

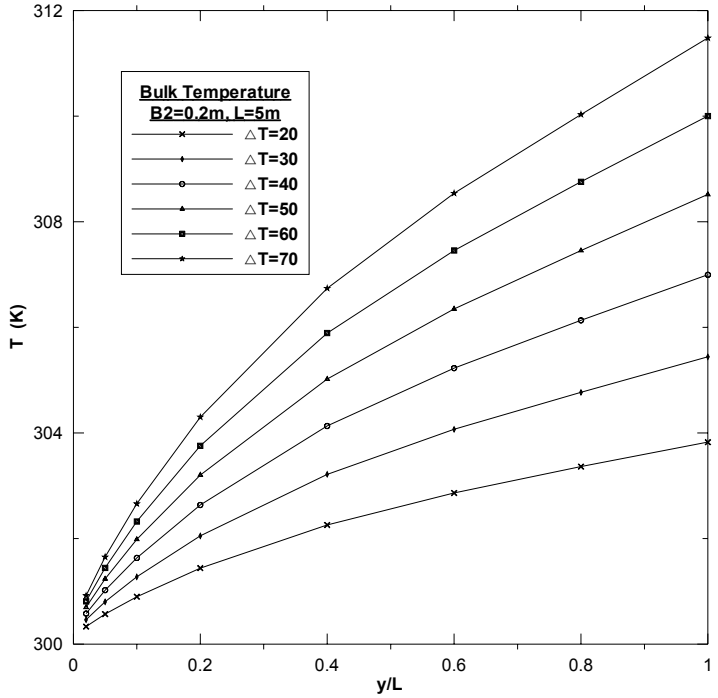

Figure 5.101: Bulk temperature distribution along the channel for channel width b = 0.2m and length L = 5m with different temperatures.

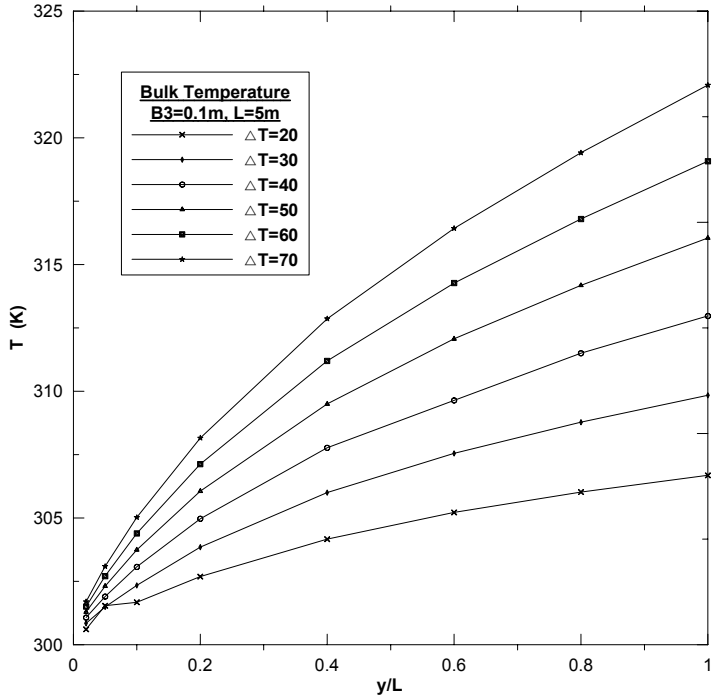

Figure 5.102: Bulk temperature distribution along the channel for channel width b = 0.1m and length L = 5m with different temperatures.

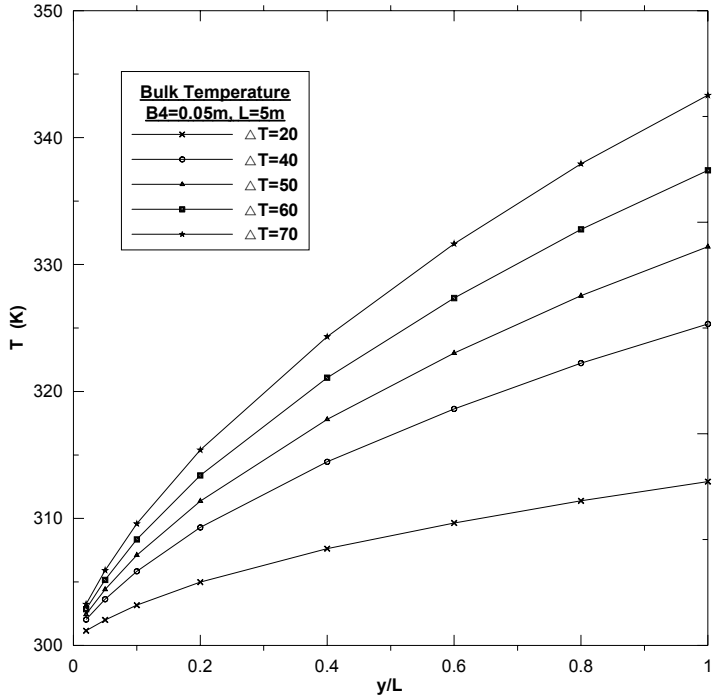

Figure 5.103: Bulk temperature distribution along the channel for channel width b = 0.05m and length L = 5m with different temperatures.

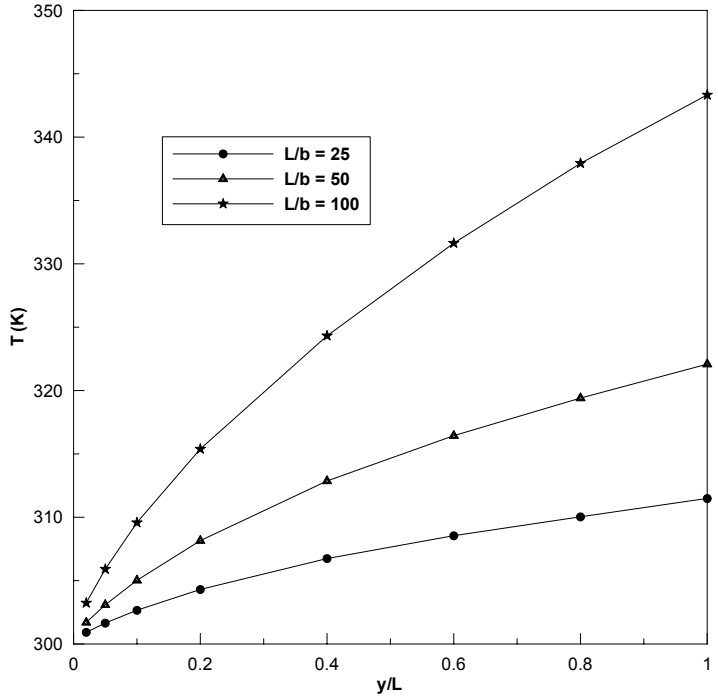

Figure 5.104: Bulk temperature distribution along the channel for $\Delta T = 70^{O}$ C and different channel aspect ratios.

Average Nusselt Number

The average Nusselt number for isothermally heated vertical surfaces for various modified Rayleigh numbers were plotted in Figure 5.105. The abscissa is the modified Rayleigh number based on the width of the channel multiplied by the inverse of the channel aspect ratio (b/L). It may be observed that the data are well correlated by this type of representation. The average Nusselt numbers for different channel aspect ratios at different modified Rayleigh number are shown in Figure 5.105. For isothermal vertical surfaces, the modified Rayleigh is calculated as follows:

$$Ra_b^* = \frac{g\beta\Delta T b^3}{\nu^2}\left(\frac{b}{L}\right) \tag{5.1}$$

The average Nusselt number data are correlated by the least-square power law which results in the following correlation:

$$\overline{Nu} = 0.64\,[Ra_b\ (b/L)]^{0.27} \tag{5.2}$$

The above correlation is shown by the solid line in Figure 5.105.The best fit over the whole range considered has a co-efficient of determination 0.99 (R^2)

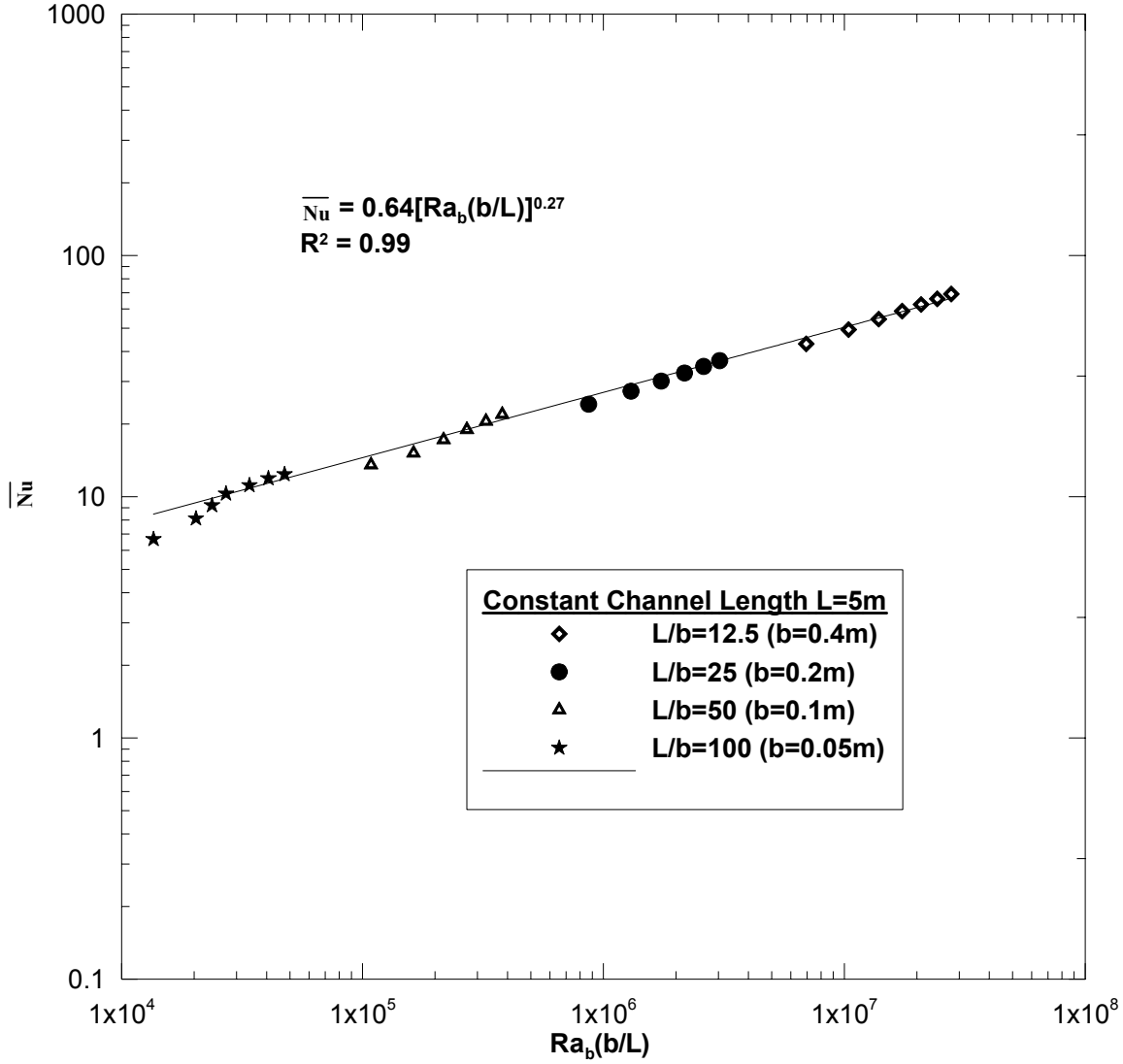

Figure 5.105: Average Nusselt number for symmetrically heated Isothermal surfaces.

5.5.2 Isoflux Vertical Surfaces

Average Nusselt Number

Figure 5.106 shows the effect of Rayleigh number on the average Nusselt number obtained for two parallel-plate vertical channel with symmetrical heat flux on both plates. The abscissa is the modified Rayleigh number based on the width of the channel multiplied by the inverse of the channel aspect. It may be observed that the data are well correlated by this type of representation. For isoflux vertical surfaces, the modified Rayleigh is calculated from

$$Ra_b^* = \frac{g\beta q_c b^4}{k\nu^2}\left(\frac{b}{L}\right) \tag{5.3}$$

this is the form of equation used my many authors (Said and Krane, 1991; Miyamoto *et al.* 1986) to correlate average Nusselt number with Rayleigh number. The average Nusselt number data are well correlated by the least-square power law

$$\overline{Nu} = 0.85\,[Ra_b\ (b/L)]^{0.21} \tag{5.4}$$

which is shown by the solid line in Figure 5.106.The best fit over the whole range considered has a co-efficient of determination 0.97 (R^2)

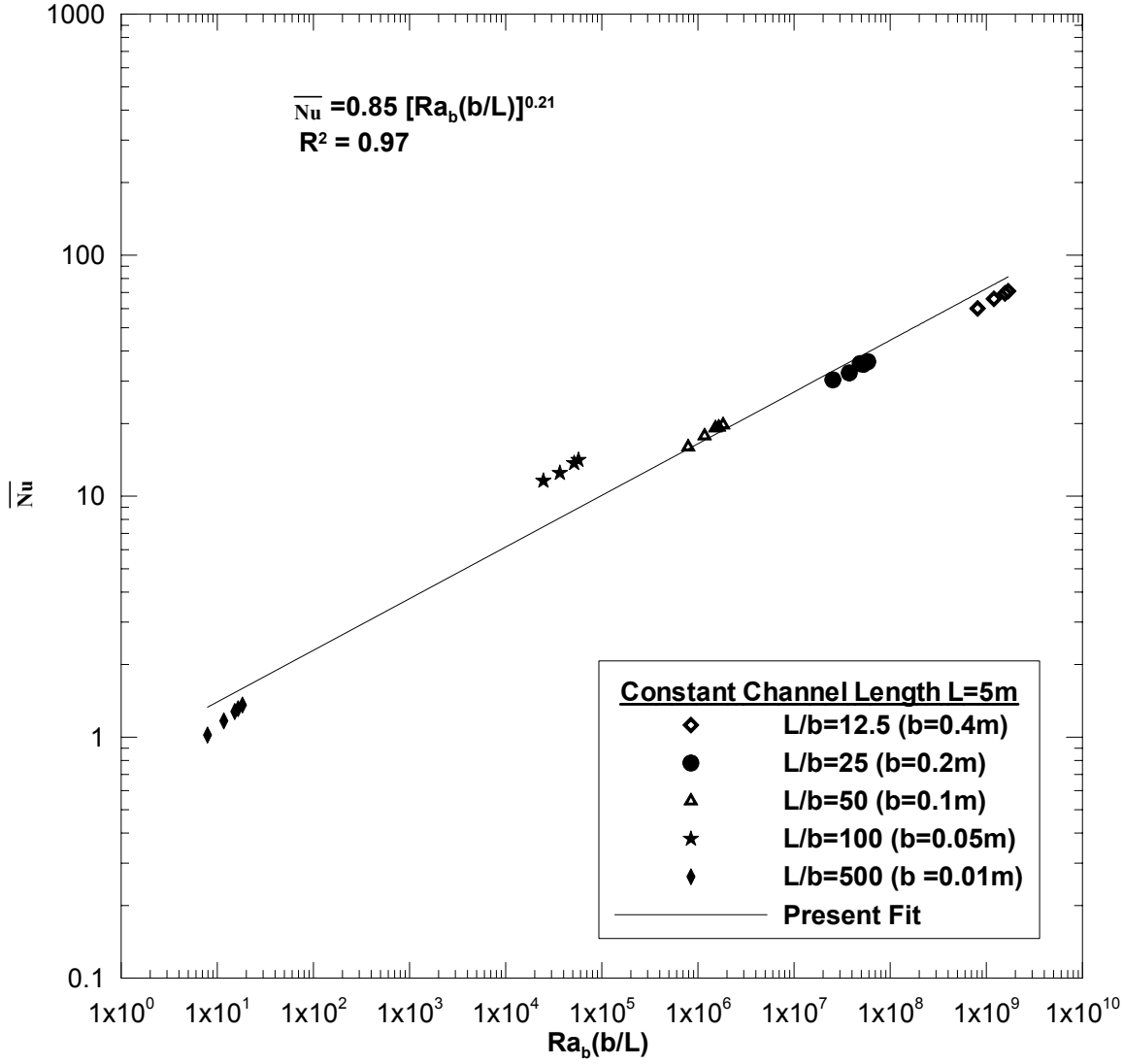

Figure 5.106: Average Nusselt number for symmetrically heated Isoflux surfaces

Chapter 6

Conclusions and Recommendations

6.1 Conclusions

The research described here constitutes a comprehensive study of the turbulent heat transfer and fluid flow characteristic of flow through buoyancy driven natural convection in vertical parallel plate channel. The general purpose computer code FLUENT is used to perform the numerical computations. The numerical procedure has been validated by comparing the present results with both experimental and numerical work in the literature for both laminar and turbulent natural convection problems. Different turbulence models have been used to study the flow and heat transfer characteristics for Rayleigh numbers in the range of 10^5 to 10^9. Different inlet boundary conditions are applied at the channel inlet to simulate complex buoyancy driven natural convention flows. During the course of investigation, various parameters such as Rayleigh number, channel aspect ratio, temperature difference between walls and ambient and different wall heat flux were systematically varied. The investigation yielded patterns of fluid flow and heat transfer presented in the form of streamlines, isotherms, velocity and temperature profiles, bulk temperature of the channel in addition to the local and average Nusselt number distribution.

The conclusions derived from the present study can be summarized as follows

1. Laminar natural convection in vertical parallel-plate channel for uniform pressure inlet condition is in good agreement with experimental results of Witz and Haag (1985).
2. The Low Reynolds number $k-\varepsilon$ M3 Model has the capability to predict flow and heat transfer characteristics in the considered range of turbulent flow regime.
3. A uniform pressure inlet condition with inlet ambient pressure and temperature boundary condition is the best assumption for simulating the actual flow processes.
4. For both laminar and turbulent flow regimes, the average Nusselt number increases with increasing modified Rayleigh number.
5. A new correlation for Nusselt number was obtained for symmetrical flow with isothermally heated surfaces in terms of modified Rayleigh number.
6. Another new correlation for Nusselt number was obtained for the case of symmetrical flow with isoflux surfaces in terms of the modified Rayleigh number.

6.2 Recommendations

1. Detail experimental flow and heat transfer data are needed to further validate the two-dimensional transport analysis and the appropriateness of the low Reynolds number $k-\varepsilon$ M3 turbulence model.
2. The scope of this study is limited by the assumption of two-dimensional, turbulent, natural convection flows. Further studies are required to extend the results of the present investigation to the three dimensional turbulent flow.
3. The heat transfer characteristics of converging-plate channels can be investigated with different converging angles.

Bibliography

1. Aung, W., Fletcher, L.S. and Sernas,V., "Developing Laminar Free Convection Between Vertical Plate Plates with Asymmetric Heating". *International Journal Heat and Mass Transfer*, Vol. 15, pp. 2293-2308, 1972.
2. Barth, T. J. and Jespersen, D., "The design and application of upwind schemes on unstructured meshes".Technical Report AIAA-89-0366, AIAA 27th Aerospace Sciences Meeting, Reno, Nevada, 1989.
3. Bejan, A., "Convection Heat Transfer" Second Edition, *Jon Wiley and Sons,Inc*, 1995.
4. Bessaih, R. and Kadja, M., "Turbulent natural convection cooling of electronic components mounted on a vertical channel". *Applied Thermal Engineering*, Vol. 20, No. 2, pp. 141-154, 2000.
5. Bessaih, R. and Kadja, M., "Numerical study of three-dimensional turbulent natural convection air cooling of heat sources simulating electronic components mounted in a vertical channel". *Journal of Enhanced Heat Transfer*, Vol. 7, No. 2, pp. 153-166, 2000.
6. Bodia, J. R. and Osterle, J. F., "The Development of Free Convection Between Heated Vertical Plates". *ASME Journal of Heat Transfer*, Vol. 84, pp. 40-44, 1962.

7. Chang, Kuo-Ping, Hung, and Ying-Huei., "Transient natural convection between vertical finite length heated plates". *Journal of Thermophysics and Heat Transfer*, Vol. 11, No. 2, pp. 203-211, 1997.
8. Chien, K. Y., "Predictions of Channel and Boundary-Layer Flows with a Low-Reynolds Number Turbulence Model". *American Institute of Aeronautics and Astronautics Journal*, Vol. 20, pp. 33-38, 1982.
9. Choudhury, D., "Introduction to the Renormalization Group Method and Turbulence Modeling". *Fluent Inc. Technical Memorandum* TM-107, 1993.
10. Dalbert, A. M., Penot F. and Peube, J. L., "Convection Naturalle Laminaire Dans un Canal Vertical Chauffe a Flux Constant". *International Journal of Heat Mass Transfer*, Vol. 24, pp.1463-1473, 1981.
11. Daloglu, A. and Ayhan, T., "Natural convection in a periodically finned vertical channel". *International Communications in Heat and Mass Transfer*, Vol. 26. No. 8, pp. 1175-1182, 1999.
12. Emanual, D., Shaigeo, K. and Atsushi, O., "Natural Convection Heat Transfer in and Asymmetrically Heated Vertical Channel Controlled by Through Flow". JSME *International Journal, Series B*, Vol. 41, No. 1, 1998.
13. Wilcox, D. C., "Turbulence Modeling for CFD". *DCW Industries*, 2000.
14. Desal, C. S and Abel, J. F., "Introduction to the Finite Element Method-A Numerical method for Engineering Analysis", CBS Publication and Distributors, Delhi, 2000.
15. Dutoya, D. and Michard, P., "A Program for Calculating Boundary Layers along Compressor and Turbine Blades". *Numerical methods in Heat Transfer*, edited by

R. W. Lewis, K. Morgan and O. C. Zienkiwicz, John Wiley and Sons, new York, 1981.

16. Elenbaas, W., "Heat Dissipation of Parallel Plates by Free Convection". *Physica 9*, pp. 1-28, 1942.
17. Fedorov, A. G. and Viskanta, R., "Turbulent natural convection heat transfer in an asymmetrically heated, vertical parallel-plate channel". *International Journal of Heat and Mass Transfer,* Vol. 40, No. 16, pp.3849-3860, 1997.
18. Fedorov, A. G., Viskanta, R and Mohamad, A. A., "Turbulent heat and mass transfer in an asymmetrically heated, vertical parallel plate channel". *International Journal of Heat and Fluid Flow*, Vol. 18, pp. 307-315, 1997.
19. Finalayson, B. A., "The Method of Weighted Residuals and Variational Principles, Academic", New York, 1972.
20. Fujii, M., Gima, S., Tomimura, T. and Zhang, X., **"**Natural Convection to Air from an Array of Vertical Parallel Plates with Discrete and Protruding Heat Sources**"**, Int. J. Heat and Fluid Flow, Vol. 17, pp. 483-490, 1996.
21. Habib, M. A., Said, S. A. M, Ahmed, S. A. and Ouwais, I., "Turbulent natural convection in vertical short channels, in: Turbulent Heat Transfer III Conference, Alaska, March 8-12, 2001.
22. Habib, M. A., Said, S. A. M., Ahmed, S. A. and Asghar, A., "Velocity characteristics of turbulent natural convection in symmetrically and asymmetrically heated vertical channels". *Experimental Thermal and Fluid Science*, Vol. 26, pp. 77-87, 2002.

23. Hall, D. A., Vliet, G. C. and Bergman, T. L., "Natural convection cooling of vertical rectangular channel in air considering radiation and wall conduction". *Journal of Electronic Packaging, Transaction of the ASME*, Vol. 121, No. 2, pp. 75-84, 1999.

24. Hanjalic, K., Kenjeres, S. and Durst, F., "Natural Convection in partitioned two-dimensional enclosures at higher Rayleigh numbers". *International Journal of Heat Mass Transfer*, Vol. 39, No. 7, pp. 1407-1427, 1996.

25. Hassid, S. and Poreh, M., "A Turbulent Energy Dissipation Model for Flows with Drag Reduction". *Journal of Fluids Engineering*, Vol. 100, pp. 107-112, 1978.

26. Hoffmann, G. H., "Improved Form of the Low-Reynolds Number $k-\varepsilon$ Turbulence Model". *Physics of Fluids*, Vol. 18, pp. 309-312, 1975.

27. Ince, N. Z and Launder, B. E., "On the computation of buoyancy-driven turbulent flow in rectangle enclosures". *International Journal of Heat and Fluid Flow*, Vol. 10, No. 2, pp. 110-117, 1989.

28. Incropera, F. P. and DeWitt, D. P., "Fundamentals of Heat and Mass Transfer", Fourth Edition, *Jon Wiley and Sons*, 1996.

29. Jaluria, Y., "Natural Convection Heat and Mass Transfer", First Edition, *Perganon press*, 1980.

30. Jones, W. P. and Launder, B. E., "The Calculation of Low-Reynolds number Phenomena with a Two-Equation Model of Turbulence". *International Journal of Heat and Mass Transfer*, Vol. 16, pp. 1119-1130, 1973.

31. Kihm, K. D., Kim, J. H. and Fletcher, L. S., "Investigation of Natural Convection Heat Transfer in Converging Channel Flows Using a Specklegram Technique". *Journal of Heat Transfer*, Vol. 115, pp. 140-147, 1993.

32. Kihm, K. D., Kim, J. H. and Fletcher, L. S., "Onset of Flow Reversal and Penetration Length of Natural Convective Flow Between Isothermal Vertical Walls". *Journal of Heat Transfer*, Vol. 117, pp.776-779, 1995.

33. Kettleborough, C. F., "Transient Laminar Free Convection Between Heated Vertical Plates Including Entrance Effects". *International Journal of Heat Mass Transfer*, Vol. 15, pp. 883-896, 1972.

34. La Pica, A, Rodono, G. and Volpes, R., "As experimental investigation on natural convection of air in a vertical channel". *International Journal of Heat Mass Transfer*, Vol. 36, pp. 611-616, 1993.

35. Lam, C. K. G and Bremhorst, K. A., "Modified Form of the $k-\varepsilon$ Model for Predicting Wall Turbulence", *Journal of Fluids Engineering*, Vol. 103, pp. 456-460, 1981.

36. Lapidus, L. and Pinder G. F., "Numerical Solution of Partial Differential Equations in Science and Engineering" *John wiley and Sons*, 1982.

37. Launder, B. E., Reece G. J. and Rodi, W., "Progress in the development of Reynolds-stress turbulence closure". Journal of Fluid Mechanics, Vol. 68, No. 3, pp. 537-566, 1975.

38. Launder, B. E. and Sharma, B. I., "Application of the Energy-Dissipation Model of Turbulence to the Calculation of Flow Near a Spinning Disc". *Letters in Heat and Mass Transfer*, Vol. 1, pp. 131-138, 1974.

39. Launder, B. E. and Shima, N., "Second-Moment Closure for the Near-Wall Sublayer: Development and Application". *AIAA Journal*, Vol. 27, No. 10, pp. 1319-1325, 1989.

40. Launder, B. E. and Spalding, D. B., "The Numerical computation of Turbulent Flow". *Computer Methods in Applied Mechanics and Engineering*, Vol. 3, pp. 269-289, March 1974.

41. Launder, B. E. and Spalding, D. B., "Lectures in Mathematical Models of Turbulence". *Academic Press Inc*., London, 1972.

42. Launder, B. E. and Spalding, D. B., "Introduction to the Modeling of Turbulence". Lecture Series-1991-02, Von Karman Institute for Fluid Dynamics, 1991.

43. Lee, Kuan-Tzong, "Natural convection heat and mass transfer in partially heated vertical parallel plates". *International Journal of Heat Mass Transfer*, Vol. 42, No. 23, pp. 4417-4425, 1999.

44. Manca, O., Nardini, S., Naso, V. and Ruocco, G., "Experiments on natural convection and radiation I asymmetrical heated vertical channels with discrete heat source". *ASME., HTD*- Vol. 317, No. 1, pp. 309-319, 1995.

45. Miyamoto, M., Katoh, Y., Kurima, J. and Sasaki, H., "Turbulent Free Convection Heat Transfer From Vertical Parallel Plates". Heat Transfer, *Proceeding of the International Heat Transfer, conference 8th 1986*, Vol. 4, pp. 1593-1598, 1986.

46. Miyatake, O. and Fujii, T., "Free Convection Heat Transfer Between Vertical Plates – One Plate Isothermally Heated and the Other Thermally Insulated". *[in Japanese]*, *kagaku Kogaku*, Vol. 36, pp. 405-412, 1972.

47. Nakamura, H., Yutaka, A. and Naitou, T., "Heat Transfer by Free Convection Between Two Parallel Flat Plates". *Numerical Heat Transfer*, Vol. 5, pp. 95-106, 1982.

48. Naylor, D., Floryan, J.M., and Tarasuk, J.D. "A Numerical Study of Developing Free Convection Between Isothermal Vertical Plates". Transaction of the ASME, *Journal of Heat Transfer*, Vol. 113, pp.620-626, 1991.

49. Naylor, D., and Tarasuk, J. D., "Natural Convective Heat Transfer in a Divided Vertical channel Par I –Numerical Study". *Journal of heat Transfer*, Vol. 115, pp. 377-387, 1993.

50. Naylor, D., and Tarasuk, J. D., "Natural Convective Heat Transfer in a Divided Vertical channel Par II –Experimental Study". *Journal of heat Transfer*, Vol. 115, pp. 387-397, 1993.

51. Nobuhide K. and Mitsugu N., "Direct numerical simulation of combined forced and natural turbulent convection in a vertical plane channel". *International Journal of Heat and Fluid Flow*, Vol. 18, pp. 88-99, 1997.

52. Oosthuzien, P. H., "A Numerical Study of Laminar Free Convective Flow Through a Vertical Open Partially Heated Plane Duct". *Fundamentals of Natural Convection- Electronic Equipment Cooling*, ASME HTD- Vol. 32, pp. 41-48, 1984.

53. Patel, V. C., Rodi, W. and Scheuerer, G., "Turbulence Models for Near-Wall and Low Reynolds Number Flows: A Review". *American Institute of Aeronautics and Astronautics Journal*, Vol.23 No. 9, pp. 1308-1319, 1984.

54. Patankar, S. V., "Numerical Heat Transfer and Fluid Flow", *Hemisphere Publishing corporation*, 1980.

55. Patankar, S. V. and Spalding, D. B., "A Calculation Procedure for Heat, Mass and Momentum Transfer in Three-dimensional Parabolic Flows", *International Journal of Heat and Mass Transfer*, Vol. 15, pp. 1777-1787, 1972.

56. Reynolds, W, C., "Computation of Turbulent Flows". *Annual Review of Fluid Mechanics*, Vol. 8, pp. 183-208, 1976.

57. Roberts, D. A. and Floryan, J. M., "Heat Transfer Enhancement in the Entrance Zone of a Vertical Channel". ASME *Journal of Heat Transfer*, Vol. 120, pp. 290-292, 1998.

58. Reynolds, O., "On the Dynamical Theory of Incompressible Viscous Fluids and the Determination of the Criterion". *Philosophical Transactions of the Royal Society of London*, *Series A*, Vol. 186, pp. 1-23, 1895.

59. Rodi, W., "Turbulence Models and Their Application in Hydraulics". *International Association for Hydraulic Research*, Delft, The Netherlands, 1980.

60. Rodi, W., "Turbulence Models and Their Application in Hydraulics- A State of the art review". University of Karlsrhe, Federal Republic of Germany, 1984.

61. Said, S. A. M., "Investigation of Natural convection in convergent vertical channels". *International Journal of Energy Research*, Vol. 20, pp. 559-567, 1996.

62. Said, S. A. M. and Krane, R. J., "An analytical and experimental investigation of natural convection heat transfer in vertical channels with a single obstruction". *International Journal of Heat Mass Transfer*, Vol. 33, No. 6, pp. 1121-1134, 1990.

63. Sarma, P. A., Prasad, B. V. and Sastri, K. S., "Laminar Natural Convection in Vertical Channels with Periodic Wall Protrusions", *Applied Scientific Research*, Vol. 54, pp. 1-22, 1995.

64. Schlichting, H., "Boundary-Layer Theory", 7th edition, *McGraw-Hill*, New York, 1979.

65. Shahin, G. A. and Floryan, J. M., "Heat Transfer Enhancement Generated by the Chimney Effect in Systems of Vertical Channels". ASME *Journal of Heat Transfer*, Vol. 121, pp. 230-232, 1999.

66. Sparrow, E. M. and Azevedo, L. F., "Vertical-channel natural convection spanning between the fully-developed limit and the single-plate boundary-layer limit". *International Journal of Heat Mass Transfer*, Vol. 28, No. 10, pp. 1847-1857, 1985.

67. Straatman, A. G., Naylor, D., Floryan, J. M. and Tarasuk, J. D., "A Study of Natural Convection Between Inclined Isothermal Plates". *Journal of Heat Transfer*. Vol. 116, pp. 243-145, 1994.

68. Tanda, G., "Experiments on natural convection from two staggered vertical plates". *International Journal of Heat Mass Transfer*, Vol. 38. No. 3, pp. 533-543, 1995.

69. Tanda, G., "Natural Convection heat transfer in vertical channels with and without transverse square ribs". *International Journal of Heat Mass Transfer*, Vol. 40, No. 9, pp. 2173-2185, 1997.

70. Tsuji, T. and Nagano, Y., "Characteristics of a turbulent natural convection boundary layer along a vertical flat plate". *International Journal of Heat Mass Transfer*, Vol. 31, No. 8, pp. 1725-1734, 1988.

71. Versteegh, T. A. M. and Nieuwstadt, F. T. M., "A direct numerical simulation of natural convection between two infinite vertical differentially heated walls scaling laws and wall functions". *International Journal of Heat Mass Transfer*, Vol. 42, pp. 3673-3679, 1999.

72. Versteegh, T. A. M. and Nieuwstadt, F. T. M., "Turbulent budgets of natural convection in an infinite, differentially heated, vertical channel". *International Journal of Fluid Flow*, Vol. 19, pp. 135-140, 1998.

73. van Driest, E. R., "On Turbulent Flow Near a Wall". *Journal of the Aeronautical Sciences*, Vol. 23, pp. 1007-1011, 1956.

74. Versteeg, H. K. and Malalasekera, W., "An Introduction to Computational Fluid Dynamics". The Finite Volume Method, *Longman Scientific and Technical*, New York, 1995.

75. von Karman, T., "Turbulence", Twenty Fifty Wilbur Wright Memorial Lecture, *Journal of Aeronautical Science*, Vol. 41, p 1109, 1937.

76. Wirtz, R. A. and Haag, T., "Effect of an Unheated Entry on Natural Convection Between Vertical Parallel Plates". *ASME Paper NO. 85*- WA/HT- 14, 1985.

77. Yakhot, V. and Steven A. O., "Renormalization Group Analysis of Turbulence. I Basic Theory". *Journal of Scientific Computing* Vol.1, No.1, pp. 3-51, 1986.

78. Yang, Z. and Shih, T. H., "New Time Scale Based $k-\varepsilon$ Model for Near-Wall Turbulence" *American Institute of Aeronautics and Astronautics Journal*, Vol. 31, No. 7, pp. 1191-1198, 1993

79. Zamora, B. and Hernandez, J., "Influence of variable property effects on natural convection flows in asymmetrically-heated vertical channels". *International Communications in Heat Mass Transfer*, Vol. 24, No. 8, pp. 1153-1162, 1997.